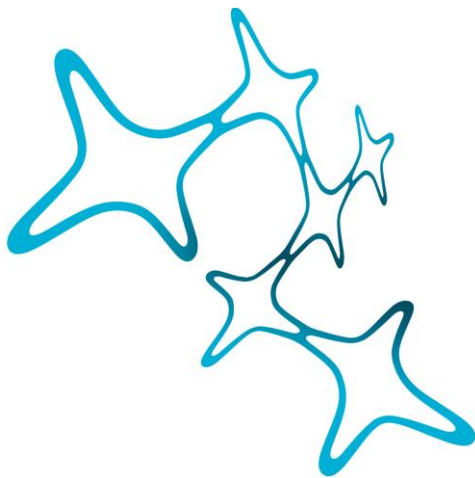


Physiology of rodent olfactory bulb interneurons

Wolfgang Bywalez



**Graduate School of
Systemic Neurosciences**

LMU Munich

Dissertation der Graduate School of Systemic Neurosciences
der Ludwig-Maximilians-Universität München

07.09.2016

Physiology of rodent olfactory bulb interneurons

Wolfgang Bywalez

Dissertation der Graduate School of Systemic Neurosciences
der Ludwig-Maximilians-Universität München

07.09.2016

First reviewer and supervisor: Prof. Dr. Veronica Egger

Second reviewer: Dr. Volker Scheuss

External reviewer: Prof. Dr. Marc Spehr

Date of oral defense: 05.04.2016

Content

Abstract	VI
1. Introduction	1
1.1. General importance of the sense of smell	1
1.2. Organs of olfactory reception	2
1.3. Olfactory receptor repertoire.....	3
1.4. Bulbar circuitry and connectivity	4
1.4.1. Main olfactory bulb layered organization.....	4
1.4.2. From the epithelium to the cortex	6
1.4.3. Circuitry in the glomerular layer and external plexiform layer	8
1.4.3.1. Glomerular layer	8
1.4.3.2. External plexiform layer.....	10
1.5. Centrifugal input to the olfactory bulb	12
1.6. Dopaminergic cells in the olfactory bulb	15
1.7. Granule cell physiology	17
1.7.1. The reciprocal granule cell – mitral cell dendrodendritic synapse	17
1.7.2. Granule cell plasticity.....	18
1.7.3. Spines	19
1.7.4. Gemmule structure	19
1.7.5. Receptor repertoire and physiology of the reciprocal arrangement	20
1.7.6. Activation modes of granule cell gemmules	23
1.8. Oscillatory activity in the olfactory bulb	24
1.9. Adult neurogenesis in the olfactory bulb	25
2. Motivation / Aims of the thesis and experimental steps	32
2.1. Project 1: Subtype diversity of dopaminergic neurons within the rat and mouse olfactory bulb glomerular layer	32
2.2. Project 2: Local postsynaptic voltage-gated sodium channel activation in dendritic spines of olfactory bulb granule cells.....	33
2.3. Contributions to non-thesis-related publications	34
3. Manuscripts	35
3.1. Subtype diversity of dopaminergic neurons within the rat and mouse olfactory bulb glomerular layer.....	35
3.2. Local postsynaptic voltage-gated sodium channel activation in dendritic spines of olfactory bulb granule cells.....	81
4. Discussion	110
4.1. Spine compartmentalization and spine function.....	110
4.2. Functional implications of bulbar physiology in discussion with recent literature	113
4.2.1. Studies with well-preserved feedback connectivity in the olfactory bulb	113
4.2.2. Recent studies on granule cell functionality	114
4.2.3. Focus on dopaminergic cell physiology and function and large-scale bulbar signal transformations.....	115
4.2.4. Rationale for lateral and columnar circuit elements.....	118
4.3. Physiological importance of adult neurogenesis	119
4.4. Multiple transmitter neurons – transmitter type determination.....	120
4.5. Implications of olfactory bulb physiology in disease and clinical aspects ..	121
4.6. Dendritic neurotransmitter release in the bulb and similar features in other brain areas	122
4.7. Perspective on bulbar circuits.....	123

4.8.	Modular arrangements in the brain with similarities to glomeruli	124
4.9.	Final remarks	126
5.	References / Bibliography	127
6.	Appendix	150
6.1.	Nomenclature / Abbreviations	150
6.2.	Acknowledgements	152
6.3.	Short scientific curriculum vitae	154
6.4.	Contributions	156
6.5.	Eidesstattliche Versicherung / Affidavit	157
6.6.	Erratum	158

Abstract

The sense of olfaction is a central gateway of perceiving and evaluating an animal's environment filled with volatile chemicals. It affects individual and social behavior in an evaluative way, i.e. by helping to find food sources, warning from dangers like toxins or predators or influencing mating choice. Already the first central station for vertebrate olfactory processing, the olfactory bulb (OB), is astonishingly complex. Its structure features several horizontal layers of signal transformation that includes a large variety of local interneurons (INs). Most of these cells are subject to adult neurogenesis, which rejuvenates and remodels the circuitry throughout life. One of those interneuron subtypes, the granule cell (GC), poses the most numerous cell type of the olfactory bulb. As the major synaptic connection of the bulb, linking different glomerular units, it participates in numerous reported tasks like odor discrimination or memory formation. Many of those capacities are attributable to the function of peculiar spines with long necks and enormous bulbar heads called gemmules. They accommodate pre- and postsynaptic specializations of the reciprocal synapse with mitral cells (MCs) that are topographically and functionally linked and feature many modes of signal integration and transmission. As of yet, the mechanistic underpinnings of activation and neurotransmitter release are not yet resolved in great detail.

This gave rise to the first project of this thesis, which focusses on the detailed granule cell gemmule physiology during local glutamatergic activation. With the help of two-photon glutamate uncaging and concomitant calcium imaging, the spine could be selectively stimulated and its physiological dynamics tested. By the use of different pharmacological agents, we could verify the importance of voltage gated sodium channels (Na_v) for local signal amplification and the involvement of NMDA and high voltage activated calcium channels (HVACCs) in the calcium elevation during local stimulation, which is important for γ -aminobutyric acid (GABA) release from the spine. The superthreshold depolarizing signal and strong calcium elevation during local input are exclusively restricted to the spine, which affirms the chemical and electrical isolation of gemmules from the rest of the cell. In this study we thereby confirmed the theoretical prediction of active computation within single spines in our system, emphasizing the functional importance of morphological compartmentalization for the cell's physiology.

The second largest population of interneurons in the olfactory bulb is located in the glomerular layer (GL) of the olfactory bulb and subsumes a plethora of different cell types, categorized in terms of molecular characteristics (mostly neurotransmitter), morphology and function. Among those, dopaminergic (DAergic) juxtglomerular cells (JGCs) form a subpopulation, which the second part of this thesis is focused on.

Innervated by the first or second synapse in the olfactory pathway, these cells exert strong influence in very early stages of olfactory signaling. The gating and transformation of inputs locally and very importantly also laterally over large distances originate from several factors. This cell grouping usually expresses two neurotransmitters at the same time, GABA and dopamine (DA), and encompass many different morphologies and synaptic arrangements with other cell types. Utilizing dopamine transporter (DAT) based staining methods in three animal populations differing in age and species, this study revealed a larger diversity of dopaminergic cell types in the glomerular layer. New 'uniglomerular' and a 'clasping' cell types were discriminated, showing distinct dendritic formations and glomerulus innervations, which was assessed with a new morphometric tool kit. The clasping cell type features dendritic specializations, densely clasping around single cell bodies. These morphological traits occur in higher abundance and complexity specifically among adult animals and could be structures of neurotransmitter output since they show strong calcium influx upon soma depolarization. Comparisons of the three animal populations showed age- and/or species-dependent changes in the subtype composition of dopaminergic JGCs. Concordant with recent research, the inclusion of age-dependent comparisons in bulbar studies turned out to be of great significance.

1. Introduction

1.1. General importance of the sense of smell

The sense of smell is often essential for the survival of animal life (Galizia and Lledo, 2013). Strongly interacting with taste, olfaction allows for the evaluation of an environment filled with chemicals. It helps to identify sources of nutrition, warns us from harmful substances like spoiled food, toxins and other sources of danger like predators or fire (Lledo et al., 2005; Stevenson, 2010). Moreover, it encompasses a social function identifying individuals like sexual partners or kin and communicates affective states like aggression or submission (Stowers et al., 2002; Lledo et al., 2005; Mutic et al., 2015). In humans, at least since antiquity, olfaction also has taken on further cultural and social aspects in the form of perfumes or religious and medicinal aromatics (Jones and Rog, 1998). Humans are categorized into the microsmatic group (as opposed to macrosmatic animals), having a relatively small epithelial surface and low sensitivity to odorants (Galizia and Lledo, 2013). Latter notion should be critically revised or differentiated, since human detection capabilities are often underrepresented and can be very sensitive for certain compounds (Sarrafchi et al., 2013). Although it may be true that humans nowadays do not critically rely on their olfactory sense in many aspects of their lives, disturbances of this system or the total loss of the sense strongly reduces life quality and can lead to depression and other disorders (Hummel and Nordin, 2005; Seo et al., 2009). The capabilities of human olfaction have been theoretically assessed to be very impressive with more than one trillion discriminable odorant stimuli (Bushdid et al., 2014), although this estimation was probably erroneous (Gerkin and Castro, 2015; Meister, 2015). Discrimination and identification of odorants is dependent on cognitive abilities (Endevelt-Shapira et al., 2014; Fagundo et al., 2015) which definitely limits the number of memorizable odorants to much lower numbers. The olfactory detectability of a chemical is strongly dependent on its volatility, with most odorous substances having a molecular weight of less than 350 Dalton (Galizia and Lledo, 2013). Therefore the number of potential volatile odorants is limited. Reception of water borne chemicals is not discussed in this thesis. Odorant molecules are very variable in size, shape, functional groups and charge and include many chemical classes (Amoore and Hautala, 1983). Among those, alcohols, aliphatic acids, aldehydes, ketones and esters; chemicals with aromatic, alicyclic,

polycyclic or heterocyclic ring structures; and innumerable substituted chemicals of each of these types, as well as combinations of them (Gaillard et al., 2004). Even if a substance is volatile, it is not necessarily received or perceived. Humans cannot smell CO₂ or CO, whereas other animals can (Jones, 2013). Most perceived odors are not single substances – coffee odor or rose odor are complex mixtures of hundreds of substances with some components being more relevant for the odor impression (Galizia and Lledo, 2013). Certain combinations of odor components blend together to form a percept in such a way that single components will not be reliably identified within the mixture (Hummel et al., 2013; Sinding et al., 2013). Concentrations of odorants have a strong impact on physiological responses as early as at the receptor level and also during further computations down to the percept level (Gross-Isseroff and Lancet, 1988; Duchamp-Viret et al., 2003). A given odorant can act on many receptors at the same time, and one receptor can get activated by several odorants (Galizia and Lledo, 2013). The combined activation pattern in space and time (which can even include inhibitory interactions with receptors), with different representations in other cross-connected processing areas like the OB, olfactory cortex and other associational brain areas encompasses the odor percept.

The following introductory parts will introduce general aspects of olfaction very roughly. On the bulbar level, circuitry and signal transduction and transformation is reviewed in greater detail. These parts cover aspects beyond the focus of the experiments of this thesis, which are helpful and necessary to understand recent physiological studies in the OB and are considered in the discussion. Both included manuscripts tackle important issues of general bulbar functionality to influence the understanding bulbar processing with the finding of (1) new cell types with innervation specificity and (2) a local depolarizing boosting mechanism and electrical function found in GC gemmules.

1.2. Organs of olfactory reception

Olfactory stimuli are registered in mammals in various subsystems of the nose which differ in anatomy, function and axonal targets (Breer et al., 2006). Interestingly, basic principles of olfactory transduction and primary processing networks are astonishingly similar across species and even phyla (Hildebrand and Shepherd, 1997). The two main nasal chemosensory systems are the main olfactory epithelium (MOE) and the vomeronasal organ (VNO). The VNO, a tube-like structure in the nasal septum is

considered a nose, mostly specialized on detecting chemical signals from other animals that transmit socially relevant information (Halpern, 2003). These signals are to a large part non-volatile and convey information about species, gender or individual identity that can induce innate behaviors and physiological reactions related to aggression (Maruniak et al., 1986; Stowers et al., 2002), parenting (Fleming et al., 1979; Saito et al., 1988) and mating (Bruce, 1959; Whitten, 1959; Singer et al., 1988; Leypold et al., 2002). However, the main olfactory bulb (MOB) is also involved in the processing of social signals and the systems are substantially cross-connected (Spehr et al., 2006; Kang et al., 2009). Two further organs have been described – the septal organ and the Grueneberg ganglion. Those organs' roles remained elusive until recently, although the septal organ was suggested to be involved in food odor detection and social sexual signaling (Breer and Strotmann, 2005). Moreover, nasal chemoreception is intertwined with trigeminal detection, which is linked to irritant or noxious stimuli with almost any odor eliciting a certain trigeminal response (Finger et al., 2003; Lin et al., 2008).

1.3. Olfactory receptor repertoire

At least five receptor gene families are currently known in vertebrates. These families are 'odorant receptors' (ORs) (Buck and Axel, 1991), two families of 'vomeronasal receptors' (V1R, V2R) (Herrada and Dulac, 1997; Matsunami and Buck, 1997; Pantages and Dulac, 2000), 'trace amine-associated receptors' (TAARs) (Borowsky et al., 2001; Bunzow et al., 2001) and 'formylpeptide receptors' (FPRs) (Le et al., 2001; Migeotte et al., 2006; Rivière et al., 2009), all of which are G-protein coupled receptors (GPCRs) (Galizia and Lledo, 2013). For the distribution of receptors in the different olfactory subsystems see Munger et al. (2009). Gene family sizes vary for receptor type and species. Humans, for example, have no functioning V2R genes (only a few pseudogenes), whereas mice have at least 100 genes and twice as many pseudogenes of this family. Rodents have approximately 1000 odorant receptor genes and humans still have, next to a large number of pseudogenes, approximately 350 functional OR genes (Galizia and Lledo, 2013). This astonishing number actually presents the biggest gene family in the mammalian genome representing 2-7% of the mouse genome, including the vomeronasal receptor families (Mombaerts, 2004).

1.4. Bulbar circuitry and connectivity

1.4.1. Main olfactory bulb layered organization

The MOB of rodents is organized in a laminar fashion with six main layers (Nagayama et al., 2014) or seven if counting the subependymal zone (SEZ). The most exterior layer is the olfactory nerve layer (ONL), consisting of axon bundles of olfactory sensory neurons. The cell bodies of those cells lie within the olfactory epithelium and send their axons into receptor-specific glomeruli. The second layer called glomerular layer (GL) is named after the roughly spherical structures of neuropil, laterally lining the outer perimeter of the olfactory bulb. Within glomeruli, synaptic connections from OSNs to projecting cells and processing interneurons are made. They are surrounded by cell bodies of periglomerular (PGCs) or juxtglomerular cells (JGCs), including projection neurons and local interneurons. PGCs directly adhere to the glomerular neuropil whereas JGC cell bodies are generally located in the GL, not necessarily directly touching the glomerular neuropil. Within the glomerular neuropil, consisting of axons, dendrites and glial processes, no cell bodies are present (Kasowski et al., 1999). Glial cells will not be further discussed, although they might play an important homeostatic and even signaling role in the olfactory bulb and certainly are essential for (adult) neurogenesis (Kozlov et al., 2006; Platel et al., 2010; Ninkovic and Gotz, 2013). Within mostly the periglomerular space, dendritic and axonal neuropil interconnects glomerular units, e.g. via short-axon cells (SACs). One type of SACs even forms a descending connection to the granule cell layer (GCL), linking the two horizontal layers vertically (Scott et al., 1987). Central to the GL lies the external plexiform layer (EPL). Only very few somata are situated in this layer, some of those belong to populations of tufted cells (TCs). These are differentiated mostly by their vertical position within the layer and additionally show physiological distinctions (Mori et al., 1983). In the EPL SACs and many different populations of interneurons occur in quite low numbers (recently summarized in Nagayama et al., 2014). Apart from those sparse cell bodies, the EPL is mainly characterized by its complex neuropil organization. All of the above mentioned resident cells extend their axons and dendrites mostly or exclusively within the EPL, but very importantly also other processes run through this layer. The apical and lateral dendrites of the olfactory bulb main projection cells, mitral and tufted cells (often combined as MTCs), connect with the apical dendrites of granule cells in reciprocal arrangements, forming the putatively most numerous synaptic connection of

the olfactory bulb in this layer. The EPL can be further subdivided by the dendritic outgrowth patterns of lateral dendrites of mitral and tufted cells, which differ in their respective synaptic numbers, arrangements and functionality (Mori et al., 1983; Fourcaud-Trocme et al., 2014; Bartel et al., 2015), or by the localization of certain interneuron cell types (Nagayama et al., 2014). The mitral cell layer (MCL) is very restricted in its vertical extent and features a dense belt of mitral cell somata as well as granule cell somata. Mitral cells themselves are not a homogeneous population but display different connectivity and biophysical properties (Padmanabhan and Urban, 2010; Angelo et al., 2012). The internal plexiform layer (IPL) is a very thin layer featuring few cell types and specialized connections from the contralateral bulb as well as cortical projections. The main cell group is horizontal cells, whose dendrites run parallel to the MCL and whose axons project into the EPL (Price and Powell, 1970c). Some multipolar neurons in this layer express acetylcholine esterase (Carson and Burd, 1980). Axons of a group of ETCs (or superficial tufted cells) project to the IPL of the other side of the same bulb (medial to lateral or vice versa) targeting GCs of the opposite side glomerular column (Lodovichi et al., 2003) via the so-called intrabulbar projection (IBP). A recent publication suggested that the projecting neurons, instead of GCs, are primarily excited via this connection by cholecystinin (CCK) (Ma et al., 2013). Additionally, axons from the mitral cells' basal side pass through the IPL (Schoenfeld et al., 1985), extending towards higher olfactory centers. The most central layer of the olfactory bulb, the granule cell layer (GCL) harbors the somata of most GCs, organized in clusters and projecting into the EPL. GCs are subclassified depending on dendritic extension patterns, (electro-)physiological properties and maturation stage (Orona et al., 1983; Petreanu and Alvarez-Buylla, 2002; Carleton et al., 2003; Naritsuka et al., 2009). Different deep short-axon cells (dSACs) and other interneurons can be found in this layer. Interestingly, some dSACs vertically cross-connect their residence deep layer and the superficial glomerular layer by selectively targeting PGCs (Eyre et al., 2008). Other dSAC types even project to cortical areas (Eyre et al., 2008). Another deep layer is sometimes discriminated, the so-called subependymal zone, harboring some progenitor cell types of olfactory bulb interneurons (Shiple and Ennis, 1996). All of the layers of the OB are conversely the target of centrifugal backprojections. The detailed connections in the GL and EPL are summarized further below and a schema of glomerular organization is shown at the end of the introduction (Fig. I2-4).

1.4.2. From the epithelium to the cortex

The following rough signal transduction towards cortical subareas is based on canonical olfactory sensory neurons (OSNs) in the MOE, computations at bulbar stations are neglected in this part. They will be in the focus of the subsequent section.

The reception of many odorants takes place at a thin epithelial sheet in the nasal cavity, the olfactory epithelium. Here, odorants bind to olfactory receptors, which are seven transmembrane, G protein-coupled receptors, expressed on the cilia of receptor neurons. The cilia extend into a mucous layer secreted by supporting cells, which, with the help of solved proteins and enzymes, facilitates accumulation, receptor binding and post-interactive removal of odorant molecules (Getchell et al., 1984). In contrast to insects (Nakagawa and Vosshall, 2009), the signal transduction mechanism in ORs of mammals is resolved mechanistically. Upon binding of the odorant, the receptors generate signals through G_{olf} , converting guanosine diphosphate to guanosine triphosphate (GTP). The GTP-bound G_{olf} activates adenylyl cyclase type III, leading to cyclic adenosine monophosphate (cAMP) production. cAMP binds and opens calcium permeable, cyclic nucleotide gated channels, raising sodium and calcium levels within the receptor cell and depolarizing the membrane. Additionally, the calcium influx opens chloride channels. This anion efflux leads to further depolarization of the membrane potentials and eventually action potential (AP) generation (Bhandawat et al., 2005; Imai and Sakano, 2008). The calcium influx is also essential for the rapid desensitization of OSNs, via several downstream second messenger signals (Matthews and Reisert, 2003). The OSN AP signal is transduced via long axons, traveling in bundles through the porous cribriform plate of the ethmoid bone and reaches the olfactory bulb. Each receptor cell usually bears only one receptor type and OSNs expressing the same receptor converge into the same few glomeruli within the OB (in rodents two approximately symmetric glomeruli along the sagittal OB axis per olfactory bulb – Mombaerts, 1996). In turn, usually every glomerulus gets input from only a single receptor type. The rodent olfactory epithelium has multiple, partially overlapping, spatial zones along its dorsoventral axis which express different OR genes and this pattern is roughly conserved in corresponding domains in the olfactory bulb (Ressler et al., 1993; Miyamichi et al., 2005). The OB map can be divided into different clusters, e.g. based on odor tuning specificity or receptor classes (Bozza et al., 2009; Matsumoto et al., 2010). Inside the glomeruli the olfactory signal is directly

or indirectly forwarded to projection neurons (ETCs, TCs, MCs) with differing levels of processing by local interneurons (Fukunaga et al., 2012; Adam et al., 2014) and with different effects on output timing (Najac et al., 2015). The intrabulbar projection of ETCs is implied in using timing cues via activity onset latency differences for concentration coding of the stimulus (Zhou and Belluscio, 2008; 2012). Mitral and tufted cells transmit their information in parallel with different latency regimes onto distinct downstream targets, summarized under the name of the olfactory cortex (OC). TC targets include the ventrorostral anterior piriform cortex (PC), anterior olfactory nucleus (posteroventral part and the pars externa) and the anterolateral part of the olfactory tubercle. MCs show a wider selection of cortical targets, including the dorsal part of the anterior olfactory nucleus (AON), the cortical part of the olfactory tubercle (OT), mostly dorsal parts of anterior piriform cortex, the tenia tecta, the posterior piriform cortex, lateral entorhinal cortex, the nucleus of the lateral olfactory tract, anterior cortical amygdaloid nucleus and posterolateral cortical amygdaloid nucleus (Igarashi et al., 2012). This divergence, as well as several recent physiological studies (Fukunaga et al., 2012; Adam et al., 2014) consolidate the different roles of those subtypes of projection neurons, which, until very recently, have often been pooled as similar in morphology and function. Additional to classical principal projecting cells, GCL short-axon type cells have been demonstrated to also project to cortical olfactory centers – specifically the OT (Kosaka and Kosaka, 2007b; Eyre et al., 2008). Higher order olfactory areas, in crosstalk with the OB, serve manifold functions (Matsutani and Yamamoto, 2008; Mandairon and Linstner, 2009; Giessel and Datta, 2014), such as constructing an odor percept (Barnes et al., 2008; Payton et al., 2012), forming associational networks (Haberly and Bower, 1989), pairing olfaction with valence or affective information (Seubert et al., 2010; Gadziola et al., 2015; Patin and Pause, 2015), or enabling multisensory integration (Wesson and Wilson, 2010; Maier et al., 2015). Therefore, constructing and shaping an odor ‘image’ in the brain is founded in extremely elaborate circuitry and the simplified notion of being able to derive and predict it just by looking at the combinatorial receptor code has to be refuted (Barnes et al., 2008; Triller et al., 2008; Mori et al., 2013; Kumar et al., 2015).

1.4.3. Circuitry in the glomerular layer and external plexiform layer

The following connectivity schemata concentrate on parts of the bulbar circuitry directly connected to the cells investigated in this thesis, particularly glomerular layer and external plexiform layer interactions. Those layers actually perform most of the signal transformation in the OB. For dopaminergic cells to some extent but especially later for GC spines, the level of detail will increase even to their receptor configuration. Further connections might only be mentioned briefly. Gap junctions will not be focused on in this dissertation, although they are known to play important roles in MOB activity at various stages, including both GL and EPL interactions. Oscillatory activity, temporal synchrony of output and gating functions by shunting are influenced by those connections (Friedman and Strowbridge, 2003; Kosaka et al., 2005; Migliore et al., 2005; Gire et al., 2012; Banerjee et al., 2015).

1.4.3.1. Glomerular layer

Within olfactory bulb glomeruli, information from glutamatergic sensory cells to glutamatergic projecting cells (MCs and TCs) is extremely convergent, with the ratio of olfactory sensory neurons exceeding the number of projection cells by approximately 1000:1 (Van Drongelen et al., 1978, Mori et al., 1999). In total, approximately 20-50 projection neurons enter an individual glomerulus via usually a single apical dendrite (Malun and Brunjes, 1996; Schoppa and Westbrook, 2001; Ke et al., 2013). From there on, convergent and divergent information of individual glomerular pathways is projected towards cortical areas (Lei et al., 2006; Stettler and Axel, 2009; Apicella et al., 2010; Igarashi et al., 2012), bearing in mind that glomerular information channels are intrinsically laterally cross-connected within several bulbar layers, mostly in the GL (Kosaka and Kosaka, 2011; Banerjee et al., 2015) and the EPL (Egger et al., 2003; Kato et al., 2013). Most of the glomerular neurons are GABAergic interneurons (>50% with a total of around 230 per glomerulus – Parrish-Aungst et al., 2007) which are usually uni- (=mono-) glomerular or contact few adjacent glomeruli (Nagayama et al., 2014). This notion excludes a population of long-range dopaminergic and GABAergic short-axon cells that can innervate several or many glomeruli over a large distance (Kiyokage et al., 2010). A minor population of GABAergic periglomerular cells can be directly driven by OSNs (up to ~30%; = type I PGCs), whereas most of them get feed-

forward input via ETCs (~70%; = type II PGCs) (Kosaka et al., 1998; Hayar et al., 2004a; Kiyokage et al., 2010). TCs and interneurons are primary targets of OSNs, with ETCs to feed-forward excite a large proportion of cells within the glomerular layer, including MCs and further interneurons (De Saint Jan et al., 2009; Kiyokage et al., 2010; Fukunaga et al., 2012; Gire et al., 2012). ETCs also release endocannabinoids onto PGCs regulating their transmitter release and even influencing other ETCs slightly (Wang et al., 2012). MCs get only minor direct OSN input (De Saint Jan et al., 2009). GABAergic cells in the GL do not display a homogeneous population of cells, they differ in several partially overlapping populations of neurochemical markers. Distinction determinants include the GABA synthesizing enzyme (GAD65 or GAD67), co-expression of dopamine, their calcium binding protein type (calbindin, calretinin, neurocalcin), receptor repertoire (Panzanelli et al., 2007) and temporal origin (Batista-Brito et al., 2008). PGCs provide presynaptic GABAergic input to sensory neuron terminals as well as pre- or postsynaptic inhibition to other GABAergic interneuron types, PGCs, SACs and projection cells (Pinching and Powell, 1971a; Murphy et al., 2005; Panzanelli et al., 2007). With apical dendrites of projection neurons, they can also form dendrodendritic reciprocal arrangements (Kosaka and Kosaka, 2005). Dopaminergic cells in the glomerular layer are very diverse, morphologically and functionally. In mice all of them co-express GABA, in rats almost all (Kosaka and Kosaka, 2007a; Kiyokage et al., 2010). Most of the dopaminergic cells are driven via ETCs, some get direct OSN input (Kiyokage et al., 2010). Their output is directed onto very diverse targets, including ETCs, OSNs, PGCs, DAergic JGCs and centrifugal terminals (Pinching and Powell, 1971c; b; Ennis et al., 2001; Gutierrez-Mecinas et al., 2005; Maher and Westbrook, 2008; Banerjee et al., 2015). The DAergic JGC proportion of glomerular neurons is in the order of ~ 10%, (approximately 50 cells per glomerulus – Parrish-Aungst et al., 2007). Laterally oriented GL short-axon cells are considered a major connecting element of glomerular vertical columns (Aungst et al., 2003). Their neurotransmitter type has been proposed to be mainly glutamatergic, but the current literature considers most of them to be part of the dopaminergic-GABAergic population although there is still discordance about the nomenclature of this cell type (Aungst et al., 2003; Kiyokage et al., 2010; Kosaka and Kosaka, 2011; Liu et al., 2013; Nagayama et al., 2014). A different short-axon cell type was in fact shown to be glutamatergic (Brill et al., 2009). It can administer direct excitatory lateral drive onto hitherto unresolved targets. Many other neuroactive substances have been found

within the OB GL, including vasopressin (Tobin et al., 2010), neuromodulators like substance P, enkephaline, nitric oxide and many more (Kosaka et al., 1998). The GL and other MOB regions are subject to circadian dynamics, which influence manifold molecular and physiological processes with regular fluctuations (Corthell et al., 2014). Cortical modulation of this layer will be summarized later on (1.5.).

1.4.3.2. External plexiform layer

Strong gating inhibitory activity on MCs and TCs is exerted by GCs and other inhibitory interneurons in the EPL, mostly targeted on lateral dendrites of the projection cells. GCs themselves can be subdivided into different populations, classified by their soma location, overall morphology, innervation of OB horizontal sublayers and cell types, or depending on cell generation age and chemical markers (Price and Powell, 1970c; Mori et al., 1983; Orona et al., 1983; Naritsuka et al., 2009; Merkle et al., 2014). The GC subtype-specific repertoire of synaptic contacts involves reciprocal boutons in the perisomatic area of MCs, purely postsynaptic spines in the proximal dendritic tree and reciprocal gemmules in either the whole EPL or in rather distal (superficial) processes (Price and Powell, 1970d; Mori et al., 1983; Orona et al., 1983; Naritsuka et al., 2009). GCs outnumber MCs by a factor of approximately 50-100 (Shepherd and Greer, 2004; Egger and Urban, 2006). Despite getting manifold inputs, the GABAergic output of axonless GCs is probably restricted to the reciprocal connections with projection cells via dendritic release mechanisms (Price and Powell, 1971d; Egger et al., 2005; Shepherd et al., 2007; cf. 1.7. and more specifically 1.7.6.). The number of GCs and their synapses connected to a single projection cell or glomerulus and their respective influence is hard to estimate for different reasons. Not all GC spines harbor a reciprocal synapse, the proximal apical and basal ones are mostly purely postsynaptic (Price and Powell, 1970d; Balu et al., 2007). Furthermore, not all GABAergic connections on projecting cells are formed by GCs and the number of synapses, marked with GABA/glycine receptor subunit markers or gephyrin (Giustetto et al., 1998; Sasso-Pognetto and Fritschy, 2000) is also not uniform throughout the EPL, depending on the sublayer innervation pattern of the respective projection cell (Panzanelli et al., 2005; Bartel et al., 2015). Even though the linear density of reciprocal synapses, marked by gephyrin on the PN side, seems consistent along a given lateral dendrite, with an average of 1.1 synapses per μm (Bartel et al., 2015), the impact on the

projection neuron differs a lot depending on the localization of the synapse. Distal connections on MCs are more likely to be involved in local dendrodendritic microcircuits and lateral inhibition whereas proximal ones seem to shape temporal coding such as synchronized MTC firing (Bartel et al., 2015). Whether most connectivity of a glomerular unit to another is mainly local or established over long-range connections and whether the connectivity is specific or random is still subject to discussion, although the long-standing proposal of a clear center-surround connectivity seems unlikely (Egger and Urban, 2006; Fantana et al., 2008; Murthy, 2011; Spors et al., 2012).

Further cell types influence computations in the EPL. Among those are somatostatin immunoreactive cells, which directly interact with MC dendrites, involving dendrodendritic reciprocal synapses (Lepousez et al., 2010). Largely overlapping populations of PV positive and CRH positive cells also interact reciprocally with projecting cells (Toida et al., 1994; Huang et al., 2013; Garcia et al., 2014a). They exert a substantial influence on OB output with broadly tuned odor sensitivity and possibly even in response to airflow-induced mechanical signals. These cells form a strong inhibitory conjunction element between MCs similar to GCs, yet more densely connected (Huang et al., 2013; Kato et al., 2013; Miyamichi et al., 2013). Additionally, they seem to modulate postnatally generated GCs directly via CRH activity (Garcia et al., 2014a). Some PV positive cells overlap with the somatostatin immunoreactive cells (Lepousez et al., 2010), possibly the ones establishing reciprocal synaptic interactions with MCs.

With their soma in even deeper bulbar layers, several dSAC types exert inhibitory influence on bulbar interneurons like GCs or even PGCs (Eyre et al., 2008; Labarrera et al., 2013; Burton and Urban, 2015). For instance, Blanes cells persistently inhibit GCs monosynaptically (Pressler et al., 2007). Some other, mostly GABAergic interneurons coexist in the GCL and EPL, which influence bulbar output (Schneider and Macrides, 1978; Brinon et al., 1999; Alonso et al., 2001). Among those, an EPL-intrinsic dopaminergic population was observed (Liberia et al., 2012). An interesting study showed that even astrocytes target projection cells and GCs in the olfactory bulb with GABA and glutamate release, leading to slow inward and outward currents that can have a strong modulatory effect on both cell types (Kozlov et al., 2006).

1.5. Centrifugal input to the olfactory bulb

The bulbar circuitry is not a hermetic system or a one-way street towards higher processing centers, but is influenced by many (mainly primary) olfactory cortical areas (Price and Powell, 1970b; Shipley and Ennis, 1996) as well as classical neuromodulatory brain centers (Shipley and Adamek, 1984), giving state dependent and experience related context to olfactory stimuli (Fletcher and Chen, 2010; Kato et al., 2012; Mandairon et al., 2014; Rothermel and Wachowiak, 2014). To understand bulbar transformations in their full physiological context (cf. studies in the discussion), cortical inputs have to be considered.

The (back-)projections of primary olfactory cortex areas mainly arise from excitatory (often glutamatergic) afferents from the AON, PC (mostly layer II and III pyramidal cells), periamygdaloid cortex, entorhinal cortex, nucleus of the lateral olfactory tract and amygdala (Shipley and Ennis, 1996; Matsutani, 2010). Many fibers do not only contact the ipsilateral bulb, but also project contralaterally (Alheid et al., 1984; Shipley and Ennis, 1996). AON glutamatergic projections target bulbar interneurons (PGCs, SACs and GCs) as well as ETCs and MCs. Activating those feedback axons *in vivo* suppresses spontaneous and odor-evoked MC activity, sometimes preceded by a temporally precise increase in firing probability (Markopoulos et al., 2012). The AON is interconnected with the OB and the PC and its projections are among the most numerous centrifugal inputs to the OB (Shipley and Adamek, 1984). This activity is coupled strongly to inhalation *in vivo* with high diversity in odorant specificity and temporal dynamics. All those properties support a role in temporal coding of bulbar activity and shaping of odor-specificity (Rothermel and Wachowiak, 2014). A special feature of AON fibers to the bulb are commissural projections via the *pars externa* that reach the contralateral side of the bulb, while *pars medialis* branches target the ipsilateral side (Davis et al., 1978; Mori et al., 1979; Luskin and Price, 1983). This projection could be used for directional cues of odor localization (Rajan et al., 2006). Olfactory cortical feedback from the PC is mainly targeted onto bulbar interneurons, GCs, SACs and JGCs in widespread areas of the bulb, to decorrelate MC output (Boyd et al., 2015; Otazu et al., 2015).

Massive cholinergic and GABAergic (Gracia-Llanes et al., 2010b; Nunez-Parra et al., 2013; Rothermel et al., 2014) fibers to the MOB originate from the basal forebrain (BF), mostly from the horizontal limb of the diagonal band of Broca (HDB). Neural pathways

are not always clear, as BF cholinergic neurons project across the limbic system and cortex and target olfactory cortical areas (Zaborszky et al., 2012), which in turn modulate OB circuitry (Rothermel et al., 2014). Muscarinic receptors are mainly distributed in the internal and external plexiform layers and periglomerular areas, whereas nicotinic receptors show a different broad distribution with concentrations in the GL and EPL (Shiple and Ennis, 1996). Interestingly, acetylcholine esterase, the transmitter cleaving enzyme, shows more intense staining at some glomeruli corresponding to regions of luteinizing hormone releasing hormone innervation (Zheng et al., 1988). Both muscarinic and nicotinic receptors on JGCs shape the inhibitory balance of glomerular circuitry (D'Souza and Vijayaraghavan, 2012; Liu et al., 2015). Many major cell types, including MTCs, and especially interneurons, both GCs and JGCs are directly targeted by cholinergic projections in a complex way (Smith et al., 2015). A direct modulatory impact on dopaminergic JGCs was also shown (Pignatelli and Belluzzi, 2008), their firing rate decreased via metabotropic muscarinic receptor activation. *In vivo*, MTC spiking is enhanced spontaneously and during inhalation and odor stimulation by this input (Rothermel et al., 2014). This input is thought to sharpen olfactory tuning curves of MTCs and enhances discrimination capabilities of projection neurons (Mandairon et al., 2006; Ma and Luo, 2012). The forebrain cholinergic system is generally implied in many animal behavioral states like attention, motivation or wakefulness (Hasselmo and Sarter, 2011; Zaborszky et al., 2012) and olfactory memory is affected by cholinergic activity (Roman et al., 1993; De Rosa et al., 2001; Fletcher and Chen, 2010). GABAergic forebrain input directly inhibits GCs and thereby impairs olfactory discrimination (Nunez-Parra et al., 2013). Glycinergic forebrain input might act similarly on GCs (Trombley et al., 1999; Zeilhofer et al., 2005).

Noradrenergic (NA) fibers from the pontine nucleus locus ceruleus (LC) show a laminar innervation pattern of the OB with heavy innervation in the IPL and GCL. Impressively, up to 40% of LC neurons project to the rat OB, mainly innervating the MCL and EPL, and the GL only at low density (Shiple et al., 1985; McLean et al., 1989). A subset of those projections also contain neuropeptide Y (Bouna et al., 1994). NA α_2 and β receptors are found in the GCL, both α receptor subtypes are present in the EPL (α_1 receptor density in the EPL is the highest in the brain – Young and Kuhar, 1980), while the GCL and IPL contain β_2 receptors. NA β_1 receptors are expressed on JGCs, MCs and TCs as well as some GCs (Yuan et al., 2003). This publication additionally demonstrates the topographical and mechanistical entanglement of different

neuromodulatory inputs with the bulbar circuitry. It illustrates interactions of noradrenergic with serotonergic inputs during an odor learning paradigm. Another recent modeling study based on experimental data shows the functional amalgamation of NA and ACh inputs on GCs (Li et al., 2015). In general, NA seems to influence excitation and inhibition of MCs directly and mainly via GCs, again in a very complex way (Jahr and Nicoll, 1982; Trombley, 1992; Hayar et al., 2001; Nai et al., 2009; Nai et al., 2010; Zimnik et al., 2013). Functionally, those connections play roles in synaptic plasticity, cell integration, learning processes and also spontaneous and reward-motivated discrimination (Brennan and Keverne, 1997; Veyrac et al., 2005; Mandairon et al., 2008). Additional to the MOB connections, NA influences accessory olfactory bulb functions, regulating pregnancy and postpartum behavior in female rats (Kaba and Keverne, 1988; Kaba et al., 1989; Kendrick et al., 1992; Raineke et al., 2010). A study by Eckmeier and Shea (2014) shows that centrifugal neuromodulation impacts bulbar processing at the level of the sensory terminals, and thereby already at the first synapse of the olfactory system.

Serotonergic fibers from distinct raphe nuclei innervate the GL (OSNs, ETCs and JGCs) (Hardy et al., 2005; Liu et al., 2012; Steinfeld et al., 2015) and GCL (GCs and other interneurons) (Hardy et al., 2005; Schmidt and Strowbridge, 2014). 5-HT_{1A} receptors are present on processes in the EPL, MCL and very few in the GCL. Cells expressing 5-HT_{1A} are located in the MCL and GCL, possibly even including glia (Whitaker-Azmitia et al., 1993). 5-HT_{2A} receptors can be found in the EPL and are strongly expressed in MTCs, only moderately in PGCs and faintly in GCs (Hamada et al., 1998). Glomeruli show both types of receptors, although with relatively low occurrence. Other receptor subtypes may be present in the bulb as well (Shipley and Ennis, 1996). Physiological studies show extensive innervation of morphologically different JGCs (Hardy et al., 2005), including dopaminergic cells (Gracia-Llanes et al., 2010a; Brill et al., 2015) from which it can directly trigger AP-independent GABA release. GCs (indirectly) and other non-GC interneurons are affected by serotonergic modulation acting via very complex physiological dynamics (Schmidt and Strowbridge, 2014; Brill et al., 2015). Serotonin directly excites ETCs and depolarizes some MCs (Brill et al., 2015). It was also shown to influence timing of bulbar output and thereby olfactory learning and exerts other modulatory effects like synchrony with respiration (McLean et al., 1993; Petzold et al., 2009; Liu et al., 2012; Schmidt and Strowbridge, 2014; Steinfeld et al., 2015).

Recently even dopaminergic projections from the substantia nigra to the OB have been discovered. The fibers terminate in the EPL, MCL and GCL and are reportedly important for proper odor discrimination (Hoglinger et al., 2015).

Inputs from the above mentioned neuromodulatory areas and from other brain regions additionally heavily innervate primary olfactory cortical areas, further extending the modulatory circuitry (Shipley and Ennis, 1996; Mori, 2014; de Almeida et al., 2015). These top-down inputs are also vital for adult neurogenesis and migration via the action of many different neurotransmitters (e.g. O’Keeffe et al., 2009; Hsieh and Puche, 2014).

The rudimentary circuit diagrams, often accompanying introductory sections of olfactory bulb publications are obviously extremely simplified for the most part. Of course this is inevitable due to space restrictions, but the generic display of an extremely reduced circuitry not specifically designed for the respective study subject is problematic. This factor and the incongruence of nomenclature for certain cell types (as obvious in e.g. Kosaka and Kosaka, 2011) is inconvenient for readers and can even lead to misconceptions in the scientific discussion. The cell type and neurotransmitter diversity of the bulb is astonishingly diverse and gets complemented by extrinsic projections, partially covered by this section. For a more detailed description of neurotransmitter diversity in the olfactory system cf. Ennis et al. (2007). At the end of the introduction, three schemata will introduce the main players of OB circuitry described in the introduction (Fig. I2), a limited circuitry that is usually shown in most OB literature (Fig. I3), and a circuitry focusing on centrifugal contacts (Fig. I4).

1.6. Dopaminergic cells in the olfactory bulb

Dopamine can influence bulbar circuitry via several populations of cells residing or terminating in the olfactory bulb – projection fibers from the substantia nigra, resident EPL interneurons and most prominently, morphologically diverse juxtglomerular cells (Kosaka and Kosaka, 2009; Pignatelli et al., 2009; Liberia et al., 2012; Hoglinger et al., 2015). Since there is only very sparse information about the EPL population and the central projection pathway, this section will be focused on the GL population. Two reported subtypes of those glomerular cells have been discriminated, as histochemically identified by the dopamine synthesizing enzyme tyrosine hydroxylase

(TH) (Kosaka and Kosaka, 2008; 2009; Kiyokage et al., 2010). The small subtype, contacting several glomeruli locally, is driven mostly indirectly (feed-forward) via ETCs, as shown by the occurrence of EPSC bursts, with only a smaller portion getting direct OSN input (70% vs. 30%, Kiyokage et al., 2010). The large subtype is exclusively ETC-driven (no direct OSN input) and shows large dendritic and axonal projections ranging several hundreds of micrometers laterally, contacting dozens of glomeruli (this study, Kosaka and Kosaka, 2009; Kiyokage et al., 2010). A clear axon with distinct sodium channel clusters has only been proposed for this large subtype (Kosaka and Kosaka, 2011). The manifold targets, as stated previously (ETCs, OSNs, PGCs, DAergic JGCs and centrifugal terminals), receive input mostly via D2-like receptor activity (Escanilla et al., 2009), although D1-like activity also plays a role, which could even produce a biphasic activation pattern in ETCs after fast GABAergic inhibition (Yue et al., 2004; Gutierrez-Mecinas et al., 2005; Liu et al., 2013). The cells' GABAergic and dopaminergic output is not yet resolved in detail, with at least some target cells getting both neurotransmitter inputs (Liu et al., 2013; Banerjee et al., 2015) albeit from different vesicles released on different time scales (Maher and Westbrook, 2008; Borisovska et al., 2013; Vaaga et al., 2014). DA release is likely to require stronger cell activation than GABA release (Maher and Westbrook, 2008; Bundschuh et al., 2012; Borisovska et al., 2013; Brill et al., 2015). Although studies about the abundance of DAergic JGNs have been made (Parrish-Aungst et al., 2007), those numbers may be underestimated since TH detection levels fluctuate with neuronal activity and maturation state (Baker, 1990; Kovalchuk et al., 2015). Additionally, the dopaminergic cell population shows changing proportions of the total bulbar neuron number throughout life (Ninkovic et al., 2007; Adam and Mizrahi, 2011). The lateral connectivity of these cells has strong implications in general bulbar information representation and computation (Banerjee et al., 2015; and discussed in more detail in 4.2.3. and 4.2.4.). Functionally, GL dopaminergic cells seem to be involved in output patterning pacemaker activity and oscillatory coupling, although this role could still be due to the close electrical and synaptic conjunction with ETCs (Pignatelli et al., 2005; Liu et al., 2013; Banerjee et al., 2015). Several studies attribute a strong gain control of bulbar output to these cells by influencing projection cells substantially (Bundschuh et al., 2012; Banerjee et al., 2015). Dopaminergic cell activation is regulated by very intricate excitability mechanisms, which have intrinsic components like a hyperpolarization activated current (I_h) (Puopolo et al., 2005; Pignatelli et al., 2013), but are also modulated by

various extrinsic (many of them centrifugal) influences – acetylcholine (ACh), noradrenaline (NA), serotonin (5-HT), histamine, or DA, to name a few (Pignatelli and Belluzzi, 2008; Borin et al., 2014; and cf. 1.5.). A recent study indicates, that bulbar corticotropin releasing hormone (CRH) could additionally influence dopaminergic JGCs (Garcia et al., 2014a).

1.7. Granule cell physiology

GCs are the reportedly most abundant cell type of the bulb, involved in many aspects of bulbar processing. Focused research involving the work of many groups revealed the important role of this axonless interneuron. Those findings include the special reciprocal synapse with projecting cells, connecting glomerular modular columns laterally, the importance of independent subcompartment signaling, and the general impact on odor processing (Shepherd et al., 2007). In this part, functionality and physiology of granule cell reciprocal signaling are introduced, including details about channel composition and working modes of the reciprocal gemmule.

1.7.1. The reciprocal granule cell – mitral cell dendrodendritic synapse

The MC-GC reciprocal synapse is the most numerous connection within the olfactory bulb with an estimated total number of 500×10^6 (Egger and Urban, 2006). Functionally it may serve many different functions such as generating or sustaining bulbar oscillations (Lagier et al., 2007), influencing projection cell output locally in a glomerular unit or laterally, leading to gain control, stimulus decorrelation and contrast enhancement (Lowe, 2002; Arevian et al., 2008; Abraham et al., 2010). Eventually, higher processing centers read out the spatial and temporal codes from projecting cells (Bathellier et al., 2008; Blauvelt et al., 2013; Haddad et al., 2013), which have been sculpted strongly by GL and EPL and especially GC reciprocal connections.

GCs sharpen odor representations and thereby discriminability and identity by limiting the lateral spread of information in the EPL (Isaacson and Strowbridge, 1998). The boundaries of a glomerular unit of information processing in layers deeper than the GL are subject to debate, but there is evidence for a vertical columnar architecture (Willhite et al., 2006; Kim et al., 2011). Different modes of transmission from the GC as already

proposed in the 60s (Rall and Shepherd, 1968) support a functional variability of the reciprocal synapse in the OB. Most of the signaling operates in subthreshold regimes, which is already sufficient to sustain oscillatory activity in the bulb (Bathellier et al., 2006). Subthreshold modes include the purely local activation of single spines that only reciprocally inhibit the stimulating mitral cell (Egger et al., 2005), or regional or global dendritic calcium and sodium spikes that can already spread inhibition laterally (Egger et al., 2005; Pinato and Midtgaard, 2005; Zelles et al., 2006). In contrast to those, global sodium channel dependent AP generation can lead to strong global signals within the whole cell (Egger et al., 2003; Egger, 2008). All the signals underlie differential channel activation on the spine or the whole cell, most of which strongly influence local and global calcium levels in the cell, the main determinant for neurotransmitter release. Release of the GC can therefore differ spatially and it involves slow and fast components (Egger, 2008), which will be explained in more detail below.

1.7.2. Granule cell plasticity

Calcium elevations and kinetics that are highly complex in granule cells (Egger and Stroh, 2009), do not only influence release but moreover shape synaptic plasticity. The interplay of GCs with MCs is subject to different forms of plasticity, including classical forms of synaptic plasticity (e.g. short-term plasticity) at the reciprocal connection (Dietz and Murthy, 2005; and unpublished results from V. Egger) or from cortical inputs (Balu et al., 2007; Gao and Strowbridge, 2009; Kato et al., 2012). Even epigenetic mechanisms like histone acetylation can facilitate aversive olfactory learning and synaptic plasticity (Wang et al., 2013). Other forms of network plasticity include the turnover of interneurons like GCs (among other cell types) in the OB, due to regionally changing cell numbers, but also by new cells exhibiting synaptic properties dissimilar to resident cells (Mouret et al., 2009; Nissant et al., 2009; Lepousez et al., 2014). Despite the continuous turnover and in contrast to dopaminergic new-born cells, the number of granule cells in the OB is relatively stable throughout a rodent's life (Ninkovic et al., 2007).

1.7.3. Spines

After being discovered by Ramon y Cajal (y Cajal, 1888), Gray resolved the synaptic connections of terminal structures onto dendritic spines (Gray, 1959). The receptive part of almost all glutamatergic synapses on dendrites of excitatory neurons, and even on some inhibitory cells are formed by spine protrusions (Chen and Sabatini, 2012; Scheuss and Bonhoeffer, 2014). Thereby a spine can be generalized as the morphological correlate of a postsynapse (Chen and Sabatini, 2012). These structures have been traditionally classified as thin (bulbar head, fine neck), mushroom shaped (broader head) and stubby (without neck). Other classical nomenclature alternatively described them as sessile or pedunculated (comparable to stubby and mushroom/thin spines, respectively) (Jones and Powell, 1969; Peters and Kaiserman-Abramof, 1970). Yet they come in many further different forms and shapes throughout the nervous system (Sorra and Harris, 2000; Ballesteros-Yanez et al., 2006). In OB granule cells, some spines display a very special appearance and arrangement with GABAergic presynaptic and manifold postsynaptic specializations intertwined (Price and Powell, 1970d; c; section 1.5.5.). A role for biochemical compartmentalization of spine structures has been widely accepted, influencing learning and plasticity mechanisms (Matsuzaki et al., 2004; Scheuss et al., 2006; Harvey and Svoboda, 2007; Scheuss and Bonhoeffer, 2014). An electrical function, however, with the spine neck and surface area of the spine as the limiting factor of electrical connectivity or isolation, and thus input impedance, are still widely debated (Svoboda et al., 1996; Araya et al., 2006; Grunditz et al., 2008; Tonnesen et al., 2014; Popovic et al., 2015). Spine channels are known to display regular channel turnover, which is an important mechanism for functionality and plasticity (Kim and Ziff, 2014). Beyond that, dendritic spines themselves (including the ones on GCs) show regular turnover with many influences like input activity patterns stabilizing or destabilizing the structure (Engert and Bonhoeffer, 1999; Kopel et al., 2012; Livneh and Mizrahi, 2012; Meyer et al., 2014; Huang et al., 2015).

1.7.4. Gemmule structure

In terms of its dimensions, the granule cell reciprocal spine differs massively from spines of other cell types. In comparison to conventional spines like on Cornu Ammonis

region 1 (CA1) pyramidal neurons in the hippocampus (Harris and Stevens, 1989), it has a 10-fold bigger spine head volume and an 3.8 times longer neck while only being 1.5 times thicker (Woolf et al., 1991). Interestingly, reciprocal spines contacting MCs in their perisomatic region seem to be likewise specifically enlarged (Naritsuka et al., 2009). The gemmule is usually filled with organelles and membranes including ribosomes or endoplasmic reticulum spanning throughout the head and neck. Particularly mitochondria are found in more than 70% of spine heads and they mostly further extend into the neck (Woolf et al., 1991). Most gemmules receive centrifugal synaptic connections from the horizontal limb of the BF and AON (Price and Powell, 1970b). Additionally, centrifugal structures from the olfactory cortex (Laaris et al., 2007) and neuromodulatory brain areas (i.e. Nunez-Parra et al., 2013 and cf. 1.5.) target GCs, sometimes specifically the spine structures. Even several MOB resident neurons other than the projecting cells synapse with GCs. Certain GABAergic dSACs terminate on GC gemmules directly, adjacent to the reciprocal synapse (Eyre et al., 2008). With the special morphology of GC gemmules (long necks, big heads, sparsely arranged on the dendrite), the potential role of a spine as a discrete chemical and electrical subcompartment (Bloodgood and Sabatini, 2005) becomes easily accessible for experimental investigation.

1.7.5. Receptor repertoire and physiology of the reciprocal arrangement

The major input to the GC reciprocal synapse is via the sensory pathway and the activation of MCs. Upon sufficient depolarization, MC lateral dendrites faithfully transmit electrical impulses over large distances including active mechanisms (Bischofberger and Jonas, 1997; Debarbieux et al., 2003). The MC presynapse of the reciprocal synapse is located on smooth dendrites, without light-microscopically accessible obvious specializations. At those locations, high threshold calcium channels are tightly coupled to glutamate release (Isaacson and Strowbridge, 1998), as well as glutamatergic autoreceptors, mainly NMDA receptors (Isaacson, 1999; Salin et al., 2001). Certainly, NMDA and AMPA glutamate receptors are the main source of synaptic activation at the GC spine and play important roles for neurotransmitter release (Schoppa et al., 1998; Chen et al., 2000). Metabotropic glutamatergic mechanisms were found to play a role at the MC side of the dendrodendritic synapse (Trombley and Westbrook, 1992), but are certainly a major influence at the apical

dendrite and, very importantly, also at the GC postsynapse (with the highest reported mGluR5 levels in the brain), where they cause direct and indirect excitation (Romano et al., 1995; Heinbockel et al., 2007; Dong et al., 2009). Dopamine mediated inhibition of high-voltage activated channels is another way to modulate glutamate release from MCs (Davila et al., 2003). Furthermore, MCs and GCs bear corticotropin releasing factor receptors, which act via many signaling pathways, including coupling to different G proteins and kinase pathways (Chen et al., 2005). It is possible that they do not affect the cells directly at the reciprocal MC-GC synapse but the releasing cells definitely have a strong impact on MC signaling (Huang et al., 2013 – and cf. 1.4.3.2.). Serotonin receptors are expressed in GCL, MCL and EPL (Pompeiano et al., 1992; 1994; Clemett et al., 2000). Whereas the transmitter might only play a minor direct role on GCs, it does affect MCs, mainly via 5-HT₂ actions (Schmidt and Strowbridge, 2014). Noradrenaline increases or decreases GABAergic inhibition of MCs via α ₁ and α ₂ activity, respectively, also acting on calcium currents in both cells (Trombley and Shepherd, 1992; Nai et al., 2009; Nai et al., 2010). GCs as well as MCs are targets of forebrain cholinergic modulation, in part directly on the gemmule (Price and Powell, 1970a). Muscarinic action seems to directly increase GC excitability, having an impact on slow signaling components (Pressler et al., 2007), although other studies found mainly inhibitory effects (Castillo et al., 1999). Moreover, its influence involves calcium release from internal stores in granule cells (Ghatpande et al., 2006) and is reported to enhance glutamate release at the dendrodendritic synapse also via other mechanisms (Ghatpande and Gelperin, 2009). There is recent contrasting *in vivo* data suggesting suppression (Ma and Luo, 2012) of spontaneous activity or mainly excitatory influence (Rothermel et al., 2014) of projecting cells by cholinergic input, which may be due to an interplay of several components of multi-layered OB inputs of these fibers. For adult-born GCs, nicotinic receptors play an important role for regulating survival and integration (Mechawar et al., 2004). Further cortical input targets GCs, although not specifically the reciprocal connection (Price and Powell, 1970a), as reviewed previously (1.5.). GABA acts on GCs both via autoreceptive pathways, as well as via targeted GABAergic terminals. The MC reciprocal synapse release site is targeted by GABA_A receptors, which is ultrastructurally outside of the postsynaptic GABAergic specialization (where the receptor is also found) and may strongly affect glutamate release (Panzanelli et al., 2004). It is known that GABA_A receptors are expressed on the GC (Nusser et al., 1999; Panzanelli et al., 2004). These

receptors on GCs (expressing the $\beta 3$ -subunit) seem to be rather clustered at the soma and dendrite stems of GCs and are not abundant on reciprocal spines (Nunes and Kuner, 2015). Conditional $\beta 3$ knockouts in GCs show less GC inhibition and therefore, the output from the bulb is changed, which even had an impact on behavior resulting in accelerated odor discrimination (Nunes and Kuner, 2015). GABA_B receptors seem to be located at GC gemmules, controlling transmitter release, probably by inhibiting HVACCs (Isaacson and Vitten, 2003). They were shown to only weakly inhibit glutamate release from mitral cell dendrites of the reciprocal synapse, but play a strong role on those cells during transmission of odor information from the OSNs (Nickell et al., 1994). GABAergic processes targeting GCs arise from the cortex and from bulbar-intrinsic inhibitory fibers of INs like Blanes cells or dSACs, which sometimes even specifically terminate on the gemmule (Eyre et al., 2008; Arenkiel et al., 2011; Nunez-Parra et al., 2013, Nunes and Kuner, 2015). Glycine also impacts GC and MC physiology in the bulb in an inhibitory fashion via glycine and GABA receptors (Trombley and Shepherd, 1994; Trombley et al., 1999). Glycine $\alpha 3$ and β receptor subunits have been reported in deeper layers with β receptors on MCs and both receptors are found in the internal granular layer. Likewise, the EPL shows strong glycine receptor immunoreactivity (van den Pol and Gorcs, 1988). Glycinergic fibers targeting the bulb might arise in the forebrain (Zeilhofer et al., 2005). To illustrate the influences of aforementioned main players of the reciprocal MC-GC arrangement, they are comprehensively summarized in a schema later on (Fig. I1).

Synaptic activation of GCs via MCs has a fast initial component and a slow component called long lasting depolarization, indicating the involvement of many different conductances. Several calcium channels play a role in GC spine physiology, especially affecting its release. The kinetics of the calcium signal after activation via mitral cells is consequently also remarkably slow and asynchronous (Isaacson and Strowbridge, 1998) and in sub-AP regimes remains strictly localized to the activated spine (Egger et al., 2003). The slow kinetics are in part due to intrinsic mechanisms like transient A-type potassium currents (Schoppa and Westbrook, 1999; Kapoor and Urban, 2006) and slow calcium extrusion (Egger and Stroh, 2009). Outside of the spine, big conductance potassium channels (BK) are involved in the physiology of GCs (Isaacson and Murphy, 2001) and can influence the cell's activation and resting dynamics. There are other slow dynamics triggered by synaptic sodium spikes that play crucial roles. An unspecific cation current (I_{CAN}) is induced in the granule cell NMDA receptor

dependently, further prolonging and increasing depolarization and calcium influx. Activation of T-type calcium channels is also implied in the asynchronous release from the spine (Egger, 2008). The nature of I_{CAN} was recently investigated and seems to be a combination of the activation of TRPC1 and TRPC4 channels (Stroh et al., 2012). Fast components of GC signaling involve glutamatergic activation via AMPA (not calcium permeable) and NMDA channels and the activation of different voltage dependent calcium channels, including HVACCs (Isaacson, 2001; Egger et al., 2005) possibly activated by voltage dependent sodium channels. Input patterns from mitral cells or from extrinsic centrifugal sources, as well as network dynamics including inhibitory elements further strongly shape the kinetics of the voltage and calcium signal in the postsynaptic granule cell (Schoppa, 2006; Arevian et al., 2008; Burton and Urban, 2015).

1.7.6. Activation modes of granule cell gemmules

Inferring from the last section, it should have become obvious that GC gemmules show a broad repertoire of receptors and channels. Several of those, as already mentioned, are differentially activated by variable modes of activation of the cell. For instance, local synaptic activation of GCs via MCs activates AMPA and NMDA receptors, as well as T-type and probably HVACCs and calcium-induced calcium release (Egger et al., 2005), involving fast and slow components. The calcium signal of this activation is strictly localized to the spine and the electrical activation at the soma is very small. Synaptic activation can also trigger low-threshold spikes, sodium or calcium spikes. Those events are certainly not confined to the activation site, but spread regionally or globally and involve additional T-type calcium channels (Egger et al., 2005; Pinato and Midtgaard, 2005), although in the frog *rana pipiens*, spontaneous active electrical events in GCs were independent of T-type channel involvement (Zelles et al., 2006). Evidently, most GC signaling modes conduct activity and release in subthreshold regimes without AP induced mechanisms. This is supported by the fact that GCs rarely spike *in vivo* (Cang and Isaacson, 2003; Margrie and Schaefer, 2003). In turn, MCs might be able to release glutamate in the subthreshold regime as well (tested in the accessory olfactory bulb in Castro and Urban, 2009). Thereby, both sides of the dendrodendritic synapse can signal in very energy-efficient subthreshold regimes. During synaptically evoked APs, global and prolonged calcium signals are evident

throughout the whole cell, which include T-type channels, HVACCs and TRPC channels (Egger et al., 2003; Egger, 2008; Stroh et al., 2012). For these global signaling modes, for instance, additional NMDA channel activation only plays a role at spines that were activated by the glutamatergic input. Thus, even in global events the signals can be inhomogeneous and involve different components. The effective spread of sub- and suprathreshold signals over large distances speaks for compact, active dendrites in GCs, also involving voltage gated sodium channels (Navs) (Chen et al., 2000; Egger et al., 2003; Thomas Kuner – personal communication). Conclusively, this signaling versatility, harnessing specific subsets of conductances in different stimulation modes, can explain the fast and asynchronous long-lasting components of GC activation and GABA release from spines to a large extent.

1.8. Oscillatory activity in the olfactory bulb

Dendrodendritic activity seems to be strongly involved in generating oscillatory activity in olfactory processing across different phyla with analogous systems, which underlines its importance (Kay, 2015). Both interneurons in the focus of this thesis are strongly involved in the generating, maintaining and shaping bulbar oscillatory activity, by strong chemical and electrical connections to another and to projection cells (Fukunaga et al., 2014). The EPL reciprocal synapse is mostly involved in the gamma frequency oscillations of the bulb and a gamma pattern temporal input facilitates output from the GC (Halabisky and Strowbridge, 2003; Lagier et al., 2007). Those fast paced oscillations are not only mediated by chemical synapses but also by gap junction connections (Friedman and Strowbridge, 2003), formed between GCs and projecting cells in the EPL as well as between the perikarya of clustered GCs (Reyher et al., 1991). Oscillations in different frequency bands allow for the temporal coordination of PNs (Poo and Isaacson, 2009), and can be behaviorally linked to olfactory fine discrimination (Beshel et al., 2007; Abraham et al., 2010; Schaefer and Margrie, 2012; Lepousez and Lledo, 2013) and learning mechanisms (Martin et al., 2007; Kay and Beshel, 2010; Martin and Ravel, 2014). This oscillatory activity is strongly affected by odor quality (Gelperin and Tank, 1990), respiratory activity (Verhagen et al., 2007; Wachowiak, 2011; Rojas-Libano et al., 2014) and behavioral state (Kay, 2003; Manabe and Mori, 2013) and modulated or even imposed by cortical feedback (Hall and Delaney, 2001; Kay, 2003; Balu et al., 2007; Boyd et al., 2012; Nunez-Parra et al.,

2013; Rothermel and Wachowiak, 2014). For instance, beta-band oscillations are strongly dependent on the intact bidirectional connectivity of OB and PC whereas gamma oscillations can be sustained by local networks (Martin et al., 2006). OB layers other than the EPL, especially the GL with its synchronized input and dendrodendritic arrangements (Schoppa and Westbrook, 2001; De Saint Jan et al., 2009; Fukunaga et al., 2012; Fukunaga et al., 2014) influence rhythmic activity in the bulb. Theta oscillations couple strongly to respiration and arise mainly from glomerular circuits and support rhythmic projection neuron discharge and pacemaker activity (Hayar et al., 2004a; Hayar et al., 2004b; Verhagen et al., 2007; Fourcaud-Trocme et al., 2014). Those slow oscillations are probably also mediated via neuron-glia gap-junctional interactions (Roux et al., 2015). Beta rhythms, coupled to piriform and entorhinal cortex and hippocampal rhythmicity in waking animals are implicated in associative learning (Vanderwolf and Zibrowski, 2001; Lowry and Kay, 2007; Martin et al., 2007). Many further bulbar cell types, mostly connected to centrifugal input (cf. 1.5.) or reciprocally connected within the bulb additionally shape oscillatory rhythms in the olfactory bulb (Eyre et al., 2008; Lepousez et al., 2010; Kato et al., 2013). Naturally, all these different oscillatory mechanisms and networks feed into another and influence each other, which leads to complex working states of bulbar output, depending on the imposition of competing or interacting oscillation regimes (David et al., 2015).

1.9. Adult neurogenesis in the olfactory bulb

Until the second half of the 20th century it was commonly believed that neurogenesis occurred exclusively during embryonic development and was arrested at birth (Colucci-D'Amato et al., 2006). This conviction, strongly fortified by leading neuroscientists like Cajal or Golgi in the early 20th century, has only started to crumble by the early 1960s when Joseph Altman and collaborators found evidence for neurogenesis in the hippocampus of rats (Altman, 1962). By the end of the 1970s, Kaplan and Hinds found neuronal adult generated cells in the rat olfactory bulb and hippocampus (Kaplan and Hinds, 1977). Nowadays, it is known that adult neurogenesis is vital for normal olfactory function and plastic, experience-dependent adjustments and rejuvenates bulbar circuitry that is subject to strong neuronal turnover (Lepousez et al., 2013). Stemming from a neurogenic niche called subventricular zone (SVZ), located between the striatum and the lateral ventricle, pluripotent precursor cells travel tangentially through

the rostral migratory stream (RMS) towards the anterior brain and into the OB, before radially migrating into the respective destination layers (Whitman and Greer, 2009). Initially, the neural stem cells have astrocyte-like characteristics and can retain their pluripotent potential regardless of the age of the animal, yet individual stem cells deplete over time (Kriegstein and Alvarez-Buylla, 2009; Barbosa et al., 2015). Upon transplantation, depending on their surrounding environment, they can form glial cell populations with astrocytic or oligodendritic characteristics (Seidenfaden et al., 2006) or assume neuronal phenotypes (Brill et al., 2008; Milosevic et al., 2008). Direct conversion of a glial precursor to a neuronal cell without any cell division is possible and may even be the predominant way to generate neurons (Barbosa et al., 2015). Stem cells in different areas of the SVZ give rise to different types of olfactory interneurons (Merkle et al., 2007). The spatial origin of a cell therefore predetermines the cell fate. The vast majority of newborn cells differentiates into GCs (Lledo and Saghatelian, 2005), smaller portions into different subtypes of JGCs (Bagley et al., 2007; Whitman and Greer, 2007a; Batista-Brito et al., 2008; Brill et al., 2008; Brill et al., 2009). Although thousands of progenitor cells arrive at the olfactory bulb every day, only a small portion gets integrated into existing circuitry. Half of the cells that mature successfully survive for longer than a month (Lledo et al., 2006). The elimination of GCs is not continuous or diffuse but occurs during a specifically timed window in the postprandial period, typically during sleep states, involving top-down inputs from the olfactory cortex (Yokoyama et al., 2011; Komano-Inoue et al., 2014).

Already on the way to full integration, considerable differentiation and plastic changes take place which may be one of the reasons for the rapid onset of functionality upon arrival at the site of their integration (Mizrahi, 2007; Nissant et al., 2009; Kovalchuk et al., 2015). The newly arriving cells do not only replace resident cells but the continuous turnover changes the population dynamics and weights, favoring a larger relative and absolute fraction of dopaminergic cells in older animals in the GL while e.g. the GC population remains stable (Ninkovic et al., 2007; Adam and Mizrahi, 2011). Adult-born GCs seem to integrate in different circuits than neonate GCs and retain distinct properties (Magavi et al., 2005; Lledo et al., 2008). There are several stages of GC maturation corresponding to morphological and (electro-)physiological properties (Petreanu and Alvarez-Buylla, 2002; Belluzzi et al., 2003; Carleton et al., 2003). A similar classification has, in part, been used to characterize JGCs as well (Mizrahi, 2007). In general, survival and integration of the newly arriving cell is extremely

complex and regulated by many factors. Sensory input (Yamaguchi and Mori, 2005; Bastien-Dionne et al., 2010; Sawada et al., 2011), bulbar-specific neurotransmitter or neurotrophic factor input (Garcia et al., 2014b; McDole et al., 2015), behavioral state (Yokoyama et al., 2011; Kopel et al., 2012), centrifugal input (Mechawar et al., 2004; Veyrac et al., 2005; Whitman and Greer, 2007b; Hsieh and Puche, 2014) in specific temporal domains (Mouret et al., 2008) play a role, interacting with specific transcriptional pathways (Ninkovic et al., 2010; Fuentealba et al., 2012; Ninkovic and Gotz, 2013). The olfactory epithelium also has a neurogenic niche, supplying the sensory area with new receptor cells throughout life. Sensory neurons regenerate regularly from basal cells in deep layers of the olfactory epithelium (Galizia and Lledo, 2013).

OB adult interneuron turnover and neurogenesis has a strong impact on existing computations and represents another avenue for plasticity in certain brain areas, which can complement classical molecular and cellular mechanisms. The function of adult neurogenesis was shown to include stimulus decorrelation (Chow et al., 2012), learning and memory (Moreno et al., 2009; Alonso et al., 2012), and to plastically adjust the system to changing demands (Bonzano et al., 2014; Livneh et al., 2014). This plasticity also applies for restoring functionality after acute neuron loss (Cummings et al., 2014; Lazarini et al., 2014). Some studies already show the potential of these cells to replace degenerated cells in other brain areas making them an attractive research target from a clinical perspective (Cave et al., 2014). Whether there is a replacement of OB interneurons via a functional RMS in adult humans is still highly debated, whereas the existence of functional SVZ neuroblasts is agreed upon (Sanai et al., 2004; Sanai et al., 2007; Wang et al., 2011; Alizadeh et al., 2015). Integration of adult generated neurons into early olfactory processing appears to be a wide spread phenomenon, encompassing insect and crustacean species, underlining its general importance (Cayre et al., 2007; Sullivan et al., 2007).

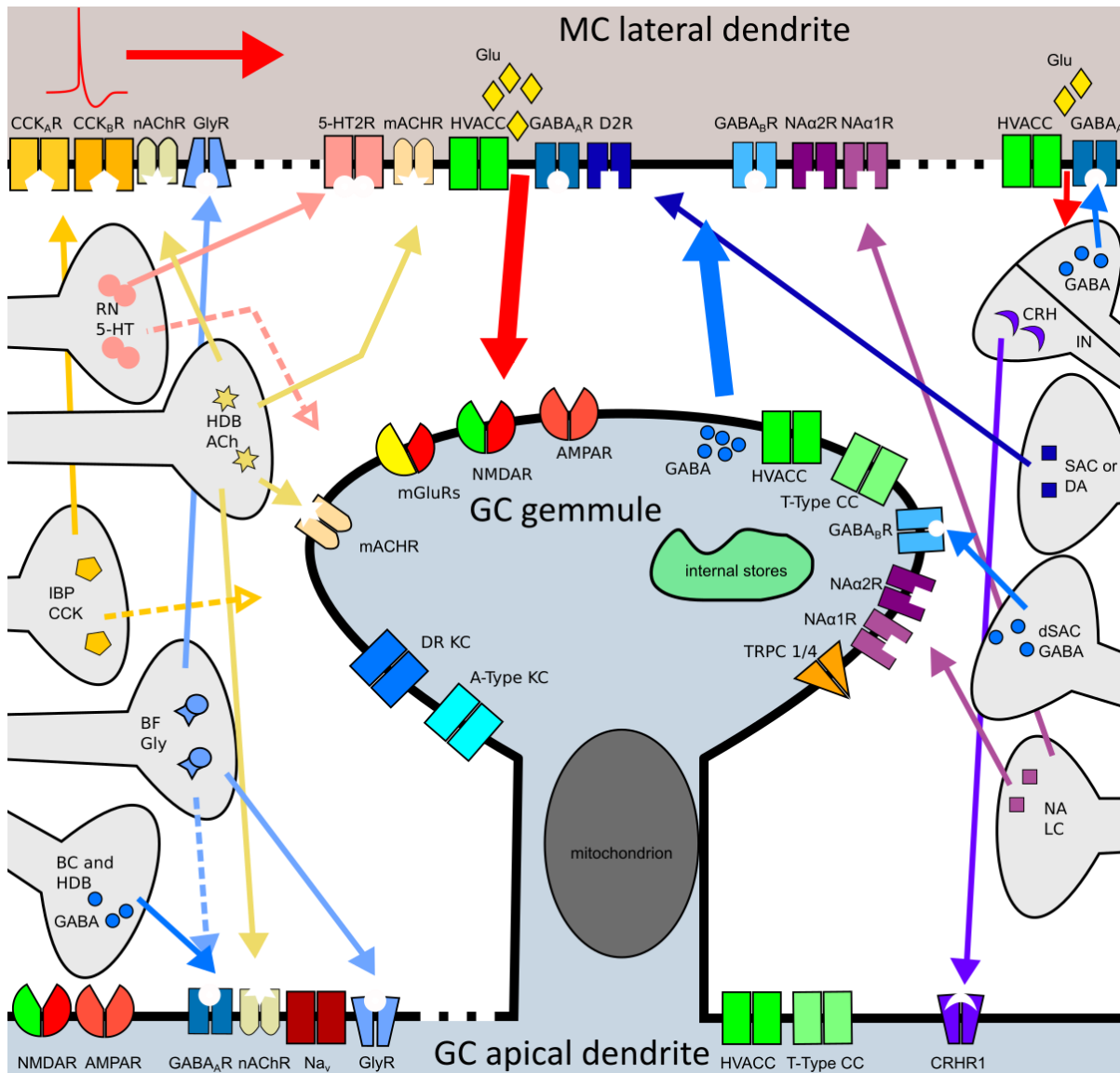


Fig 11: Mitral cell – granule cell reciprocal synapse interactions

The exact subcellular localization of channels on the gemmule spine head or the adjacent dendrite has not been demonstrated for all of the channels, although some have been specifically located at the spine head or dendrite respectively (see referred literature in 1.7.5.). Wherever the localization is known, it has been established in the schema. Certainly, not all channels involved in the overall physiology of the granule cell are mentioned and displayed, only the ones implicated to have a strong specific impact on the reciprocal synapse or the ones which are located directly on the spine head. The same applies for the channels indicated here on the mitral cell side. No channels involved in somatic signaling or the specific repertoire of the apical mitral cell dendrite are included in this depiction.

The abbreviations used here are not necessarily commonly used in the literature or the rest of the manuscript. “R” generally stands for receptor, an additional number or (subscript) capital or Greek letter indicates the specific subtype and will not be mentioned in these explanations. Nomenclature abbreviations for receptors will not be repeated for the respective neurotransmitter again or vice versa. ‘CCK’: Cholecystikinin, ‘n’ or ‘m’ ‘AChR’: nicotinic or muscarinic acetylcholine receptor, ‘GlyR’: glycine receptor, ‘5-HT’: serotonin, ‘Glu’: glutamate, ‘GABA’: gamma-aminobutyric acid, ‘D’ or ‘DA’: dopamine, ‘NA’: noradrenaline, ‘mGluRs’: metabotropic glutamate receptors, ‘NMDAR’: N-Methyl-D –aspartic acid receptor, ‘AMPA’: α -amino-3-hydroxy-5-methyl-4-isoxazolepropionic acid receptor, ‘HVACC’: high voltage activated calcium channel, ‘CC’ calcium channel, ‘DR KC’: delayed rectifier potassium channel, ‘KC’: potassium channel, ‘TRPC’: transient receptor potential channel, ‘Na_v’: voltage gated sodium channel, ‘RN’: raphe nuclei, ‘HDB’: horizontal limb of the diagonal band of Broca, ‘IBP’: intrabulbar projection, ‘BF’: basal forebrain, ‘BC’: Blanes cell, ‘CRH’: corticotropin releasing hormone, ‘IN’ interneuron, ‘SAC’: short-axon cell, ‘SN’: substantia nigra, ‘dSAC’: deep short-axon cell, ‘LC’: locus ceruleus.

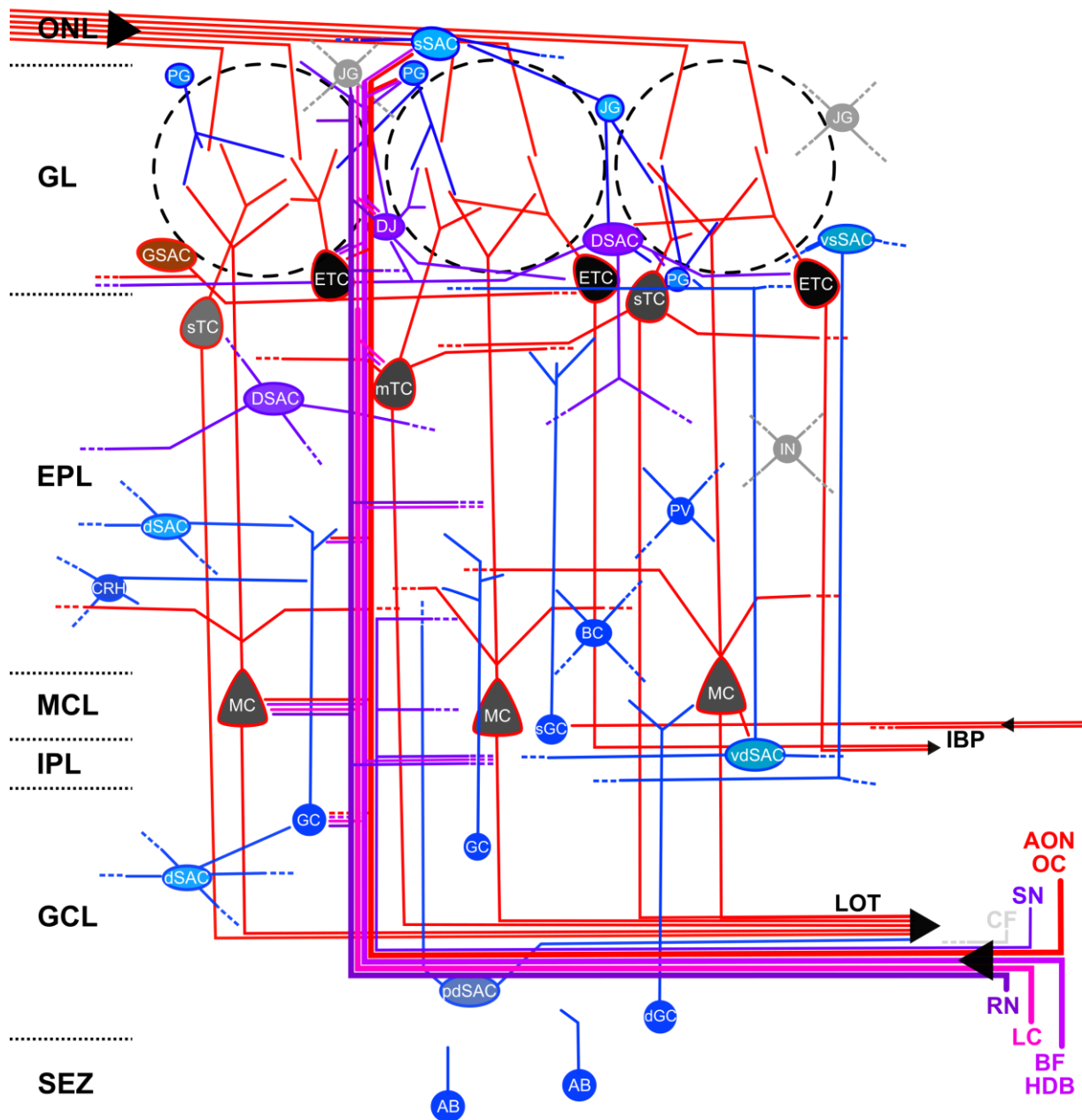


Fig. 12: Extensive schematic circuitry of the olfactory bulb

Blue lines indicate mostly inhibitory processes, red lines primarily excitatory ones. Magenta/purple colors indicate modulatory influence, which can be inhibitory or excitatory, depending on the transmitter and the respective receptors. Similar cells are indicated with similar cell body colors. The discriminated layers include olfactory nerve layer (ONL), glomerular layer (GL), external plexiform layer (EPL), mitral cell layer (MCL), internal plexiform layer (IPL), granule cell layer (GCL), subependymal zone (SEZ). IBP stands for intrabulbar projection from the other side of the ipsilateral bulb. LOT stands for the lateral olfactory tract. Centrifugal input is divided in fibers from the anterior olfactory nucleus (AON), olfactory cortex (OC), substantia nigra (SN), raphe nuclei (RN), locus ceruleus (LC), basal forebrain (BF), horizontal limb of the diagonal band of Broca (HDB), or unspecified further centrifugal fibers (CF). The following cell types are discriminated (top left to bottom right): periglomerular cell (PG), unspecified juxtglomerular cell (JG), superficial short-axon cell (sSAC), glutamatergic SAC (GSAC), superficial tufted cell (sTC), external TC (ETC), local dopaminergic JGC (DJ), dopaminergic SAC (DSAC), vertical column superficial SAC (vsSAC), medial TC (mTC), unspecified deep SAC (dSAC), parvalbumin positive interneuron (PV), unspecified interneuron (IN), corticotropin-releasing hormone positive cell (CRH), Blanes cell (BC), mitral cell (MC), superficial granule cell (sGC), vertical column deep SAC (vdSAC), granule cell (GC), projecting deep SAC (pdSAC), deep GC (dGC), adult-born neural progenitor cell (AB). Abbreviations used here are not necessarily common in literature.

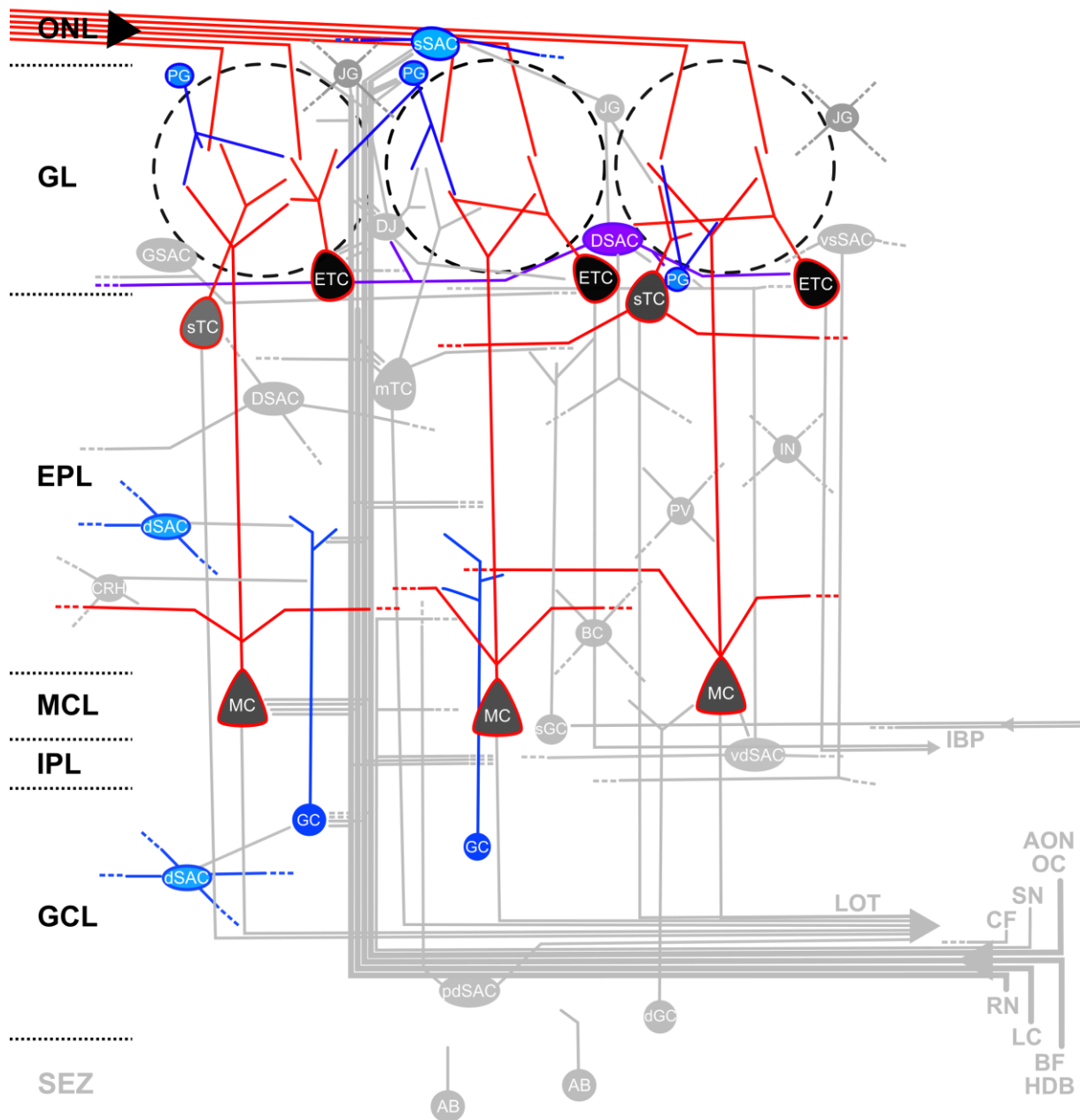


Fig. 13: Reduced circuitry diagram of the olfactory bulb

Colors and abbreviations as in the previous diagram. In most of the classical and even current literature (research papers as well as reviews) on bulbar processing a simplified wiring diagram, often similar to this one, or an even more reduced one (excluding the grey, faded structures) is depicted. In only very few instances this should be appropriate. Even if a certain study focusses their interest on a specific part of the circuitry, many elements central to the focused part are usually left out.

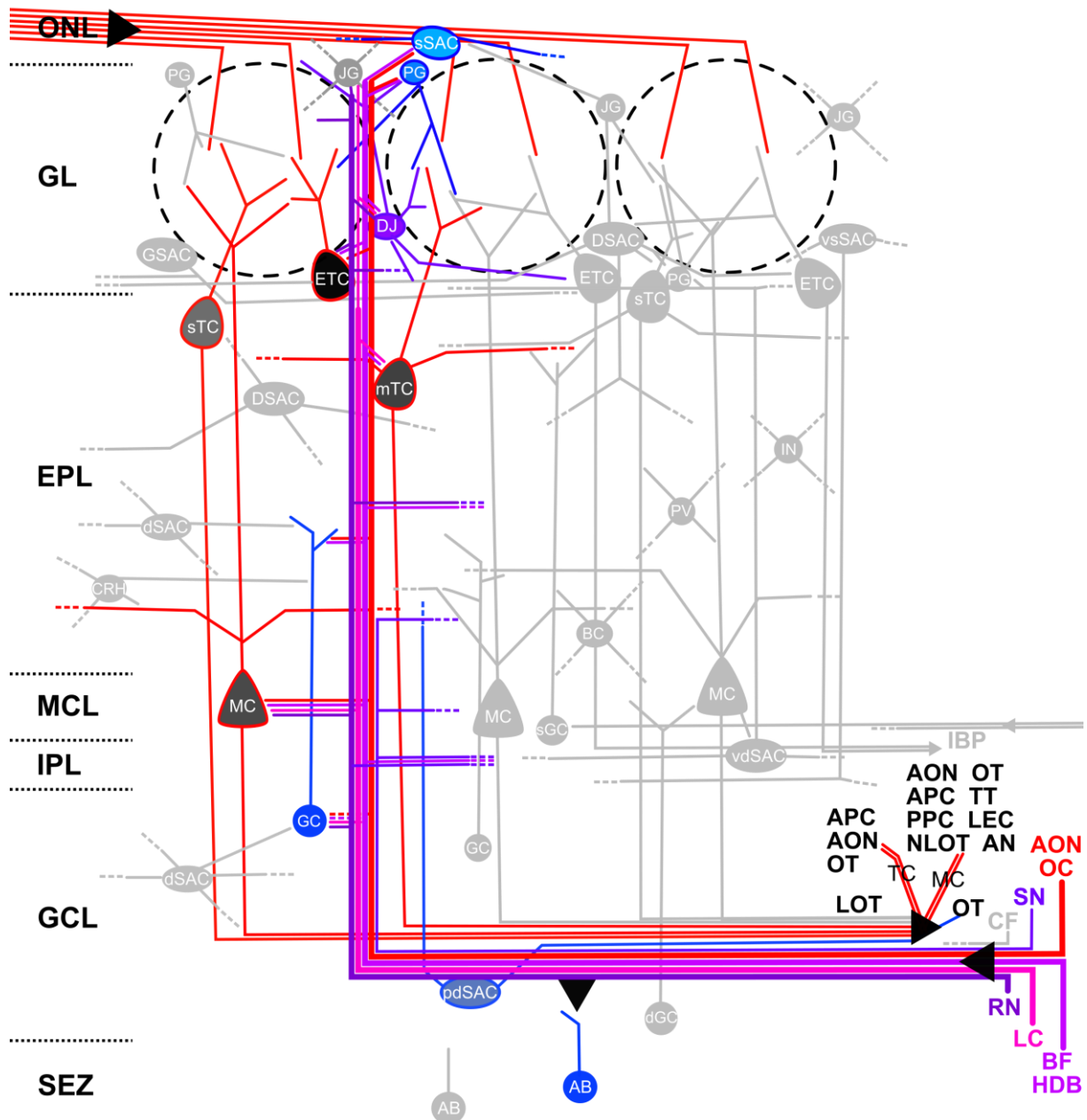


Fig. 14: Schematic circuitry of the olfactory bulb focusing on the projections from the bulb to cortical areas and respective backprojections to the bulb

Colors and abbreviations as in previous diagrams. Faded grey structures should be ignored for the sake of clarity. The target extrabulbar structure abbreviations are as follows. Anterior piriform cortex (APC), anterior olfactory nucleus (AON), olfactory tubercle (OT), tenia tacta (TT), posterior piriform cortex (PPC), lateral entorhinal cortex (LEC), nucleus of the lateral olfactory tract (NLOT), amygdaloid nuclei (AN). Note the arrow of the backprojections towards the olfactory bulb adult-born cells. Several modulatory influences target progenitor cells throughout their migration (cf. sections on centrifugal input and neurogenesis). The sampled literature did not elaborate if these interactions are also mediated in the SEZ, which is why the arrow is rather unspecifically targeted. Some of the centrifugal terminations to bulbar cells are only discussed in the publications in terms of laminar innervation without cell type specificity due to experimental limitations or focus on other brain regions. Therefore the extent and variety of specific targets are certainly underrepresented.

2. Motivation / Aims of the thesis and experimental steps

The experiments of this thesis were focused on morphological and physiological aspects of interneurons in the rodent olfactory bulb. Serious transformations are imposed on the information stream that passes through the olfactory bulb towards higher brain centers. The two main lateral layers involved in bulbar signal processing are the glomerular layer and the external plexiform layer. The GL includes a population of DAergic and GABAergic cell types that can act on fast and slower modulatory timescales on local and long-range glomerular circuitry. DAergic cells in the GL are traditionally marked with TH, which, like any other dopaminergic marker, is prone to only label a subset of all dopaminergic cells due to e.g. protein fluctuations (Cave and Baker, 2009). Indications in the literature for the possibility of further dopaminergic cell types, like a monoglomerular cell (Kosaka and Kosaka, 2009), and the sparsity of physiological data on these cells were the motivation for the first study.

The EPL is contacted by granule cells via their apical dendrites, forming reciprocal synapses with mitral cell lateral dendrites. Complex activation and signaling modes are utilized in granule cells, which were experimentally tested over many decades by now (Egger et al., 2005; Shepherd et al., 2007). Still, this cell type and the reciprocal connection hold many unresolved questions, especially concerning synaptic activation and dendritic integration. In these cells with especially voluminous and long spines, the general debate over an electrical role of spines could also be addressed (Svoboda et al., 1996; Grunditz et al., 2008; Bloodgood et al., 2009). The reciprocal connection and its function upon localized monosynaptic input was central to the second study. Both projects included electrophysiology and especially imaging techniques, the field of expertise of Veronica Egger's lab.

2.1. Project 1: Subtype diversity of dopaminergic neurons within the rat and mouse olfactory bulb glomerular layer

The diversity of cell types with different neurochemical configuration in the OB is astonishing and regularly new cell types get added to the variety (Merkle et al., 2014; Nagayama et al., 2014). Adult neurogenesis in the olfactory bulb is a research hot-topic, not least due to its potential in the clinical sector to use neural stem cells as a

replacement for degenerated neuron populations (Cave et al., 2014). Progress in imaging technology and genetic tools allow for new venues of research adding a temporal dimension to the investigation of the highly plastic and changing circuitry. The availability of a transgenic mouse line (DAT::Cre^{ERT2}/CAG::GFP), which inducibly labels a different subset of dopamine transporter (DAT) positive neurons from previous studies with a putative high incidence of adult-born cells, was a valuable tool to get insight into specific changes of adult circuits (provided by Jovica Ninkovic's lab). The first project of this thesis aimed at (1) morphologically classifying dopaminergic cell types in the glomerular layer in juvenile rats and adult mice and (2) utilizing the dopaminergic fluorescent marker FFN102 for olfactory bulb acute brain slices for the wild-type experiments. This approach gave us the possibility to look for differences between species and changes with different ages of animals/cells and to detect dopaminergic cells not stained with TH markers. The DAergic JGC group was traditionally classified into two different subtypes, a local medium sized type and a large type (Kiyokage et al., 2010), although some reports already hinted at a larger diversity (Kosaka and Kosaka, 2009). The discovery of new cell types with the help of very detailed morphometry was accompanied by noticing differences in their innervation patterns with respect to the surrounding glomerular structures. (3) To get an empirical grasp on the subject of glomerulus innervation, a new analysis tool was drafted and utilized. The discovery of specific cell structures ('clasps') in one of the newly described subtypes of dopaminergic cells also invited for (4) physiological analysis of this cell type using calcium imaging. In those experiments, the goal was to investigate the calcium dynamics in the dendritic tree of the cells within subcellular compartments and with respect to the innervated neuropil volumes (intraglomerular versus extraglomerular). The interesting results fit well with other current literature and the manuscript is submitted to the Journal of Comparative Neurology.

2.2. Project 2: Local postsynaptic voltage-gated sodium channel activation in dendritic spines of olfactory bulb granule cells

Granule cell physiology has always been the main research focus of Veronica Egger's lab. Many pre- and mainly postsynaptic GC key players in the physiology of the reciprocal connection have been identified and tested throughout previous work. Central to those results was the discovery of several different modes of transmission capabilities of granule cells, depending on the activation mechanism and the

differential involvement of subsets of receptors and channels (e.g. Egger et al., 2005; Egger, 2008; Stroh et al., 2012). The chemical compartmentalization of the gemmule in terms of calcium elevation during synaptic stimulation was already evident from previous experiments (Egger et al., 2003; Egger et al., 2005). With the acquisition of new equipment, new aspects of the synaptic transmission between mitral cell and granule cell could be dissected in this project. (1) The first goal was to establish stable and repeatable stimulation and recording conditions during single spine two-photon glutamate uncaging in a whole-cell patched granule cell. After being able to repeatedly and physiologically activate single gemmules, (2) the involvement of receptors and channels during a fictive, short, physiological local transmission event was assessed with various pharmacological tools. Especially the role of local activation of high-voltage activated calcium channels was of great interest, since their role in this circuitry could not be tested directly using different stimulation conditions beforehand. Their involvement could be critical for connecting the local spine signal to the concept of the spine as an electrical compartment (e.g. Grunditz et al., 2008). Deriving a putative role of the spine in shaping electrical input properties from experimental results, (3) a collaboration with Andreas Herz's lab in Munich was formed. This led to the development of an elaborate computational model of synaptic gemmule excitation, which could replicate the measured data to complement the experimentally established mechanisms during local spine activation. The results of this project were published in *Neuron* in February 2015.

2.3. Contributions to non-thesis-related publications

MRZ-99030 – A novel modulator of A β aggregation: II – Reversal of A β oligomer-induced deficits in long-term potentiation (LTP) and cognitive performance in rats and mice – Rammes et al., 2015, published in *Neuropharmacology*.

Conducting calcium imaging measurements of somatically evoked single action potentials and action potential trains in hippocampal slice CA1 pyramidal neurons of mice. Comparative measurements during normal physiology and during pharmacological application of the MRZ-99030 aggregation modulator.

3. Manuscripts

3.1. Subtype diversity of dopaminergic neurons within the rat and mouse olfactory bulb glomerular layer

Contributions:

Wolfgang Bywalez (W.B.) and Veronica Egger (V.E.) designed experiments. W.B., V.E. and Michael Lukas (M.L.) interpreted data. W.B. and Tiffany Ona Jodar (T.O.J.) performed experiments. W.B., T.O.J. and V.R. analyzed data. W.B. and V.E. wrote the manuscript. W.B. prepared the figures. W.B., V.E. and M.L. critically revised the manuscript. Jovica Ninkovic (J.N.) provided transgenic animals.

Title: Subtype diversity of dopaminergic neurons within the rat and mouse olfactory bulb glomerular layer

Authors: Wolfgang Georg Bywalez^{1,2}, Tiffany Ona Jodar², Michael Lukas², Jovica Ninkovic^{4,5,6}, Veronica Egger^{1,2,3}

Affiliations

1. Systems Neurobiology, Department II of Biology, Ludwig-Maximilians-Universität München, Bavaria, 82152 Planegg-Martinsried, Germany

2. Neurophysiology, Institute of Zoology, Universität Regensburg, 93040 Regensburg, Bavaria, Germany

3. Regensburg Center of Neuroscience (RCN), Universität Regensburg, 93040 Regensburg, Bavaria, Germany

4. Institute for Stem Cell Research, Helmholtz Zentrum München, German Research Center for Environmental Health (GmbH), 85764 Neuherberg, Bavaria, Germany

5. Institute of Physiological Genomics, Ludwig-Maximilians-Universität München, Schillerstrasse 46, 80336 München, Bavaria, Germany

6. Cluster for Systems Neurology (SyNergy) and BioMedical Center (BMC), Ludwig-Maximilians-Universität München, Bavaria, 82152 Planegg-Martinsried, Germany

Abbreviated title: Diversity of olfactory bulb glomerular DAT+ neurons

Name of Associate Editor: Thomas E. Finger

Key words: juxtglomerular cells, subcellular compartments, glomerular innervation analysis, calcium imaging, dendrites, two-photon imaging, morphological reconstruction

Corresponding author: Wolfgang G. Bywalez, Institute of Zoology, Universitätsstr. 31, 93040 Regensburg, Germany, Phone +49(0)941/943-4334, Fax +49(0)941/943-3052, Wolfgang.Bywalez@biologie.uni-regensburg.de

Abstract

Within the glomerular layer of the rodent olfactory bulb, numerous subtypes of local interneurons contribute to early processing of incoming sensory information. These circuits operate in highly complex, compartmentalized intra- and juxtglomerular arrangements and partially undergo adult remodeling. Here we have identified dopaminergic glomerular neurons based on their expression of dopamine transporter (DAT) and characterized their dendritic innervation pattern with respect to individual glomeruli, using fluorescent labeling via patch pipettes and 3D reconstruction of dendrites and glomerular structures based on two-photon imaging data. Among the DAT+ cells, in addition to several cell types that have been identified previously via markers of tyrosine hydroxylase, we describe two new subtypes. The first of these new subtypes resembles the classical GABAergic periglomerular cell with dendrites projecting mostly into a single glomerulus. The second cell type projects its dendrites locally into the interglomerular space, similar to smaller short-axon type cells that were already known. However, these dendrites form striking morphological structures that clasp mostly around several juxtglomerular cell bodies. Interestingly, these clasps are especially complex and abundant in adult animals, indicating a potential role for late circuit modifications. All dendrites, including the clasping structures, show robust dendritic Ca^{2+} entry evoked by backpropagating action potentials and therefore might contain release sites for either GABA and/or dopamine. The relative distribution of subtypes differs between juvenile and adult populations and/or species. Overall, we show that glomerular dopaminergic neurons dispose of high subtype diversity and thus are probably involved in many aspects of early olfactory sensing.

Introduction

Dopaminergic juxtglomerular cells (DA JGCs) in the olfactory bulb (OB) play an important role in the physiology of mammalian olfaction, influencing a wide range of odor processing tasks. Those include odor discrimination (Tillerson et al., 2006), olfactory learning (Coopersmith et al., 1991), stimulus gating, gain control and pacemaker activity (Pignatelli et al., 2005; Liu et al., 2013; Banerjee et al., 2015) and are required for adjusting the bulbar network to changes in the odor environment (Brunjes et al., 1985; Baker, 1990; Bonzano et al., 2014). Social behavior dependent on odor memory was shown to correlate with dopamine levels in the bulb (Serguera et al., 2008) and neurodegenerative disease, e.g. Parkinson (Ansari and Johnson, 1975; Huisman et al., 2004) can be associated with substantial changes in the numbers of OB dopaminergic cells and ensuing changes of the network activity.

In mice, all juxtglomerular tyrosine hydroxylase expressing (TH+) cells co-express GABA (Gall et al., 1987; Parrish-Aungst et al., 2007), which also holds true for the majority of TH+ cells in the rat (Kosaka and Kosaka, 2007). GABA and DA are believed to be packaged into different vesicles and to be released independently (Borisovska et al., 2013), probably in part onto different postsynaptic targets (Pinching and Powell, 1971b; Cave and Baker, 2009). These include olfactory sensory neurons (OSNs), mitral and tufted cells (MCs, TCs), external tufted cells (ETCs) and glomerular interneurons (Cave and Baker, 2009).

The phenomenon of massive adult neurogenesis in the olfactory bulb occurs specifically for several subtypes of interneurons, namely granule cells and glomerular interneurons, the latter including the dopaminergic subpopulation (Lledo et al., 2006; Ninkovic et al., 2007). Adult-born bulbar neurons in general have the ability to integrate very rapidly into the operating circuitry (Mizrahi, 2007; Panzanelli et al., 2009; Kovalchuk et al., 2015) and do not simply replenish old cells. Instead, the relative proportions of the distinct cell populations may change in the lifespan of an animal – in the case of DA JGCs there is a net increase in later ages (Ninkovic et al., 2007; Adam and Mizrahi, 2011). On top of these changes in population composition individual cells also exhibit considerable structural and physiological plasticity of their dendritic processes (Mizrahi, 2007; Livneh and Mizrahi, 2011; Livneh et al., 2014), which contributes to some of the initially mentioned functions, such as olfactory learning or

adjustment to changes in the olfactory environment (Adam and Mizrahi, 2011; Livneh and Mizrahi, 2012; Livneh et al., 2014).

So far, two distinct dopaminergic cell types have been agreed upon, based mainly on their soma size and more recently additionally on neurite morphology and the existence of an axon initial segment (Pignatelli et al., 2005; Kosaka et al., 2008; Kiyokage et al., 2010; Chand et al., 2015): (1) neurons with smaller, round somata (average diameter 9 μm), innervating several adjacent glomeruli (“oligoglomerular innervation”, on average 5-8, Kiyokage et al., 2010) and (2) neurons with larger, elliptical somata (11 μm) and a classical axon initial segment, spanning lateral distances across many glomeruli (“polyglomerular innervation”, on average 39, Kiyokage et al., 2010). However, both subtypes have also been characterized as projecting with their dendrites mostly into the interglomerular space in the manner of short axon cells (SACs); thus the precise dendritic and axonal innervation patterns of TH+ cells are subject to debate (Kiyokage et al., 2010; Kosaka and Kosaka, 2011; Nagayama et al., 2014; and see discussion). Concerning adult neurogenesis, the smaller subtype is known to be generated both at early and adult age (Kosaka and Kosaka, 2009).

Here we describe dopamine transporter expressing (DAT+) neuron subtypes of the glomerular layer as established in acute mouse or rat brain slices with two different labels, that have not been used so far for morphological identification of bulbar dopaminergic neurons: (1) an in-vitro live-stain for DAT+ cells (FFN102, Rodriguez et al., 2013), used in adult mice and juvenile rats and (2) a mouse line with DAT+ cells labeled by GFP after tamoxifen induction in adult animals (Rieker et al., 2011). Individual labeled neurons were stained with fluorescent dye and reconstructed from two-photon scans along with the contours of innervated glomeruli. Since a glomerulus is a strongly subcompartmentalized and inhomogeneous structure (Kasowski et al., 1999; Kosaka and Kosaka, 2005) lacking a clear distinction between periglomerular and intraglomerular neuropil at the ultrastructural level (Pinching and Powell, 1971c; b), we also analyzed the innervation patterns of cell types with respect to subglomerular volumes. This approach may serve to morphologically differentiate glomerular neurons in general, help to identify their putative synaptic partners and eventually to establish a more refined picture of their network interactions during odor sensing.

Materials and Methods

Animals and slice preparation

Rats and mice were decapitated under deep anesthesia with isoflurane according to the stipulations of the German law governing animal welfare (Tierschutzgesetz) and according to the EU directive 2010/63/EU, as approved by the Bavarian state government (Regierung von Oberbayern). Brains were removed and horizontal olfactory bulb brain slices (300 μm thick) were prepared of juvenile rats of either sex (postnatal days 11-18, Wistar) as well as adult wild-type (WT) mice (postnatal weeks 16-40, BL-6) and adult DAT-GFP mice of either sex (postnatal weeks 16 – 20, DAT::CreER^{T2}/CAG::GFP also in BL-6 background) (Nakamura et al., 2006; Rieker et al., 2011). In this transgenic line, GFP is expressed in a subset of DAT+ cells in adult animals after tamoxifen induction. Briefly, the DAT-GFP mice received intraperitoneal tamoxifen (T-5648, Sigma, St Louis, MO, USA) injections (15 mg/kg body weight; AZ 552-1-54-2531-144/07) on 5 consecutive days, the last one 10-20 days before slice preparation. The slices of transgenic animals were incubated in carbogen gas (95% O₂, 5% CO₂) infused artificial cerebrospinal fluid (ACSF, composition: 125 mM NaCl, 26 mM NaHCO₃, 1.25 mM NaH₂PO₄, 20 mM glucose, 2.5 mM KCl, 1 mM MgCl₂, and 2 mM CaCl₂), in a heated water bath at 33°C for 30 min and then kept at room temperature (22°C) until experimentation. For identification of dopaminergic cells in wild-type mouse and rat acute brain slices were incubated in ACSF containing 10 μM of the fluorescent pH-responsive probe FFN102 (Abcam, Cambridge, MA, USA) for 45 min (30 min at 33°C and a further 15 min at room temperature) for identification of dopaminergic cells, adapted from the in-vitro protocol specified in (Rodriguez et al., 2013). Before experimentation, FFN102-treated slices were washed with ACSF without FFN102 (which was also used during electrophysiological recording and imaging) in the recording chamber for at least 15 min to get rid of excessive background staining and to allow for unambiguous identification of genuinely FFN+ cells.

Immunohistochemistry and confocal microscopy

Acute OB slices were prepared from DAT::CreER^{T2}/CAG::GFP mice (similarly to the slices for in-vitro experimentation, 250 μm thick) and fixed in 4% paraformaldehyde in

phosphate buffer (PB, pH 7.4) with 0.5% Triton X-100 overnight at 4°C. After washing in PB, the slices were blocked in 5% normal goat serum and 2.5% bovine serum albumin + 0.5% Triton X-100 in PB (blocking solution) for 3 hours. After washing in phosphate buffered saline (PBS), slices were incubated in blocking solution + primary antibodies (chicken anti-TH 1:200, mouse anti-GFP 1:250, goat anti-OMP 1:500 – all from Abcam) for 48h. After several washing steps in PBS, the secondary antibodies were applied (donkey anti-chicken Cy3, 1:400, Jackson ImmunoResearch Laboratories, West Grove, PA, USA; donkey anti mouse Alexa Fluor 488 conjugate, 1:200, Abcam; donkey anti-goat Alexa Fluor 405, Abcam) for 24h in blocking solution. After multiple rinsing steps in PBS, the slices were embedded with Vectashield mounting medium (Vector Laboratories, Burlingame, CA, USA) and covered by coverslips.

Immunostained slices were scanned with a Leica TCS SP5-2 confocal laser-scanning microscope (Leica Microsystems, Mannheim, Germany) equipped with a HCX PL APO lambda blue 63x/NA1.4 immersion oil objective (Leica). Fluorochromes have been visualized with excitation wavelengths of 405nm (Alexa Fluor 405), 488nm (Alexa Fluor 488) and 561nm (Cy3) with respective emission filters. For each optical section the images were collected sequentially for the three fluorochromes. Serial 8-bit stacks with a z-step of 1 µm and a resolution of 512x512 pixels and a pixel width of 481.5 nm have been acquired. Images were averaged from 5 successive scans. Images were then homogeneously adjusted in brightness and contrast with Fiji (ImageJ; Schindelin et al., 2012). Cells were also counted in Fiji, from 3 scanned slices.

Two-photon imaging and electrophysiology

Fluorescence was recorded on a Femto-2D microscope (Femtonics, Budapest, HU), equipped with a tunable, Verdi-pumped Ti:Sa laser (Chameleon Ultra I, Coherent, Glasgow, Scotland). The microscope disposed of three detection channels (green fluorescence (epi and trans), red (epi) and infrared light (trans)) and was equipped with a 60x Nikon Fluor water-immersion objective (NA 1.0; Nikon Instruments, Melville, NY, USA) and controlled by MES v4.5.613 software (Femtonics).

After identification of FFN102+ or GFP+ cells, in WT rats and mice, in the green channel at an excitation wavelength of 760 nm or 900 nm, respectively, individual fluorescent cell bodies were patched in whole-cell mode with patch pipettes (resistance 6-8Mohm), filled with an intracellular solution (composition: 130 mM K-methylsulfate,

10 mM HEPES, 4 mM MgCl₂, 2.5 mM Na₂ATP, 0.4 mM NaGTP, 10 mM Na-phosphocreatine, 2 mM ascorbate, 0.1 mM). Electrophysiological recordings were made with an EPC-10 amplifier using Patchmaster v2x60 software (both HEKA Elektronik, Lambrecht/Pfalz, Germany). For FFN102 experiments, the red fluorescent dye Alexa Fluor 594 (50 μM, Invitrogen, Carlsbad, CA, USA) was added to the intracellular solution to allow for the detailed visualization of all cell processes and to subsequently image the dendritic fine structure. In the case of DAT-GFP mouse calcium imaging experiments, the calcium indicator OGB-1 (100 μM, Invitrogen) was added for both calcium imaging and process visualization. Fluorescence transients were acquired at 800nm laser excitation. Data were mostly collected from glomeruli within the medial surface of the olfactory bulb.

All experiments were performed at room temperature (22°C). The patched juxtglomerular neurons were held near their resting potential of -60 to -70 mV and the access resistance was monitored. For a coarse electrophysiological classification, depolarizing step pulses were applied for 500 ms each. Starting at and returning to resting membrane potential after each sweep, the cell was injected with a current of -90 pA, which was increased by +30 pA for in total 10 steps (therefore ending at +180 pA). In calcium imaging experiments values of > 25 pA of holding current were unacceptable and the experiment was rejected). A shift in baseline fluorescence F_0 of more than 15% between the first and the last measurement of each region of interest (ROI) also led to a rejection of the experiment.

After sufficient filling of the dendritic tree (at least 15 min), stacks of scans of the entire cell were recorded at 1 μm z-resolution. Each scan included 2 images, recorded in the red (Alexa) or green (OGB-1) fluorescent channel and at the same time in the trans-infrared channel of the microscope, to gather information on both the dendritic tree and glomerular structure. The xy-resolution was 900x900 or 1000x1000 pixels with a pixel width of 0.098 to 0.24 μm, trading off between resolution and coverage of the stained cellular neurites by the xy-window. All cells except for the long-range projecting subtype fit within one or two scanning windows and were fully sampled.

In several instances we noted upon reconstruction that cells had been incompletely scanned, mostly because the stack's z-coordinate was not set deep enough. These neurons were not used for detailed morphological analyses, but most could be

classified and included in the total numbers for cell subtype distributions across animal groups (Fig. 7 B).

During calcium imaging experiments, structures of interest were imaged in free line-scanning mode with a temporal resolution of ~ 1 ms. At a given dendritic location, several consecutive focal line-scans during somatically evoked single action potentials (sAPs) (by an injected current step of 1000 pA for 1 ms) or action potential trains (AP trains) (15 stimuli at 50 Hz) were recorded (duration 1.5 s), averaged and smoothed. Dendritic calcium transients $\Delta F/F$ in DAT+ clasping cells relative to the resting fluorescence F_0 were analyzed, with their decay measured in terms of half duration $\tau_{1/2}$ (Egger et al., 2003). Decay half duration values were capped at 5 s, because a higher value could not be reliably extrapolated. Post-hoc data analysis was performed using custom macros written in IGOR Pro 5 (Wavemetrics, Lake Oswego, OR, USA).

Reconstruction and analysis of cellular morphology

To measure the cell body dimensions of glomerular neurons, we approximated the somatic shape as oval within single x-y-slices. We calculated the mean diameters d for any given soma from the slice with the largest oval cross-sectional area A and perimeter P as follows (cf. Heyt and Diaz, 1975):

$$d = 1.55 A^{0.625} / P^{0.25}$$

The morphology of dopaminergic juxtglomerular cell dendrites was reconstructed with Fiji plugin Simple Neurite Tracer (SNT) (Longair et al., 2011) from the fluorescence z-stack scans. Thin, putative axonal structures could neither be unambiguously discriminated in all cases nor fully recovered, which is a drawback of reconstructions from live TPLSM imaging data (Blackman et al., 2014; and results).

The following morphometric parameters were extracted from SNT analysis tools and other ImageJ calculations: 3D coordinates, total process length, soma dimensions, number of branches and end-points. In this context, a branch is defined as a part of the cell bounded by any two junction points. Both spines and other endings are counted as terminal points. The number of primary dendrites was established according to the following criterion: Any primary dendrite had to account for > 10% of the total process length and to stem from the cell soma or a main dendrite bifurcating more proximal

than 15 μm . All other morphometric analyses were derived or computed from those values, except for the innervation analysis (see below).

Reconstruction of glomeruli for DAT+ uniglomerular and clasping cells

The glomerular contours were reconstructed from the TPLSM trans-infrared z-stacks with the ImageJ plugin TrakEM2 (Cardona et al., 2012). A glomerular counterstain was not required due to the good visibility of glomerular contours in the trans-IR-TPLSM channel and thus both dendritic and glomerular data could be gathered in the very same coordinate system, allowing for a precise innervation analysis. For FFN-stained slices, the green channel PMT overlay of the FFN staining with the trans-IR channel yielded additional contrast between cell bodies and glomerular neuropil (Fig.1 A). Contours were determined by tracing the border between the ring-like arrangement of JGC somata and the glomerular neuropil on the glomerulus inside for each successive z-slice. The TrakEM2 "interpolate gaps" tool allows to interpolate the areas between two traced slices, which we sometimes applied for traced z-slices close to the midline of a glomerulus and no more than 3 μm apart to ensure high structural accuracy. Even though the images became more blurry in deeper parts of the brain slice (depending on the brain slice quality, age of the animal etc.), the transition between contrast-rich somata and the grainy neuropil was still detectable for most scanned glomeruli. In cases where the visibility of deep glomerular contours was compromised the data was discarded.

In 2 of the 15 cells sampled for innervation analysis the deeper part of the glomerulus was not scanned completely although the dendrites were fully recovered. In these cases the respective glomerulus was completed virtually in order to reduce errors in volume and average radius measurements (see below) by the following procedure: First the glomerular cross-sectional area at the deepest z-slice was determined and matched to the z-slice with the most similar area size of the top z-side of the glomerulus. Then the remaining slices on the top side until the end of the glomerulus were added to the incomplete part in mirrored order and aligned to the center of gravity of the deepest contour, resulting in an added volume of 10 and 28 % of the total volume, respectively.

Innervation analysis

Prior to the methodical description of this new analysis approach, we define three auxiliary terms: (1) “glomerular neuropil” refers to the intraglomerular tissue, but not to the surrounding cell bodies or the periglomerular neuropil, (2) a cell’s “home glomerulus” is either the only glomerulus innervated within its neuropil, or the glomerulus with the largest fraction of the cell’s process length adjacent to its neuropil (within the glomerular “outer shell”, see below). (3) The glomerular “intermediate zone” denotes the transition zone from the periglomerular cell body layer/neuropil to the intraglomerular neuropil; it has been characterized with light microscopy and at an ultrastructural level (Pinching and Powell, 1971c; b; and see discussion).

As to the nomenclature of neuronal subtypes, we have named DAT+ cell subtypes dopaminergic “uniglomerular”, “clasping”, or “undersized” cells, respectively (see results for criteria of classification). As in previous literature, the term “periglomerular cell” (PGC) refers to uniglomerular neurons with their soma directly adjacent to the dendritically innervated glomerular neuropil, and the broader term “juxtglomerular cell” (JGC) encompasses all glomerular layer neurons (e.g. Nagayama et al. 2014), including any subtypes of DAT+ cells described here. Finally, the large dopaminergic cells with long lateral processes and a distinct axon, which have been called short axon cells (Kiyokage et al., 2010), inhibitory juxtglomerular association neuron, or even dopaminergic external tufted cells (Kosaka and Kosaka, 2011), are called “dopaminergic large lateral association neuron” in this manuscript.

For analysis of the glomerular innervation by a reconstructed dendritic tree, the reconstruction data were exported into Microsoft Excel 2007 and then to Word 2007 (both Microsoft, Redmond, WA, USA) text files where the data were reformatted and then imported into IGOR via custom-written software. Pixel coordinates were converted into metric coordinates. Next, the coordinate systems of the two reconstructions – tuft and home glomerulus – were aligned. After this step, 3-D voxel representations with a voxel side length of 1 μm were generated both of the dendritic tree (Hellwig, 2000; Egger et al., 2008) and of the home glomerulus. The tuft voxel representation did not account for dendritic diameters.

In some instances there were gaps in the glomerular surface representation due to an insufficient density of data points in the reconstruction (mainly in contour lines that

happened to run parallel to the x- or the y-axis for several μm). In these cases we used a custom-written filling algorithm which extended the reconstructed surface by 1-2 μm . The maximal error in glomerular volume due to this procedure was on the order of < 5 %.

The voxel representations were used to determine the following parameters: (1) Total amount of 1 μm voxels within a glomerulus, (2) glomerular volume, glomerular center of mass and mean glomerular radius (3) fractional innervation of shells as described below.

For analyzing the relation between a glomerular layer neuron and its home glomerulus, an intuitive approach would be to conduct a 3-D Sholl-type analysis (Sholl, 1953) originating from the center of mass of the glomerulus rather than from the soma of the neuron. However, since glomeruli were usually not spherical or ellipsoid in shape, we could not apply a straightforward 3-D analysis of innervation based on equally spaced spherical (or ellipsoidal) glomerular shells. Instead, shell volumes were calculated based on the real glomerular, that is, in terms of expanding or shrinking the reconstructed glomerular surface by a certain radial distance from the center of mass of the glomerulus. The fraction of innervation was then determined by counting all tuft voxels of the 1 μm representation within the volume of a shell and normalizing the number to the total number of tuft voxels within the glomerular neuropil.

To allow for a quantitative analysis of intra- versus inter-glomerular innervation and for the inclusion of an intermediate zone we discriminated the following three volumes (cf. also Fig. 6 A): The “outer shell” was an extra layer with 15 μm thickness around the identified glomerulus neuropil-to-soma border, i.e. the reconstructed glomerular surface, to include the closely adjacent cell body layer around the glomerulus in the analysis. The choice of 15 μm is intended to include any directly adjacent juxtglomerular cell body in this volume, even large JGCs like the large dopaminergic lateral association subtype and external tufted cells (Nagayama et al., 2014). The inside of the glomerulus was subdivided into (1) the “inner shell”, a volume extending for $\frac{1}{4}$ th of the glomerular mean radius from the neuropil-to-soma border towards the glomerulus centroid ($8 \pm 2 \mu\text{m}$, $n = 15$) and (2) the “core”, which was the remaining inner volume. In most glomeruli the volumes of inner shell and core were roughly the same (fraction inner shell of total glomerular volume 0.57 ± 0.04 , $n = 15$). The combined

inner and outer shell volume should incorporate the “intermediate zone”, while the combined core and inner shell volumes represent the neuropil of the home glomerulus.

Statistical analysis

Statistical significances have been assessed in SigmaPlot 13.0 (Systat Software, Inc., San Jose, CA, USA). A student's t-test or Rank Sum test was used for all comparisons except for paired data (e.g. within the same cell) where the non-parametric Wilcoxon test was used. For correlations, a linear regression analysis was utilized (SigmaPlot) to determine R square values (R^2). Data are presented as mean values of parameters \pm standard deviation (S.D.).

Results

The DAT-based approaches used in this study have revealed two more dopaminergic subtypes in addition to the known cell types described in the introduction, and also allowed us to investigate whether there are subtype-specific differences across the three tested animal populations. One DAT⁺ subtype closely resembles a classical GABAergic periglomerular cell type whose dendrites project into a single glomerulus. The other cell type shows unique dendritic structures that have not been described so far, and which apparently innervate mainly the cell bodies of other subtypes of glomerular neurons via dense clasps. To further characterize these clasp structures, we also investigated the dendritic Ca²⁺ dynamics of this cell type.

3. Identification and reconstruction of dopaminergic cells in rat/mouse olfactory bulb slices

In our hands, the dopamine transporter substrate FFN102 reliably labeled subsets of glomerular neurons in acute brain slices of rat and mouse olfactory bulbs. Initially, FFN102 was described as a dopaminergic marker with high specificity and transmission sensor in the ventral midbrain and striatum (Rodriguez et al., 2013). Aside from stained cell bodies and sometimes stained proximal dendrites, we observed small fluorescent puncta throughout the glomerular neuropil as well as juxtglomerular zones of the glomerular layer (Fig. 1 A and B). Those are likely to correspond to synaptic DA reuptake sites at presynapses (Rodriguez et al., 2013). To confirm and complement our observations based on FFN102 we also used a tamoxifen-inducible mouse line (DAT::CreER^{T2}/CAG::GFP, cf. Rieker et al. 2011). Induction of GFP expression with low tamoxifen levels in adult animals showed labeled cells exclusively in the glomerular layer with strong fluorescence in cell bodies and upon high laser illumination also in dendritic processes (Fig. 1 C). Interestingly, quantifications of the immunohistological stainings in this transgenic line against TH showed a large subset of TH⁺ cells that were not co-stained with GFP ($51 \pm 7\%$ of all stained cells), corresponding to dopaminergic cells without strong Cre activity after tamoxifen induction (Fig. 1 D). On the other hand those stainings also revealed a substantial population of TH⁻ GFP⁺ cells ($31 \pm 4\%$ of all stained cells, Fig. 1 D). A third population of cells showed an overlap of both markers ($18 \pm 8\%$ of all stained cells, Fig. 1 D). These observations

might be explained with a low induction rate (for more explanations of the labeling pattern cf. discussion).

For morphological reconstruction, GFP+ or FFN102+ cells were labeled intracellularly with additional fluorescent dyes via whole-cell patching and scanned using TPLSM. While the dendrites could be reconstructed, the fluorescence signal from thin, putative axonal structures was not bright enough except for the initial parts of some axons. In parallel, the surrounding tissue was scanned and the 3D-surface of the glomerular neuropil was reconstructed (see methods). This approach – simultaneous sampling of detailed individual cell structure and the surrounding glomerular tissue – allows to precisely determine neuronal morphometrics relative to glomerular contours (Fig. 1 E, F, supplementary movie S1).

2. Morphological subtype diversity of juxtaglomerular DAT+ cells

2.1 The DAT+ uniglomerular cell

Within both the rat and mouse populations of FFN+ cells, we have regularly observed a uniglomerular subtype that morphologically resembles a classical periglomerular cell (Figure 2). The existence of this dopaminergic PGC subtype has already been suggested (Kosaka and Kosaka, 2009; Nagayama et al., 2014) even though its exact dendritic morphology has not been verified in any preceding study. Accordingly, we characterized this subtype by the confinement of at least 50% of its total reconstructed neurite length extending into a single “home glomerulus” (on average $81 \pm 16\%$, $n = 9$; see Methods). Within the glomerular neuropil these neurites had the appearance of classical dendrites and ramified extensively in roughly spherical volumes. Some cells innervated almost the entire glomerular volume, while most innervated only a smaller part of the home glomerulus, proximal to the cell body (3 vs. 6 cells) (see e.g. Fig. 2 A, D, F vs. Fig. 2 B, C, E, G). The extraglomerular processes were thin and usually did not branch extensively nor show spines, therefore they probably corresponded to axons. They never extended into other glomeruli’s neuropils, and also could not be followed any further than beyond one adjacent glomerulus from the soma. Some uniglomerular cell dendrites bore spines or spine-like protrusions ($n = 5$ of 9 cells), yet

with quite variable density and appearance in each cell. The larger uniglomerular cells also tended to show a higher density of spiny structures. The soma size was in accordance with earlier descriptions of periglomerular cells (average mean diameter of all pooled cells $10.3 \pm 1.8 \mu\text{m}$, $n = 9$) and did not significantly deviate from the other DAT+ cell types described here, except for the large lateral association neurons (see 2.3). For the analysis of other morphological parameters see Table 1 and Fig. 7. Interestingly, the uniglomerular DAT+ type was not found among the DAT-GFP+ neurons (Fig. 7, but see 2.3 and discussion).

2.2 The DAT+ clasping cell

Clasping cells were observed across all three animal groups. Most neurites of these cells (or sometimes all) were found to be ramifying in the interglomerular space of the glomerular layer (Fig. 3). If these cells ever entered glomerular neuropil, they did so only in a restricted fashion, namely within mostly superficial volumes of one particular home glomerulus, and no other additional glomeruli ($n = 6$ out of 12). Thus the DAT+ clasping cells might be involved in synaptic interactions in the glomerular intermediate zones (Pinching and Powell, 1971c). This hypothesis is further tested below (see section 4 and discussion). For each cell, several primary neurites were found to extend around several glomeruli for a few hundred micrometers in tortuous shapes. In general, there was no obvious orientation of the neurite trees relative to the glomerular layer or the home glomerulus, but they never grew into the external plexiform layer (EPL). While there is a partial overlap of the characteristics of this cell type with descriptions in previous studies (e.g. the “oligoglomerular” cells in Kiyokage et al., 2010, see discussion), there were locally ramifying neurite structures, which to our knowledge have not been described so far: extremely dense neurite specializations, that were found to clasp around single targeted cell bodies and sometimes also to enter the glomerular neuropil. To classify as a clasping cell in our study, a given cell had to show at least two of these clasp structures. See section 2.4 for a more detailed description of clasp identification.

Our approach did not allow to determine whether all DAT+ clasping cells bear an axon (but see e.g. Fig. 5 C, methods and discussion). In any case, the clasp-bearing processes, which included most or sometimes all of the major neurites, are presumably dendrites since they were bearing spine-like protrusions (albeit with very variable abundance) and also otherwise resembled classical dendritic structures. Since the

dendrites of most other bulbar neuron types and in particular also dopaminergic JGCs are known to release neurotransmitter (Schoppa, 2005), we suggest that the clasping dendrites may act as presynaptic structures as well. This idea is further supported by the calcium imaging data described below (2.4).

The soma size was in the medium range (average mean diameter of all pooled cells $9.6 \pm 2.0 \mu\text{m}$, $n = 12$), and not significantly different from the soma size of DAT+ uniglomerular cells. Many other morphological properties of clasping and uniglomerular dendrites were also highly similar across rat FFN populations (Table 1). DAT+ clasping cells were found in all examined animal populations (FFN mice, FFN rats, GFP mice; Fig. 7 A, B). Across these animal groups, we observed a substantially increased complexity of the DAT+ clasping dendrites for the GFP+ population in comparison to FFN mice and especially to juvenile FFN rats, as reflected in total process length, branch and end point numbers and numbers of clasps (compare Fig. 3 A – D to 3 E, F and 3 G, H, Fig. 7, Table 1).

2.3 Other DAT+ cell types

Here we describe in brief the remainder of the encountered DAT+ cell types (Fig. 4). A large lateral association neuron with a usually elongated soma (size $13.6 \pm 1.3 \mu\text{m}$, long axis oriented along the glomerular neuropil border) and a lateral dendritic extent of several hundreds of micrometers within the glomerular layer (cf. Kiyokage et al., 2010) was observed in the FFN+ rat and mouse populations. Those dendrites did not branch extensively, in contrast to the two previously described cell types, and bore distinct spines with bulbar heads. Aside from the long lateral dendrites this cell type also was observed to bear an axon, extending towards and sometimes into the EPL (no full reconstruction possible, see methods; Fig. 4 A, C). Such cells were not observed in the GFP labeled DAT+ population, speaking against adult-stage generation, as already reported (Kosaka and Kosaka, 2009).

In all three of our samples there were also cells with medium or smaller size somata, which could not be classified into the uniglomerular or clasping populations based on our characterizations (see 2.1. and 2.2). In several instances they resembled the morphology of either one of these cell types to a large extent (Fig. 4 B, D). Since they did not meet the previously defined criteria and on average also showed a reduced

complexity compared to both the clasping and uniglomerular cells (Table 1), they were pooled as “intermediate cells”.

Finally, there was a population of morphologically much reduced cells within all tested animal groups (Fig. 4 E, F). These “undersized” cells bore rather short neurites (on average $244 \pm 171 \mu\text{m}$ total process length, $n = 14$) with few branches and never more than two primary dendrites, and displayed no distinct innervation patterns. In the DAT-GFP mice none of those cells showed spiking upon step depolarization. Their morphology was not analyzed any further.

Among the fluorescent cells we also very rarely encountered astrocytes (Fig. 4 G). They could be identified by their morphological appearance (mostly star-like, sometimes polar or elongate dendritic orientation with very elaborate, varicose processes, branching throughout their whole length, and a lack of electrical excitability (Bailey and Shipley, 1993).

3. DAT+ clasping cell dendrites and substructures: Morphology and Ca^{2+} dynamics

The cell clasps found on DAT+ clasping cells (2.2) were identified according to the following criteria: (1) formed by at least two processes extending from the same parent dendrite, (2) embracing a single cell body from several spatial directions, such that (3) the soma is encompassed by the dendrite(s) for the length of at least half the mean cell diameter (see Fig. 5 A, supplementary movies S2 and S3). These dendritic specializations were highly abundant in adult-born GFP+ cells (DAT-GFP animals, number of clasps 7.4 ± 2.3 , $n = 6$), and were, to a lesser extent, also observed in the corresponding FFN+ cells from rats (2.8 ± 0.5 , $n = 4$) and mice (3.5 ± 0.7 , $n = 2$; cf. Table 1 and Fig. 7 C).

For any given DAT+ clasping cell, the cell bodies embraced by the clasps can belong to the outer shells of several different glomeruli, including the cell’s home glomerulus. The mean diameter of clasped cells ($8.0 \pm 1.6 \mu\text{m}$, range $5.2 \mu\text{m} - 11.7 \mu\text{m}$, $n = 78$, Fig. 5 E) overlaps with the diameter distributions of either other PGCs or ETCs (e.g. Nagayama et al., 2014), but was too small for the dopaminergic large lateral association neurons. No FFN label was seen in clasped cells. Aside from the dense clasp structures, some dendrites were entering the neuropil also in a very tightly packed fashion (see e.g. bundles in Fig. 5B).

Next, we asked whether the clasp structures are likely to release transmitter. Dopaminergic JGCs are known to fire action potentials, which is probably one of the mechanisms important for dendritic neurotransmitter release (Maher and Westbrook, 2008). Therefore we first tested the excitability of DAT+ clasping cells. Upon prolonged depolarization of DAT+ clasping cells from their resting potential via somatic injection of current steps we observed firing patterns mainly of the continuous, non-accommodating spiking type (13 of 21 cells), some of the accommodating type (5 of 21 cells, example in Fig. 5 C), and very few instances of no spike generation (3 of 21 cells; nomenclature according to McQuiston and Katz, 2001). Bursting was never observed in DAT+ clasping cells. All firing cells showed a low spiking threshold, with spikes observed at the first depolarizing current injection step of 30 pA in 13 of 18 neurons and at 60 pA in all of 18.

Dendritic release upon AP firing would require that single Aps can reliably produce substantial calcium transients in the dendrites of adult-born DAT+ clasping cells. This was tested with TPLSM calcium imaging. Single somatically evoked Aps (sAP) elicited substantial calcium influx in a major part of DAT+ clasping cell dendrites (Fig. 5 C right). These signals were not saturating, since trains of 20 Aps at 50 Hz recorded in the same locations resulted in larger $\Delta F/F$ transients, which usually reached a plateau during the train stimulation at a level expected for 100 μM OGB-1 (sAP $15 \pm 10\%$ $\Delta F/F$ vs. train $150 \pm 74\%$ $\Delta F/F$ in 155 locations, $P < 0.001$, paired t-test). In general, $\Delta F/F$ transients decayed with a very slow half duration, on the order of one to three seconds, sometimes even more slowly (on average 2.5 ± 1.2 s, $n = 94$).

As expected for neurons that feature dendritic release of transmitter (Egger et al., 2003) sAP-mediated $\Delta F/F$ did not decrease with distance from the soma; rather individual $\Delta F/F$ amplitudes were completely uncorrelated to the distance of the recording site (Fig. 5 C, G, $R^2 = 0.0008$).

In clasping cells that innervated the glomerular neuropil, calcium signals measured in dendrites within innervated glomeruli were not significantly different from those on the outside (for sAPs $15 \pm 5\%$ $\Delta F/F$, $n = 18$ vs. $16 \pm 13\%$ $\Delta F/F$, $n = 141$, n.s., Wilcoxon test, Fig. 5 F), which is also true for the decay half durations (2.2 ± 1.1 s, $n = 12$ vs. 2.5 ± 1.3 s, $n = 82$, n.s.). Neither were the transient amplitudes in clasping structures different from those in non-clasping dendrite sections across all clasping cells ($13 \pm 8\%$ $\Delta F/F$, $n = 46$ vs. $16 \pm 11\%$ $\Delta F/F$, $n = 110$, n.s., Fig. 5 F). Decay half-durations were

also not significantly different in clasping vs. non-clasping structures (2.2 ± 1.1 s vs. 2.6 ± 1.3 s, n.s.). There was also no significant trend for $\Delta F/F$ and $\tau_{1/2}$ in paired data sets (clasping versus non-clasping structures within the same cells, Fig. 5F, paired t test, both n.s.). We observed no correlations of any of the parameter combinations of $\Delta F/F$, distance or decay half-time in either of the populations (not shown, R^2 values range from 0.005 to 0.071).

These observations indicate a substantial, slowly decaying AP-mediated Ca^{2+} entry in conventional dendrites and clasp subcompartments in most investigated DAT+ clasping cells, which may allow for dendritic release from both compartments.

3. Innervation analysis

DAT+ uniglomerular and clasping cells in any given animal group were quite similar in terms of several common morphological parameters (soma size, number of primary dendrites, total process length, branch number; see Table 1 and Fig. 7). Therefore we sought to discriminate these subtypes via the differential innervation of the inter- and intra-glomerular space, in particular in relation to their respective home glomerulus. We performed a 3-D-overlay of neuronal reconstructions with the reconstruction of their home glomerulus and determined the relative innervation in three selected volumes of the glomerulus: the core, inner and outer shell (Fig. 6 A; see methods).

First, we compared the fraction of the innervated voxels of the glomerular neuropil (inner shell + core) to the tuft voxels within the outer shell (Fig. 6 B), which yielded highly significant differences (average 0.32 ± 0.20 , $n = 8$ in clasping cells vs. 18.73 ± 16.32 , $n = 7$ in uniglomerular cells; Mann-Whitney Test, $P < 0.001$). Even though numbers for the individual animal groups were small, very similar results emerged (FFN+ mouse 0.25 ± 0.35 vs. 30.67 ± 27.26 , respectively, $n = 2$; FFN+ rat 0.27 ± 0.25 vs. 17.95 ± 7.64 , respectively, $n = 2$, cf. Fig. 6 B). We also considered the shell region (inner + outer shell) as a whole in order to cover the intermediate zone, and compared this volume to the complete covered volume (core + inner + outer shell). This fractional innervation also displayed a highly significant difference (Fig. 6 C, average 0.93 ± 0.07 , $n=8$ in clasping cells vs. 0.40 ± 0.17 , $n=7$ in uniglomerular cells; Mann-Whitney Rank Sum Test, $P < 0.001$). Again, the individual animal populations yielded similar results

(FFN+ mouse 0.96 ± 0.05 vs. 0.27 ± 0.14 , respectively, $n = 2$; FFN+ rat 0.99 ± 0.01 vs. 0.33 ± 0.02 , respectively, $n = 2$, cf. Fig. 6 C). Briefly, both measures of glomerular innervation proved to be very distinct for the cell types, i.e. clasping cells innervate almost exclusively the shell regions, whereas uniglomerular cells primarily innervate the inner shell and the core.

Discussion

3. Labeling of dopaminergic cells: TH versus DAT

We have investigated the morphology of DAT⁺ cells in the glomerular layer of the olfactory bulb using a new in-vitro marker (FFN102, Rodriguez et al., 2013) as well as a transgenic mouse line expressing GFP under a DAT promoter induced in adult animals with a possible higher incidence for adult-born cells. FFN specificity as established by the overlap with DAT⁺ immunoreactive cells is reportedly extremely high (Rodriguez et al., 2013). Immunolabeling for TH and GFP in the induced DAT::CreER^{T2}/CAG::GFP transgenic line yielded three labeled cell populations: TH⁺ GFP⁻ cells, TH⁺ GFP⁺ cells, and TH⁻ GFP⁺ cells. The rather low occurrence of TH⁺ GFP⁺ cells (18% of stained cells) indicates a moderate induction success because of lower concentrations of tamoxifen in comparison to other studies (Mori et al., 2006). Therefore, many of the observed large fraction of TH⁺ GFP⁻ cells are still likely to bear DAT, but were not induced by the tamoxifen injections, although the specificity of the DAT::Cre line is solid, as shown in earlier DAT antibody stainings (Ninkovic et al., 2010).

The observation of TH⁻ GFP⁺ cells could be explained by the following reasons. In a previous study with an inducible CreER^{T2} line recombination was very efficient in migrating adult-born cells (Mori et al., 2006). A subset of dopaminergic cells could therefore also show higher accessibility or susceptibility to tamoxifen as also observed for the GLAST::CreER^{T2} animals (Mori et al., 2006). TH and DAT are rather late determinant markers of dopaminergic cells in their differentiation (Cave and Baker, 2009; Ninkovic et al., 2010; Kovalchuk et al., 2015), but a high number of GFP⁺ TH⁻ cells could nevertheless argue for some DAT expression in still migrating cells.

It is generally accepted, that adult animals show increased numbers of dopaminergic cells compared to juvenile animals due to adult neurogenesis (Ninkovic et al., 2007; Whitman and Greer, 2007a; Adam and Mizrahi, 2011). TH levels are known to fluctuate in bulbar dopaminergic cells in correlation to sensory activity and therefore some of the TH⁻ cells can be explained by expression levels below detectability, in partially in immature cells or even resident cells which did not receive substantial sensory activation (Baker, 1990; Cave and Baker, 2009). The scenario of populations of cells that express TH but no DAT or vice versa is rather unrealistic as it has not been

observed or reported so far in the olfactory bulb, although this explanation should not be dismissed completely. A high number of GFP+ TH- cells in our study is dissimilar to another recent non-inducible DAT::Cre based study which reports a reasonably strong overlap of TH and DAT staining (85% overlap, Banerjee et al., 2015). This can also be interpreted as a high number of adult-born cells showing specifically the DAT marker but not the TH marker in our induction approach. Moreover, transgenic expression of a fluorescent marker under the TH promoter would probably also yield a higher overlap with our DAT+ cells, since the fluctuating detection reliability of TH is most prone to result in false negatives in antibody assays directed against the formed protein (Cave and Baker, 2009). However, such differences might of course also be attributed to the choice of species and the respective staining and detection methods. Conclusively, both our study and others indicate that DAT-based labels and TH-based labels stain partially different populations of dopaminergic cells.

Indeed, we observed two dopaminergic subtypes that had not yet been classified with TH-based approaches and show hitherto unknown dendritic specializations. This observation further supports that DAT labeling is not fully overlapping with TH labeling (see also Fig. 1 D). Our observation of rather undifferentiated “undersized” DAT+ cells that have also not been reported before as such within the glomerular layer is also in agreement with not fully mature cells bearing the induced DAT label. These cells are possibly either newly arriving cells, still morphologically and physiologically undifferentiated or pre-apoptotic (see also 3. Classification of cell types).

Although in our hands FFN+ neurons were slightly compromised with respect to their physiological health (e.g. higher leak currents than DAT-GFP+ cells), FFN labeling might be used for functional imaging as described in (Rodriguez et al., 2013). We occasionally observed the destaining of a subset of fluorescent puncta – probably indicating synaptic dopamine transmission (Rodriguez et al., 2013) – correlated to somatically elicited action potential trains in FFN+ cells (data not shown). This feature of FFN102 might also help to discriminate GABAergic and dopaminergic output synapses of dopaminergic JGNs. Thus, in our view DAT is a valuable marker complementing TH, similar to the parallel use of the vesicular GABA transporter (VGAT), and the synthesizing enzyme isoforms glutamate decarboxylase 65 or 67 (GAD65, GAD67) for research on GABAergic neurons and circuits (Parrish-Aungst et al., 2007).

2. Reconstruction of dendrites and glomeruli

Detailed morphological reconstructions based on fluorescence measurements in acute slices with TPLSM are superior to the classical biocytin-based methods with respect to efficiency and to z-shrinkage. The latter is not an issue due to reconstruction from data in living tissue. Therefore parameters such as volumes, dendritic lengths and innervation densities can be accurately determined (Egger et al., 2008; Blackman et al., 2014). Also, reconstruction of glomerular contours from embedded material requires a counterstain, whereas no extra staining was required to visualize glomerular borders in the acute slice preparation. However, recovery of axonal structures is clearly limited (see also below). Thus the method used here is an effective means for analysis of dendritic glomerular innervation patterns, also for non-dopaminergic JGCs.

3. Classification of cell types

We have consistently observed both the classical dopaminergic subtypes that have been reported previously based on TH+, and additional subtypes, including a uniglomerular cell type and rather undifferentiated DAT+ cells. The SAC-like classical cells comprise the previously known large lateral association neurons and a smaller subtype that is denoted here as DAT+ clasping cell since its dendrites bear structural specializations that resemble somatic clasps.

Between the DAT+ uniglomerular and the DAT+ clasping cell subtypes there is a less well defined spectrum of morphologies, classified here as “intermediate cells”. These cells neither showed multiple clasp structures nor did they project with the majority of their dendrites into the home glomerulus. Since these intermediate cells were on average morphologically less complex than either uniglomerular or clasping cells, part of them might still be in the process of differentiation into either subtype, which is also supported by the following considerations: With less strict criteria for categorization, intermediate cells could be largely reclassified as either uniglomerular or clasping. For example, reducing the fraction of required intraglomerular total process length from 50% to 30% would result in a notable increase of uniglomerular cell numbers in all populations, including the DAT+ GFP mouse population, where none of the cells did make the 50% cut-off. Next, reducing the numbers of cell clasps to zero or one would reunite most of the remaining intermediate cells into one group with the DAT+ clasping cells: a medium-range, mainly interglomerular, small SAC-like cell type. Future

investigations, perhaps including axonal reconstructions and/or imaging new cells at various time points (e.g. time-lapse imaging or brainbow/confetti stainings), will be required to ultimately settle the identity of intermediate cells.

The still much less complex “undersized” cells (Fig. 4 E, F) are unlikely to be insufficiently filled cells of one of the other categories because they usually filled quickly and showed no truncations. So far, such undersized cells have not been reported specifically among the dopaminergic JGN population in the GL (but see Pignatelli et al., 2009 for a description of a reservoir of immature TH⁺ neurons in the EPL). Similarly undifferentiated cells have been observed in the olfactory bulb and classified as immature neurons on their way to synaptic integration based on morphological and physiological analysis (granule cells: Carleton et al., 2003; PGN/JGCs Mizrahi, 2007; Kovalchuk et al., 2015). As reported for the undersized cells here, early stages of these cells also did not fire proper Na⁺ spikes. Therefore undersized cells could be immature DAT⁺ glomerular neurons or alternatively pre-apoptotic cells, since reportedly a large number of arriving cells gets eliminated and not integrated into the bulbar circuitry (Winner et al., 2002).

In any case, in our view the existence of both these undersized cells and part of the intermediate cells reflects the participation of certain subtypes of DA neurons in ongoing adult neurogenesis and remodeling in the olfactory bulb (see also discussion below).

As already mentioned in the introduction, Kiyokage et al. (2010) described two dopaminergic subtypes based on their innervation patterns, termed oligoglomerular and polyglomerular, which otherwise both resemble SAC-like cells. While the polyglomerular subtype clearly corresponds to the large lateral association neuron that we also encountered, a matching of the oligoglomerular subtype to our cells is less obvious. We found the dendrites of both DAT⁺ claspings and DAT⁺ uniglomerular cells to innervate no more than the central neuropil of one glomerulus, whereas Kiyokage et al. (2010) report the innervation of several or many glomeruli by all the TH⁺ cells in their study. They also discriminated uniglomerular cells, however these were not TH⁺.

These discrepancies might be explained by the following technical differences: (1) Their label for dopaminergic cells was TH, not DAT (see discussion above). The fact that a uniglomerular dopaminergic cell has not been comprehensively reported so far

(but see e.g. Kosaka and Kosaka, 2009) supports the view that this cell type is likely to be labeled more efficiently via the more recent DAT-based approaches, perhaps reflecting a reduced activity of these neurons compared to the SAC-like subtypes. Such differences in labeling efficiency may also extend to other dopaminergic cell populations, e.g. the “undersized” cells reported here. Uniglomerular cells might also be generated preferably at embryonic/perinatal times, since they were mostly detected in juvenile animals and much less in adult rats.

(2) Whether a glomerulus was classified as innervated or not might also have differed, due to the different reconstruction technique and detail.

(3) Kiyokage et al. (2010) reconstructed detailed morphologies in biocytin-filled cells in fixed slices with a confocal microscope, whereas we recorded our image stacks in acute tissue with TPLSM. Since the axons of short-axon like cells are particularly thin (hence also the historical insufficient axonal staining and misnaming of short-axon cells), we presume that the fluorescence from these structures was too weak for sufficient resolution in our scans, except for the initial parts of some axons (probably e.g. Fig. 2 A – D, 4 A and C; Blackman et al., 2014) . On the other hand, the biocytin method is much more sensitive and therefore should recover axonal processes (also pointed out by Kosaka and Kosaka, 2011) although Kiyokage et al. (2010) chose to not differentiate between dendrites and axons because of their similar appearance. Notably, so far the existence of axons has not been demonstrated directly for dopaminergic glomerular neurons except for the large lateral association neurons (Chand et al., 2015). However, we clearly see axon-like structures in the uniglomerular subtype and also consider it highly likely that DAT+ clasping cells feature axons.

Although Kiyokage et al. (2010) have not specifically reported clasp-like structures, some of their cells might show such features even though this cannot be properly judged from z-projections (e.g. their Fig. 5 B, top panels). Therefore we propose that their oligoglomerular subtype is likely to overlap at least to some extent with the DAT+ clasping cells reported here. In this case the extended glomerular innervation of this subtype would be performed by its axon (which is lacking from our reconstructions), while the dendrites project mostly interglomerularly with the exception of a single “home glomerulus” that is superficially innervated (see results). In line with this view DAT+ cell bodies were reported to respond to odors in a sparse fashion which is highly correlated across a given glomerulus (Banerjee et al. 2015) – an observation that is most parsimoniously explained as the result of a predominantly local dendritic

innervation. This description yields further implications for the input and output connectivity of DAT+ clasping cells (see below).

Since Kiyokage et al. (2010) report on two different main sources of input to oligoglomerular cells (ETC driven versus olfactory nerve driven) it is conceivable that a further diversification of this subtype will emerge. If clasping cells do indeed overlap with oligoglomerular cells, we would expect them to be primarily driven by ETCs because of their dendritic innervation pattern. A possible umbrella-term to encompass both these dopaminergic juxtaglomerular cells that are in contact with several glomeruli with mainly interglomerular dendritic projections could be “local range dopaminergic neurons”.

Interspecies differences between mice and rats have been observed with respect to glomerular neuron subtype composition (Kosaka and Kosaka, 2005). We were able to find all the discriminated cell types – the two new subtypes, clasping cells and uniglomerular cells, as well as large lateral association cells, undersized cells and a substantial amount of intermediate cells in both juvenile rats and adult mice using FFN staining. Although the overall number of cells in this study is not sufficient to provide a sound estimate of relative abundances of cell types, most cell types occurred with roughly similar frequencies with the exception of DAT+ uniglomerular cells that were far less common in the adult mouse compared to the juvenile rat. This observation might be explained by an increasing relative fraction of clasping cells with age due to neurogenesis and thus is probably not mainly related to interspecies differences (Fig. 7 B). Shifts in subtype composition have been previously observed for bulbar interneurons in studies on adult neurogenesis (Ninkovic et al., 2007; Batista-Brito et al., 2008; Adam and Mizrahi, 2011). In our study, neurogenesis is also a probable factor contributing to change in subtype composition, if considering the inducible DAT-GFP line as a model with an increased proportion of adult-born cells compared to the other populations. In this scenario, neurogenesis possibly has an almost negligible contribution to the uniglomerular subtype and a very substantial influence on the clasping cell subtype. In future research, it would be interesting to investigate subtype-specifically, if cell types and subtype morphology can be determined by the cell age and not only by animal age (Livneh and Mizrahi, 2011).

Both FFN and DAT-GFP very rarely labeled astrocytes. Apparently this subset of astrocytes expresses the dopamine transporter and therefore could participate at least in the neurotransmitter clearance in the glomerular layer (as reported for other brain areas, cf. Karakaya et al., 2007). Other astrocytes in the bulb were reported to directly participate in neurotransmission (Kozlov et al., 2006). The contribution of astrocytes to bulbar network function will therefore be an interesting target for future research.

3. Function of DAT+ clasping cells

Electrophysiological measurements of excitability and dendritic TPLSM Ca^{2+} imaging were focused on the DAT-GFP+ clasping cells. First of all, because the function of the hitherto not described clasp structures is of particular interest. In addition, as mentioned above, FFN+ cells were often compromised in their physiological properties, and thus were not suitable for investigation of active properties. Overall, adult-induced DAT+ clasping cells would readily respond with trains of action potentials to prolonged depolarization. We never observed low-threshold spikes, a firing pattern that was found to be characteristic for external tufted cells and also for a subset of classical periglomerular cells, but less for short-axon like cells (McQuiston and Katz, 2001; Hayar et al., 2004). A previous study of TH+ bulbar neurons has already isolated various active conductances (Na_v , K_v and Ca_v currents), with no difference between the small and the large DA neuron subtype (Pignatelli et al., 2005).

Highly active dendrites are rather common within the circuitry of the olfactory bulb, due to its various dendrodendritic synaptic interactions. In several neuron types Ca^{2+} dynamics evoked by (backpropagating) action potentials, $(\Delta F/F)_{AP}$, have been used as a readout for the presence of active dendritic conductances. Mitral cells feature a complex dendritic tuft at the terminus of their apical dendrite that widely innervates the neuropil of a single glomerulus and is known to perform reciprocal dendrodendritic interactions with various partners (Pinching and Powell, 1971b). These tufts were observed to show higher $(\Delta F/F)_{AP}$ than the apical dendrite just below the tuft, and to increase with distance from the root of the tuft (Yuan and Knopfel, 2006) even though the apical dendrite itself is also known to be highly active (Chen et al., 1997). External tufted cells, which also innervate the glomerular neuropil and are considered the theta pace-makers of the bulb (Hayar et al., 2004) display substantial $(\Delta F/F)_{AP}$, in particular

in cooperation with burst potentials. While this signal was found to decrease in more distal branches, there was a direct correlation between $(\Delta F/F)_{AP}$ amplitudes and postsynaptic signaling in JGC partners, proof of transmitter release from these dendrites (Masurkar and Chen, 2012). Other bulbar neurons include the GABAergic granule cells that show considerable $(\Delta F/F)_{AP}$ especially within their output region in the apical dendrite (Egger et al., 2003; Egger et al., 2005; Pinato and Midtgaard, 2005).

Here we find that dendrites of DAT-GFP+ clasping cells also fit the notion of releasing dendrites since they showed substantial $(\Delta F/F)_{AP}$ which did not decrease with distance from the soma. Moreover, the $(\Delta F/F)_{AP}$ signals decayed extremely slowly, which cannot be explained via buffering by the added dye and thus could promote asynchronous release of transmitter, similar to what has been suggested for granule cells (Egger and Stroh, 2009). Since dopamine has been proposed to get released only upon sufficiently strong or prolonged stimulation (Maher and Westbrook, 2008; Bundschuh et al., 2012), it is interesting to note that the remarkably slow decay of Ca^{2+} reported here will result in strong summation of both postsynaptic and AP-evoked Ca^{2+} transients within a time frame of seconds. Therefore a sequence of action potentials, whether combined with local glutamatergic input or not, is likely to foster release of dopamine, even if it occurs at a low frequency such as e.g. the prominent bulbar theta rhythm mentioned above. It remains to be elucidated whether this slow decay is a result of slow extrusion or a very high buffering capacity.

However, we did not observe any significant differences in $(\Delta F/F)_{AP}$ signals in clasping versus non-clasping dendritic compartments. Thus it seems unlikely that clasps could be exclusive or preferred release sites compared to the remainder of the dendrite, and output synapses may be located in either compartment. Therefore our findings on $(\Delta F/F)_{AP}$ do not implicate any specific function for clasps in this respect.

Alternatively, clasps might be involved in circuit formation in both juvenile and adult animals. The advent of elaborate time-lapse imaging techniques in the last few years revealed a remarkable morphological plasticity of adult-born bulbar cells throughout their life-span. This remodeling can be influenced by factors like sensory activity and animal age and affects for example synaptic turnover and dendritic branching (Mizrahi, 2007; Livneh and Mizrahi, 2011; 2012). Our observations imply that the DAT+ clasping cells may also undergo such remodeling, as is reflected by very variable structural features (branches, terminal points, number of clasps – cf. Table 1 and Fig. 7 C) of this

cell type across animal populations. In particular, the increase of the numbers of clasping structures in cells of young FFN rats to adult FFN mice to adult-induced DAT-GFP mice suggests a special importance of clasps for adult-born neurons, possibly during early time points of integration. In this respect, they might also serve as compartments sensing some kind of input from resident structures – diverse chemical signals and synaptic activity are known to support integration of adult-born cells (Whitman and Greer, 2007b; Khodosevich et al., 2013; Garcia et al., 2014b; Kovalchuk et al., 2015). In this case a migrating cell might develop clasps as guiding structures to its final spatial position in the glomerular layer. Therefore the clasps might even be transient in nature, helping the cell survive, migrate or integrate into the glomerular circuitry. Such a special, transient function could be related to the reported increased sensitivity and odorant promiscuity for adult-born cells in the olfactory bulb in early stages of integration (Livneh et al., 2014). If those structures were not transient but persistent, they might still change in complexity, which could also explain their different appearance and frequency of occurrence in the three populations. Thus time-lapse in-vivo imaging in conjunction with specific markers for adult-born DAT+ cells might be required to further elucidate a potential role of clasps in circuit integration.

Because of the diversity of morphologies that we found it is conceivable that, as Livneh et al. (2014) suggests, adult-born cells in the olfactory bulb do not serve a predetermined role in OB function, but rather integrate and adapt according to circuit demands. They might specifically influence computations in distinct glomerular or inter-glomerular compartments in response to changing odor environments (Adam and Mizrahi, 2011; Livneh and Mizrahi, 2012; Bonzano et al., 2014).

In future studies, a larger sample might refine subtype classification by including other criteria such as odor responses, conductance profiles or molecular markers. In any case, a temporal dimension that takes into account both animal age and cell age is important for a realistic portrayal of glomerular neuron subtype diversity.

5. Circuits: possible DAT+ cell inputs and outputs

5.1. Conclusions from innervation analysis

The detailed innervation analysis used here allowed to quantitatively differentiate cell types by their peri- and intraglomerular innervation patterns. A similar approach was used previously to characterize glomerular innervation by projection neurons in the

silkmoth (Kazawa et al., 2009; Namiki and Kanzaki, 2011). In addition, we have performed the analysis in relation to different glomerular volumes (shells vs. core, Fig. 6), which allowed us to characterize the special dendritic innervation pattern of the DAT+ clasping cell type. It either only ramifies in interglomerular space (sometimes very closely to the intraglomerular neuropil) or sometimes also clearly inside the intraglomerular neuropil of one single home glomerulus where it is mostly restricted to the superficial volume (inner shell).

We hypothesize that this superficial projection might correspond to a targeting of the so-called intermediate zone, which denotes a transition between periglomerular and intraglomerular neuropil as described by Pinching and Powell (1971c; b) – for these considerations one has to bear in mind that the term for periglomerular cells used in this reference might include more cell types than our restricted use of this term (see methods): Ultrastructurally this zone is characterized by portions of juxtaglomerular dendrites and projecting axon terminals (possibly including tapering glial wrappings) about to enter the glomerulus, as well as specific synaptic arrangements. Additionally, the neuropil around the cell bodies shows an irregular outline and retains the ‘grainy’ characteristic of periglomerular neuropil. As to synaptic interactions in this zone, periglomerular cells receive connections from terminals of superficial short-axon or other periglomerular cells and also ETC collaterals or centrifugal fiber terminals. Another arrangement features mitral and tufted cell dendritic processes contacting a PGC via a reciprocal synapse in close proximity to another contact on the PGC by a short-axon cell terminal. Even olfactory nerve terminals can interdigitate with the periglomerular neuropil in the intermediate zone (for all observations cf. Pinching and Powell, 1971c; b). In the light of this description and our results on DAT+ cell morphologies, dopaminergic neurons are likely to take on roles of short-axon cells and other types of JGCs (mainly clasping and uniglomerular subtype, respectively).

The innervation analysis approach taken here could also easily be generalized to investigate the specific innervation of other known glomerular subcompartments such as olfactory nerve termination zones and dendrodendritic interaction zones (Chao et al., 1997; Kasowski et al., 1999; Kosaka and Kosaka, 2005). For example, olfactory nerve termination zones could be reconstructed based on presynaptic fluorescent labeling (Wachowiak and Cohen, 2001) to determine their specific innervation by the dendrites of glomerular layer neurons.

5.2. Targets of clasp structures

Which cell type might be actually targeted by the clasp structures themselves? Since the clasped cells were not found to be FFN+ (dopaminergic) and their somatic size distribution did not encompass very large cells, it is unlikely that large lateral association neurons are contacted by clasps. Previous studies have described functional influence of dopaminergic cells on mitral and tufted cells (Bundschuh et al., 2012; Livneh et al., 2014; Banerjee et al., 2015), both of which can be excluded as candidate partners because of their soma size and location. Additionally, ETCs and GABAergic JGCs are known to be targeted by dopaminergic cells (Pinching and Powell, 1971a; c; Maher and Westbrook, 2008; Liu et al., 2013), which would conform with the measured cell body sizes of clasped cells.

Our calcium imaging experiments support a putative presynaptic function of clasping structures. However, it remains to be proven at the ultrastructural level that clasps are indeed output structures. If so, clasps would be a rare example for chemical dendrosomatic synapses, which so far have been found mainly in sympathetic ganglia and in type S granule cells which innervate mitral cell bodies (Naritsuka et al., 2009).

5.3. Further glomerular synaptic interactions of DAT+ cells

Due to the mostly interglomerular dendritic projection, most sensory synaptic activation of DAT+ clasping cells is likely to be provided in feed-forward mode via ETCs, which was also recently corroborated for DAT+ JGCs in general (Kiyokage et al., 2010; Adam et al., 2014; Banerjee et al., 2015). A direct OSN activation of DAT+ clasping cells is only probable via an innervated home glomerulus although olfactory nerve fibers can occasionally also reach the intermediate neuropil (Pinching and Powell, 1971c). On the other hand, since most of the clasping cells' dendrites are restricted to the environment of one particular home glomerulus it is likely that most (feed-forward) drive will actually originate from a single odorant receptor type.

Since the dendrites of DAT+ uniglomerular cells mostly innervated intraglomerular neuropil these neurons are expected to receive inputs from intraglomerular synapses similar to other periglomerular neurons. If these cells indeed release dopamine from their dendrites (as also implied by the occurrence of regular FFN+ puncta in the

neuropil observed here) they could provide dopaminergic signaling to all kinds of intraglomerular synaptic arrangements. Little is known on the spread and function of classical PGN axonal projections (Nagayama et al., 2014), thus also the projections of DAT+ uniglomerular cell axons remain to be elucidated.

In addition, DAT+ cell types in general also receive inputs via gap-junctions or centrifugal fibers (Pinching and Powell, 1971c; Banerjee et al., 2015). Inhibitory control of dopaminergic JGNs has barely been investigated so far, but might involve contacts from classical GABAergic periglomerular cells, other dopaminergic JGNs and possibly autoinhibition, as well as centrifugal fibers, e.g. cholinergic input (Pinching and Powell, 1971c; a; Maher and Westbrook, 2008; Pignatelli and Belluzzi, 2008; Nagayama et al., 2014).

Many exotic cell contacts have been observed in glomerular circuits, like dendro-dendritic, dendro-somatic and somato-somatic contacts, mainly between ETCs and PGCs (Pinching and Powell, 1971a). PGCs were mostly identified by their soma locations, which may also have included several subtypes of dopaminergic cells reported in this manuscript. As somato-somatic contacts were close to the projection cell axon hillock (Pinching and Powell, 1971a), this connection might exert strong influence on bulbar output. Further ultrastructural studies that account for the high neuronal subtype diversity in the glomerular layer and also contacts from other bulbar layers as well as centrifugal terminals from cortical and neuromodulatory centers (Matsutani and Yamamoto, 2008) are needed to disentangle the complex glomerular circuitry.

So far, GABAergic and dopaminergic signaling from dopaminergic juxtaglomerular cells has not been studied at the level of individual synapses yet (Maher and Westbrook, 2008; Borisovska et al., 2013; Liu et al., 2013). The functional properties of these synapses are likely to turn out as yet another cornerstone for the functional versatility of dopaminergic cells. In any case, due to the broad complementary dendritic and axonal innervation patterns the diverse ensemble of DA neuron subtypes described here is likely to be involved in highly various aspects of glomerular processing. Thus our study fortifies the essential, broad role of dopamine in odor sensing.

Our findings also help to explain the strong diversity of odor response patterns of DAT+ cells observed *in vivo* by Banerjee et al. (2015), since dissimilar cell types are unlikely to respond in unison: due to the complementary innervation patterns demonstrated here, they will be activated and modulated by odorants via different synaptic pathways. Further *in vivo* studies followed by morphological reconstruction are required to unravel the response patterns of the individual subtypes.

Other acknowledgments.

We would like to thank Hortenzia Jacobi and Anne Pietryga-Krieger for technical assistance and Ilona Grunwald Kadow and Magdalena Götz for comments on the manuscript and to Magdalena Götz for support in obtaining funding.

Conflict of interest statement.

No conflicts.

Role of authors.

All authors take responsibility for the integrity of the data and the accuracy of the data analysis. Study concept and design: W.B., V.E. Acquisition of data: W.B. and T.O.J., histology W.B. and J.N.. Analysis and interpretation of data: W.B., V.E. T.O.J. and M.L.. Figure preparation W.B., (supplement also T.O.J.). Drafting of the manuscript: W.B. and V.E.. Critical revision of the manuscript for important intellectual content: M. L. Statistical analysis: W.B. and V.E.. Obtained funding: V.E., J.N.. Administrative, technical, and material support: W.B., T.O.J., V.E., M.L., J.N.. Study supervision: W.B. and V.E.

References

- Adam Y, Livneh Y, Miyamichi K, Groysman M, Luo L, Mizrahi A. 2014. Functional transformations of odor inputs in the mouse olfactory bulb. *Frontiers in Neural Circuits* 8.
- Adam Y, Mizrahi A. 2011. Long-Term Imaging Reveals Dynamic Changes in the Neuronal Composition of the Glomerular Layer. *The Journal of Neuroscience* 31(22):7967-7973.
- Ansari KA, Johnson A. 1975. Olfactory function in patients with Parkinson's disease. *J Chronic Dis* 28(9):493-497.
- Bailey MS, Shipley MT. 1993. Astrocyte subtypes in the rat olfactory bulb: morphological heterogeneity and differential laminar distribution. *J Comp Neurol* 328(4):501-526.
- Baker H. 1990. Unilateral, neonatal olfactory deprivation alters tyrosine hydroxylase expression but not aromatic amino acid decarboxylase or gaba immunoreactivity. *Neuroscience* 36(3):761-771.
- Banerjee A, Marbach F, Anselmi F, Koh MS, Davis MB, Garcia da Silva P, Delevich K, Oyibo HK, Gupta P, Li B, Albeanu DF. 2015. An Interglomerular Circuit Gates Glomerular Output and Implements Gain Control in the Mouse Olfactory Bulb. *Neuron* 87(1):193-207.
- Batista-Brito R, Close J, Machold R, Fishell G. 2008. The distinct temporal origins of olfactory bulb interneuron subtypes. *Journal of Neuroscience* 28(15):3966-3975.
- Blackman AV, Grabuschnig S, Legenstein R, Sjöström PJ. 2014. A comparison of manual neuronal reconstruction from biocytin histology or 2-photon imaging: morphometry and computer modeling. *Front Neuroanat* 8:65.
- Bonzano S, Bovetti S, Fasolo A, Peretto P, De Marchis S. 2014. Odour enrichment increases adult-born dopaminergic neurons in the mouse olfactory bulb. *Eur J Neurosci* 40(10):3450-3457.
- Borisovska M, Bensen AL, Chong G, Westbrook GL. 2013. Distinct modes of dopamine and GABA release in a dual transmitter neuron. *J Neurosci* 33(5):1790-1796.
- Brunjes PC, Smith-Crafts LK, McCarty R. 1985. Unilateral odor deprivation: effects on the development of olfactory bulb catecholamines and behavior. *Brain Res* 354(1):1-6.
- Bundschuh ST, Zhu P, Scharer YP, Friedrich RW. 2012. Dopaminergic modulation of mitral cells and odor responses in the zebrafish olfactory bulb. *J Neurosci* 32(20):6830-6840.
- Cardona A, Saalfeld S, Schindelin J, Arganda-Carreras I, Preibisch S, Longair M, Tomancak P, Hartenstein V, Douglas RJ. 2012. TrakEM2 software for neural circuit reconstruction. *PLoS One* 7(6):e38011.
- Carleton A, Petreanu LT, Lansford R, Alvarez-Buylla A, Lledo PM. 2003. Becoming a new neuron in the adult olfactory bulb. *Nat Neurosci* 6(5):507-518.
- Cave JW, Baker H. 2009. Dopamine systems in the forebrain. *Advances in experimental medicine and biology* 651:15-35.
- Chand AN, Galliano E, Chesters RA, Grubb MS. 2015. A distinct subtype of dopaminergic interneuron displays inverted structural plasticity at the axon initial segment. *J Neurosci* 35(4):1573-1590.
- Chao TI, Kasa P, Wolff JR. 1997. Distribution of astroglia in glomeruli of the rat main olfactory bulb: Exclusion from the sensory subcompartment of neuropil. *The Journal of Comparative Neurology* 388(2):191-210.
- Chen WR, Midtgaard J, Shepherd GM. 1997. Forward and backward propagation of dendritic impulses and their synaptic control in mitral cells. *Science* 278(5337):463-467.
- Coopersmith R, Weihmuller FB, Kirstein CL, Marshall JF, Leon M. 1991. Extracellular dopamine increases in the neonatal olfactory bulb during odor preference training. *Brain Research* 564(1):149-153.
- Egger V, Nevian T, Bruno RM. 2008. Subcolumnar dendritic and axonal organization of spiny stellate and star pyramid neurons within a barrel in rat somatosensory cortex. *Cereb Cortex* 18(4):876-889.
- Egger V, Stroth O. 2009. Calcium buffering in rodent olfactory bulb granule cells and mitral cells. *J Physiol* 587(Pt 18):4467-4479.

- Egger V, Svoboda K, Mainen ZF. 2003. Mechanisms of lateral inhibition in the olfactory bulb: Efficiency and modulation of spike-evoked calcium influx into granule cells. *J Neurosci* 23:7551-7558.
- Egger V, Svoboda K, Mainen ZF. 2005. Dendrodendritic synaptic signals in olfactory bulb granule cells: Local spine boost and global low-threshold spike. *J Neurosci* 25:3521-3530.
- Gall CM, Hendry SH, Seroogy KB, Jones EG, Haycock JW. 1987. Evidence for coexistence of GABA and dopamine in neurons of the rat olfactory bulb. *J Comp Neurol* 266(3):307-318.
- Garcia I, Bhullar PK, Tepe B, Ortiz-Guzman J, Huang L, Herman AM, Chaboub L, Deneen B, Justice NJ, Arenkiel BR. 2014a. Local corticotropin releasing hormone (CRH) signals to its receptor CRHR1 during postnatal development of the mouse olfactory bulb. *Brain Struct Funct*.
- Garcia I, Quast KB, Huang L, Herman AM, Selever J, Deussing JM, Justice NJ, Arenkiel BR. 2014. Local CRH signaling promotes synaptogenesis and circuit integration of adult-born neurons. *Dev Cell* 30(6):645-659.
- Hayar A, Karnup S, Ennis M, Shipley MT. 2004. External tufted cells: a major excitatory element that coordinates glomerular activity. *J Neurosci* 24(30):6676-6685.
- Hellwig B. 2000. A quantitative analysis of the local connectivity between pyramidal neurons in layers 2/3 of the rat visual cortex. *Biol Cybern* 82(2):111-121.
- Heyt J, Diaz J. 1975. Pressure drop in flat-oval spiral air duct. *ASHRAE Transactions* 81(Part 2):221-230.
- Huisman E, Uylings HB, Hoogland PV. 2004. A 100% increase of dopaminergic cells in the olfactory bulb may explain hyposmia in Parkinson's disease. *Mov Disord* 19(6):687-692.
- Karakaya S, Kipp M, Beyer C. 2007. Oestrogen regulates the expression and function of dopamine transporters in astrocytes of the nigrostriatal system. *J Neuroendocrinol* 19(9):682-690.
- Kasowski HJ, Kim H, Greer CA. 1999. Compartmental organization of the olfactory bulb glomerulus. *J Comp Neurol* 407(2):261-274.
- Kazawa T, Namiki S, Fukushima R, Terada M, Soo K, Kanzaki R. 2009. Constancy and variability of glomerular organization in the antennal lobe of the silkworm. *Cell Tissue Res* 336(1):119-136.
- Khodosevich K, Lazarini F, von Engelhardt J, Kaneko H, Lledo PM, Monyer H. 2013. Connective tissue growth factor regulates interneuron survival and information processing in the olfactory bulb. *Neuron* 79(6):1136-1151.
- Kiyokage E, Pan YZ, Shao Z, Kobayashi K, Szabo G, Yanagawa Y, Obata K, Okano H, Toida K, Puche AC, Shipley MT. 2010. Molecular identity of periglomerular and short axon cells. *J Neurosci* 30(3):1185-1196.
- Kosaka K, Kosaka T. 2005. synaptic organization of the glomerulus in the main olfactory bulb: compartments of the glomerulus and heterogeneity of the periglomerular cells. *Anat Sci Int* 80(2):80-90.
- Kosaka K, Kosaka T. 2007. Chemical properties of type 1 and type 2 periglomerular cells in the mouse olfactory bulb are different from those in the rat olfactory bulb. *Brain Res* 1167:42-55.
- Kosaka T, Komada M, Kosaka K. 2008. Sodium channel cluster, betaIV-spectrin and ankyrinG positive "hot spots" on dendritic segments of parvalbumin-containing neurons and some other neurons in the mouse and rat main olfactory bulbs. *Neurosci Res* 62(3):176-186.
- Kosaka T, Kosaka K. 2009. Two types of tyrosine hydroxylase positive GABAergic juxtglomerular neurons in the mouse main olfactory bulb are different in their time of origin. *Neurosci Res* 64(4):436-441.
- Kosaka T, Kosaka K. 2011. "Interneurons" in the olfactory bulb revisited. *Neurosci Res* 69(2):93-99.
- Kovalchuk Y, Homma R, Liang Y, Maslyukov A, Hermes M, Thestrup T, Griesbeck O, Ninkovic J, Cohen LB, Garaschuk O. 2015. In vivo odourant response properties of migrating adult-born neurons in the mouse olfactory bulb. *Nat Commun* 6:6349.
- Kozlov AS, Angulo MC, Audinat E, Charpak S. 2006. Target cell-specific modulation of neuronal activity by astrocytes. *Proc Natl Acad Sci U S A* 103(26):10058-10063.

- Liu S, Plachez C, Shao Z, Puche A, Shipley MT. 2013. Olfactory bulb short axon cell release of GABA and dopamine produces a temporally biphasic inhibition-excitation response in external tufted cells. *J Neurosci* 33(7):2916-2926.
- Livneh Y, Adam Y, Mizrahi A. 2014. Odor processing by adult-born neurons. *Neuron* 81(5):1097-1110.
- Livneh Y, Mizrahi A. 2011. Long-term changes in the morphology and synaptic distributions of adult-born neurons. *J Comp Neurol* 519(11):2212-2224.
- Livneh Y, Mizrahi A. 2012. Experience-dependent plasticity of mature adult-born neurons. *Nat Neurosci* 15(1):26-28.
- Lledo PM, Alonso M, Grubb MS. 2006. Adult neurogenesis and functional plasticity in neuronal circuits. *Nat Rev Neurosci* 7(3):179-193.
- Longair MH, Baker DA, Armstrong JD. 2011. Simple Neurite Tracer: open source software for reconstruction, visualization and analysis of neuronal processes. *Bioinformatics* 27(17):2453-2454.
- Maher BJ, Westbrook GL. 2008. Co-transmission of dopamine and GABA in periglomerular cells. *J Neurophysiol* 99(3):1559-1564.
- Masurkar AV, Chen WR. 2012. The influence of single bursts versus single spikes at excitatory dendrodendritic synapses. *Eur J Neurosci* 35(3):389-401.
- Matsutani S, Yamamoto N. 2008. Centrifugal innervation of the mammalian olfactory bulb. *Anatomical science international* 83(4):218-227.
- McQuiston AR, Katz LC. 2001. Electrophysiology of interneurons in the glomerular layer of the rat olfactory bulb. *J Neurophysiol* 86(4):1899-1907.
- Mizrahi A. 2007. Dendritic development and plasticity of adult-born neurons in the mouse olfactory bulb. *Nat Neurosci* 10(4):444-452.
- Mori T, Tanaka K, Buffo A, Wurst W, Kuhn R, Gotz M. 2006. Inducible gene deletion in astroglia and radial glia--a valuable tool for functional and lineage analysis. *Glia* 54(1):21-34.
- Nagayama S, Homma R, Imamura F. 2014. Neuronal organization of olfactory bulb circuits. *Front Neural Circuits* 8:98.
- Nakamura T, Kurokawa K, Kiyokawa E, Matsuda M. 2006. Analysis of the Spatiotemporal Activation of Rho GTPases Using Raichu Probes. *Methods in Enzymology*. Vol Volume 406: Academic Press. p 315-332.
- Namiki S, Kanzaki R. 2011. Heterogeneity in dendritic morphology of moth antennal lobe projection neurons. *J Comp Neurol* 519(17):3367-3386.
- Naritsuka H, Sakai K, Hashikawa T, Mori K, Yamaguchi M. 2009. Perisomatic-targeting granule cells in the mouse olfactory bulb. *The Journal of Comparative Neurology* 515(4):409-426.
- Ninkovic J, Mori T, Gotz M. 2007. Distinct modes of neuron addition in adult mouse neurogenesis. *J Neurosci* 27(40):10906-10911.
- Ninkovic J, Pinto L, Petricca S, Lepier A, Sun J, Rieger MA, Schroeder T, Cvekl A, Favor J, Gotz M. 2010. The transcription factor Pax6 regulates survival of dopaminergic olfactory bulb neurons via crystallin alphaA. *Neuron* 68(4):682-694.
- Panzanelli P, Bardy C, Nissant A, Pallotto M, Sassoe-Pognetto M, Lledo PM, Fritschy JM. 2009. Early synapse formation in developing interneurons of the adult olfactory bulb. *J Neurosci* 29(48):15039-15052.
- Parrish-Aungst S, Shipley MT, Erdelyi F, Szabo G, Puche AC. 2007. Quantitative analysis of neuronal diversity in the mouse olfactory bulb. *The Journal of Comparative Neurology* 501(6):825-836.
- Pignatelli A, Ackman J, Vigetti D, Beltrami A, Zucchini S, Belluzzi O. 2009. A potential reservoir of immature dopaminergic replacement neurons in the adult mammalian olfactory bulb. *Pflugers Archiv-European Journal of Physiology* 457(4):899-915.
- Pignatelli A, Belluzzi O. 2008. Cholinergic modulation of dopaminergic neurons in the mouse olfactory bulb. *Chemical senses* 33(4):331-338.
- Pignatelli A, Kobayashi K, Okano H, Belluzzi O. 2005. Functional properties of dopaminergic neurones in the mouse olfactory bulb. *J Physiol* 564(Pt 2):501-514.

- Pinato G, Midtgaard J. 2005. Dendritic sodium spikelets and low-threshold calcium spikes in turtle olfactory bulb granule cells. *J Neurophysiol* 93(3):1285-1294.
- Pinching AJ, Powell TP. 1971a. The neuron types of the glomerular layer of the olfactory bulb. *J Cell Sci* 9(2):305-345.
- Pinching AJ, Powell TP. 1971b. The neuropil of the glomeruli of the olfactory bulb. *J Cell Sci* 9(2):347-377.
- Pinching AJ, Powell TP. 1971c. The neuropil of the periglomerular region of the olfactory bulb. *J Cell Sci* 9(2):379-409.
- Rieker C, Engblom D, Kreiner G, Domanskyi A, Schober A, Stotz S, Neumann M, Yuan X, Grummt I, Schutz G, Parlato R. 2011. Nucleolar disruption in dopaminergic neurons leads to oxidative damage and parkinsonism through repression of mammalian target of rapamycin signaling. *J Neurosci* 31(2):453-460.
- Rodriguez PC, Pereira DB, Borgkvist A, Wong MY, Barnard C, Sonders MS, Zhang H, Sames D, Sulzer D. 2013. Fluorescent dopamine tracer resolves individual dopaminergic synapses and their activity in the brain. *Proc Natl Acad Sci U S A* 110(3):870-875.
- Schindelin J, Arganda-Carreras I, Frise E, Kaynig V, Longair M, Pietzsch T, Preibisch S, Rueden C, Saalfeld S, Schmid B, Tinevez JY, White DJ, Hartenstein V, Eliceiri K, Tomancak P, Cardona A. 2012. Fiji: an open-source platform for biological-image analysis. *Nat Methods* 9(7):676-682.
- Schoppa NE. 2005. Neurotransmitter mechanisms at dendrodendritic synapses in the olfactory bulb. *Dendritic Neurotransmitter Release*: Springer. p 101-115.
- Serguera C, Triaca V, Kelly-Barrett J, Banhaabouchi MA, Minichiello L. 2008. Increased dopamine after mating impairs olfaction and prevents odor interference with pregnancy. *Nat Neurosci* 11(8):949-956.
- Sholl DA. 1953. Dendritic organization in the neurons of the visual and motor cortices of the cat. *J Anat* 87(4):387-406.
- Tillerson JL, Caudle WM, Parent JM, Gong C, Schallert T, Miller GW. 2006. Olfactory discrimination deficits in mice lacking the dopamine transporter or the D2 dopamine receptor. *Behav Brain Res* 172(1):97-105.
- Wachowiak M, Cohen LB. 2001. Representation of odorants by receptor neuron input to the mouse olfactory bulb. *Neuron* 32(4):723-735.
- Whitman MC, Greer CA. 2007a. Adult-generated neurons exhibit diverse developmental fates. *Dev Neurobiol* 67(8):1079-1093.
- Whitman MC, Greer CA. 2007b. Synaptic integration of adult-generated olfactory bulb granule cells: basal axodendritic centrifugal input precedes apical dendrodendritic local circuits. *J Neurosci* 27(37):9951-9961.
- Winner B, Cooper-Kuhn CM, Aigner R, Winkler J, Kuhn HG. 2002. Long-term survival and cell death of newly generated neurons in the adult rat olfactory bulb. *European Journal of Neuroscience* 16(9):1681-1689.
- Yuan Q, Knopfel T. 2006. Olfactory nerve stimulation-evoked mGluR1 slow potentials, oscillations, and calcium signaling in mouse olfactory bulb mitral cells. *J Neurophysiol* 95(5):3097-3104.

Figures

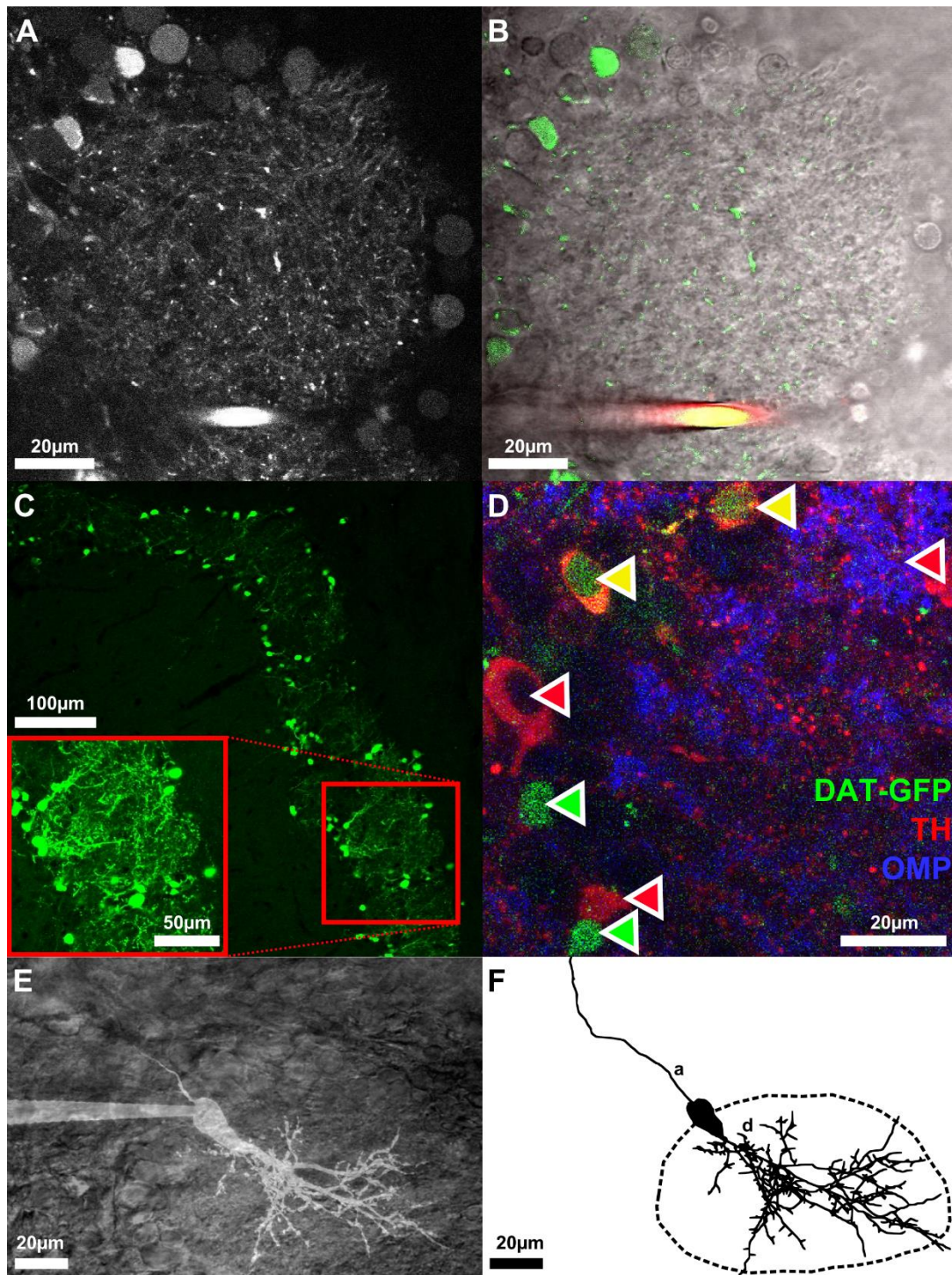


Fig. 1 DAT cell labeling techniques

(A), (B) Representative live FFN102 labeling of the glomerular and periglomerular neuropil in an adult WT mouse brain slice. (A) Green fluorescence channel of the TPLSM, with some brightly stained puncta within the glomerular neuropil as well as some labeled cell bodies at the glomerulus borders. (B) Same region in the trans-infrared detection channel shown in grey overlaid with the green FFN102 fluorescence from (A). (C) Maximal z-projection scan of an olfactory bulb slice with tamoxifen-induced DAT-GFP+ cells from adult mice surrounding the glomeruli. The inset shows a rescan at higher magnification. (D) Pseudo-colored confocal single plane image of the glomerular layer from the same transgenic mouse line with adult-induced DAT-GFP+ cells. Immunostaining against GFP is shown in green, against TH in red and against olfactory marker protein (OMP) in blue. Note the partially non-overlapping populations of DAT+ and TH+ cells depicted by colored arrows (red: exclusive TH signal, green: exclusive DAT signal, yellow: DAT and TH signal). (E) Maximal z-projection of the red channel of an Alexa-594 patch-pipette-filled neuron overlaid with the single z-plane of the trans-infrared channel that showed the maximal extent of the innervated glomerulus. (F) Maximal z-projection of the fully reconstructed cell from (E), including an outline of the glomerulus and marking putative axonal ("a") vs. dendritic ("d") structures. A similar representation of cells and glomeruli is also used in figures 2 through 4.

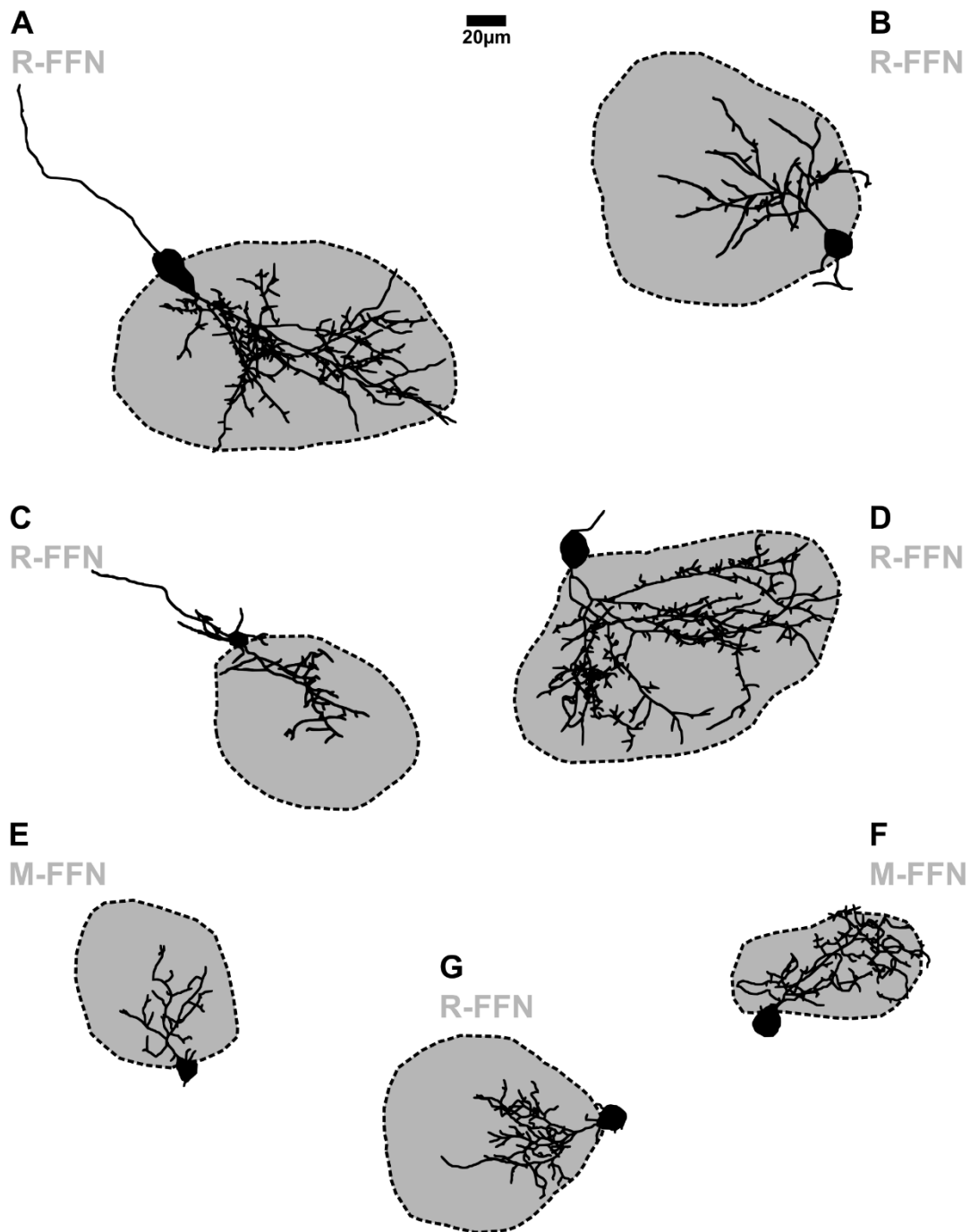


Fig. 2 DAT+ uniglomerular cells

Maximal z-projections of representative reconstructed uniglomerular cells with their corresponding surrounding glomeruli. The dark shading indicates that the glomerulus is innervated. R-FFN indicates FFN102+ cells from juvenile rat, M-FFN labels FFN102+ cells from adult wild-type mouse.

Note the differing fractions of intraglomerular innervation with sparse or no extraglomerular processes, as well as the differing degree of branching and spine density across individual cells.

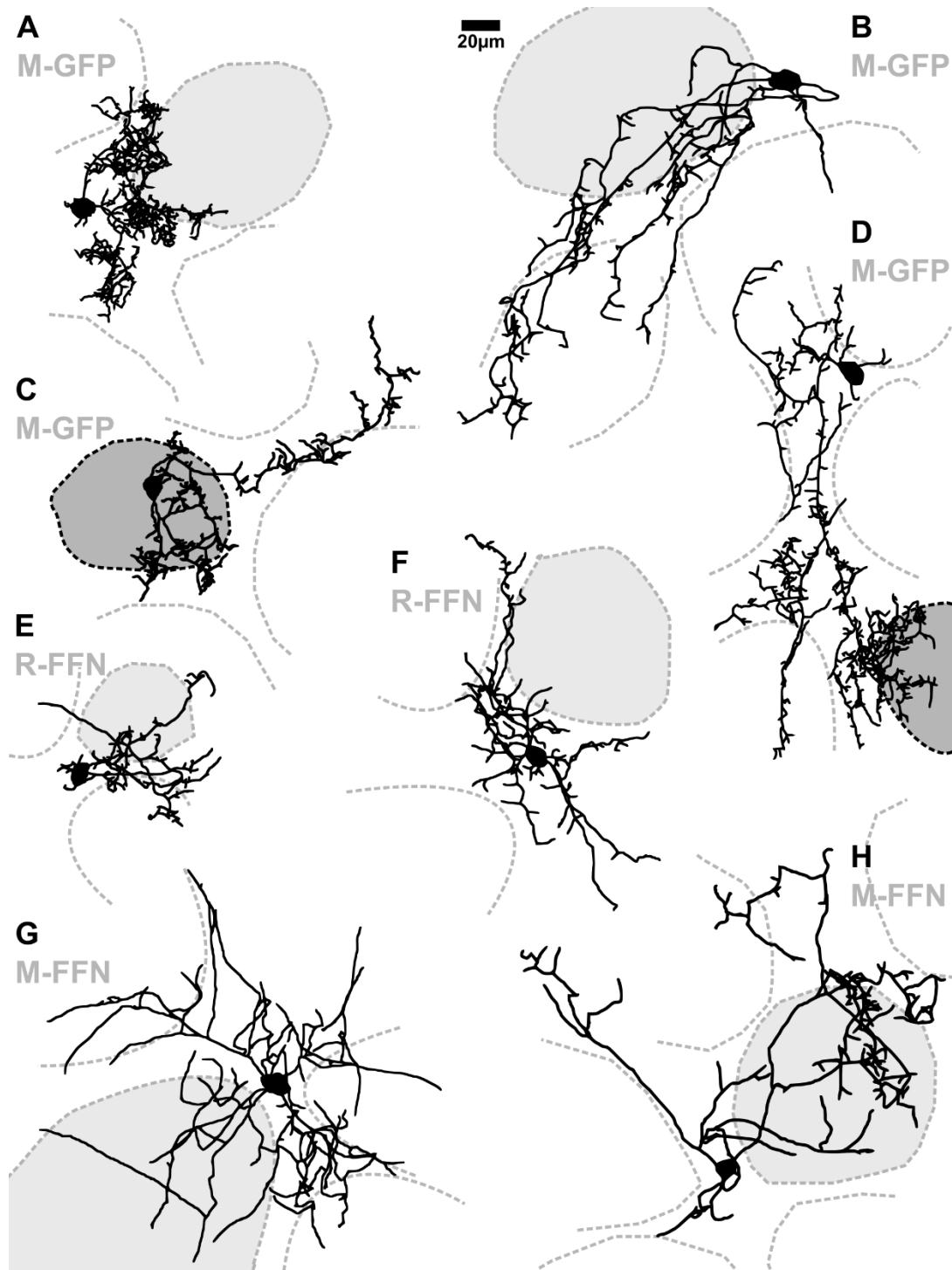


Fig. 3 DAT+ clasping cells

Maximal z-projections of representative clasp cell reconstructions with indicated surrounding glomeruli. The “home glomerulus” is shaded for each cell (see methods). Darker shades indicate that the glomerulus is innervated within its neuropil (C and D). Non-shaded structures are surrounding glomeruli, which were not innervated and do not constitute the home glomerulus. The clasp cell population includes cells from FFN102 stained juvenile wild-type rats and adult wild-type mice (R-FFN and M-FFN, respectively), as well as adult-induced GFP labeled transgenic mouse cells (M-GFP). Most dendritic structures including cell body clasps do not innervate intraglomerular neuropil, with the exception of a few superficially innervating branches, also including clasps (C and D). Note the increased complexity of M-GFP clasping cells.

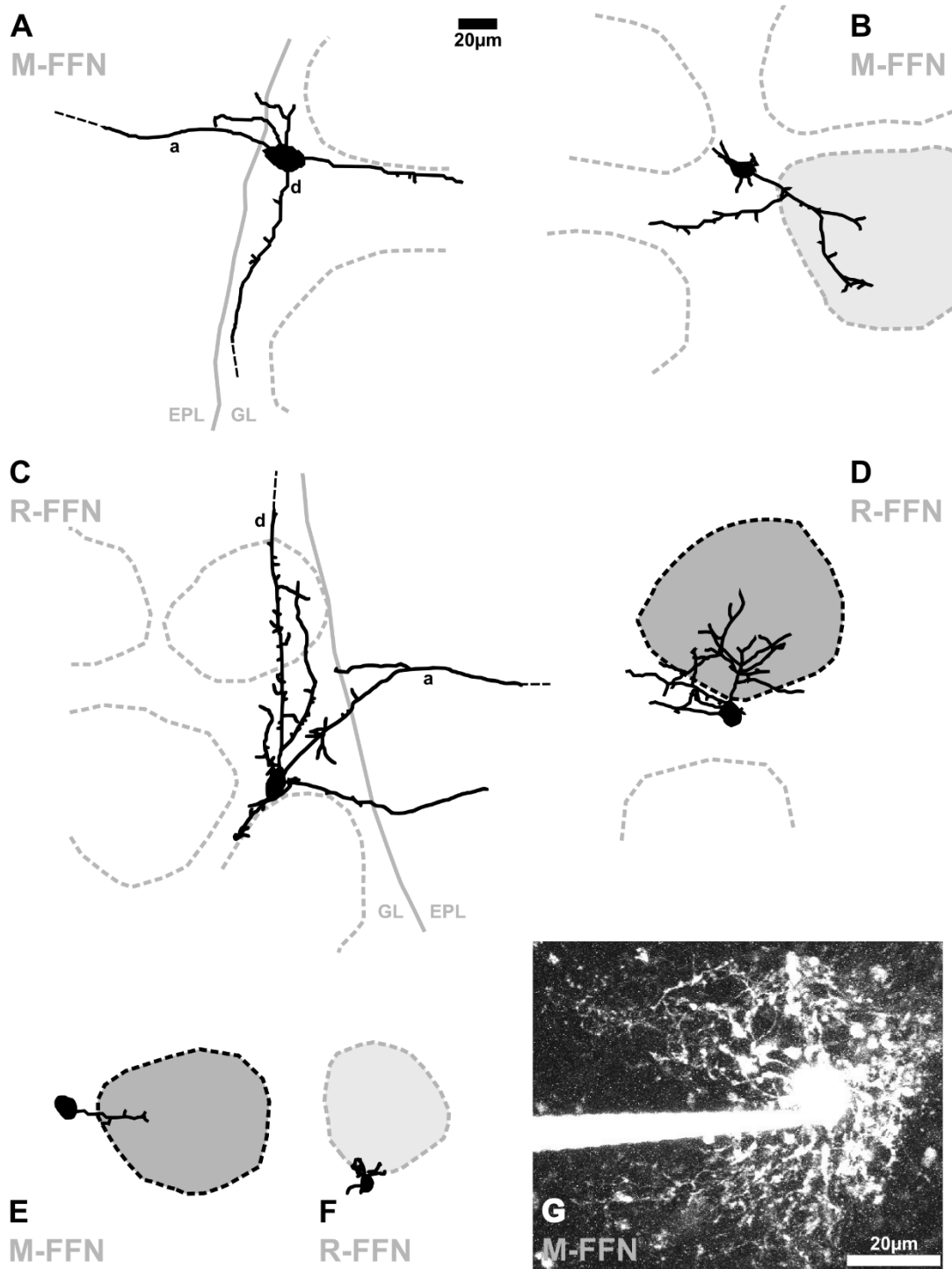


Fig. 4 Other DAT+ cells

Maximal z-projections of representative reconstructions of other cell types. Shading of glomeruli similar to Fig. 3. Panels (A) and (C) feature large lateral association cells with large dendrites (“d”) and an axon (“a”) extending from the glomerular layer (GL) into the external plexiform layer (EPL) (border to glomerular layer marked with grey solid line). Panels (B) and (D) feature “intermediate cell” morphologies. The cell in (B) is entirely extraglomerular without showing any clasp structures, the one in (D) shows substantial dendritic innervation of both the intraglomerular and extraglomerular space. Cells (E) and (F) show very reduced morphologies (“undersized cells”). (G) shows a patched FFN+ astrocyte.

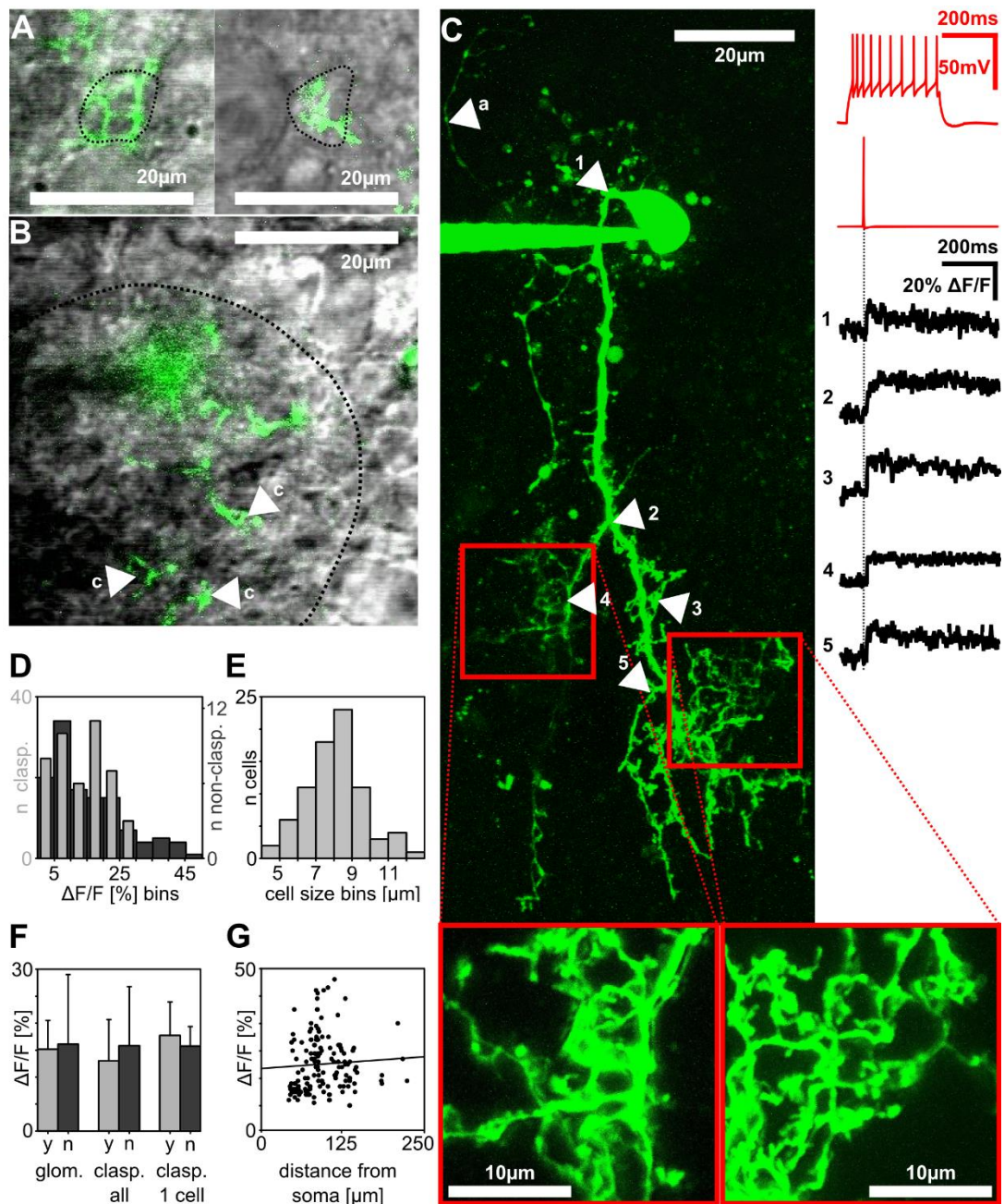


Fig. 5 DAT+ clasp cell dendrites: Clasp structures and AP-evoked Ca^{2+} signals

(A) Two different clasp structures around cell bodies (left and right), with a dotted line indicating the somatic outline of the clasped cell. (B) Exemplary, tight clasp structures (“c”) within the glomerular neuropil, with a dotted line indicating the glomerular border. (A) and (B) show single z-plane scans from the green channel overlaid with the trans-infrared channel in grey. (C) Maximal z-projection of the OGB-1 filled adult-induced clasp cell from Fig. 3 D (insets at bottom: magnified rescans of clasp structures), Numbered arrows in the scan correspond to the locations of the numbered averaged $\Delta F/F$ transients on the right, time-locked to the evoked somatic action potential (red trace directly above the black $\Delta F/F$ traces). The voltage recording on the top right shows this cell’s slightly accommodating firing pattern upon step depolarization (+120 pA current injection). In the scan, the arrow “a” points out a putative stained axon. It is thinner than the other, dendritic, structures and bears no visible spines or clasps. (D) Distributions of $\Delta F/F$ amplitudes in clasp (left y-axis) and non-clasp (right y-axis) (5% $\Delta F/F$ per bin). (E) Distribution of the size of somata contacted by clasp structures (1 μm bins starting at “4-5” μm mean diameter). (F) Average $\Delta F/F$ amplitudes in different cell substructures or neuropils. The two left bars compare population means (\pm S.D.) of calcium transients inside the home glomerulus’ neuropil (y) to outside (n). The middle bars compare population means of clasp structures (y) to non-clasp structures (n). The right bars show within-cell comparisons of the averaged clasp (y) vs. non-clasp structures (n) within individual cells. No significant differences were found in any case. (G) depicts $\Delta F/F$ versus the distance of its dendritic location from the soma. No significant correlation emerged.

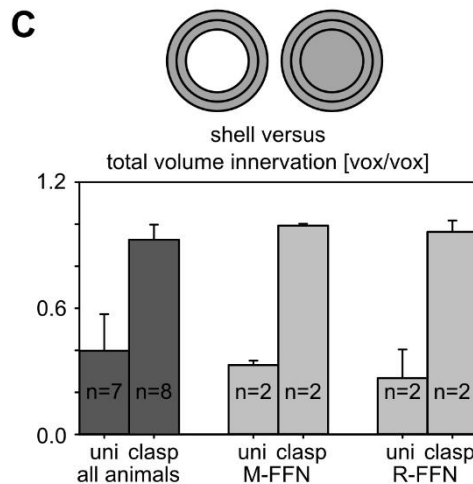
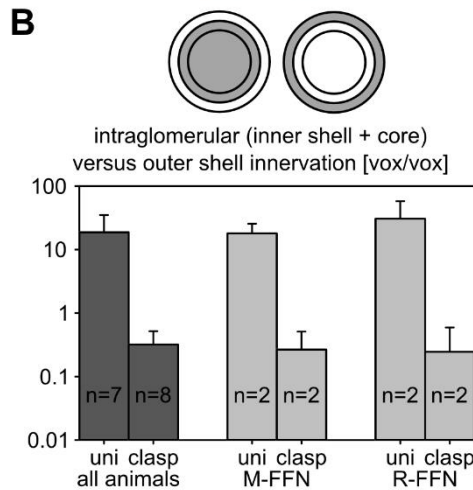
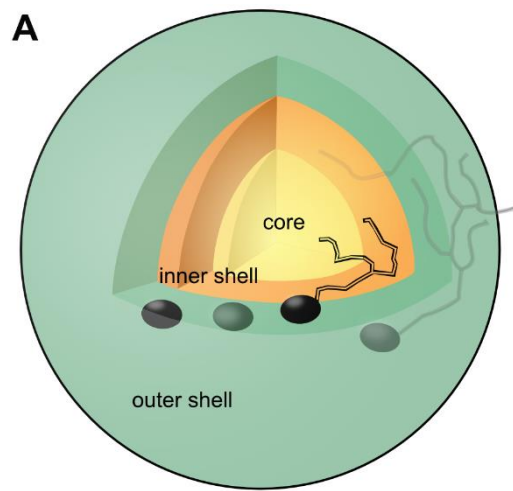


Fig. 6 Glomerular innervation by DAT+ clasp (clasp) and uniglomerular (uni) cells

(A) Schema of the three analyzed home glomerulus volumes: an outer shell comprising directly adjacent glomerular cell bodies (green), an inner shell with a depth of 1/4th of the mean glomerular radius (orange) and a core region (yellow; see methods). (B) illustrates the different shell region innervation of the two analyzed cell types – uniglomerular cell and clasp cell – as fraction of intraglomerular dendritic voxels divided by the outer shell voxels (vox) for all pooled cells (left), or two subpopulations (FFN+ mice and FFN+ rats, middle and right, respectively). (C) illustrates the fractional innervation of cell types in the combined shell volume (inner + outer shell), which incorporates the intermediate zone, relative to the total glomerular volume (shells + core), again for all pooled cells (left) or differentially for two subpopulations (FFN+ mice and FFN+ rats, middle and right, respectively).

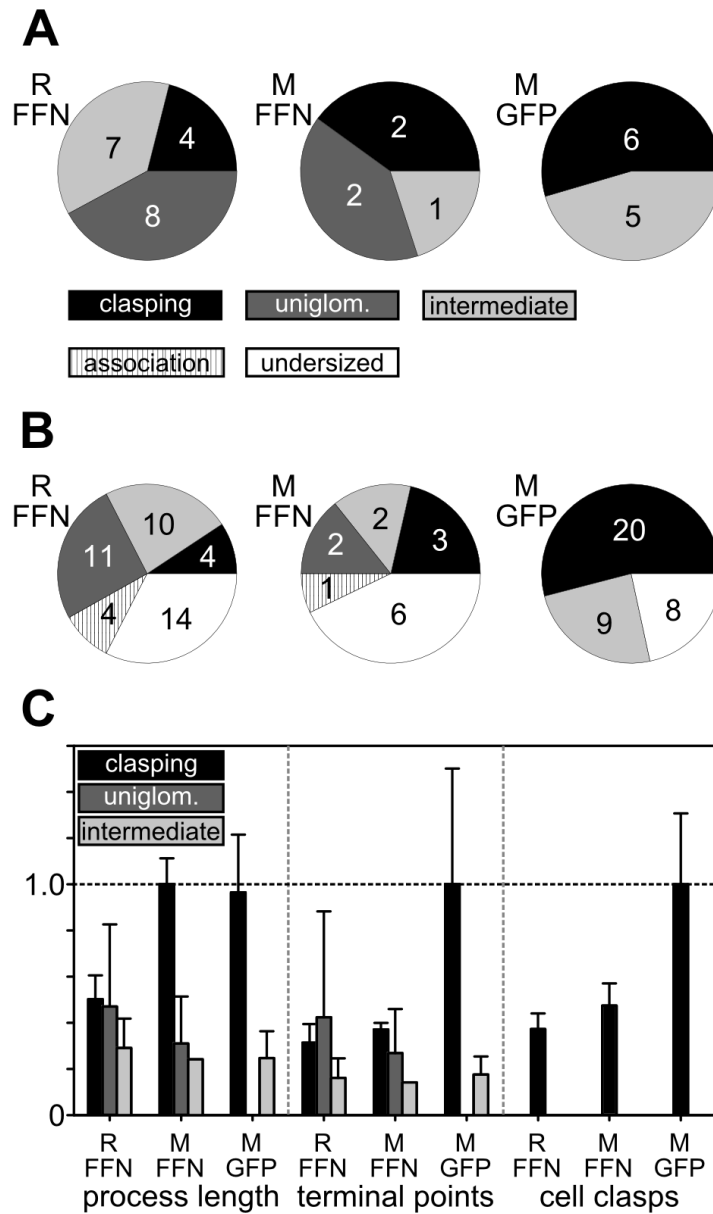


Fig. 7 Subtype distribution of cells and main morphological parameters

Panel (A) shows the population-separated distributions of three compared cell types (claspings cells, depicted in black shading in all panels, uniglomerular (uniglom.) cells - light grey, intermediate cells - dark grey), which only include perfectly captured cells used for detailed morphological parameter analysis (see Table 1 and Fig. 7 C). (B) These pie charts show the categorization of all patched cells (including also the large lateral “association” type and “undersized” cells – marked with striped and white shading, respectively). This assembly also contains incomplete scans or scans with insufficient filling (see methods/discussion). Panel (C) compares the three cell types normalized to the parameter’s respective maximum for morphological parameters, separated for each animal population (numbers from the cells pooled in A), in order to illustrate the variability between cell types, both within and across animal populations. Notice for example the higher complexity of adult-induced (M-GFP) claspings cells (black bars), compared to the wild-type populations (R-FFN or M-FFN).

Parameter	Animal	Clasping	Uniglom.	Intermediate
soma mean diameter [μm]	R-FFN	8.7 ± 1.6	10.6 ± 1.9	10.3 ± 2.1
	M-FFN	9.0 ± 2.4	8.9 ± 1.4	11.8
	M-GFP	10.4 ± 2.3		7.1 ± 1.7
primary dendrites [#]	R-FFN	3.3 ± 0.5	3.3 ± 0.9	3.5 ± 1.2
	M-FFN	5.0 ± 4.2	3 ± 0	4
	M-GFP	3.3 ± 1.2		2.2 ± 0.8
total process length [μm]	R-FFN	1138 ± 236	1068 ± 255	659 ± 289
	M-FFN	2270 ± 256	704 ± 462	547
	M-GFP	2188 ± 570		560 ± 265
branches [#]	R-FFN	162 ± 52	206 ± 217	78 ± 44
	M-FFN	185 ± 6	126 ± 93	74
	M-GFP	444 ± 278		85 ± 38
end points [#]	R-FFN	75 ± 20	102 ± 110	39 ± 20
	M-FFN	89 ± 7	65 ± 46	34
	M-GFP	240 ± 120		42 ± 19
cell clasps [#]	R-FFN	2.8 ± 0.5		
	M-FFN	3.5 ± 0.7		
	M-GFP	7.4 ± 2.3		

Table 1: Morphological parameters from cell reconstructions

Parameter numbers are stated as average (\pm S.D.). Numbers for individual cell populations are given in Fig. 7 A, with selected relative comparisons in Fig. 7 C.

Fig. S1: 3-D visualization of a reconstructed uniglomerular neuron and its innervated reconstructed glomerulus

The depicted cell corresponds to the maximal projection shown in Fig. 2 D.

Fig. S2 and 3: Visualization of clasping structures in z-stack movies

Videos depict successive focal z-images of TPLSM stacks. Each of the videos shows dendritic structures of a patched cell “clasping” around a targeted cell body. The red PMT image shows the dendritic structure, the tIR image (light-blue with dark contrast) shows the periglomerular neuropil including cell bodies. S2 shows a very complex clasping phenotype around a single cell body (in the center of the video). In this cell, the nucleus can be quite clearly seen. S3 shows a less strongly clasped cell body in the center of the video. The cell outline is quite clear in this example.

3.2. Local postsynaptic voltage-gated sodium channel activation in dendritic spines of olfactory bulb granule cells

Contributions:

Veronica Egger (V.E.) and Wolfgang Bywalez (W.B.) designed experiments and established a functional setup. W.B., Vanessa Rupprecht (V.R.), and V.E. performed experiments and analyzed data. V.E., W.B., Dinu Patirniche (D.P.) and Martin Stemmler (M.S.) wrote the manuscript. W.B., V.E. and D.P. prepared the figures. D.P. performed the simulations, in close collaboration with M.S., Andreas Herz (A.H.), V.E. and W.B.. Dénes Pálfi (De.Pa.) and Balázs Rózsa (B.R.) provided DNI-caged glutamate and data on DNI properties. W.B., V.E., D.P., A.H., M.S., and V.R. edited and revised the manuscript and all authors approved the final version.

Local Postsynaptic Voltage-Gated Sodium Channel Activation in Dendritic Spines of Olfactory Bulb Granule Cells

Wolfgang G. Bywalez,^{1,2} Dinu Patirniche,³ Vanessa Rupprecht,² Martin Stemmler,³ Andreas V.M. Herz,³ Dénes Pálfi,^{4,5} Balázs Rózsa,^{4,5} and Veronica Egger^{2,*}

¹Systems Neurobiology, Department II of Biology, Ludwig-Maximilians-Universität München, 82152 Martinsried, Germany

²Neurophysiology, Institute of Zoology, Universität Regensburg, 93040 Regensburg, Germany

³Computational Neuroscience, Department II of Biology, Ludwig-Maximilians-Universität München, 82152 Martinsried, Germany

⁴Two-Photon Imaging Center, Institute of Experimental Medicine, Hungarian Academy of Sciences, 1039 Budapest, Hungary

⁵Faculty of Information Technology and Bionics, Pázmány Péter Catholic University, 1083 Budapest, Hungary

*Correspondence: veronica.egger@ur.de

<http://dx.doi.org/10.1016/j.neuron.2014.12.051>

SUMMARY

Neuronal dendritic spines have been speculated to function as independent computational units, yet evidence for active electrical computation in spines is scarce. Here we show that strictly local voltage-gated sodium channel (Na_v) activation can occur during excitatory postsynaptic potentials in the spines of olfactory bulb granule cells, which we mimic and detect via combined two-photon uncaging of glutamate and calcium imaging in conjunction with whole-cell recordings. We find that local Na_v activation boosts calcium entry into spines through high-voltage-activated calcium channels and accelerates postsynaptic somatic depolarization, without affecting NMDA receptor-mediated signaling. Hence, Na_v -mediated boosting promotes rapid output from the reciprocal granule cell spine onto the lateral mitral cell dendrite and thus can speed up recurrent inhibition. This striking example of electrical compartmentalization both adds to the understanding of olfactory network processing and broadens the general view of spine function.

INTRODUCTION

Dendritic potentials are likely to invade spines with almost no loss. In the opposite direction, synaptic input is strongly attenuated from the spine toward the dendrite (e.g., Brown et al., 1988; Palmer and Stuart, 2009; Popovic et al., 2014). However, if the spine neck resistance is sufficiently high, synaptic spine potentials could become amplified and synapses could directly recruit high-voltage-activated conductances solely within the spine without a coincident backpropagating action potential. This idea, put forward by theorists (e.g., Jack et al., 1975; Miller et al., 1985; Segev and Rall, 1988), now finds more and more experimental support (Araya et al., 2007; Grunditz et al., 2008; Bloodgood et al., 2009; Harnett et al., 2012). Activating

voltage-dependent conductances could induce synaptic plasticity, e.g., through local NMDA receptors. As spine neck morphology governs the resistance, such synaptic plasticity could be regulated by plastic changes in spine neck length (Bloodgood and Sabatini, 2005; Grunditz et al., 2008; Harnett et al., 2012; Tonnesen et al., 2014; Araya et al., 2014). Several studies, though, have cast doubt on the notion that spine neck resistances could be sufficiently high to allow for local synaptic amplification (Koch and Zador, 1993; Svoboda et al., 1996; Palmer and Stuart, 2009). Here we provide functional evidence that the postsynaptic activation of voltage-dependent sodium and calcium conductances can occur exclusively within spines.

At the mitral cell to granule cell (GC) synapse of the olfactory bulb, postsynaptic calcium directly triggers GABA release from the reciprocal GC spine (Shepherd et al., 2007). The relevant ΔCa^{2+} most likely involves a contribution from high-voltage-activated Ca^{2+} channels (HVACCs) (Isaacson and Strowbridge, 1998; Isaacson, 2001), just as in conventional presynaptic terminals, notwithstanding the fact that their activation would require a depolarization of the spine head by ~ 20 – 40 mV. Postsynaptic Ca^{2+} signals are strictly localized to reciprocal spine heads and include substantial contributions of NMDAR- and VACC-mediated Ca^{2+} entry, while AMPARs are Ca^{2+} impermeable (Egger et al., 2003, 2005; Jardemark et al., 1997). These observations suggest that spines act as electrically isolated compartments to amplify voltage signals and thereby permit calcium entry, even though GCs exhibit somatic resting potentials both in vitro and in vivo of below -70 mV (e.g., Wellis and Scott, 1990; Margrie and Schaefer, 2003; Egger et al., 2003). The density of voltage-gated sodium channels (Na_v s) on GC dendrites is likely to be high, as indicated by the efficient, Na_v -dependent conduction of action potentials (Egger et al., 2003) and the occurrence of Na^+ spikelets in frog and turtle GC dendrites (Pinato and Midtgaard, 2005; Zelles et al., 2006). Moreover, reciprocal GC spines feature long necks, most of which contain mitochondria (Woolf et al., 1991; cf. Figures 2A, 3A, and S2D), promoting electrical isolation. All these findings support the idea that the GC reciprocal spine acts as a “mini-neuron” that can generate synaptic output on its own (Egger and Urban, 2006). Thus, we hypothesized that dendritic Na_v s boost postsynaptic Ca^{2+} entry and help activate HVACCs during unitary synaptic inputs to GC spines.

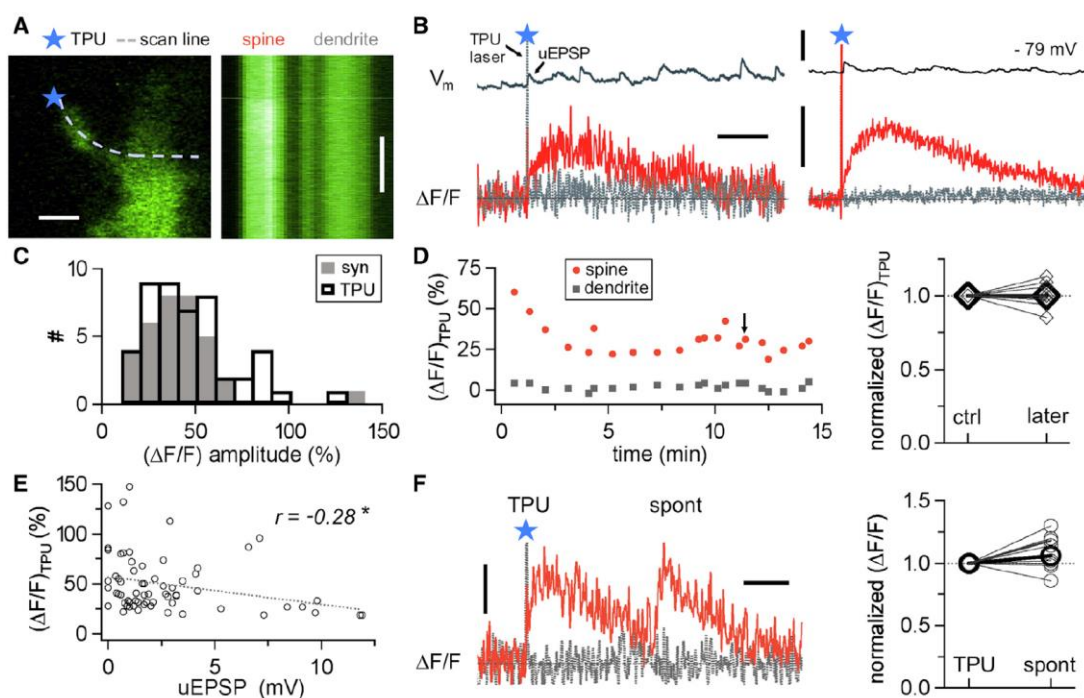


Figure 1. TPU-Evoked Ca^{2+} Spine Signals and Somatic EPSPs Are Equivalent to Synaptically Evoked Signals

(A) Left: spine and dendrite filled with $100\ \mu\text{M}$ OGB-1 with scan line and TPU site. Right: line scan during uncaging. Scale bars: $1\ \mu\text{m}$, $500\ \text{ms}$.
 (B) Left: the individual response from (A), voltage recording at soma (top), Ca^{2+} transient in spine (red) and dendrite (gray) (bottom). Right: averaged response ($n = 20$). Scale bars: 25% , $200\ \text{ms}$, $2\ \text{mV}$.
 (C) Distribution of $\Delta F/F$ amplitudes for TPU-evoked and synaptic data (latter from Egger et al., 2005).
 (D) Left: response amplitudes over time in the above experiment; arrow: individual response from (B). Right: spine-wise comparison of averaged normalized $(\Delta F/F)_{\text{TPU}}$ amplitudes separated by intervals of 10–25 min ($n = 12$, bold: average change \pm SD to 1.00 ± 0.07 of control).
 (E) Relation of $(\Delta F/F)_{\text{TPU}}$ to uEPSP amplitude ($n = 65$).
 (F) Left: individual $(\Delta F/F)_{\text{TPU}}$ along with later spontaneous response. Scale bars are as in (B). Right: spine-wise comparison of averaged normalized spontaneous and TPU-evoked amplitudes ($n = 8$, bold: average spontaneous amplitude \pm SD 1.09 ± 0.15 of TPU).
 See also Figure S1.

RESULTS

To enable postsynaptic pharmacological interference with Na_v s and HVACCs, we bypassed release from the mitral cell presynapse via two-photon uncaging (TPU) of MNI-caged glutamate (Matsuzaki et al., 2001) and the novel compound DNI-caged glutamate (Chiovini et al., 2014) in acute juvenile rat olfactory bulb slices, in combination with somatic whole-cell current-clamp recordings. Simultaneous two-photon Ca^{2+} imaging allowed for a local readout of changes in spine Ca^{2+} (Carter and Sabatini, 2004). GCs were filled with the Ca^{2+} -sensitive dye OGB-1 at a concentration of $100\ \mu\text{M}$ for comparison with previously recorded spontaneous and evoked synaptic Ca^{2+} data (Egger et al., 2003, 2005). Similarly to these studies, we exclusively investigated GC spines within the external plexiform layer of the olfactory bulb. These spines are known to predominantly form reciprocal connections with mitral and tufted cell dendrites (Price and Powell, 1970).

Uncaging-Evoked Signals Mimic Synaptic Signals

It is crucial to avoid unphysiologically strong uncaging stimuli as an undue activation of AMPARs might cause an artificial activa-

tion of voltage-dependent conductances (Sabatini and Bloodgood, 2008). We therefore investigated whether TPU would yield stable spine Ca^{2+} transients $(\Delta F/F)_{\text{TPU}}$ and somatic electrical signals similar to our previous synaptic data $(\Delta F/F)_{\text{syn}}$. Figure 1 summarizes various tests of this requirement. First, we observed that Ca^{2+} transients were strictly localized to the spine head and that properties such as the distribution of $(\Delta F/F)_{\text{TPU}}$ amplitudes, $(\Delta F/F)_{\text{TPU}}$ rise time, and decay kinetics agreed with the previously obtained evoked and spontaneous synaptic data in the absence of caged compounds ($n = 48$ spines; Figures 1A–1C; Table S1). Also, uncaging excitatory postsynaptic potentials (uEPSPs) recorded at the GC soma closely mimicked previously recorded spontaneous unitary EPSPs associated with local spine Ca^{2+} transients in the absence of caged compounds with respect to amplitude, rise time, and decay (Egger et al., 2003; Table S1). uEPSP amplitudes were weakly negatively correlated with $(\Delta F/F)_{\text{TPU}}$ amplitudes (Figure 1E), with several $(\Delta F/F)_{\text{TPU}}$ responses lacking detectable somatic EPSPs (for $\sim 15\%$ of all spines). Occasionally, we observed spontaneous $(\Delta F/F)_{\text{syn}}$ along with uncaging-evoked events in the same spine, again showing a high similarity (Figure 1F). Sufficient stability of $(\Delta F/F)_{\text{TPU}}$ and uEPSP responses was established via long-term

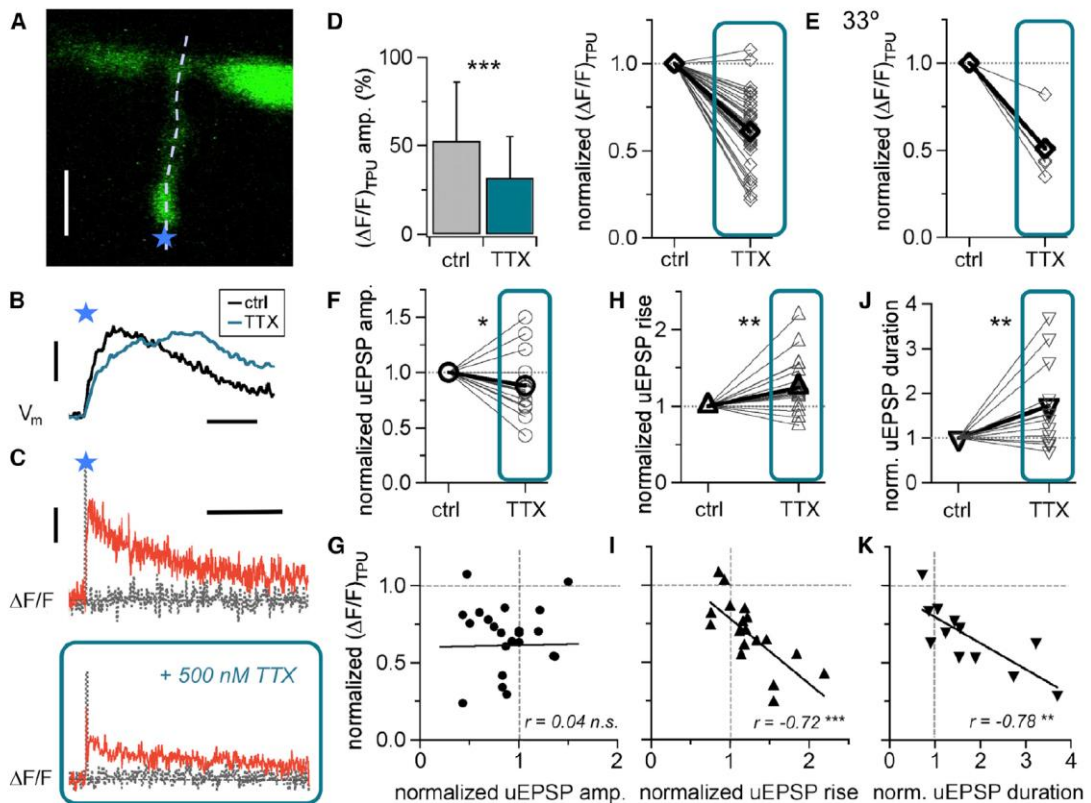


Figure 2. Sodium Channels Boost Postsynaptic Spine Ca^{2+} Signals and Accelerate the Rising Phase of the EPSP in Most Spines

(A) Spine with scan line and TPU site. Scale bar: 2 μm .

(B) Averaged uEPSP recorded at the soma during control and in the presence of TTX. Scale bars: 0.5 mV, 10 ms.

(C) Averaged $(\Delta F/F)_{\text{TPU}}$ in spine and dendrite from (A), (B) during control (top), and in the presence of TTX (bottom). Scale bars: 25%, 500 ms.

(D) Effect of TTX on $(\Delta F/F)_{\text{TPU}}$ amplitudes ($n = 34$ spines). Left: averaged absolute amplitudes \pm SD ($54\% \pm 33\%$ versus $33\% \pm 22\%$, $p < 0.0001$). Right: spine-wise amplitudes normalized to control (bold: average change \pm SD to 0.63 ± 0.20 of control).

(E) Effect of TTX on $(\Delta F/F)_{\text{TPU}}$ amplitudes at near physiological temperature ($n = 5$ spines). Spine-wise amplitudes normalized to control (bold: average change \pm SD to 0.51 ± 0.18 of control).

(F–K) Top: spine-wise parameters normalized to control (bold: average change). Bottom: individual data points for $(\Delta F/F)_{\text{TPU}}$ amplitude in TTX normalized to their control values versus the change in the respective parameter. Solid line: linear fit to data.

(F) Spine-wise analysis of uEPSP amplitudes: average \pm SD 0.88 ± 0.30 of control, $n = 23$, $p2 < 0.05$.

(G) No correlation between TTX effects on $(\Delta F/F)_{\text{TPU}}$ and uEPSP amplitude.

(H) Spine-wise analysis of uEPSP rise time change: average \pm SD 1.24 ± 0.37 of control, $n = 18$, $p2 < 0.02$.

(I) Strong correlation between TTX effects on $(\Delta F/F)_{\text{TPU}}$ amplitude and uEPSP rise time ($p2 < 0.001$).

(J) Spine-wise analysis of uEPSP duration change: average \pm SD 1.78 ± 0.98 of control, $n = 12$, $p2 < 0.05$.

(K) Strong correlation between TTX effects on $(\Delta F/F)_{\text{TPU}}$ amplitude and uEPSP duration ($p2 < 0.005$).

See also Figure S2.

recordings at individual spines over 12–30 min (ratios early to late interval $(\Delta F/F)_{\text{TPU}}$ amplitude 0.98 ± 0.08 , $n = 12$, uEPSP amplitude 1.04 ± 0.15 , $n = 7$, uEPSP rise time 1.05 ± 0.13 , $n = 7$, all not significant, Figure 1D).

As to the influence of morphological parameters, Figure S1A shows that uEPSP amplitudes did not depend on the distance of an activated spine from the GC soma, whereas there was a significant positive correlation for uEPSP rise times as expected from dendritic filtering. $(\Delta F/F)_{\text{TPU}}$ response amplitudes also tended to increase with distance, reminiscent of a similar increase in Ca^{2+} transients elicited by backpropagating action potentials (Egger et al., 2003). The spine neck length had no in-

fluence on any of these parameters (Figure S1B). Spontaneous data in the absence of caged compounds closely overlapped with these measurements (Figures S1A and S1B).

From all these observations, we infer that the Ca^{2+} and electrical signals evoked by uncaging are equivalent to synaptic signals with respect to the parameters investigated here.

Sodium Channel Blockade Decreases Spine Ca^{2+} Signals and Slows Postsynaptic Potentials

Next, we investigated a possible contribution of Na_v activation to postsynaptic GC signals (Figure 2). After blocking Na_vs by wash-in of 500 nM TTX, we observed a substantial reduction of the

$(\Delta F/F)_{\text{TPU}}$ amplitude in most spines ($n = 33$, total $p < 0.001$, [Figures 2A–2D](#)), which was uncorrelated with the distance of the spine from the soma ($r = 0.07$, $p1 > 0.5$; average distance $123 \pm 69 \mu\text{m}$) and also not correlated with the initial amplitude of $(\Delta F/F)_{\text{TPU}}$ ($r = -0.17$, $p2 = 0.33$). $(\Delta F/F)_{\text{TPU}}$ rise times were also slowed down by TTX application ([Figure S2A](#), $n = 29$, $p2 < 0.005$), indicating a rapid activation of Ca^{2+} conductances via Na_v s. Thus, Na_v s play a major role in postsynaptic GC spine Ca^{2+} entry.

Active mechanisms could increase the reliability of postsynaptic Ca^{2+} signals, as boosting could produce unitary ΔV_m depolarizations instead of the stochasticity inherent in postsynaptic AMPA/NMDAR signaling (described by e.g., [Franks et al., 2003](#)). Alternatively, if the number of available Na_v s within the spine was low and thus Na_v activation was stochastic (e.g., [Schneidman et al., 1998](#)), Na_v blockade should reduce the variability of postsynaptic Ca^{2+} signals. Upon analysis of the coefficient of variation across $(\Delta F/F)_{\text{TPU}}$ amplitudes of individual responses in a subset of experiments (those with sufficient signal-to-noise ratios in the presence of TTX), we found a consistent increase in variability in TTX (CV ratio TTX versus control 1.64 ± 0.49 , $n = 15$, $p2 < 0.001$), refuting the second hypothesis. Thus, Na_v activation serves to both increase and homogenize postsynaptic Ca^{2+} signals.

The amplitude of somatically recorded uEPSPs was slightly reduced ($p1 < 0.05$, [Figure 2F](#)), while their rise time was slowed down more strongly, by $\sim 25\%$ on average ($p < 0.02$, [Figure 2G](#)). The integral of uEPSPs did not change significantly in TTX ($0.19 \pm 0.15 \text{ mV}\cdot\text{s}$ versus $0.24 \pm 0.16 \text{ mV}\cdot\text{s}$, $p2 = 0.12$), with a considerable variance between experiments. However, upon normalization of the integral to the uEPSP amplitude the resulting uEPSP duration increased significantly in TTX, indicating a slower decay of the uEPSP ([Figure 2H](#)).

Similar changes in $(\Delta F/F)_{\text{TPU}}$ amplitude and uEPSP amplitude and rise time were also observed in control experiments conducted at near-physiological temperature ([Figure 2E](#), uEPSP data not shown, $n = 5$).

Remarkably, the relative TTX-induced increase in EPSP rise time was highly correlated with the magnitude of the blocking effect on $(\Delta F/F)_{\text{TPU}}$ ($r = -0.72$, $p < 0.001$, $n = 18$, [Figure 2I](#)). Thus, the more uncaging-evoked local Ca^{2+} signals were reduced by TTX, the more the associated uEPSP, as measured at the soma, was slowed down in its rising phase. A similar effect was observed for the magnitude of the TTX-induced increase in uEPSP duration ($r = -0.78$, $p2 < 0.005$, $n = 12$, [Figure 2K](#)). Such a substantial correlation was not observed with respect to EPSP amplitude changes in TTX nor for $(\Delta F/F)_{\text{TPU}}$ rise time ([Figures 2G and S2B](#)).

The pronounced effect of TTX on uEPSP rise time and duration did not depend on the respective spines' distance from the soma ([Figure S2C](#)); there was also no correlation with the mixed effect of TTX on uEPSP amplitude (data not shown). Occasionally, we could record the action of TTX on more than one spine of the same GC. In several instances, TTX affected $(\Delta F/F)_{\text{TPU}}$ in immediately adjacent spines in a highly non-uniform manner ($n = 3$ GCs; [Figure S2D](#)).

Since basal spontaneous EPSP rates in GCs are usually high (e.g., [Figure 1B](#)), more global pathways of TTX action could suppress network activity and might also cause the observed decel-

eration of EPSP rise times, e.g., by changing the electric properties of the GC dendrite. However, we could replicate increased rise times via intracellular Na_v blockade with $10 \mu\text{M}$ QX-314 (versus a control group of spines, $n = 15$ spines each group, $p < 0.001$, [Figure S2E](#)), whereas the uEPSP amplitude was similar across groups ($p = 0.30$). Accordingly, longer rise times of spontaneous EPSPs (which may originate also from non-reciprocal spines) resulted after patching with QX ($p1 < 0.01$, $3.0 \pm 0.6 \text{ ms} < 1 \text{ min}$ post whole-cell configuration versus $4.3 \pm 2.1 \text{ ms} > 20 \text{ min}$ later, $n = 27$ EPSPs each condition, from 3 GCs), while there was no significant change in amplitude.

Altogether, we observe that blocking Na_v s significantly affects both uncaging-evoked individual spine Ca^{2+} entry and somatic EPSP kinetics in a correlated manner, pointing toward a mechanism operating within the activated spine.

High-Voltage-Activated Ca^{2+} Channels Mediate the Extra Ca^{2+} Entry

To test the hypothesis that Na_v s contribute to extra ΔCa^{2+} via HVACCs, we blocked N/P/Q-type Ca^{2+} channels with $1 \mu\text{M}$ ω -conotoxin MVIIC (CTX; [Bloodgood and Sabatini, 2007](#)). [Figures 3A–3E](#) show the resulting substantial decrease of $(\Delta F/F)_{\text{TPU}}$ ($p < 0.001$, $n = 24$), similar to the effect of TTX, albeit with no significant changes of uEPSP amplitude and rise time. On average, the CTX effect on ΔCa^{2+} was occluded by prior blockade with TTX ($n = 14$, [Figure 3F](#)); prior CTX also occluded the TTX effect ($n = 8$, [Figure 3F](#)). Thus, HVACCs are not likely to become activated without support from Na_v -mediated depolarization and most of the extra ΔCa^{2+} that is blocked away in TTX is actually due to HVACC activation. We conclude that HVACCs are the main source of postsynaptic Ca^{2+} entry arising from Na_v activation but that there is no HVACC-mediated electrical contribution to somatic uEPSPs.

Interaction of Other Sources of Postsynaptic Ca^{2+} with Na_v Activation

To investigate whether known sources of GC Ca^{2+} entry other than HVACCs, in particular T-type Ca^{2+} channels (T-channels), release from internal stores and NMDARs ([Egger et al., 2003, 2005](#)), could contribute to increased ΔCa^{2+} due to Na_v activation, we performed experiments in which we first blocked the source of Ca^{2+} and then applied 500 nM TTX ([Figures 4A–4D](#)).

NMDARs are known to prominently contribute to GC postsynaptic signaling, both electrically and with respect to ΔCa^{2+} ([Schoppa et al., 1998](#); [Isaacson and Strowbridge, 1998](#); [Egger et al., 2005](#)). The application of $25 \mu\text{M}$ D-APV strongly reduced $(\Delta F/F)_{\text{TPU}}$, to 0.37 ± 0.17 of control ($p1 < 0.025$, $n = 6$, [Figure 4D](#)). Subsequent wash-in of TTX further substantially reduced the remaining Ca^{2+} signal ($p1 < 0.05$, $n = 5$, [Figure 4B](#)). Thus, Na_v -induced ΔCa^{2+} does not require NMDAR activation. Since NMDAR activation depends on postsynaptic depolarization, we also studied whether prior blockade of Na_v s could prevent or limit NMDAR activation. To this end, we added $25 \mu\text{M}$ D-APV in a subset of the occlusion experiments mentioned above where both TTX and CTX were already present. In this case, APV substantially reduced the Ca^{2+} signal even further ($p2 < 0.01$, $n = 8$, [Figures 4A and 4B](#)). The total effect of APV and TTX or TTX/CTX

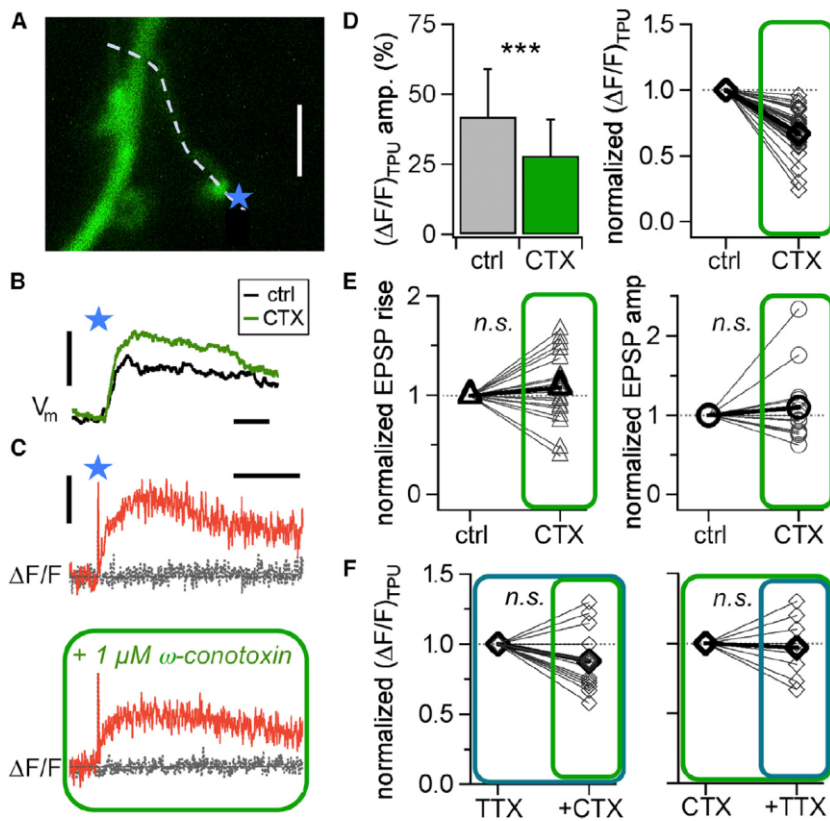


Figure 3. High-Voltage-Activated Ca^{2+} Channels Mediate Most of the Extra Ca^{2+} Entry Caused by Na_v Activation

(A) Spine with scan line and TPU site. Scale bar: 2 μm .

(B) Averaged uEPSP recorded at the soma of cell in (A) during control and in the presence of 1 μM ω -conotoxin MVIIC (CTX). Scale bars: 0.5 mV, 10 ms.

(C) Averaged $(\Delta\text{F}/\text{F})_{\text{TPU}}$ in spine and dendrite from (A) during control (top) and in the presence of CTX (bottom). Scale bars: 25%, 500 ms.

(D) Effect of CTX on $(\Delta\text{F}/\text{F})_{\text{TPU}}$ amplitudes ($n = 24$ spines). Left: averaged absolute amplitudes \pm SD ($42\% \pm 17\%$ versus $28\% \pm 13\%$, $p < 0.001$). Right: spine-wise amplitudes normalized to control (bold: average change \pm SD to 0.67 ± 0.19).

(E) Spine-wise effect of CTX on normalized uEPSP amplitudes (left, $n = 20$, bold: average change \pm SD 1.10 ± 0.42 , n.s.) and rise times (right, $n = 19$, average \pm SD 1.08 ± 0.35 , n.s.).

(F) Left: TTX before CTX ($n = 14$). Average effect of CTX on individual amplitudes normalized to control (bold: average change \pm SD to 0.88 ± 0.22 of control). Right: CTX before TTX ($n = 8$). Average effect of TTX on individual amplitudes normalized to control (bold: average change \pm SD to 0.94 ± 0.26 of control).

All TTX applications in the presence of blockers of Ca^{2+} entry described in this section reduced $(\Delta\text{F}/\text{F})_{\text{TPU}}$ in a manner indistinguishable from the effect of TTX

together on $(\Delta\text{F}/\text{F})_{\text{TPU}}$ was a reduction to 0.18 ± 0.13 of control without drugs ($p2 < 0.001$, $n = 15$, Figure 4D). We conclude that NMDAR-mediated Ca^{2+} signaling at the reciprocal spine occurs by and large independently of Na_v activation and that NMDARs and HVACCs are the two main sources of postsynaptic Ca^{2+} in most spines.

To investigate the role of T-channels, we applied 10 μM mibefradil, which has been shown previously to block low-threshold Ca^{2+} spikes in GCs (Egger et al., 2005) and also a substantial fraction of Ca^{2+} entry mediated by backpropagating action potentials (Egger et al., 2003). Mibefradil slightly reduced $(\Delta\text{F}/\text{F})_{\text{TPU}}$ (0.90 ± 0.11 of control, $n = 5$, n.s., Figure 4D). In the presence of mibefradil, TTX still substantially reduced $(\Delta\text{F}/\text{F})_{\text{TPU}}$ ($p1 < 0.025$, $n = 6$, Figure 4C). Thus, T-channels are likely to contribute only marginally to Na_v -mediated Ca^{2+} entry.

To interfere with Ca^{2+} release from internal stores, we applied 10 μM thapsigargin while continuously stimulating GCs, which has been shown previously to reduce GC postsynaptic Ca^{2+} signals (Egger et al., 2005). This treatment reduced $(\Delta\text{F}/\text{F})_{\text{TPU}}$ in four out of six spines (total average n.s., 0.81 ± 0.15 of control, $n = 6$, Figure 4D). Again, the effect of TTX in the presence of thapsigargin was as strong as without this drug ($p1 < 0.05$, $n = 6$, Figure 4C). Due to the small overall effects of mibefradil and thapsigargin on $(\Delta\text{F}/\text{F})_{\text{TPU}}$, the reverse experiment—i.e., first TTX and then the blockers—could not be conducted because small changes in small $\Delta\text{F}/\text{F}$ signals cannot be reliably determined in most spines.

alone shown in Figure 2D, with $p2$ values ranging from 0.86 to 0.2. In summary, Ca^{2+} sources other than HVACCs do not substantially contribute to Na_v -mediated Ca^{2+} entry.

Role of K^+ Channels

Voltage-gated K^+ conductances (K_v) are likely to activate during Na_v -mediated depolarization and thus play a role in the observed effects of Na_v blockade on V_m and $\Delta\text{F}/\text{F}$. Charge efflux through K_v s counteracts the additional Na_v -mediated charge influx, which will affect how much remaining charge reaches the soma. Reduced repolarization might explain why Na_v blockade slows down the somatic EPSP rise and fall but hardly affects the EPSP amplitude (Figures 2F–2K). Various K_v channels, ranging from A-type ($\text{Kv}4$) to delayed rectifier K^+ channels (K_{DR}), are present or likely to be expressed in GC dendrites (Schoppa and Westbrook, 1999; $\text{Kv}2.1, 2.2$: Hwang et al., 1993; $\text{Kv}1.1, 2.3, 6$: Veh et al., 1995). In addition, Ca^{2+} -activated K^+ currents could be diminished in the course of the observed reduction of Ca^{2+} entry in TTX. Candidates for such interactions in GCs include in particular big conductance Ca^{2+} -activated K^+ (BK) currents (Isaacson and Murphy, 2001). Small conductance Ca^{2+} -activated K^+ channels are locally activated via NMDARs in hippocampal CA1 neuron spines (Bloodgood and Sabatini, 2007; Wang et al., 2014) but have not been detected in GCs (Maher and Westbrook, 2005). If K^+ channels made a major contribution to repolarization, pharmacological blockade of these channels should result in a substantial increase in ΔCa^{2+}

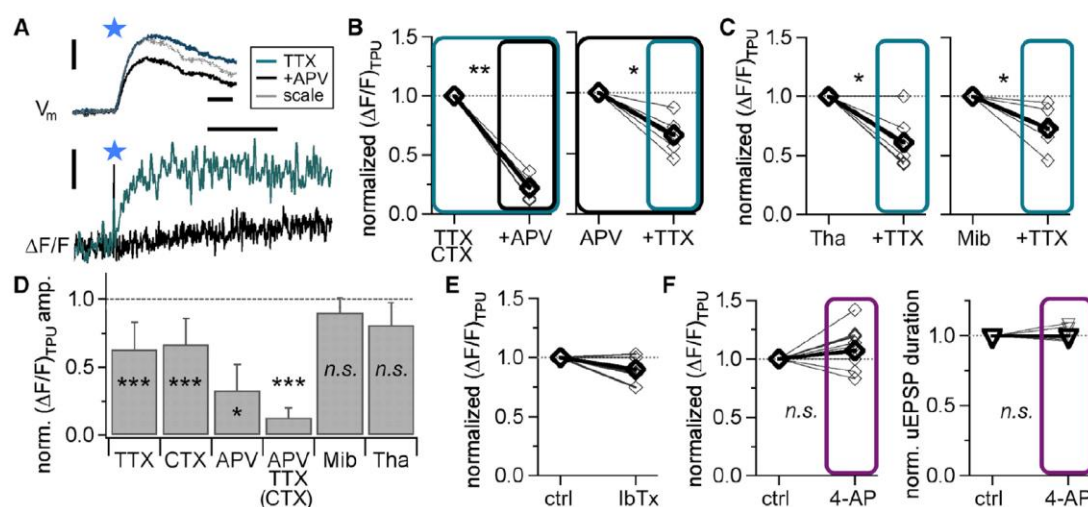


Figure 4. NMDA Receptors and Other Sources of Ca^{2+} Aside from HVACCs Are Not Required for Boosting of Ca^{2+} ; Big Conductance Ca^{2+} -Activated-Type and A-Type K^+ Currents Do Not Contribute to Repolarization

(A) Top: averaged uEPSP recorded at the soma in the presence of 500 nM TTX and upon addition of 25 μM D-APV. Scale bars 1 mV, 10 ms. Gray trace: EPSP in APV scaled to the same amplitude as in TTX alone. Note the similar rise time in APV. Bottom: averaged $(\Delta F/F)_{\text{TPU}}$ in the corresponding spine in the presence of 500 nM TTX and upon addition of 25 μM D-APV. Scale bars: 25%, 500 ms.

(B) Left: spine-wise effect of 25 μM D-APV on normalized $(\Delta F/F)_{\text{TPU}}$ amplitudes in the presence of 500 nM TTX + 1 μM CTX (left, $n = 9$, bold: average change 0.20 ± 0.09 , $P_2 < 0.01$). Right: the reverse experiment: Spine-wise effect of 500 nM TTX on normalized $(\Delta F/F)_{\text{TPU}}$ amplitudes in the presence of 25 μM D-APV ($n = 5$, average \pm SD 0.65 ± 0.16 , $p_1 < 0.05$).

(C) Spine-wise effect of TTX on $(\Delta F/F)_{\text{TPU}}$ amplitudes in the presence of 10 μM thapsigargin (left; $n = 6$, bold: average change \pm SD 0.61 ± 0.22 , $p_1 < 0.05$) and 10 μM mibefradil (right; $n = 6$; bold: average change \pm SD 0.73 ± 0.17 , $p_1 < 0.025$).

(D) Cumulative display of the effect of various compounds on $(\Delta F/F)_{\text{TPU}}$ amplitude normalized to control, i.e., to $(\Delta F/F)_{\text{TPU}}$ amplitude in the absence of any compound. For TTX and CTX, compare Figures 2D and 3D. Other average values \pm SD: APV 0.33 ± 0.19 , $n = 7$, APV and TTX (and CTX for 9 spines) 0.18 ± 0.13 , $n = 15$, mibefradil 0.90 ± 0.11 , $n = 5$, thapsigargin 0.81 ± 0.17 , $n = 6$.

(E) The BK channel blocker iberiotoxin (100 nM) does not affect $(\Delta F/F)_{\text{TPU}}$ amplitude ($n = 6$, bold: average change \pm SD 0.90 ± 0.10 , n.s.).

(F) Left: effect of 5 mM 4-AP on $(\Delta F/F)_{\text{TPU}}$ amplitude ($n = 12$, bold: average change \pm SD 1.07 ± 0.17 , n.s.). Right: effect of 5 mM 4-AP on uEPSP duration ($n = 6$, bold: average change 1.00 ± 0.05 , n.s.).

due to prolonged NMDAR and voltage-activated Ca^{2+} channel opening and in an increase in duration of the somatic uEPSP.

We tested the role A-type $\text{Kv}4$ channels play using 5 mM 4-aminopyridine (4-AP; Schoppa and Westbrook, 1999; Wang et al., 2014). While a few spines (4 out of 12) showed a substantial increase in $(\Delta F/F)_{\text{TPU}}$ by more than 15% relative to control, this increase was not significant across all spines (Figure 4F). With respect to uEPSPs, we observed no significant changes in amplitude (2.3 ± 2.6 mV control versus 2.0 ± 2.0 mV 4-AP, $n = 8$), rise time (2.8 ± 0.8 ms control versus 3.2 ± 1.2 ms 4-AP, $n = 7$), or duration (46 ± 15 ms control versus 46 ± 14 ms 4-AP, $n = 6$; Figure 4F). 4-AP also did not modulate the effect of subsequent wash-in of TTX on $(\Delta F/F)_{\text{TPU}}$ amplitudes ($p_2 < 0.02$, $n = 7$, average change 0.57 ± 0.19 ; $p_2 = 0.48$ versus effect of TTX alone, data not shown). While we cannot rule out that A-type $\text{Kv}4$ channels might limit postsynaptic Ca^{2+} entry in a subset of spines, they seem unlikely to play a major role in local reciprocal spine activation or the time course of the somatic EPSPs.

We also investigated a possible role of BK channels as these channels were found to mediate GC somatic inhibitory currents following extrasynaptic NMDAR activation (Isaacson and Murphy, 2001), and NMDAR-mediated Ca^{2+} entry substantially contributes to $(\Delta F/F)_{\text{syn/TPU}}$ (Egger et al., 2005; see also above and Figures 4A–4C). Wash-in of iberiotoxin (IbTx, 100 nM, e.g.,

Wang et al., 2014) did not significantly change $(\Delta F/F)_{\text{TPU}}$ (Figure 4E) or modify uEPSP shapes, since there were no consistent changes in amplitude (1.8 ± 1.4 mV control versus 1.7 ± 1.1 mV IbTx), rise time (3.0 ± 0.6 ms control versus 3.2 ± 1.2 ms IbTx), or normalized integral (59 ± 30 ms control versus 59 ± 33 ms IbTx, all $n = 4$). Thus, BK channels are unlikely to be present on reciprocal spines and are probably restricted to perisomatic compartments (Knaus et al., 1996; Isaacson and Murphy, 2001).

As mentioned above, we found that the EPSP duration increases in TTX and that this effect is strongly correlated to the effect of TTX on $(\Delta F/F)_{\text{TPU}}$ (Figures 2J and 2K). These observations suggest that a voltage-dependent conductance activated by Na_v -mediated depolarization in the spine contributes to slow repolarization, which would match the properties of K_{DR} channels.

Simulation of $V_m(t)$ and $[\text{Ca}^{2+}](t)$ within GC Spines

We turned to a minimalist compartmental model in NEURON (Hines and Carnevale, 1997) to show how the interaction of K_v and Na_v currents and possibly filtering by the spine neck resistance could explain the initially puzzling experimental observations in Figures 2F–2K. (1) The normalized EPSP integral (or EPSP duration) increased in TTX, rather than decreasing; in fact, the stronger the effect of TTX on $(\Delta F/F)_{\text{TPU}}$, the longer the

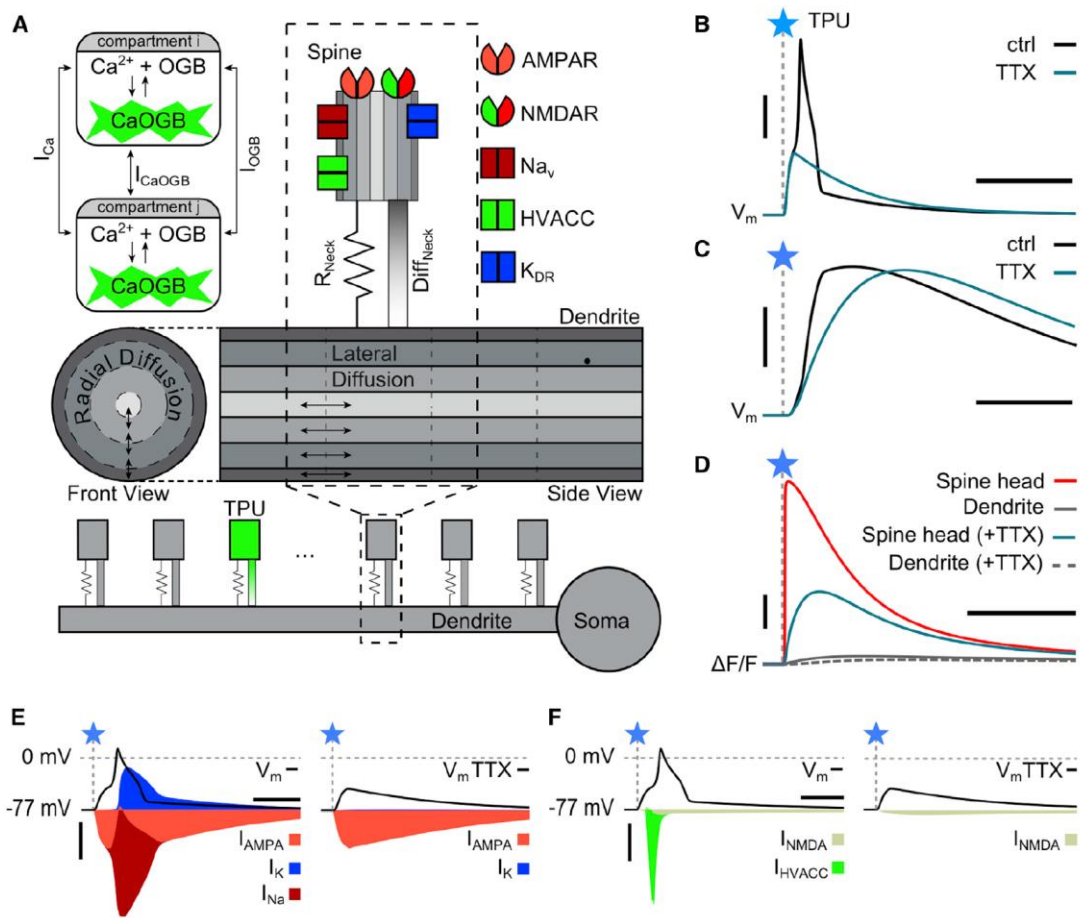


Figure 5. Simulation of Spine Head Depolarization and Ca^{2+} Transient

(A) Schematic representation. The granule cell model features a soma and a dendrite of length $200\ \mu\text{m}$, along which 50 spines are spaced equally. The spine at a distance of $80\ \mu\text{m}$ receives a pulse of $1\ \text{mM}$ glutamate for $1\ \text{ms}$, which causes electrical and diffusive currents. The electrical and diffusive couplings between the spine head and the dendrite are represented by two independent parameters, the spine neck resistance R_{neck} and the area ratio α (see [Supplemental Experimental Procedures](#)). Three types of molecules diffuse both longitudinally and radially within the spine head and the main dendrite: free Ca^{2+} , the fluorescent dye OGB-1, and the bound CaOGB; the binding and unbinding of Ca^{2+} is simulated within each compartment.

(B) Simulated membrane potential $V_m(t)$ in the spine head in control conditions and with Na_v blockade (“TTX”). Scale bars: $20\ \text{mV}$, $10\ \text{ms}$.

(C) Simulated $V_m(t)$ at the soma, as above. Scale bars: $0.5\ \text{mV}$, $10\ \text{ms}$.

(D) Simulated CaOGB transient in the spine head and the corresponding dendritic segment in control conditions and “in TTX.” Scale bars: 10% , $500\ \text{ms}$.

(E) Na_v , AMPAR, and K_{DR} current contributions to the postsynaptic event. Left: control conditions. Right: the same experiment with Na_v blocked. Scale bars: $20\ \text{pA}$, $5\ \text{ms}$.

(F) NMDAR and HVACC current contributions to the postsynaptic event. Left: control conditions. Right: the same experiment with Na_v blocked. Scale bars: $0.5\ \text{pA}$, $5\ \text{ms}$.

See also [Figure S3](#); the parameter set of the simulations shown in (B)–(F) is listed in [Table S4](#).

somatic EPSP duration was. (2) While the rise of the EPSP was decelerated in TTX, the EPSP amplitude barely changed.

The model simulated both the membrane potential $V_m(t)$ and Ca^{2+} dynamics, as shown in [Figure 5A](#), with Na_v , AMPAR, HVACC, NMDAR, and K_{DR} conductances in the spine head as free parameters (see [Supplemental Experimental Procedures](#)). The coupling between spine and dendrite was summarized by an electrical resistance and a diffusive coupling term for Ca^{2+} , the last two free parameters of the model.

A high resistance in the spine neck acts as a voltage divider, so that Na_v activation produces a local Na^+ spike that is

restricted to the spine head ([Figure 5B](#)). Under TTX, this action potential is blocked and the stimulus-induced depolarization is less but decays more gradually. In the absence of TTX, spike repolarization by the K_{DR} conductance causes the voltage time course in the spine to undershoot the voltage time course with TTX ([Figure 5B](#)). The Na^+ spike causes the somatic EPSP rise time to become faster, but the subsequent voltage undershoot in the spine means that the somatic EPSP also decays faster ([Figure 5C](#)). Indeed, the somatic EPSP under TTX can be larger than without TTX. Ca^{2+} entry into the spine is reduced in TTX; very little Ca^{2+} reaches the dendrite ([Figure 5D](#)). K_{DR} currents

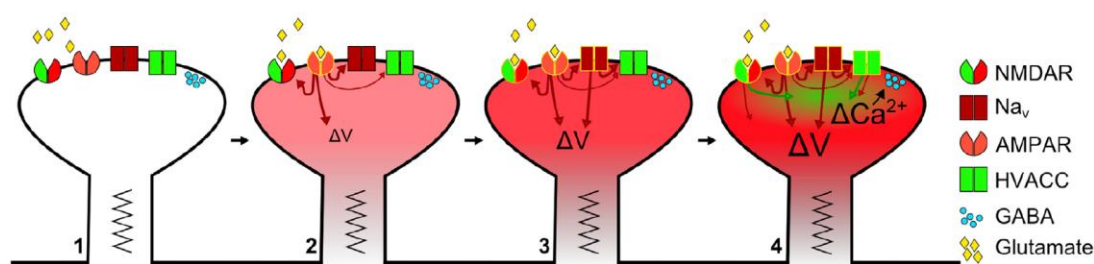


Figure 6. Summary of the Activation Sequence in Spines Containing Na_v s

Activated channels are indicated by yellow edges, depolarizing currents by red arrows and Ca^{2+} entry by green arrows. (1) Schematic spine with conductances essential for postsynaptic signaling (see legend on the right). (2) Upon binding of glutamate, first AMPARs get activated, leading to depolarization of the spine. (3) AMPAR-mediated depolarization of the spine activates Na_v s, which in turn drive additional depolarization. (4) In the strongly depolarized spine HVACCs open, thus substantially increasing the spine calcium level and possibly promoting release of GABA. The delayed opening of NMDARs via AMPAR-mediated depolarization also contributes to the postsynaptic rise in Ca^{2+} .

are only substantially activated when a local Na^+ spike occurs (Figure 5E).

We performed a wide-ranging parameter scan to find parameter combinations that would match the experimental results (Figure S3). This analysis yielded predictions for the lower limits on R_{neck} , AMPAR, and Na_v conductances, such that local Na^+ spikes can still occur. In particular, R_{neck} must be larger than 1 G Ω . Even though several experimental findings were not built into the model, such as the decoupling of somatic uEPSP amplitude and spine ΔCa^{2+} (Figure 1E) or the dissociation between somatic uEPSP amplitude and rise time with respect to the effect of Na_v blockade (Figures 2F–2I), the model was able to replicate these findings.

DISCUSSION

Our study provides evidence that Na_v s can contribute to postsynaptic Ca^{2+} entry via HVACC activation as summarized in Figure 6, with the entire cascade localized in a single spine. The initial depolarization within this activation sequence is provided by Ca^{2+} -impermeable AMPARs, since simultaneous blockade of NMDARs and VACCs was shown to almost entirely block Ca^{2+} entry, and NMDAR-mediated synaptic currents in GCs reach their maximum well past the peak of the AMPAR-mediated component (Isaacson and Strowbridge, 1998; Schoppa et al., 1998; Egger et al., 2005; this study). The pharmacological blockade of the Na_v -mediated Ca^{2+} entry by ω -conotoxin (Figure 3), as well as the increase in the rise time of $(\Delta F/F)_{\text{TPU}}$ (Figure S2A) in TTX, strongly indicate that most of the Ca^{2+} enters through HVACCs. Similar to classical axonal release of GABA, GC spine HVACCs are likely to contribute to the release of GABA onto the mitral cell (Isaacson, 2001), further substantiating the view of the reciprocal synapse as an independent microcircuit (Shepherd et al., 2007).

Activated Na_v s Are Localized in the Spine

The observed effects do not originate from other neurons, as transmitters were uncaged locally and as both extra- and intracellular Na_v blockade led to the same results. The strong correlation of the TTX-induced uEPSP rise time increase with the purely local change in $(\Delta F/F)_{\text{TPU}}$ and the independence of any

of the observed TTX-mediated effects on the spine's location relative to the soma (e.g., Figure S2C), including the differential action of TTX on neighboring spines, strongly indicate that the underlying mechanism is localized in the spines, not in the dendrites. Thus, we conclude that the amplification of Ca^{2+} entry is most likely a direct effect of Na_v activation within the spine head.

The Na_v -mediated effects do show a broad variability across spines (Figures 2D, 2F, 2H, 2J, and S2A). This observation could result from a variance in the number of Na_v s across spines, be they adjacent or not. Different subtypes of GCs with respect to the level of Na_v channel expression or GCs in different maturational stages (Carleton et al., 2003) are a less likely source of variability because TTX differentially affected nearby spines on the same cell (Figure S2D)—if some GCs would express considerably less Na_v s per se, then all their spines should show only minor TTX effects. Alternatively, the threshold for Na_v activation could not or barely have been met in some spines in our sample.

Interestingly, in experiments with amplitudes sufficiently large for analysis of individual $\Delta F/F$ responses Na_v blockade resulted in an increase of the coefficient of variation. This finding requires further elucidation but it seems possible to conclude that spine spikes are all-or-none events that warrant fairly uniform ΔV_m in the spine head. A similar proposal with respect to spine function has been made for the location dependence of EPSPs (Gulledge et al., 2012).

Passive GC Dendrites during Local Spine Inputs

The local Na_v -based amplification mechanism reported here is different from the perisomatic dendritic boosting of distal EPSPs known from CA1 and cortical pyramidal neurons, which is typically promoted by depolarized V_m (reviewed in Spruston et al., 2007). The latter mechanism is generally unlikely to occur in GCs because of their characteristically low resting potential of ~ -80 to -70 mV (Egger et al., 2003) and small unitary EPSPs whose size is not correlated to the distance relative to the soma (~ 2 mV at soma, Table S1, Figure S1). Thus, dendrite-based mechanisms are unlikely to exert any major influence on unitary signals from GC synapses. Coincident inputs, on the other hand, are known to activate dendritic conductances in GCs such as low-threshold VACCs (Pinato and Midtgaard, 2005; Egger et al., 2005).

Role of K_v Channels

A-type K^+ channels are known to play important roles in GC signaling, such as governing the latency of GC global Na^+ spikes (Schoppa and Westbrook, 1999). However, we could not find evidence for a prominent role of A-type channels at the level of individual reciprocal synapse activation. This observation is in line with ultrastructural data (Kollo et al., 2008), where $Kv4.2$ and $Kv4.3$ channels in GCs were found to be localized in the somatic membrane and not observed in the dendrites or reciprocal spines. Nevertheless, other A-type channels might be present in GC spines and dendrites, since Schoppa and Westbrook observed a dendritic expression of I_A . Therefore, A-type channels are more likely to be involved in broader activation of GCs when large EPSPs or global Na^+ spikes could activate I_A in dendrites and/or at the soma.

Local repolarization in spines is thus most probably due to delayed-rectifier currents I_{DR} , which have also been detected in GC dendrites (Schoppa and Westbrook, 1999). Here we have found indirect evidence for a slowly repolarizing conductance that is Na_v activated, which is supported by the mathematical spine model (Figures 2J, 2K, and 5E). While current-clamp mode and the high excitability of bulbar slices have prohibited a general block of K_{DR} conductances with the current broad-band pharmacological tools in our preparation, more subtle pharmacological tools and more detailed analysis of K_{DR} expression in GC dendrites could certainly help, in the future, to reveal the molecular identity of the involved K_{DR} family members. For now, there are several candidate members of both the $Kv1$ and $Kv2$ subfamilies that were found to be expressed in GCs and/or the external plexiform layer (Hwang et al., 1993; Veh et al., 1995). The active properties of GC spines reported here seem to suggest the involvement of a K_{DR} subtype that would otherwise be found in axons.

NMDA Receptor Activation versus Na_v Activation

NMDAR-mediated signaling at the reciprocal spine was found to occur mostly independently of Na_v activation. Obviously, AMPAR-mediated depolarization in the presence of TTX is already sufficient to lift the Mg^{2+} block. Thus, passive amplification via the spine input resistance that is dominated by R_{neck} can assist in activating NMDARs, confirming similar observations in CA1 pyramidal neuron spines (Grunditz et al., 2008).

The only noticeable difference between TPU-evoked and synaptic signals in our experiments was a slightly, but significantly larger contribution of NMDARs to $(\Delta F/F)_{TPU}$ versus $(\Delta F/F)_{syn}$ ($p < 0.05$, APV blockade of $(\Delta F/F)_{syn}$ to 0.51 ± 0.17 of control, $n = 9$, Egger et al., 2005, versus 0.37 ± 0.17 in the data above). In some cases of large reciprocal spine heads the uncaging beam may have been positioned suboptimally with respect to the postsynaptic density, causing the activation of a larger fraction of extrasynaptic NMDARs. However, since we observed no significant interaction between NMDAR activation and Na_v activation on postsynaptic ΔCa^{2+} , a potential overestimate of NMDAR currents results, at most, in an underestimate of the relative contribution of Na_v effects.

While NMDARs can contribute to GABA release from GC spines (Isaacson and Strowbridge, 1998; Chen et al., 2000), it is also known that AMPAR-mediated depolarization is sufficient

to mediate GABA release via HVACCs (Isaacson, 2001). Thus, the Na_v -mediated pathway is capable of causing release from GCs. In summary, our findings on the functional presence of Na_v , HVACC, and K_{DR} in GC reciprocal spines confirm the idea of these spines as functionally equivalent to “miniature axonal branches” (Price and Powell, 1970), not only on the ultrastructural but also the molecular and biophysical level. Thus, the output from GC reciprocal spines is also likely to occur in a similar manner as output from classical boutons.

Spine Morphology and Filtering

While Araya et al. (2007) have observed a systematic decrease of neocortical pyramidal cell spine uEPSP amplitudes recorded at the soma to a fraction of ~ 0.7 of control after wash-in of TTX, in our case Na_v channel blockade had little effect on uEPSP amplitudes but rather delayed their rise times (Figure 2F). We also observed a dissociation between the effects of Na_v blockade on uEPSP amplitude versus uEPSP rise time with respect to the correlation to the reduction of $(\Delta F/F)_{TPU}$ —only TTX’s effect on $(\Delta F/F)_{TPU}$ was strongly and negatively correlated to the rise time of the somatic uEPSP. Our data and simulations show that the local spine Ca^{2+} signals themselves and the uEPSP amplitudes recorded at the soma are decoupled (cf. also Figure 1E), potentially allowing for the multiplexing of modes of information transfer between GC spines. Spine ΔCa^{2+} and electrical signals at the soma are similarly uncorrelated in recordings and simulations of CA1 pyramidal neuron spines (Sobczyk et al., 2005; Bloodgood and Sabatini, 2007; Grunditz et al., 2008) and thus the observed uncoupling might reflect a more general principle of neuronal design.

The spine neck resistance R_{neck} and the main dendrite filter the Na^+ spine spike before it reaches the soma. Spine neck length seems not to be a good indicator of R_{neck} as we observe no correlation between the estimated spine neck length versus somatic uEPSP size or $(\Delta F/F)_{TPU}$ in the spine. These observations differ from observations in L5 pyramidal cells (Araya et al., 2006, 2014) but are in line with a recent STED study in hippocampal pyramidal cells (Takasaki and Sabatini, 2014). Another similar STED study has closely investigated possible links between spine morphology and compartmentalization and proposed a linear relation between R_{neck} and diffusive coupling (Tønnesen et al., 2014). In our simulations there were no a priori assumptions on the relation between R_{neck} and diffusive coupling. In the case of GC spines, diffusive coupling might depend on the presence or absence of a mitochondrion (Woolf et al., 1991), which might be uncorrelated with neck length. Further ultrastructural investigations will be required to unravel these apparent discrepancies.

Function of Local Na_v Activation in Sensory Processing

Our data suggest that Na_v -enhanced synaptic depolarization of GC reciprocal spines serves to provide temporally precise feedback inhibition to mitral cells via accelerated Ca^{2+} entry. Such fast recurrent feedback could play several important and possibly interrelated roles in olfactory processing. First, fast feedback can govern mitral cell spiking latency on the sub-millisecond timescale, which might be crucial for discriminating between similar odors (Schaefer and Margrie, 2012). Second, dendrodendritic interactions between mitral cells and granule cells drive fast oscillations in the gamma range (Nusser et al., 2001; Neville and

Haberly, 2003; Lepousez and Lledo, 2013). Third, the observed reduction in somatic/dendritic EPSP rise time due to spine Na_v activation will also serve to accelerate Na^+ or Ca^{2+} spike generation at somatic or dendritic spike initiation sites and thus is likely to speed up lateral inhibition of other mitral cells.

Indeed, a recent publication by Fukunaga et al. (2014) provides impressive evidence for a role of GCs in fast olfactory processing by optogenetic silencing of GCs in vivo. The observed average hyperpolarization of the GC somatic V_m by >-20 mV during silencing is likely to spread to the dendrite because of the electrotonic compactness of GCs (Egger et al., 2003) and thus could reduce both the Na_v /HVACC- and NMDAR-mediated local Ca^{2+} entry into reciprocal spines we have reported here. The authors confirm their earlier hypothesis that GC signaling controls the precise latency of mitral cell responses during odor perception and further elucidate the major role of GCs in driving fast gamma oscillations. In this context, it is tempting to speculate that Na_v density might be upregulated in adult-born GCs compared to early-born GCs, as adult-born GCs have a stronger impact on gamma oscillations and facilitate learning of difficult tasks (Alonso et al., 2012).

Interestingly, a similar speed-up of synaptic transmission occurs between rod bipolar and retinal AII amacrine cells—another type of axonless sensory inhibitory neuron—and this is also mediated by postsynaptic Na_v activation (Nelson, 1982; Tian et al., 2010). Thus, Na_v -mediated dendritic mechanisms may serve to endow the apparently simple circuitry of early sensory input modules—such as the olfactory bulb and the retina—with extra modes of computation that assist in fine-tuning the primary representation of the sensory stimulus.

EXPERIMENTAL PROCEDURES

Animal Handling, Slice Preparation, and Electrophysiology

Olfactory bulb brain slices (thickness 300 μm) were prepared of juvenile rats of either sex (postnatal days 11–17, Wistar), in accordance with the rules laid down by the EC Council Directive (86/89/ECC) and German animal welfare legislation. Slices were incubated in a water bath at 33°C for 30 min and then kept at room temperature (22°C) until recordings were performed. Olfactory bulb granule cells were visualized by gradient contrast and recorded in whole-cell current-clamp mode. Patch pipettes (pipette resistance 6–8 M Ω) were filled with an intracellular solution containing the following substances: 130 mM K-methylsulfate, 10 mM HEPES, 4 mM MgCl_2 , 2.5 mM Na_2ATP , 0.4 mM NaGTP, 10 mM Na-phosphocreatine, 2 mM ascorbate, 0.1 mM OGB-1 (Ca^{2+} indicator, Invitrogen), at pH 7.3. The extracellular ACSF was bubbled with carbogen and contained: 125 mM NaCl, 26 mM NaHCO_3 , 1.25 mM NaH_2PO_4 , 20 mM glucose, 2.5 mM KCl, 1 mM MgCl_2 , and 2 mM CaCl_2 . The following pharmacological agents were bath applied in some experiments: muscimol (10 μM , Tocris Bioscience), ω -conotoxin MVIIC (CTX, 1 μM , Alomone), TTX (500 nM, Alomone), D-APV (25 μM , Tocris), mibefradil (10 μM , Tocris), iberiotoxin (100 nM, Tocris), 4-AP (5 mM, Tocris), and thapsigargin (10 μM , Tocris). To ensure store depletion, we analyzed data in the presence of thapsigargin no earlier than after a period of >5 min of repeated stimulation of the spine. QX-314 was added to the intracellular solution in the experiments that excluded effects of TTX outside of GCs (10 μM , Santa Cruz Biotechnology). Electrophysiological recordings were made with an EPC-10 amplifier and Patchmaster v2.60 software (both HEKA Elektronik). Experiments were performed at room temperature (22°C), except for the set of control experiments at near-physiological temperature (32°C–34°C; temperature control via TC-324B, Warner Instruments). GCs were held near their resting potential of below -70 mV (Egger et al., 2003); if GCs required >25 pA of holding current, they were rejected.

In pharmacological experiments, we waited for at least five, respectively, 10 min after wash-in of the drugs TTX, mibefradil, APV, 4-AP resp. CTX, iberiotoxin, and thapsigargin.

Combined Two-Photon Imaging and Uncaging

Imaging and uncaging were performed on a Femto-2D-uncage microscope (Femtonics). Two tunable, Verdi-pumped Ti:Sa lasers (Chameleon Ultra I and II, respectively, Coherent) were used in parallel, set to 840 nm for excitation of OGB-1 and to 730–750 nm for uncaging, depending on the compound. The two laser lines were directly coupled into the pathway of the microscope with a polarization cube (PBS102, Thorlabs) and two motorized mirrors. As caged compounds, we used either MNI-caged glutamate trifluoroacetate (MNI, Femtonics) or DNI-caged glutamate (DNI), respectively. MNI was used in 2.5 mM concentration and DNI in 0.6 mM in a closed perfusion circuit with a total volume of 12 ml. Caged compounds were washed in for at least 10 min before starting measurements. The uncaging laser was switched using an electro-optical modulator (Pockels cell model 350-80, Conoptics). The uncaging pulse duration was 0.5–1 ms. The spine of interest was moved to the center of the scanning field and the uncaging pulse power was adjusted to the depth of the measured spine, corresponding to a laser power of approximately 15 mW at the uncaging site (Sobczyk et al., 2005). We roughly calibrated the attenuation of the uncaging laser beam within the tissue by imaging fluorescent spheres below thin olfactory bulb slices (50–200 μm thick) with the transfluorescence PMT detector (Chaigneau et al., 2011). The uncaging beam was positioned at ~ 0.5 μm distance from the outer circumference of the spine head image. Structures of interest were imaged in free line-scanning mode (mostly a single spine and its adjacent dendrite) with a temporal resolution of ~ 1 ms. Line scanning was interleaved with short uncaging intervals during which the focal spot was jumped to the preselected location within ~ 50 μs . The scan position was checked and readjusted if necessary before each measurement to account for drift. The microscope was equipped with a 60 \times Nikon Fluor water-immersion objective (NA 1.0; Nikon Instruments). Green fluorescence was collected both in the epi- and transfluorescence mode. The microscope was controlled by MES v4.5.613 software (Femtonics).

Uncaging Stability

Experiments with MNI versus DNI application yielded similar results with respect to $(\Delta F/F)_{\text{TPU}}$ and uEPSP amplitudes and kinetics and thus were pooled (Table S2). In a few GCs, intermittent bouts of depolarizations could be observed in the recorded cells upon wash-in of the caged compounds. These bouts are likely due to the caged compounds' inherent interferences with GABA_A receptor activation and/or dissociated free glutamate and occurred both in MNI and DNI. If those activity bouts compromised data acquisition, e.g., by raising the resting fluorescence F_0 , 10 μM muscimol was added to the bath solution before recording of control data. For example, there were 2 out of 33 spines recorded in the presence of muscimol in the TTX pharmacology dataset and 7 out of 24 spines in the CTX pharmacology dataset. We tested for possible changes in two ways: (1) via comparing uncaging data from the same spine before and after wash-in of muscimol, with no major changes observed ($n = 4$ expts, Table S3) and (2) via comparing the data with and without muscimol from the CTX set; again, no significant differences in $(\Delta F/F)_{\text{TPU}}$ amplitude and rise time and uEPSP amplitude and rise time were detected.

Data Analysis and Statistics, Estimate of Spine Neck Length, and Simulations

See Supplemental Experimental Procedures.

SUPPLEMENTAL INFORMATION

Supplemental Information includes Supplemental Experimental Procedures, three figures, and four tables and can be found with this article online at <http://dx.doi.org/10.1016/j.neuron.2014.12.051>.

AUTHOR CONTRIBUTIONS

W.G.B., V.R., and V.E. performed experiments and analyzed data. V.E. wrote the manuscript. D. Patimiche performed the simulations, in close collaboration

with M.S., A.V.M.H., W.G.B., and V.E. D. Pálfi and B.R. provided DNI-caged glutamate and data on DNI properties, and all co-authors except for D. Pálfi and V.R. assisted in writing the manuscript.

ACKNOWLEDGMENTS

We thank V. Scheuss for advice on uncaging, H. Jacobi for technical assistance, B. Grothe for hosting the V.E. laboratory in Munich, and A. Schaefer and A. Roth for comments on the manuscript. This work was funded by the German Federal Ministry for Education and Research (BMBF, 01GQ1104, V.E.; 01GQ1410A, A.V.M.H.), DFG-SPP 1392 (Integrative Analysis of Olfaction; W.G.B., V.E.), with additional equipment funding by LMU-GSN and DFG-SFB 870. The development of DNI-Glu was supported by FP7-ICT-2011-C 323945 (3x3D imaging) and OTKA K105997 (B.R.). There are competing financial interests: B.R. is a founder of Femtonics Kft and a member of its scientific advisory board.

Received: May 15, 2014

Revised: November 7, 2014

Accepted: December 15, 2014

Published: January 22, 2015

REFERENCES

- Alonso, M., Lepousez, G., Sebastien, W., Bardy, C., Gabellec, M.M., Torquet, N., and Lledo, P.M. (2012). Activation of adult-born neurons facilitates learning and memory. *Nat. Neurosci.* *15*, 897–904.
- Araya, R., Jiang, J., Eisenthal, K.B., and Yuste, R. (2006). The spine neck filters membrane potentials. *Proc. Natl. Acad. Sci. USA* *103*, 17961–17966.
- Araya, R., Nikolenko, V., Eisenthal, K.B., and Yuste, R. (2007). Sodium channels amplify spine potentials. *Proc. Natl. Acad. Sci. USA* *104*, 12347–12352.
- Araya, R., Vogels, T.P., and Yuste, R. (2014). Activity-dependent dendritic spine neck changes are correlated with synaptic strength. *Proc. Natl. Acad. Sci. USA* *111*, E2895–E2904.
- Bloodgood, B.L., and Sabatini, B.L. (2005). Neuronal activity regulates diffusion across the neck of dendritic spines. *Science* *310*, 866–869.
- Bloodgood, B.L., and Sabatini, B.L. (2007). Ca²⁺ signaling in dendritic spines. *Curr. Opin. Neurobiol.* *17*, 345–351.
- Bloodgood, B.L., Giessel, A.J., and Sabatini, B.L. (2009). Biphasic synaptic Ca influx arising from compartmentalized electrical signals in dendritic spines. *PLoS Biol.* *7*, e1000190.
- Brown, T.H., Chang, V.C., Ganong, A.H., Keenan, C.L., and Kelso, S.R. (1988). Biophysical properties of dendrites and spines that may control the induction and expression of long-term synaptic potentiation. In *Long-Term Potentiation: From Biophysics to Behavior*, S. Deadwyler and P. Landfield, eds. (New York: Liss), pp. 201–264.
- Carleton, A., Petreanu, L.T., Lansford, R., Alvarez-Buylla, A., and Lledo, P.M. (2003). Becoming a new neuron in the adult olfactory bulb. *Nat. Neurosci.* *6*, 507–518.
- Carter, A.G., and Sabatini, B.L. (2004). State-dependent calcium signaling in dendritic spines of striatal medium spiny neurons. *Neuron* *44*, 483–493.
- Chaigneau, E., Wright, A.J., Poland, S.P., Girkin, J.M., and Silver, R.A. (2011). Impact of wavefront distortion and scattering on 2-photon microscopy in mammalian brain tissue. *Opt. Express* *19*, 22755–22774.
- Chen, W.R., Xiong, W., and Shepherd, G.M. (2000). Analysis of relations between NMDA receptors and GABA release at olfactory bulb reciprocal synapses. *Neuron* *25*, 625–633.
- Chiovini, B., Turi, G.F., Katona, G., Kaszás, A., Pálfi, D., Maák, P., Szalay, G., Szabó, M.F., Szabó, G., Szadai, Z., et al. (2014). Dendritic spikes induce ripples in parvalbumin interneurons during hippocampal sharp waves. *Neuron* *82*, 908–924.
- Egger, V., and Urban, N.N. (2006). Dynamic connectivity in the mitral cell-granule cell microcircuit. *Semin. Cell Dev. Biol.* *17*, 424–432.
- Egger, V., Svoboda, K., and Mainen, Z.F. (2003). Mechanisms of lateral inhibition in the olfactory bulb: efficiency and modulation of spike-evoked calcium influx into granule cells. *J. Neurosci.* *23*, 7551–7558.
- Egger, V., Svoboda, K., and Mainen, Z.F. (2005). Dendrodendritic synaptic signals in olfactory bulb granule cells: local spine boost and global low-threshold spike. *J. Neurosci.* *25*, 3521–3530.
- Franks, K.M., Stevens, C.F., and Sejnowski, T.J. (2003). Independent sources of quantal variability at single glutamatergic synapses. *J. Neurosci.* *23*, 3186–3195.
- Fukunaga, I., Herb, J.T., Kollo, M., Boyden, E.S., and Schaefer, A.T. (2014). Independent control of gamma and theta activity by distinct interneuron networks in the olfactory bulb. *Nat. Neurosci.* *17*, 1208–1216.
- Grunditz, A., Holbro, N., Tian, L., Zuo, Y., and Oertner, T.G. (2008). Spine neck plasticity controls postsynaptic calcium signals through electrical compartmentalization. *J. Neurosci.* *28*, 13457–13466.
- Gulledge, A.T., Carnevale, N.T., and Stuart, G.J. (2012). Electrical advantages of dendritic spines. *PLoS ONE* *7*, e36007.
- Harnett, M.T., Makara, J.K., Spruston, N., Kath, W.L., and Magee, J.C. (2012). Synaptic amplification by dendritic spines enhances input cooperativity. *Nature* *491*, 599–602.
- Hines, M.L., and Carnevale, N.T. (1997). The NEURON simulation environment. *Neural Comput.* *9*, 1179–1209.
- Hwang, P.M., Fotuhi, M., Bredt, D.S., Cunningham, A.M., and Snyder, S.H. (1993). Contrasting immunohistochemical localizations in rat brain of two novel K⁺ channels of the Shab subfamily. *J. Neurosci.* *13*, 1569–1576.
- Isaacson, J.S. (2001). Mechanisms governing dendritic gamma-aminobutyric acid (GABA) release in the rat olfactory bulb. *Proc. Natl. Acad. Sci. USA* *98*, 337–342.
- Isaacson, J.S., and Murphy, G.J. (2001). Glutamate-mediated extrasynaptic inhibition: direct coupling of NMDA receptors to Ca²⁺-activated K⁺ channels. *Neuron* *31*, 1027–1034.
- Isaacson, J.S., and Strowbridge, B.W. (1998). Olfactory reciprocal synapses: dendritic signaling in the CNS. *Neuron* *20*, 749–761.
- Jack, J.J.B., Noble, D., and Tsien, R.W. (1975). *Electric Current Flow in Excitable Cells*. (Oxford: Oxford University Press).
- Jardemark, K., Nilsson, M., Muyderman, H., and Jacobson, I. (1997). Ca²⁺ ion permeability properties of (R,S) alpha-amino-3-hydroxy-5-methyl-4-isoxazolepropionate (AMPA) receptors in isolated interneurons from the olfactory bulb of the rat. *J. Neurophysiol.* *77*, 702–708.
- Knaus, H.G., Schwarzer, C., Koch, R.O., Eberhart, A., Kaczorowski, G.J., Glossmann, H., Wunder, F., Pongs, O., Garcia, M.L., and Sperk, G. (1996). Distribution of high-conductance Ca²⁺-activated K⁺ channels in rat brain: targeting to axons and nerve terminals. *J. Neurosci.* *16*, 955–963.
- Koch, C., and Zador, A. (1993). The function of dendritic spines: devices subserving biochemical rather than electrical compartmentalization. *J. Neurosci.* *13*, 413–422.
- Kollo, M., Holderith, N., Antal, M., and Nusser, Z. (2008). Unique clustering of A-type potassium channels on different cell types of the main olfactory bulb. *Eur. J. Neurosci.* *27*, 1686–1699.
- Lepousez, G., and Lledo, P.M. (2013). Odor discrimination requires proper olfactory fast oscillations in awake mice. *Neuron* *80*, 1010–1024.
- Maher, B.J., and Westbrook, G.L. (2005). SK channel regulation of dendritic excitability and dendrodendritic inhibition in the olfactory bulb. *J. Neurophysiol.* *94*, 3743–3750.
- Margrie, T.W., and Schaefer, A.T. (2003). Theta oscillation coupled spike latencies yield computational vigour in a mammalian sensory system. *J. Physiol.* *546*, 363–374.
- Matsuzaki, M., Ellis-Davies, G.C., Nemoto, T., Miyashita, Y., Iino, M., and Kasai, H. (2001). Dendritic spine geometry is critical for AMPA receptor expression in hippocampal CA1 pyramidal neurons. *Nat. Neurosci.* *4*, 1086–1092.

- Miller, J.P., Rall, W., and Rinzel, J. (1985). Synaptic amplification by active membrane in dendritic spines. *Brain Res.* 325, 325–330.
- Nelson, R. (1982). All amacrine cells quicken time course of rod signals in the cat retina. *J. Neurophysiol.* 47, 928–947.
- Neville, K.R., and Haberly, L.B. (2003). Beta and gamma oscillations in the olfactory system of the urethane-anesthetized rat. *J. Neurophysiol.* 90, 3921–3930.
- Nusser, Z., Kay, L.M., Laurent, G., Homanics, G.E., and Mody, I. (2001). Disruption of GABA_A receptors on GABAergic interneurons leads to increased oscillatory power in the olfactory bulb network. *J. Neurophysiol.* 86, 2823–2833.
- Palmer, L.M., and Stuart, G.J. (2009). Membrane potential changes in dendritic spines during action potentials and synaptic input. *J. Neurosci.* 29, 6897–6903.
- Pinato, G., and Midtgaard, J. (2005). Dendritic sodium spikelets and low-threshold calcium spikes in turtle olfactory bulb granule cells. *J. Neurophysiol.* 93, 1285–1294.
- Popovic, M.A., Gao, X., Carnevale, N.T., and Zecevic, D. (2014). Cortical dendritic spine heads are not electrically isolated by the spine neck from membrane potential signals in parent dendrites. *Cereb. Cortex* 24, 385–395.
- Price, J.L., and Powell, T.P. (1970). The morphology of the granule cells of the olfactory bulb. *J. Cell Sci.* 7, 91–123.
- Sabatini, B.L., and Bloodgood, B.L. (2008). Short course syllabus: Optical Stimulation of Synapses by 2-Photon-Mediated Glutamate Uncaging. https://am2012.sfn.org/index.aspx?pagename=ShortCourse1_2008.
- Schaefer, A.T., and Margrie, T.W. (2012). Psychophysical properties of odor processing can be quantitatively described by relative action potential latency patterns in mitral and tufted cells. *Front. Syst. Neurosci.* 6, 30.
- Schneidman, E., Freedman, B., and Segev, I. (1998). Ion channel stochasticity may be critical in determining the reliability and precision of spike timing. *Neural Comput.* 10, 1679–1703.
- Schoppa, N.E., and Westbrook, G.L. (1999). Regulation of synaptic timing in the olfactory bulb by an A-type potassium current. *Nat. Neurosci.* 2, 1106–1113.
- Schoppa, N.E., Kinzie, J.M., Sahara, Y., Segerson, T.P., and Westbrook, G.L. (1998). Dendrodendritic inhibition in the olfactory bulb is driven by NMDA receptors. *J. Neurosci.* 18, 6790–6802.
- Segev, I., and Rall, W. (1988). Computational study of an excitable dendritic spine. *J. Neurophysiol.* 60, 499–523.
- Shepherd, G.M., Chen, W.R., Willhite, D., Migliore, M., and Greer, C.A. (2007). The olfactory granule cell: from classical enigma to central role in olfactory processing. *Brain Res. Brain Res. Rev.* 55, 373–382.
- Sobczyk, A., Scheuss, V., and Svoboda, K. (2005). NMDA receptor subunit-dependent [Ca²⁺] signaling in individual hippocampal dendritic spines. *J. Neurosci.* 25, 6037–6046.
- Spruston, N., Stuart, G.J., and Hausser, M. (2007). Dendritic integration. In *Dendrites*, G.J. Stuart, N. Spruston, and M. Hausser, eds. (New York: Oxford University Press), pp. 351–400.
- Svoboda, K., Tank, D.W., and Denk, W. (1996). Direct measurement of coupling between dendritic spines and shafts. *Science* 272, 716–719.
- Takasaki, K., and Sabatini, B.L. (2014). Super-resolution 2-photon microscopy reveals that the morphology of each dendritic spine correlates with diffusive but not synaptic properties. *Front. Neuroanat.* 8, 29.
- Tian, M., Jarsky, T., Murphy, G.J., Rieke, F., and Singer, J.H. (2010). Voltage-gated Na channels in All amacrine cells accelerate scotopic light responses mediated by the rod bipolar cell pathway. *J. Neurosci.* 30, 4650–4659.
- Tønnesen, J., Katona, G., Rózsa, B., and Nägerl, U.V. (2014). Spine neck plasticity regulates compartmentalization of synapses. *Nat. Neurosci.* 17, 678–685.
- Veh, R.W., Lichtinghagen, R., Sewing, S., Wunder, F., Grumbach, I.M., and Pongs, O. (1995). Immunohistochemical localization of five members of the Kv1 channel subunits: contrasting subcellular locations and neuron-specific co-localizations in rat brain. *Eur. J. Neurosci.* 7, 2189–2205.
- Wang, K., Lin, M.T., Adelman, J.P., and Maylie, J. (2014). Distinct Ca²⁺ sources in dendritic spines of hippocampal CA1 neurons couple to SK and Kv4 channels. *Neuron* 81, 379–387.
- Wellis, D.P., and Scott, J.W. (1990). Intracellular responses of identified rat olfactory bulb interneurons to electrical and odor stimulation. *J. Neurophysiol.* 64, 932–947.
- Woolf, T.B., Shepherd, G.M., and Greer, C.A. (1991). Serial reconstructions of granule cell spines in the mammalian olfactory bulb. *Synapse* 7, 181–192.
- Zelles, T., Boyd, J.D., Hardy, A.B., and Delaney, K.R. (2006). Branch-specific Ca²⁺ influx from Na⁺-dependent dendritic spikes in olfactory granule cells. *J. Neurosci.* 26, 30–40.

Neuron

Supplemental Information

Local Postsynaptic Voltage-Gated Sodium Channel Activation in Dendritic Spines of Olfactory Bulb Granule Cells

**Wolfgang G. Bywalez, Dinu Patirniche, Vanessa Rupprecht, Martin Stemmler, Andreas
V.M. Herz, Dénes Pálfı, Balázs Rózsa, and Veronica Egger**

Supplemental Information

Supplemental Figure Legends

Figure S1, related to Figure 1: A spine's position influences mainly the uEPSP rise time as recorded at the soma, while its neck length shows no obvious influence. Plotted versus spine distance from soma in **(A)** and versus estimated spine neck length in **(B)**: EPSP amplitude, EPSP rise time and $\Delta F/F$ amplitude. The open symbols represent TPU data; these are fitted with the dotted lines and their correlation coefficient is given. The solid symbols represent spontaneous synaptic data.

Figure S2, related to Figure 2: Na_v blockade affects also $(\Delta F/F)_{\text{TPU}}$ rise time; TTX effects on uEPSPs are not related to distance from soma and intracellular Na_v blockade also results in increased EPSP rise times.

(A) Effect of 500 nM TTX on $(\Delta F/F)_{\text{TPU}}$ rise time. Spine-wise amplitudes normalized to control (n = 29; bold: average change \pm S.D. to 1.50 ± 0.79 of control; $P_2 < 0.005$).

(B) Individual data points normalized to their control show a potential, weak correlation between TTX effects on $(\Delta F/F)_{\text{TPU}}$ amplitude and rise time (n.s.). Solid line: Linear fit to data.

(C) Individual data points for uEPSP rise time and uEPSP duration in TTX normalized to their control values versus the distance from soma, and linear fits to data.

(D) Left: Z-projection of granule cell scan with two neighboring, consecutively stimulated spines (white boxes 1, 2). Upper left: magnified scans of the stimulated spines. Scale bars in insets: 5 μm , scale bar below 25 μm . Right: Averaged $(\Delta F/F)_{\text{TPU}}$ in spine 1 and spine 2 in control conditions and in TTX. Scale bars: 25 %, 500 ms. In 7 out of 10 GCs with at least 2 measured spines in the same cell the TTX-induced reduction of $(\Delta F/F)_{\text{TPU}}$ differed by more than 20 % between spines,

(E) Intracellular Na_v blockade achieved by 10 mM QX-314 in the internal solution does not significantly affect EPSP amplitudes but increases rise times. Left: Control of Na_v blockade

via test of action potential generation. Black trace recorded right after establishment of whole-cell configuration, blue trace 10 min later. Scale bars: 10 mV, 2 ms. Middle, left: uEPSP amplitudes and rise times recorded 20 min after whole-cell configuration and control values from set of spines matched to same average distance from soma ($n = 15$ each set, TTX values shown for comparison). Average \pm S.D. uEPSP rise time 5.2 ± 2.1 ms QX vs. 2.5 ± 1.9 ms control, amplitude 1.8 ± 1.1 mV QX vs. 2.6 ± 2.6 mV control.

Figure S3, related to Figure 5: Detailed analysis of the model parameter sets that passed the following three criteria designed to capture the experimental findings: somatic EPSPs of less than 5 mV amplitude and rise times up to 5 ms, and evoked spine-head CaOGB signals within 150 % $\Delta F/F$. These conditions were satisfied by about 5000 parameter combinations out of the more than 100 000 combinations that were drawn uniformly from the seven-dimensional parameter space. To characterize the simulation results, two measures were used. M1 quantifies differences between EPSPs under control and TTX condition, similarly, M2 captures differences in the fluorescence signal.

(A) Population data illustrating the interdependencies between parameters in the model. Within each subpanel, every parameter set that passed the three criteria is shown by one point; rows and columns denote the quantities of interest, which, apart from R_{Neck} and the aspect ratio α , are the respective ionic currents, integrated over time. Grey points represent parameter sets for which $M1 < 0.1$ and $M2 < 0.05$; yellow points mark solutions with $M1 \geq 0.1$ and magenta points correspond to $M2 \geq 0.05$. Since magenta points are plotted above yellow points, solutions that satisfy both criteria appear as red. The case shown in **Fig. 5** is indicated by black asterisks in (A-C). The respective parameter values are listed in **Table S4**.

(B) The measure M1 denotes the Euclidean distance in the EPSP-rise time/EPSP amplitude space between the control and TTX scenarios; M1 values larger than zero reflect parameter combinations for which blocking Na_v s changes the EPSP wave form. Conversely, a M1 value

of zero means that blocking Na_vs does not influence the EPSP shape, which is only possible if the Na_vs are not activated in the control case.

(C) The measure M2 represents the relative change (control vs TTX) of the maximal fluorescence signal amplitude within the spine-head. A M2 value of zero means that the influx of Ca^{2+} did not change, implying that the dynamics of the CaOGB signal in the spine head is not affected by blocking the Na_vs . M2 values larger than zero are cases in which the CaOGB signal in the control case exceeds the signal in TTX.

(D-F) Histogram of the sampled parameter values. Parameter combinations that did not meet both the M1 and the M2 criterion are shown by black bars; color code of the other solutions as in (A).

(G,H) Correlations within every panel in (A-C), computed for those parameter values that lead to solutions that exceed the M1 (G) and M2 (H) thresholds, respectively. An arrow pointing straight up represents an r-value of 1, whereas an arrow pointing straight down represents an r-value of -1. P-values: * < 0.05, ** < 0.01, *** < 0.001.

Supplemental Tables

Table S1, related to Figure 1

		Stimulation type							
		TPU		synaptic evoked			synaptic spontaneous		
Parameter		mean ± SD	n	mean ± SD	n	P	mean ± SD	n	P
$\Delta F/F$	amplitude spine (%)	46 ± 24	48	40 ± 21	34	ns	45 ± 15	26	ns
	rise time (ms)	80 ± 50	35	84 ± 28	22	ns	70 ± 36	19	ns
	ratio slow : fast spines	30:70		28:72			n.a.		
	$t_{1/2}$ (ms) fast spines	720 ± 300	27	600 ± 300	30	ns	n.a.		
	amplitude dendrite (%)	2 ± 3	48	3 ± 4	34	ns	1 ± 3	24	ns
EPSP	amplitude (mV)	3.2 ± 3.3	45				3.1 ± 2.7	19	ns
	rise time (ms)	3.4 ± 1.9	39				2.9 ± 1.9	11	ns
	decay half time (ms)	30 ± 11	26				29 ± 21	13	ns
	mean distance to soma (μm)	90 ± 68	39				105 ± 69	26	ns

Legend Supplemental Table S1: Comparison of two-photon uncaging evoked signals and synaptic signals.

Synaptic evoked: evoked mitral cell input data from Egger et al. (2005)

Synaptic spontaneous: Spontaneous responses in the absence of caged compound with Ca^{2+} transient localized to spine head (from Egger et al. 2003 and additional observations). Spontaneous EPSPs were coincident with a spontaneous $\Delta F/F$ transient localized exclusively to a spine in the external plexiform layer. The decay kinetics of spontaneous $\Delta F/F$ events could not be analysed because frequently the spontaneous event was either cut off by the end of the scan or overlapped in its decay with evoked $\Delta F/F$ events.

Slow spines: all spines with $\Delta F/F$ half duration $\tau_{1/2} > 1.5$ s (Egger et al., 2005)

Amplitude dendrite: measured in immediately adjacent dendritic shaft

Mean distance to soma: This value was also included as it influences EPSP rise times (see Fig. S1).

P: Mann-Whitney test of difference between TPU and synaptic data sets; since synaptic evoked EPSPs were not unitary, they are not included here.

Table S2, related to Experimental Procedures

		Substance				P
		DNI-Glu		MNI-Glu		
Parameter		mean \pm SD	n	mean \pm SD	n	
$\Delta F/F$	amplitude spine (%)	44 \pm 22	26	51 \pm 27	29	ns
	rise time (ms)	79 \pm 69	26	90 \pm 53	25	ns
	amplitude dendrite (%)	3 \pm 3	24	2 \pm 3	27	ns
EPSP	amplitude (mV)	3.0 \pm 3.3	25	3.0 \pm 3.1	24	ns
	rise time (ms)	3.9 \pm 1.7	25	2.7 \pm 2.0	18	ns
	decay half time (ms)	32 \pm 9	13	27 \pm 13	13	ns

Legend Supplemental Table S2: Comparison of TPU evoked signals using either 0.8 mM DNI-Glu or 2.5 mM MNI-Glu. Possible statistical differences were analysed with the Mann-Whitney-Test.

Table S3, related to Experimental Procedures

		Condition		
		Control	Muscimol	Average ratio Muscimol/Control
Parameter		mean \pm SD	mean \pm SD	mean \pm SD
$\Delta F/F$	amplitude spine (%)	47 \pm 21	44 \pm 24	0.91 \pm 0.16
	rise time (ms)	79 \pm 52	73 \pm 52	0.95 \pm 0.49
uEPSP	amplitude (mV)	1.4 \pm 1.1	0.9 \pm 0.5	0.90 \pm 0.57
	rise time (ms)	5.7 \pm 2.3	4.3 \pm 1.7	0.87 \pm 0.58

Legend Supplemental Table 3: Control for side-effects of 10 μ M muscimol.

All data are from TPU-evoked signals before and after wash-in of muscimol (n = 4 spine signals in 3 cells).

Table S4, related to Supplemental Experimental Procedures

Type	Model Name	Reference	Parameter value in Fig.5
AMPAR	ampa5.mod	Destexhe, A., Mainen, Z.F., and Sejnowski, T.J. (1998). Kinetic models of synaptic transmission. In <i>Methods in Neuronal Modeling</i> . Koch, C., Segev, I., eds.(Cambridge, USA: MIT Press), pp. 1-25.	4781 pS
NMDAR	nmda5.mod	Ibid.	96 pS
Na _v	na12.mod	Author: Zach Mainen, Salk Institute, 1994, zach@salk.edu	2246 pS/μm ²
K _{DR}	kdrmt.mod	Migliore, M., Cavarretta, F., Hines, M.L., and Shepherd, G.M. (2014). Distributed organization of a brain microcircuit analysed by three-dimensional modeling: the olfactory bulb. <i>Front Comput Neurosci</i> . 8:50. doi: 10.3389/fncom.2014.00050.	3130 pS/μm ²
HVACC	capn.mod	Li, G., and Cleland, T.A. (2013). A two-layer biophysical model of cholinergic neuromodulation in olfactory bulb. <i>J. Neurosci</i> . 33:3037-3058.	3.3 pS/μm ²
Diffusion-Reaction	cadif.mod	Carnevale, N. T., and Hines, M.L. (2003). <i>The NEURON Book</i> , Chapter 9. Cambridge, Cambridge University Press.	α = 0.41 μm
Neck resistance			R _{neck} = 1.42 GΩ

Legend Supplemental Table S4: References for components of the model described in Supplemental Methods and values of the parameters used for the simulation shown in Fig 5.

Supplemental Experimental Procedures

Data analysis and statistics

Changes in calcium were measured relative to the resting fluorescence F_0 in terms of $\Delta F/F$ as described previously (Egger et al., 2005). Off-line data analysis was performed using custom macros written in IGOR Pro (Wavemetrics, Lake Oswego, OR, USA) and MES (Femtonics) and custom MATLAB (MathWorks, Ismaning, Germany) scripts.

For analysis, consecutive $(\Delta F/F)_{\text{TPU}}$ recordings and somatic uEPSPs in the same spine and pharmacology condition were averaged and smoothed. If the uEPSP average was not overly contaminated by noise such as spontaneous activity and/or an instable baseline, uEPSP rise times were analysed in terms of the interval between 20% and 80% of total uEPSP amplitude; the same holds for the rise time of $(\Delta F/F)_{\text{TPU}}$. Integration of uEPSPs and measurement of half time of decay (to 50% of the total EPSP amplitude) was performed only on averaged data. The duration of uEPSPs was measured in terms of the integral normalized to the uEPSP amplitude. If contamination by spontaneous transients in the average occurred in the second half of the averaged uEPSP and duration values were to be compared in two conditions for the same spine, i.e. in the absence and presence of a pharmacological compound, the integral value was taken until the contaminated time in both conditions; if contaminations occurred earlier on, data were rejected. Therefore our paired data sets represent an underestimate of integral differences.

The coefficient of variation was analysed in a subset of TTX experiments, with sufficient signal-to-noise ratio of individual $(\Delta F/F)$ recordings in the presence of TTX and at least 5 recorded traces in control and TTX. There was no bias towards experiments with a large effect of TTX on $(\Delta F/F)_{\text{TPU}}$ amplitudes (average reduction to 0.71 ± 0.14 of control). We also included some experiments in the analysis with other drugs present that did not exert any major effect on $(\Delta F/F)$ (7 out of 15 with either thapsigargin or mibefradil or 4-AP).

If necessary, the $(\Delta F/F)$ amplitudes of spontaneous events were analysed by subtraction of a fit to the decay phase of $(\Delta F/F)_{\text{TPU}}$. If more than one spontaneous event was observed in a given spine, amplitude values were averaged.

Experiments were discarded if the change in resting fluorescence F_0 between control measurements and in the presence of drugs exceeded 15% of control or if other disrupting changes were observed, like strong alterations of spine morphology, dendritic swellings or electrophysiological signs of cell deterioration.

For the cumulative comparison of $(\Delta F/F)_{\text{TPU}}$ and $(\Delta F/F)_{\text{syn}}$ in **Fig. 1C** and in **Table S1**, data were matched for similar numbers of spines and similar average distance from soma, since the latter is significantly correlated to $(\Delta F/F)_{\text{TPU}}$ and uEPSP rise time, as shown in **Fig. S1B,C**. To compare control experiments and experiments with intracellular QX-314 we also matched the set of control spines for the same average distance from soma of $\sim 80 \mu\text{m}$ to eliminate possible effects of dendritic location on EPSP rise times, as shown in **Fig. S1B**. The measurement of spontaneous EPSP rise times was performed for 25 EPSPs in each group (right after break-in vs. 20 min later).

To assess statistical significance levels, the non-parametric Wilcoxon matched-pairs signed-ranks test was applied for comparing paired data sets (e.g., control TPU transients and ensuing transients after pharmacology wash-in in the same spine), while the non-parametric Mann-Whitney test was used to compare unpaired data (e.g. TPU data vs. synaptic data from different sets of neurons). The given P values refer to non-directional tests unless stated otherwise (P2 and P1, respectively). Significance of correlations was established with a t-test (vassarstats.net).

Estimate of spine neck length

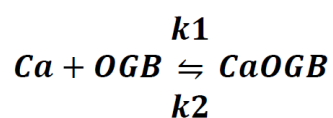
To estimate the length of spine necks (**Fig. S1B**), we evaluated the fluorescence intensity along the scan line connecting the dendrite and the spine head. We measured the distance between the fluorescence maxima in spine head and shaft and subtracted from this distance

the added mean radii of GC spine heads and dendritic shafts as estimated earlier ($\sim 1.1 \mu\text{m}$; Egger and Stroh, 2009 and Woolf et al., 1991). This estimate neglects differences in spine head shape and the extent of spine necks in the z-dimension; however, most spines were in a similar focal plane as their parent dendrites.

Simulations

General Framework. The simulations described in this paper were exclusively done via the NEURON extension for Python (Hines et al., 2009); data analysis and manipulation was performed within Python. Mechanisms which described ion channels or receptors were used “as is” presented in previous publications (see **Table S4**) and were left unmodified, with the exception of the NMDA receptor where an extra Ca^{2+} current was introduced. The NMDAR-mediated Ca^{2+} -current had the same driving force as the one used for the HVACC and a conductance 0.2 times the set NMDAR-conductance. The diffusion-reaction system was modified such that also the buffer (OGB-1) and the complex (CaOGB) were capable of radially and longitudinally diffuse diffusing within the volume, along with the ion of interest (Ca^{2+}).

The model's internal Ca^{2+} diffusion and buffering dynamics were implemented separately from the voltage dynamics. The model allowed us to investigate how fluorescent molecules spread from the spine head into the dendrite. The diffusing species propagate both longitudinally, between adjacent segments, as well as radially, between the four shells of a segment, according to their respective diffusion constants. The diffusing species are: free Ca^{2+} , the fluorescent dye OGB-1 and the fluorescing CaOGB complex. Within every shell of every compartment the following buffering reaction takes place:



Here, k_1 and k_2 are the binding and the unbinding rates, respectively. Concentration differences in any of the three species lead to a flux

$$J_i = -D_i \cdot \nabla c_i$$

where $i \in \{Ca, OGB, CaOGB\}$.

The spine neck dictates the electrical as well as the chemical compartmentalization of dendritic spines. As Ca^{2+} carries only a small fraction of the total electrical current, we segregated these two components and analyzed them separately.

The molar current, J_i , between the spine head and the dendritic shaft is:

$$J_i = -D_i \int_{A_{Neck}} \frac{c_i^{head} - c_i^{dend}}{L_{Neck}} da$$

where A_{Neck} is the cytoplasmatic cross-sectional area of the spine neck, L_{Neck} is the neck length, and c_i^{head} and c_i^{dend} are the concentrations of ionic species i in the spine head and dendrite, respectively. If the integrand above is constant, then:

$$J_i = -D_i \frac{A_{Neck}}{L_{Neck}} (c_i^{head} - c_i^{dend}) = -D_i \cdot \alpha \cdot (c_i^{head} - c_i^{dend})$$

where α is the aspect ratio of the spine neck, measured in μm . In accordance with the experimental data, we considered long spine necks, i.e., aspect ratios smaller than unity.

Simulation setup. The granule cell was modelled as a soma with one dendrite attached; the compartments had purely passive electrical properties but included the detailed description of the diffusion-reaction process, as sketched above. 50 equally spaced compartments which represent the spine heads were distributed along the dendrite; the connection to the dendrite happened via two separate processes: one set the spine neck resistivity while the other

adjusted the diffusion rate of the diffusing species between the spine head and the dendrite as previously described. In addition to the passive properties and the diffusion-reaction formalism, the following mechanisms were implemented in every spine head: AMPA receptors, NMDA receptors, Na_v channels, K_{DR} channels and HVACCs. Before starting the simulation, all cell compartments were initialized with the resting membrane potential (-77 mV) and a concentration of the fluorescent buffer of 100 μM . After 50 ms a glutamate pulse (10 mM for 1 ms) was simulated, leading to the opening of the AMPA and NMDA receptors. The total simulated time was 2 sec.

Parameter-space scan. For every run, one parameter combination was selected by drawing a random number from a uniform distribution for every parameter of interest. The parameters of interest were (range of distribution in brackets): g_{AMPA} (20 – 5000 pS), g_{NMDA} (20 – 600 pS), $g_{\text{bar_Na}_v}$ (20 – 5000 pS), $g_{\text{bar_K}_{\text{DR}}}$ ((20 – 5000)•10 pS), $g_{\text{bar_HVACC}}$ (1 – 300 pS), R_{Neck} (0.1 – 5.0 $\text{G}\Omega$) and α (0.01 – 1.00 μm). After the run was completed, the resulting current, voltage and concentration traces were kept if the simulation result fulfilled the following criteria:

- a) The EPSP amplitude measured at the soma was between 0 and 5 mV.
- b) The EPSP rise time (from 20% to 80% of the EPSP amplitude) at the soma was between 0 and 5 ms.
- c) The CaOGB signal in the spine-head did not rise above 150% $\Delta\text{F}/\text{F}$.

If all of these criteria were fulfilled, the simulation was run again to investigate the effects of TTX in that particular scenario, i.e. the Na_v conductance was set to 0, while all other parameter values were kept.

More than 100.000 parameter combinations were tested, of which approx. 5000 fulfilled the criteria listed above. For this set of runs, we measured the charge flowing through the AMPAR, NMDAR, Na_v, K_{DR}, and HVACC channels and defined two metrics:

- a) M1 – the Euclidean distance in the EPSP-amplitude/EPSP-rise time space defined as:

$$M1 = \sqrt{(\Delta V - \Delta V_{TTX})^2 + (\Delta T - \Delta T_{TTX})^2}$$

where ΔV and ΔT are the EPSP amplitude and the rise time, respectively, and the subscript TTX refers to the run in which the Na_v channels were blocked.

- b) M2 – the relative change of the maximal amplitude of the CaOGB signal in the spine-head. Thus:

$$M2 = \frac{\max(\mathbf{CaOGB}) - \max(\mathbf{CaOGB}_{TTX})}{\max(\mathbf{CaOGB})}$$

Using these two metrics we applied a simple threshold criterion ($M1 > 0.1$; $M2 > 0.05$) to investigate the parametric dependencies. Because Na_v, K_{DR} and HVACC are voltage-dependent, we chose to evaluate the integral of these currents, rather than using the conductance value set at the initialization of the run.

Supplemental References

Egger, V., and Stroh, O. (2009). Calcium buffering in rodent olfactory bulb granule cells and mitral cells. *J. Physiol.* 587, 4467-4479.

Hines, M.L., Davison, A.P., and Muller, E. (2009). NEURON and Python. *Front.*

Neuroinformatics 3, 10.3389/neuro.11.001.2009.

See also **Table S4**.

Figure S1
Bywalez et al.

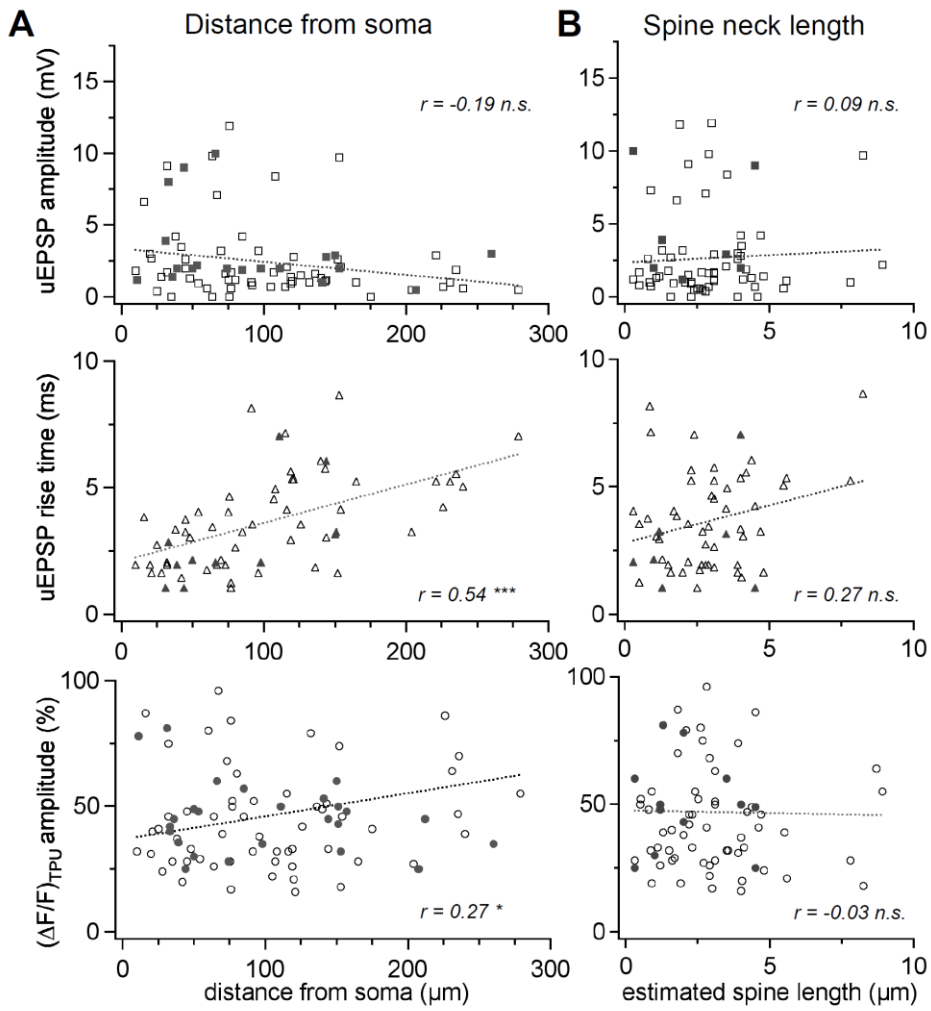


Figure S2 Bywalez et al

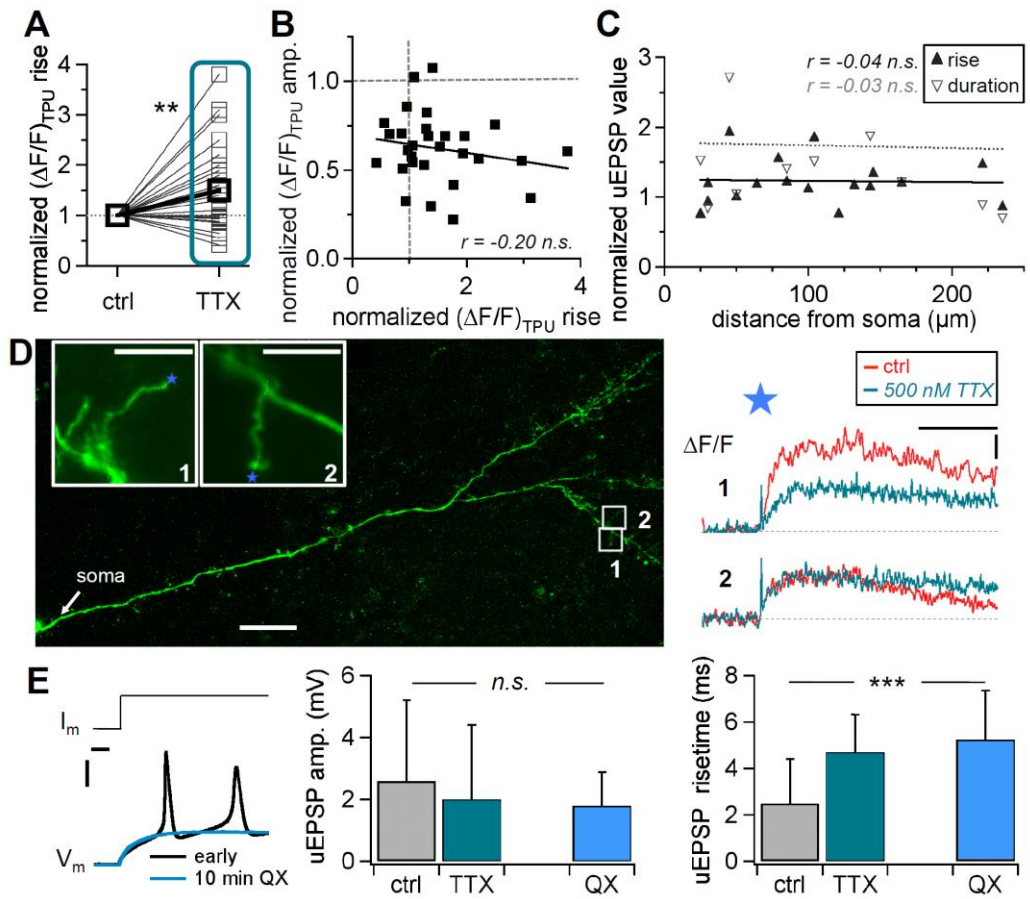
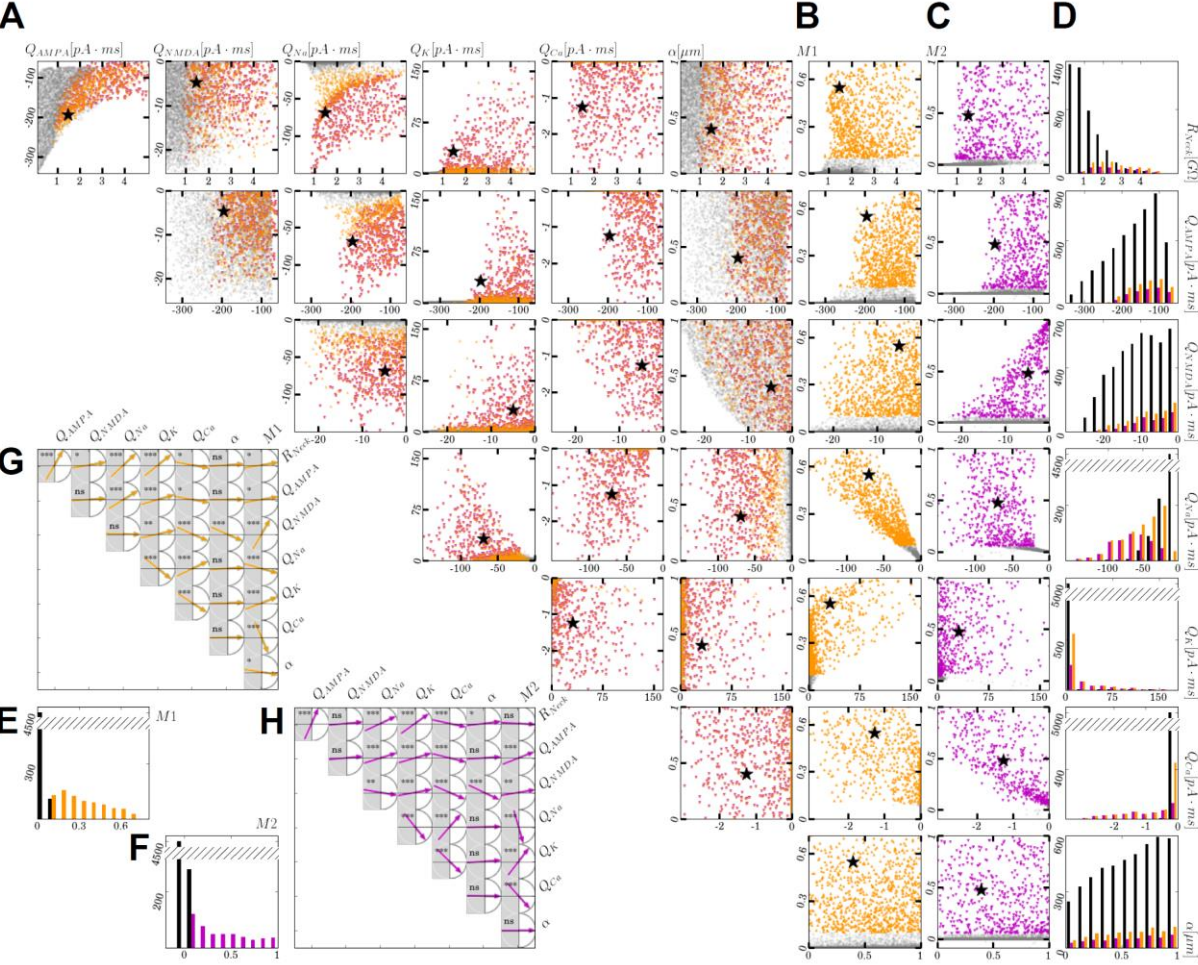


Figure S3 Bywalez et al.



4. Discussion

Two experimental studies focused on the morphology and physiology of bulbar interneurons in mouse and rat bulbar slice preparations.

The dopaminergic study demonstrated the viability of DAT based marker methods (FFN102 and a transgenic inducible DAT construct) to mark bulbar dopaminergic cells, partially different from previously described TH positive cells, which unveiled new cell types. A new glomerular innervation analysis tool was successfully utilized to discriminate the new cell types despite similar morphology appearance in some instances. Densely clustered dendritic specializations clasping mainly around single cell bodies have been observed in one of the new cell types. The whole dendritic tree of these clasping cells shows substantial calcium influx upon somatic stimulation, opening up the possibility of neurotransmitter release in clasping and non-clasping compartments. Different abundance and morphology of subtypes in the three tested populations emphasize a developmental dimension in this cell population dependent on animal age, cell age and/or species.

Experiments on OB GCs showed for the first time the purely local activation of HVACCs by a Na_v -dependent boosting mechanism in a subset of GC spines. The strong and complex activation mechanism in those spine heads involves a sequence of several channels, tested with pharmacology and supported by computational modeling. Local physiological activation includes Na_v s, AMPARs, NMDARs, HVACCs and K_{DRS} and excludes several other contributors, like internal calcium stores, T-type calcium channels, A-type or big conductance potassium channels. Despite a very strong local depolarization of the spine, the electrical signal reaching the GC soma is very small, speaking for a strong attenuating influence of the spine neck. This supports a functional role of GC spines in electrical compartmentalization, which could also be replicated in the theoretical model.

4.1. Spine compartmentalization and spine function

Many excitatory connections in the central nervous system are made onto the heads of dendritic spines. Those structures can be transient, motile and plastic, and are only very rarely stable (Alvarez and Sabatini, 2007). It is known that a spine's morphology can substantially change during plasticity events and the alterations are also thought

to affect the synaptic weights (Coss and Globus, 1978). Their morphology or geometry correlates with AMPA receptor repertoire and thereby determines synaptic strength (Matsuzaki et al., 2004). Recent high-resolution microscopy experiments and modeling studies additionally show some evidence for the spine neck morphology and plasticity having a functional impact on the synapse and the electrical regimes it is working in (Araya et al., 2014; Tonnesen et al., 2014). Small input compartments with a highly resistant junction to the dendrite open up the possibility of electrical amplification that can strongly influence the spine's physiology by employing high-voltage activated conductances (Miller et al., 1985; Segev and Rall, 1998; Spruston, 2008). Some reports, including our own, indicate some instances of special spine morphologies in which the input resistance could be high enough (reaching $G\Omega$ range) for such amplification processes to work (Grunditz et al., 2008; Bywalez et al., 2015).

Other reports refute the idea of spines serving as electrical compartments and describe the neck resistance as too low to have any effect (Svoboda et al., 1996; Popovic et al., 2015). In the latter, very recent report, evidence suggests that with an estimated resistance of only 30 $M\Omega$, electrically, spines behave as if they were located directly on dendrites (Popovic et al., 2015). Regarding the different viewpoints on the electrical role of spines, this subject has to be looked at with advanced techniques, directly visualizing the voltage in all compartments and resolving the spine morphology with super-resolution techniques and with spine type specificity. In Bywalez et al. (2015), the frequent activation of high voltage activated channels during local input with just small or no electrical signal reaching the soma (Fig. 2 and 3) indicates a very strong depolarization of the spine locally. This observation is most likely explained by a strong attenuation through the highly resistant neck, as discussed in the publication.

Diffusion observations in these experimentally tested cells support the notion of highly isolated granule cell spines. The fluorescent filling of distant spine heads in the EPL, bearing the reciprocal pre- and postsynaptic elements, took much longer than the filling of dendrites which they protruded from or the filling of proximal shorter spines (personal observations - not shown or quantified in the manuscript). Decay times of fluorescence recovery experiments of some other studies seemed to span a large range with several extremely slowly decaying signals in well isolated spines (Bloodgood and Sabatini, 2005; Grunditz et al., 2008). Although the quantified slow calcium dynamics (Table S1) and slow filling observations of this GC study do in fact parallel the observations of the

dye diffusion experiments used in the referenced studies, they can unfortunately not simply be compared directly. This is due to the fact that several channels or transporters on the cell membrane or on internal stores such as the endoplasmic reticulum distort the kinetics by actively moving calcium between the respective compartments (Grienberger and Konnerth, 2012). Moreover, size, polarity, buffering and many other molecular factors of biologically inactive fluorescent dye, as opposed to calcium, are different. Therefore, a comparison of calcium dynamics between different spine types should serve as a better indicator of the special isolation of gemmules. In this respect, the calcium dynamics of other structures like hippocampal or neocortical spines show much faster (diffusive) kinetics than gemmules, with fast exponential spine calcium decay rates and diffusional leak into the dendrite (Majewska et al., 2000; Cornelisse et al., 2007). Synaptic activation of the gemmule leads to slow, usually linearly or only slowly exponentially decaying calcium transients without a distinct calcium elevation in the dendrite (cf. Fig 1 of Bywalez et al., 2015; Egger et al., 2005). The slow calcium dynamics in GCs are mostly due to very slow extrusion mechanisms, which could functionally be coupled to asynchronous release dynamics of the spine that can shape bulbar output patterns (Egger and Stroh, 2009). Moreover, the exceptional isolation and uncoupling of the spine head compartment can at the same time foster independent signaling by leaving the rest of the cell largely unaffected. Interestingly, in the dopaminergic JGC study, all compared subcompartments of the cell showed surprisingly slow calcium decay kinetics upon somatic AP generation (results section 3). The functional underpinnings of this observation could not be elucidated yet, but these dynamics might play a role in (slow) transmitter release or intracellular signaling. Whether these dynamics change with cell age, maturation state, animal age, or are limited to the clasping cell type, form interesting questions for future research. In general, compartmental calcium accumulations can lead to neurotransmitter release (Halabisky et al., 2000; Egger and Stroh, 2009), induce long-term plasticity events (Cummings et al., 1996; Malenka and Nicoll, 1999), regulate ion channels such as other calcium conductances (Budde et al., 2002), and are involved in morphological change like dendritic growth (Sin et al., 2002) or spine formation and reshaping (Jourdain et al., 2003; Oertner and Matus, 2005).

With granule cells being able to signal in multiple modes partially independent of the rest of the cell (Egger et al., 2005), and with their plastic regulation of connectivity to projecting cells by synaptic plasticity and adult neurogenesis (Dietz and Murthy, 2005;

Nissant et al., 2009), it makes them potent all-round talents influencing bulbar computations in local and far-range circuitry.

4.2. Functional implications of bulbar physiology in discussion with recent literature

4.2.1. Studies with well-preserved feedback connectivity in the olfactory bulb

With powerful methodological advances, recent physiological bulbar research tends to focus on *in vivo* experiments, sometimes even in awake animals, and/or modeling studies that often include neuromodulatory aspects. The motivations behind this are reasonable, as bulbar interneurons and their main synaptic partners, projecting cells, are strongly influenced by cortical and modulatory feedback fibers, which cannot be investigated in acute brain slices and only to a limited extent in anesthetized animals. Traditional anesthesia mixtures are known to have a strong impact on several centrifugal and possibly local inputs (Rinberg et al., 2006; Kato et al., 2012; Mion and Villeveille, 2013), which should be taken into consideration. In fact, some studies in awake rodents show substantially changed representations of odors in the bulbar circuitry and different output dynamics from anesthetized animals, which include dynamic sniff-shaped temporal and spatial information, containing more odorant aspects like concentration and odor value (Nunez-Parra et al., 2014). Thus, sensory representation in the olfactory system is strongly dependent on the behavioral state of the animal. During wakefulness, GCs are highly active compared to the anesthetized state (Kato et al., 2012), leading to a sparsification and temporal decorrelation of MC responses to odorants in the awake state. This study also revealed that repeated odor exposure leads to odor specific, experience dependent, long term changes in mitral cell output, which is absent in anesthetized animals. Using whole-cell recordings in awake mice, Kollo et al. (2014) reported highly heterogeneous baseline firing rates of bulbar projection cells with a substantial population (one third) of ‘silent’ projection cells showing very low firing rates at rest. Upon strong sensory input, those silent cells became particularly active, whereas cells with high baseline activity showed either only weak excitation or even hyperpolarization. Therefore, upon odor stimulation, these silent cells could have a disproportionately strong influence on signal transduction compared to the other cells.

4.2.2. Recent studies on granule cell functionality

Odor evoked as well as spontaneous MTC firing seems to underlie respiratory patterning via OSN-relayed odorant and mechanoreceptive stimuli (Grosmaître et al., 2007; Carey and Wachowiak, 2011). This phasic modulation strongly influences the GC membrane potential, which has an impact on GABA release since it can also occur in subthreshold regimes (Egger et al., 2005). Recent studies showed a substantial, stereotyped modulation of GC activity by respiration under anesthesia and during wakefulness, yet strongly desynchronized firing responses in awake states. This is probably due to a much more extensive active modulatory network interfering with the sensory input channel (Czakoff et al., 2014; Youngstrom and Strowbridge, 2015). Labarrera et al. (2013) propose that, although GCs are predominantly excited via sniff shaped olfactory stimuli, the spiking output is gated via tonic inhibitory regulation. This tonic regulation could involve many inhibitory inputs, discovered over the last few years, including bulbar cells (dSACs, Blanes cells – Pressler and Strowbridge, 2006; Eyre et al., 2008; Burton and Urban; 2015), as well as many centrifugal pathways (cf. e.g. Nunez-Parra et al., 2013; Fig. I1, and section 1.5) and even astrocytic influences (cf. Kozlov et al., 2006; or similar to observations in the cerebellum – Lee et al., 2010). Recent publications focusing on the impact of cortical feedback and neuromodulatory areas on GC physiology complement the knowledge gained with earlier studies in *in vitro* preparations significantly. Cortical drive can activate, inhibit or modulate GCs in a state-dependent manner via many pathways (Balu et al., 2007; Nunez-Parra et al., 2013; Li et al., 2015, section 1.5). Yet the recent discovery of many local bulbar inputs to GCs and MCs even opens up new research possibilities in slice experiments (Eyre et al., 2008; Huang et al., 2013). In this respect, one study conducted in acute slices experimentally tested an extended circuit framework of mitral cell and granule cell interactions: Burton and Urban (2015) included the regulation of GCs via deep short-axon cells, which are also activated via the projection cells and thereby feed-forward inhibit GCs to decorrelate and temporally distribute their output onto projection cells. The importance of this thesis' experimental GC study and the mechanistic findings on general spine function alongside with the special function of a subset of reciprocal spines on granule cells provides a useful physiological basis for any kind of research on GCs.

4.2.3. Focus on dopaminergic cell physiology and function and large-scale bulbar signal transformations

A large amount of functional *in vivo* data suggests important roles for dopaminergic JGCs in odor processing. These cells, combining local circuitry and lateral connections, broadly distribute odor input as low amplitude signals over large glomerular areas irrespective of the odorant or the input-activated glomeruli (Banerjee et al., 2015). DAT+ cell activation implements gain control and decorrelation of mitral cell odor representations by primarily interacting with the driving ETCs via gap junctions and chemical synapses in a graded fashion (Banerjee et al., 2015). The interesting effects of synaptic and gap junctional coupling to ETCs could associate them with shaping the synchrony of oscillations and it also entangles the roles of both cells in their attributed pacemaker activity (Hayar et al., 2004a; Pignatelli et al., 2005; Masurkar and Chen, 2012; Liu et al., 2013).

A different study, conducted on non-differentiated juxtglomerular cells, did not report a similarly far-spread lateral activity throughout the glomerular layer (Homma et al., 2013). It is possible that with their odor stimulation and activity detection cut-off (to separate neuronal from glial signals), and temporal filtering methods they did not pick up the low amplitude signals or did not choose to mention them as such. The mostly local occurrence of inhibited glomeruli around excited ones (as derived from their figures) could be explained by connections from oligoglomerular dopaminergic cells (Kiyokage et al., 2010) or the clasping cells in this thesis' dopaminergic report (Fig. 3). Since GABAergic periglomerular cells are mostly uniglomerular (Nagayama et al., 2014) and morphologically comparable to the dopaminergic uniglomerular cells (Fig. 2), most of the lateral inhibitory action is probably exerted by local range dopaminergic cells. The net inhibition of the adjacent glomerular neuropil and many surrounding cell bodies in Homma et al. (2013) speaks for some inhibitory influence of odor stimulus-driven interneurons onto excitatory cells. Some targeted cells are most probably ETCs, since they drive many cell types of their 'parent' glomerulus and their inhibition lowers the excitatory response of the glomerulus massively. Any cell's 'parent' glomerulus corresponds to the odor responsive glomerulus, which shows an overall odorant response similar to the respective surrounding cell. Excitation of the odor-responsive glomerulus and inhibition of an adjacent one is not likely to be explained by far-spread involvement of gap junctions but rather by synaptic connections. In what way

GABAergic and dopaminergic synapses interact in this activity could not be resolved in any of the *in vivo* reports yet. The clustering of activated or inhibited cells in the vicinity of their parent glomerulus additionally supports the previously discussed conclusion of the dopaminergic project, that probably the drive of excitatory cells as well as regional lateral inhibitory cells, respectively, originates from a single glomerulus, the parent glomerulus (Homma et al., 2013). It is quite certain that the 'home' glomerulus, the way we termed it in our manuscript, equates to the parent glomerulus for uniglomerular cells. In clasping cells this uniglomerular drive is very probable as well – despite the fact that some of the dendrites surround several other adjacent glomeruli. These other processes are most likely inhibitory output structures (as discussed in the dopaminergic cell report), which is also supported by the observation of inhibited glomeruli in Homma et al. (2013). In this respect, again, it would be interesting to find out on which cell structures the driving input to dopaminergic cells is located. Furthermore, the question remains on which dendritic portions output structures can be found and to what extent those regions possibly overlap. The presence of additional responsive cells (strong rise in inhibited responses) and conversion of excited to inhibited cell responses with increasing odorant concentration as described by Homma et al. (2013) is unlikely to be explained by uniglomerular cell type actions with fast-acting neurotransmitters alone. Rather the reported modulatory divergent functions of dopaminergic cells (Liu et al., 2013), with two active neurotransmitters and gap junctional coupling to excitatory cells (Banerjee et al., 2015), leading to gain control of bulbar output computations, is suitable to elicit such actions. Dopamine transmission might be reserved to strong activation of the cell (Maher and Westbrook, 2008) or at least certainly follows different release mechanisms from the GABAergic transmission (Borisovska et al., 2013). Other neuromodulatory actions could additionally participate in the reported *in vivo* circuitry behavior found in Homma et al. (2013), but as proposed earlier, anesthesia during the experiments might have interfered with those pathways.

In a chronic-window implantation *in vivo* study, functional transformations of odor inputs were tested by imaging large areas of the dorsal bulbar circuitry, differentiating the response properties of distinct cell populations (Adam et al., 2014). Interestingly, the viral vector for introducing GCaMP reporters into their interneuron population yielded a very high transfection rate for TH+ cells (45%). The number represents a massive selective overrepresentation of this specific cell type compared to the normal

proportion of dopaminergic cells of all bulbar interneurons, which rather lies on the scale of little more than 6% (percentage of TH+ cells among all bulbar chemospecifically stained neurons – constituting 11% in the GL and only 3% in the EPL and 1% in the IPL – Parrish-Aungst et al., 2007). Therefore, a large proportion of the observations of this transfected group is reflective of dopaminergic cell activity which, curiously, is not specifically mentioned in the manuscript. The study shows several trends, using short and persistent odor exposure experiments and activity correlation comparisons over large areas of the bulbar surface: The parallel output streams of the olfactory bulb by MCs and TCs (Fukunaga et al., 2012) are indeed very different in spatial, temporal and individual versus correlated population responses. TCs relay a rather undistorted, precisely timed, low threshold activated and fast adapting signal of glomerular inputs to cortical areas. MC information is highly complex in space and time, with a distorted representation of the odor inputs. The interneuron response (including many DAergic JGCs) is correlated locally with short stimuli. Using prolonged odor stimulation, they show the most temporally diverse signals with a strong decrease in correlation, probably being subject to strong influence by interneurons themselves. Very importantly, their activation is coupled to the MC decorrelation in intra and inter-glomerular inhibition, fitting very well to the other functional reports.

Another *in vivo* study assessed the influence of glomerular interneuron circuitry in diverse processing mechanisms (Fukunaga et al., 2014). In consent with other publications, theta rhythm phase segregation of MCs and TCs is mediated within the glomerular layer circuitry and the theta rhythm itself is mediated by feedforward inhibition mechanisms of glomerular interneurons. Inhibitory INs change their output dependent on odorant concentration and, in addition to that, conversion of inhibitory responses to excitatory responses can be observed in projection cells, posing a complementary observation to the response changes of JGCs observed in Homma et al. (2013). Parallel glomerular excitatory and inhibitory feed-forward pathways are also concluded to be a non-topographical contrast enhancement mechanism (Fukunaga et al., 2014), as suggested by (Cleland and Sethupathy, 2006).

4.2.4. Rationale for lateral and columnar circuit elements

In bulbar processing, a clear center-surround (Mexican hat) organization of glomeruli and odor columns laterally has been disproven on many occasions. Further, strict chemotopic arrangements in terms of chemical class or structure seem unlikely on a glomerular level (Cleland and Sethupathy, 2006; Willhite et al., 2006; Fantana et al., 2008; Soucy et al., 2009). Yet, there exist some functional reports speaking in favor of lateral proximal and even longer-range meaningful connectivity. First, a quite invariant topography of glomeruli across individuals even in different phyla defies a completely meaningless arrangement (Ressler et al., 1994; Vassar et al., 1994; Imai et al., 2010). The study by Auffarth et al. (2011) shows a clustered glomerular organization correlated with perceptual quality and valence of the tested odorants. Perceptual quality representations have also been found in the piriform cortex (Howard et al., 2009). The study by Soucy et al. (2009), arguing against the idea of chemical mapping between nearby glomeruli, found at least some coarse domains of chemotopy and enhanced similarity on distance ranges on the scale of ~ 1 mm, which is within the range of large dopaminergic connections (Aungst et al., 2003; Kosaka and Kosaka, 2008). Interglomerular lateral inhibition in the GL was shown to functionally suppress output cells from other glomeruli over large distances (~ 600 μm) in bulbar slices (Whitesell et al., 2013). Furthermore, inside the EPL, PV cells make dense connections to output cells, within their process reach (~200 μm), regulating gain control functions of MCs regionally and strongly cross-connecting them (Kato et al., 2013; Miyamichi et al., 2013). The proximity of inhibited glomeruli to odor-stimulated ones (Homma et al., 2013) and the sheer existence of interglomerular laterally confined connections indicates putative topographical cues. The high complexity and variety of odor stimuli, (taking odorant mixtures into account, posing the majority of natural odor stimuli) presents an intricate, multidimensional odor space, which has to be represented in neuronal networks in an adequately sophisticated and thereby complicated manner. Combinatorial, plastic and experience dependent representations have to be in place to deal with this challenge. Olfactory stimulus decorrelation, a central task of bulbar transformations, can be computationally explained by intra-glomerular as well as interglomerular connectivity (Cleland and Linster, 2012). Since the neuronal substrates for both are in fact present, it is conceivable that both mechanisms play a role. Conclusively, it is very probable that the OB organization relies on topographical (Aungst et al., 2003; Auffarth et al., 2011; Kato et al., 2013) and sparse random and

selective connectivity mechanisms shaped by experience (Willhite et al., 2006; Fantana et al., 2008; Livneh and Mizrahi, 2012; Yu et al., 2014) in GL, EPL and other bulbar layers. Most GCs probably make non-topographical and non-predetermined, but rather experience dependent connections with mitral cells, with strong adult neurogenesis as a further factor of circuit plasticity. Dopaminergic cells could serve both organizational rules (topographical vs. random), probably with subtype-dependent efficiency: Large lateral-association cells generated in embryonic and perinatal stages (Kosaka and Kosaka, 2009) probably serve a topographic organization with their synaptic functions, although they can additionally participate in the global connectivity maps of gap-junction-connected networks. Local range cells spanning few adjacent glomeruli can serve both functions, associating local clusters either by inherent topographical design but also 'on demand' in an experience dependent manner via e.g. adult neurogenesis (Bonzano et al., 2014; Livneh et al., 2014). Uniglomerular cells are most likely involved in exclusively intraglomerular processing, although the role of the putative axon is unresolved yet.

By and large, the mentioned studies can thus be joined to a functionally coherent account of bulbar computations and yet again support specific roles of GCs and dopaminergic JGCs for output dynamics. In addition to that, the reported local and lateral transformations in the GL are in line with the subtype diversity of dopaminergic cells found in our study.

4.3. Physiological importance of adult neurogenesis

Very few brain areas exhibit adult neurogenesis, as it is an extremely costly and complex process, considering the remarkable diversity of cells produced in adult stages in the bulb. It seems that the sense of olfaction is particularly experience-dependent and utilizes substantial plastic circuit adaptations via the elimination and integration of neurons (Lazarini and Lledo, 2011). As introduced earlier, bulbar interneurons show a strong neurochemical diversity (Parrish-Aungst et al., 2007) and integrating neurons complement the adult circuitry with a yet broader diversity, since they differ in temporal origin and precursor-cell specific neurogenic area in the ventricle (Batista-Brito et al., 2008; Lledo et al., 2008; Merkle et al., 2014). Moreover, they show maturation-dependent physiological differences (Carleton et al., 2003; Mizrahi, 2007;

Livneh et al., 2014; Kovalchuk et al., 2015) and retain distinct properties from early-born cells even after full integration (Mouret et al., 2009; Nissant et al., 2009; Lepousez et al., 2014; Merkle et al., 2014). Moreover, it is interesting to mention the coexistence of different maturational states of adult born neurons at any given time in the operating circuitry in the bulb. Parallels to neuronal integration in the hippocampus suggest the necessity of adult neurogenesis for experience dependent association and learning mechanisms (Marin-Burgin et al., 2012). Changing receptual and perceptual needs in a new odor environment or with changing physiological states of an animal is often accompanied with changes in adult neurogenesis (Feierstein, 2012). In odor-enriched environments, the number of adult-born dopaminergic cells is adaptively upregulated (Bonzano et al., 2014). In the context of reproductive and social behavior, adult neurogenesis is strongly changed in both main and accessory olfactory bulb, which again bridges those organs' often proposed functional divide (Larsen and Grattan, 2012; Peretto and Paredes, 2014).

4.4. Multiple transmitter neurons – transmitter type determination

Dale postulated that neurons function as chemical units, although not necessarily with only one transmitter (Dale, 1935; Strata and Harvey, 1999). The classical notion of any neuron releasing only a single neurotransmitter was subsequently manifested in the literature as Dale's Principle in the early to mid-20th century (Eccles et al., 1954). This was considered to be the rule for decades and has only been refuted in recent neuroscience (Trudeau and Gutierrez, 2007; Vaaga et al., 2014). The coexistence of two or more neurotransmitters in the same neuron being co-released or co-transmitted has been observed in many combinations: among these the coexistence of a classical neurotransmitter and a neuropeptide, fast and slow-acting modulatory neurotransmitters like in DAergic JGNs, or even excitatory and inhibitory neurotransmitters have been found (Jan et al., 1979; Jonas et al., 1998; Vaaga et al., 2014). Not even the combination of DA and GABA is restricted to bulbar juxtglomerular neurons, as both transmitters can be expressed by cells in striatal culture neurons (Max et al., 1996) or in the retina (Huang and Moody, 1998). Latter study suggests that the expression of more than one neurotransmitter may only be a transient state of the neuron. In other systems like the hypothalamus, shifting

neurotransmitter phenotypes following changes in circuit signaling, have been observed as well (Liu et al., 2008). If such a transformation also occurred in the bulb, it could serve as another explanation for differences of abundance and detectability of different dopaminergic JGC subtypes (broadly discussed in the dopaminergic manuscript). Factors influencing the dopaminergic phenotype may include sensory and local circuit activity, age of the animal or the cell, as well as OB internal or external signaling cues (Matsushita et al., 2002). At least afferent activity or the lack thereof was already shown to directly influence bulbar JGC TH expression (Baker, 1990; Saino-Saito et al., 2004) and to counter-adaptively regulate D2 receptor expression (Guthrie et al., 1991).

4.5. Implications of olfactory bulb physiology in disease and clinical aspects

Olfactory dysfunction is a commonly used early indicator for neurodegenerative diseases like Parkinson's disease (PD) or Alzheimer's disease (AD) (Attems et al., 2014). Pathological changes can be observed in the olfactory epithelium, cortical structures, but also prominently in the olfactory bulb. While several diseases have an impact on olfaction, the causes and specific underlying mechanisms seem to be different in PD and AD. PD patients seem to be impaired in basic perceptual olfaction tasks, whereas AD patients show impairment in higher-order olfactory tasks involving cognitive processes (Rahayel et al., 2012). PD and associated diseases probably involve dopamine terminal dysfunctions and abnormalities of the basal ganglia and the olfactory tract and the degeneration of substantia nigra fibers to the OB (Scherfler et al., 2013; Hoglinger et al., 2015). The dopaminergic fibers from the substantia nigra terminate in EPL, GCL and MCL and therefore probably have a strong impact on the EPL computations between MCs and GCs, which could underlie the phenotypic deficits. In AD, olfactory deficits seem to be a cause of olfactory bulb and olfactory tract atrophy (Thomann et al., 2009). Protein aggregates formed by tau proteins are commonly found in patients with neurodegenerative disorders. Additionally, beta-amyloid clusters in AD patients, and alpha-synuclein aggregates in PD patients are abundant, respectively (Mundinano et al., 2011). The strong increase in dopaminergic glomerular neurons in both AD and PD is likely to be a compensatory mechanism for the early degeneration of other neurotransmitter systems influencing bulbar circuitry (Huisman et al., 2004; Mundinano et al., 2011). The generation of new dopaminergic

cells counteracting functional deficits of bulbar circuitry speaks for the integration of new-born cells depending on changing demands in bulbar circuitry (as discussed in Livneh et al., 2014 and the dopaminergic study of this thesis). Adult neurogenesis and integration is impaired in neurodegenerative diseases as well (Neuner et al., 2014). This study showed reduced dendritic differentiation, spine formation or stability and survival of adult-born GCs in a mouse model of increased alpha-synuclein aggregation. Clinical research and related studies have already shown the usefulness of SVZ stem cells or bulbar neural stem cells in replacing degenerated neurons therapeutically (Cave et al., 2014; Marei et al., 2015), which is why detailed research on those cells is very relevant.

4.6. Dendritic neurotransmitter release in the bulb and similar features in other brain areas

Dendritic neurotransmitter release is common in OB neurons. In fact, dendrodendritic contacts are even more abundant than axo-dendritic or axo-somatic synapses and include direct synaptic contacts as well as more diffuse spillover signaling (Schoppa, 2005). Reciprocal arrangements can be found in several layers, most prominently including the glomerular layer (between PGCs and apical dendrites of MTCs – Kasowski et al., 1999) and the EPL (between projecting cells and interneurons – Rall et al., 1966; Huang et al., 2013). Dendrodendritic (reciprocal) arrangements and electrical coupling appear to be vital and effective for sustaining oscillatory activity of the OB and its associated functions in temporally precise and effective signaling (Friedman and Strowbridge, 2003). Dendritic release is widely utilized in other brain areas, including further sensory systems like the auditory or visual system, cortical areas, substantia nigra and many more (Ludwig, 2005; Koch and Magnusson, 2009). Brain regions outside of the OB also show dendrodendritic arrangements, including the lateral geniculate nucleus (Famiglietti, 1970). Axo-dendritic reciprocal arrangements between interneurons and principal cells can be found in the neocortex (Holmgren et al., 2003) and even reciprocal dendrodendritic arrangements can be found, e.g. in the thalamus (Harding, 1971).

In the thalamus, GABAergic interneurons regulate the flow of information relayed to the cortex. Interneurons can release GABA from axonal and dendritic structures. The dendritic structure is involved in a complex synaptic arrangement called thalamic triad.

The GABAergic interneuron forms dendrodendritic reciprocal synapses with the proximal axon of glutamatergic thalamocortical neurons. The third component is formed by the retinogeniculate axon terminal on both other structures. All those components interact and mainly the interneuron dendrite additionally receives massive neuromodulatory input (Cox, 2014), which is a strong commonality to the arrangement between PGC (or GC) and MC. Additionally, impressive physiological similarities of thalamic interneurons and bulbar interneurons have been recognized. Thalamic INs show differential sodium and calcium spike dependent signaling in fast and slow temporal windows resembling studies in the bulb (Egger et al., 2005; Acuna-Goycolea et al., 2008; Egger, 2008). Thus, the occurrence of these astonishing resemblances in different brain systems again fortifies the value of such a functional design.

4.7. Bulbar Circuits

Division of labor in a meaningful and cross-connected way has proven to be a successful concept in countless areas of life. It is integral to any kind of complex organization such as running a workgroup or a university or assembling a car from its parts. Likewise, specialization of single organs and connecting the elements in a meaningful way is essential in biological systems, on the level of the organism itself, the organization of the brain from subregions, or circuit modules of the subsystems and even beyond that. For a primary sensory processing center located beyond the very first synapse of the olfactory pathway, the olfactory bulb shows an astonishing complexity (Shepherd, 1991).

Local computation in the olfactory bulb is organized in several microcircuits with distinct and complementary functions (cf. e.g. Cleland, 2014; Fukunaga et al., 2014). These subsystems comprise local intraglomerular connections (Kosaka and Kosaka, 2005) and cross-glomerular lateral circuitry (Banerjee et al., 2015) in the GL - both use dopaminergic juxtglomerular cells as central elements and junction points to connect those circuits. In deeper local and lateral inter-columnar circuitry, granule cells are the pivotal elements (Egger et al., 2005). Glomerular columns are cross-connected with the other side of the ipsilateral bulb via ETCs, probably targeting projection cells and possibly GCs (Lodovichi et al., 2003; Ma et al., 2013). Deep and superficial bulbar layers are cross-connected, obviously by common projecting cells but also specifically via distinct populations of short-axon cell types signaling unidirectionally between

those layers (Scott et al., 1987; Eyre et al., 2008). Both cell types analyzed in this thesis, GCs and dopaminergic JGCs, are also subject to centrifugal input from many olfactory cortex feedback projections and neuromodulatory regions with ipsilateral and contralateral fibers extending the processing loops immensely (Shiple and Adamek, 1984; Kay and Brunjes, 2014).

The principal neurons of a glomerular module show strong selectivity for their input and retain similarities that are not common with most of the other glomerular units whereas juxtglomerular cells are more variable (Tan et al., 2010; Kikuta et al., 2013). Yet still, sister mitral cells transmit non-redundant information as shown by different temporal activity patterns (Dhawale et al., 2010) and targets of sister mitral cells in the PC are not shared (Ghosh et al., 2011; Miyamichi et al., 2011). Large scale bulbar odor processing, as discussed before (4.2.), is connecting these microcircuits with other distinct lateral modules (Kikuta et al., 2013; Adam et al., 2014). Without combinatorial co-activation of several units plus the lateral influence on other modules and the pattern readout by higher cortical areas, animals would not be able to discriminate such a broad variety of odorants, which is essential for an animal's fitness (Galizia and Lledo, 2013).

Therefore, much rather than only acting as a forwarding relay station with only localized, secluded computations, the olfactory bulb receives rich and various centrifugal input (Price and Powell, 1970b; Davis and Macrides, 1981; Luskin and Price, 1983), exerting a powerful influence on early stages of olfactory processing. Massive and diverse connections couple the local processing to the physiological, affective and behavioral state of the animal and strongly influence processes like learning and memory with subcellular plasticity mechanisms and regulation of neural integration (Kiselycznyk et al., 2006; Martin et al., 2006; Fletcher and Chen, 2010; Moreno et al., 2012; Blauvelt et al., 2013; Cauthron and Stripling, 2014; Rothermel and Wachowiak, 2014).

4.8. Modular arrangements in the brain with similarities to glomeruli

The olfactory bulb glomerulus is the prime and most distinguishable example of a glomerular arrangement in the brain with many cells participating in its circuitry demarcating its outline. Further smaller glomerular structures can be found in other

regions like the cerebellum, substantia gelatinosa and trigeminal nucleus (Pinching and Powell, 1971b). Common to those compared structures is evidently a complex synaptic interaction and connection pattern of several major sets of processes – an incoming axon, a dendrite and processes of interneurons. The delimitation of some of the involved processes (e.g. the olfactory sensory neurons ending in and not extending contacts beyond the glomeruli) and a glial lamellar ensheathing, are features similar to all those glomerular structures (Pinching and Powell, 1971b). Other organizationally and functionally comparable network modules to olfactory bulb glomeruli have been reported in many different brain structures, in vertebrates and non-vertebrates (Akert and Steiger, 1967). With converging axons contacting cross-connected dendrites of many neurons, the OB glomerulus is similar to barrels in rodent somatosensory cortex (Woolsey and Van der Loos, 1970), cortical columns (Mountcastle, 1957; Hubel and Wiesel, 1962), striasomes (Goldman and Nauta, 1977), or thalamic formations in the lateral geniculate nucleus (Kay and Sherman, 2007; and cf. the previous section about thalamic connectivity), but has several functional differences as well. The most important common task of these modules could be input specific signal transformation enhancing the signal-to-noise ratio (Chen and Shepherd, 2005).

In the thalamocortical barrels, input terminates in layer IV, which can be seen as analogous to the olfactory nerve terminal zones within glomeruli. Location-specific interneuron innervation is also similar to the selectivity of certain juxtglomerular neuron types, although the topographic arrangement of barrels and their respective cells is much clearer than in the OB, which does not deal with clear topographic stimuli (Egger et al., 2008; Giessel and Datta, 2014; Egger et al., 2015). The common principals in different brain areas support the view of an advantageous efficient function of such a structural organization in signal processing.

On an even larger scale, the bulbar processing structure has been compared to primary cortical areas or a thalamic processing relay in that it shows bottleneck convergence of input and modulation by a wide range of regions like the brainstem and other extrinsic sources (Xu et al., 2000; Neville and Haberly, 2004; Kay and Sherman, 2007). These influences reportedly shape gain control, contrast enhancement and oscillatory coupling at this very early level (Hayar et al., 2001; Kay, 2005; Kay and Sherman, 2007). Additionally, the olfactory processing system may have served as a blueprint for other cortical areas throughout evolution and the driving force for

neocortical expansion (Shepherd, 2011; Rowe and Shepherd, 2015). In turn, to primary targets of OB output like the piriform cortex, functions of higher order association cortices of other sensory systems are attributed to (Johnson et al., 2000).

4.9. Final remarks

Connecting all the complex interactions of the olfactory bulb circuitry is certainly a question of complex integrative and systemic research. In contrast, our partitioned and reductionist experimental approach in acute slices on single cell or even subcellular level was perfectly suitable to answer certain detailed fundamental questions that are the logical substrate of the conceptual large-scale questions. In two studies, the efforts of this thesis elucidated mechanisms of granule cell spine function and expanded the diversity of dopaminergic cell types in comprehensive discussion with other recent studies. This endeavor provides very relevant insight into the processing of odor information at the level of the olfactory bulb, which can be threaded into an increasingly clearer emerging picture of understanding principles of olfaction and, consequently, fundamental neurobiological processes.

5. References / Bibliography

- Abraham NM, Egger V, Shimshek DR, Renden R, Fukunaga I, Sprengel R, Seeburg PH, Klugmann M, Margrie TW, Schaefer AT, Kuner T. 2010. Synaptic inhibition in the olfactory bulb accelerates odor discrimination in mice. *Neuron* 65(3):399-411.
- Acuna-Goycolea C, Brenowitz SD, Regehr WG. 2008. Active dendritic conductances dynamically regulate GABA release from thalamic interneurons. *Neuron* 57(3):420-431.
- Adam Y, Livneh Y, Miyamichi K, Groysman M, Luo L, Mizrahi A. 2014. Functional transformations of odor inputs in the mouse olfactory bulb. *Frontiers in Neural Circuits* 8.
- Adam Y, Mizrahi A. 2011. Long-Term Imaging Reveals Dynamic Changes in the Neuronal Composition of the Glomerular Layer. *The Journal of Neuroscience* 31(22):7967-7973.
- Akert K, Steiger U. 1967. [On the glomeruli in the central nervous system of vertebrates and invertebrates]. *Schweiz Arch Neurol Neurochir Psychiatr* 100(2):321-337.
- Alheid GF, Carlsen J, De Olmos J, Heimer L. 1984. Quantitative determination of collateral anterior olfactory nucleus projections using a fluorescent tracer with an algebraic solution to the problem of double retrograde labeling. *Brain Res* 292(1):17-22.
- Alizadeh R, Hassanzadeh G, Soleimani M, Joghataei MT, Siavashi V, Khorgami Z, Hadjighassem M. 2015. Gender and age related changes in number of dopaminergic neurons in adult human olfactory bulb. *J Chem Neuroanat* 69:1-6.
- Alonso JR, Briñón JG, Crespo C, Bravo IG, Arévalo R, Aijón J. 2001. Chemical organization of the macaque monkey olfactory bulb: II. Calretinin, calbindin D-28k, parvalbumin, and neurocalcin immunoreactivity. *Journal of Comparative Neurology* 432(3):389-407.
- Alonso M, Lepousez G, Wagner S, Bardy C, Gabellec M-M, Torquet N, Lledo P-M. 2012. Activation of adult-born neurons facilitates learning and memory. *Nat Neurosci* 15(6):897-904.
- Altman J. 1962. Are new neurons formed in the brains of adult mammals? *Science* 135(3509):1127-1128.
- Alvarez VA, Sabatini BL. 2007. Anatomical and physiological plasticity of dendritic spines. *Annu Rev Neurosci* 30:79-97.
- Amoore JE, Hautala E. 1983. Odor as an aid to chemical safety: odor thresholds compared with threshold limit values and volatilities for 214 industrial chemicals in air and water dilution. *J Appl Toxicol* 3(6):272-290.
- Angelo K, Rancz EA, Pimentel D, Hundahl C, Hannibal J, Fleischmann A, Pichler B, Margrie TW. 2012. A biophysical signature of network affiliation and sensory processing in mitral cells. *Nature* 488(7411):375-378.
- Apicella A, Yuan Q, Scanziani M, Isaacson JS. 2010. Pyramidal cells in piriform cortex receive convergent input from distinct olfactory bulb glomeruli. *The Journal of neuroscience : the official journal of the Society for Neuroscience* 30(42):14255-14260.
- Araya R, Jiang J, Eisenthal KB, Yuste R. 2006. The spine neck filters membrane potentials. *Proc Natl Acad Sci U S A* 103(47):17961-17966.
- Araya R, Vogels TP, Yuste R. 2014. Activity-dependent dendritic spine neck changes are correlated with synaptic strength. *Proceedings of the National Academy of Sciences* 111(28):E2895-E2904.
- Arenkiel BR, Hasegawa H, Yi JJ, Larsen RS, Wallace ML, Philpot BD, Wang F, Ehlers MD. 2011. Activity-induced remodeling of olfactory bulb microcircuits revealed by monosynaptic tracing. *PLoS One* 6(12):e29423.
- Arevian AC, Kapoor V, Urban NN. 2008. Activity-dependent gating of lateral inhibition in the mouse olfactory bulb. *Nat Neurosci* 11(1):80-87.
- Attems J, Walker L, Jellinger KA. 2014. Olfactory bulb involvement in neurodegenerative diseases. *Acta Neuropathol* 127(4):459-475.
- Auffarth B, Gutierrez-Galvez A, Marco S. 2011. Continuous spatial representations in the olfactory bulb may reflect perceptual categories. *Frontiers in Systems Neuroscience* 5.

- Aungst JL, Heyward PM, Puche AC, Karnup SV, Hayar A, Szabo G, Shipley MT. 2003. Centre-surround inhibition among olfactory bulb glomeruli. *Nature* 426(6967):623-629.
- Bagley J, LaRocca G, Jimenez DA, Urban NN. 2007. Adult neurogenesis and specific replacement of interneuron subtypes in the mouse main olfactory bulb. *BMC Neurosci* 8:92.
- Baker H. 1990. Unilateral, neonatal olfactory deprivation alters tyrosine hydroxylase expression but not aromatic amino acid decarboxylase or gaba immunoreactivity. *Neuroscience* 36(3):761-771.
- Ballesteros-Yanez I, Benavides-Piccione R, Elston GN, Yuste R, DeFelipe J. 2006. Density and morphology of dendritic spines in mouse neocortex. *Neuroscience* 138(2):403-409.
- Balu R, Pressler RT, Strowbridge BW. 2007. Multiple modes of synaptic excitation of olfactory bulb granule cells. *J Neurosci* 27(21):5621-5632.
- Banerjee A, Marbach F, Anselmi F, Koh MS, Davis MB, Garcia da Silva P, Delevich K, Oyibo HK, Gupta P, Li B, Albeanu DF. 2015. An Interglomerular Circuit Gates Glomerular Output and Implements Gain Control in the Mouse Olfactory Bulb. *Neuron* 87(1):193-207.
- Barbosa JS, Sanchez-Gonzalez R, Di Giaino R, Baumgart EV, Theis FJ, Götz M, Ninkovic J. 2015. Live imaging of adult neural stem cell behavior in the intact and injured zebrafish brain. *Science* 348(6236):789-793.
- Barnes DC, Hofacer RD, Zaman AR, Rennaker RL, Wilson DA. 2008. Olfactory perceptual stability and discrimination. *Nat Neurosci* 11(12):1378-1380.
- Bartel DL, Relu L, Hsieh L, Greer CA. 2015. Dendrodendritic synapses in the mouse olfactory bulb external plexiform layer. *J Comp Neurol* 523(8):1145-1161.
- Bastien-Dionne PO, David LS, Parent A, Saghatelian A. 2010. Role of sensory activity on chemospecific populations of interneurons in the adult olfactory bulb. *J Comp Neurol* 518(10):1847-1861.
- Bathellier B, Buhl DL, Accolla R, Carleton A. 2008. Dynamic ensemble odor coding in the mammalian olfactory bulb: Sensory information at different timescales. *Neuron* 57(4):586-598.
- Bathellier B, Lagier S, Faure P, Lledo PM. 2006. Circuit properties generating gamma oscillations in a network model of the olfactory bulb. *J Neurophysiol* 95(4):2678-2691.
- Batista-Brito R, Close J, Machold R, Fishell G. 2008. The distinct temporal origins of olfactory bulb interneuron subtypes. *Journal of Neuroscience* 28(15):3966-3975.
- Belluzzi O, Benedusi M, Ackman J, LoTurco JJ. 2003. Electrophysiological differentiation of new neurons in the olfactory bulb. *J Neurosci* 23(32):10411-10418.
- Beshel J, Kopell N, Kay LM. 2007. Olfactory bulb gamma oscillations are enhanced with task demands. *J Neurosci* 27(31):8358-8365.
- Bhandawat V, Reiser J, Yau KW. 2005. Elementary response of olfactory receptor neurons to odorants. *Science* 308(5730):1931-1934.
- Bischofberger J, Jonas P. 1997. Action potential propagation into the presynaptic dendrites of rat mitral cells. *J Physiol* 504 (Pt 2):359-365.
- Blauvelt DG, Sato TF, Wienisch M, Knopfel T, Murthy VN. 2013. Distinct spatiotemporal activity in principal neurons of the mouse olfactory bulb in anesthetized and awake states. *Front Neural Circuits* 7:46.
- Bloodgood BL, Giessel AJ, Sabatini BL. 2009. Biphasic Synaptic Ca Influx Arising from Compartmentalized Electrical Signals in Dendritic Spines. *PLoS Biology* 7(9):e1000190.
- Bloodgood BL, Sabatini BL. 2005. Neuronal activity regulates diffusion across the neck of dendritic spines. *Science* 310(5749):866-869.
- Bonzano S, Bovetti S, Fasolo A, Peretto P, De Marchis S. 2014. Odour enrichment increases adult-born dopaminergic neurons in the mouse olfactory bulb. *Eur J Neurosci* 40(10):3450-3457.
- Borin M, Fogli Iseppa A, Pignatelli A, Belluzzi O. 2014. Inward rectifier potassium (Kir) current in dopaminergic periglomerular neurons of the mouse olfactory bulb. *Front Cell Neurosci* 8:223.
- Borisovska M, Bensen AL, Chong G, Westbrook GL. 2013. Distinct modes of dopamine and GABA release in a dual transmitter neuron. *J Neurosci* 33(5):1790-1796.

- Borowsky B, Adham N, Jones KA, Raddatz R, Artymyshyn R, Ogozalek KL, Durkin MM, Lakhani PP, Bonini JA, Pathirana S. 2001. Trace amines: identification of a family of mammalian G protein-coupled receptors. *Proceedings of the National Academy of Sciences* 98(16):8966-8971.
- Bouna S, Gysling K, Calas A, Araneda S. 1994. Some noradrenergic neurons of locus ceruleus-olfactory pathways contain neuropeptide-Y. *Brain Res Bull* 34(4):413-417.
- Boyd AM, Kato HK, Komiyama T, Isaacson JS. 2015. Broadcasting of Cortical Activity to the Olfactory Bulb. *Cell reports* 10(7):1032-1039.
- Boyd AM, Sturgill JF, Poo C, Isaacson JS. 2012. Cortical feedback control of olfactory bulb circuits. *Neuron* 76(6):1161-1174.
- Bozza T, Vassalli A, Fuss S, Zhang JJ, Weiland B, Pacifico R, Feinstein P, Mombaerts P. 2009. Mapping of class I and class II odorant receptors to glomerular domains by two distinct types of olfactory sensory neurons in the mouse. *Neuron* 61(2):220-233.
- Breer H, Fleischer J, Strotmann J. 2006. The sense of smell: multiple olfactory subsystems. *Cell Mol Life Sci* 63(13):1465-1475.
- Breer H, Strotmann J. 2005. The septal organ: a "mini-nose" with dual function. *ChemoSense* 7(2):1-7.
- Brennan P, Keverne E. 1997. Neural mechanisms of mammalian olfactory learning. *Progress in neurobiology* 51(4):457-481.
- Brill J, Shao Z, Puche AC, Wachowiak M, Shipley MT. 2015. Serotonin increases synaptic activity in olfactory bulb glomeruli. *Journal of Neurophysiology*.
- Brill MS, Ninkovic J, Winpenny E, Hodge RD, Ozen I, Yang R, Lepier A, Gascon S, Erdelyi F, Szabo G, Parras C, Guillemot F, Frotscher M, Berninger B, Hevner RF, Raineteau O, Gotz M. 2009. Adult generation of glutamatergic olfactory bulb interneurons. *Nat Neurosci* 12(12):1524-1533.
- Brill MS, Snapyan M, Wohlfrom H, Ninkovic J, Jawerka M, Mastick GS, Ashery-Padan R, Saghatelian A, Berninger B, Gotz M. 2008. A Dlx2-and Pax6-dependent transcriptional code for periglomerular neuron specification in the adult olfactory bulb. *Journal of Neuroscience* 28(25):6439-6452.
- Brinon JG, Martinez-Guijarro FJ, Bravo IG, Arevalo R, Crespo C, Okazaki K, Hidaka H, Aijon J, Alonso JR. 1999. Coexpression of neurocalcin with other calcium-binding proteins in the rat main olfactory bulb. *J Comp Neurol* 407(3):404-414.
- Bruce HM. 1959. An exteroceptive block to pregnancy in the mouse.
- Buck L, Axel R. 1991. A novel multigene family may encode odorant receptors: a molecular basis for odor recognition. *Cell* 65(1):175-187.
- Budde T, Meuth S, Pape HC. 2002. Calcium-dependent inactivation of neuronal calcium channels. *Nat Rev Neurosci* 3(11):873-883.
- Bundsuh ST, Zhu P, Scharer YP, Friedrich RW. 2012. Dopaminergic modulation of mitral cells and odor responses in the zebrafish olfactory bulb. *J Neurosci* 32(20):6830-6840.
- Bunzow JR, Sonders MS, Arttamangkul S, Harrison LM, Zhang G, Quigley DI, Darland T, Suchland KL, Pasumamula S, Kennedy JL. 2001. Amphetamine, 3, 4-methylenedioxymethamphetamine, lysergic acid diethylamide, and metabolites of the catecholamine neurotransmitters are agonists of a rat trace amine receptor. *Molecular pharmacology* 60(6):1181-1188.
- Burton SD, Urban NN. 2015. Rapid Feedforward Inhibition and Asynchronous Excitation Regulate Granule Cell Activity in the Mammalian Main Olfactory Bulb. *J Neurosci* 35(42):14103-14122.
- Bushdid C, Magnasco MO, Vosshall LB, Keller A. 2014. Humans Can Discriminate More than 1 Trillion Olfactory Stimuli. *Science* 343(6177):1370-1372.
- Bywalez WG, Patirniche D, Rupprecht V, Stemmler M, Herz AV, Palfi D, Rozsa B, Egger V. 2015. Local postsynaptic voltage-gated sodium channel activation in dendritic spines of olfactory bulb granule cells. *Neuron* 85(3):590-601.
- Cang J, Isaacson JS. 2003. In vivo whole-cell recording of odor-evoked synaptic transmission in the rat olfactory bulb. *J Neurosci* 23(10):4108-4116.

- Carey RM, Wachowiak M. 2011. Effect of sniffing on the temporal structure of mitral/tufted cell output from the olfactory bulb. *J Neurosci* 31(29):10615-10626.
- Carleton A, Petreanu LT, Lansford R, Alvarez-Buylla A, Lledo PM. 2003. Becoming a new neuron in the adult olfactory bulb. *Nat Neurosci* 6(5):507-518.
- Carson KA, Burd GD. 1980. Localization of acetylcholinesterase in the main and accessory olfactory bulbs of the mouse by light and electron microscopic histochemistry. *Journal of Comparative Neurology* 191(3):353-371.
- Castillo PE, Carleton A, Vincent JD, Lledo PM. 1999. Multiple and opposing roles of cholinergic transmission in the main olfactory bulb. *J Neurosci* 19(21):9180-9191.
- Castro JB, Urban NN. 2009. Subthreshold Glutamate Release from Mitral Cell Dendrites. *Journal of Neuroscience* 29(21):7023-7030.
- Cauthron JL, Stripling JS. 2014. Long-term plasticity in the regulation of olfactory bulb activity by centrifugal fibers from piriform cortex. *J Neurosci* 34(29):9677-9687.
- Cave JW, Wang M, Baker H. 2014. Adult subventricular zone neural stem cells as a potential source of dopaminergic replacement neurons. *Front Neurosci* 8:16.
- Cayre M, Scotto-Lomassese S, Malaterre J, Strambi C, Strambi A. 2007. Understanding the regulation and function of adult neurogenesis: contribution from an insect model, the house cricket. *Chem Senses* 32(4):385-395.
- Chen AM, Perrin MH, DiGruccio MR, Vaughan JM, Brar BK, Arias CM, Lewis KA, Rivier JE, Sawchenko PE, Vale WW. 2005. A soluble mouse brain splice variant of type 2 α corticotropin-releasing factor (CRF) receptor binds ligands and modulates their activity. *Proceedings of the National Academy of Sciences of the United States of America* 102(7):2620-2625.
- Chen Y, Sabatini BL. 2012. Signaling in dendritic spines and spine microdomains. *Curr Opin Neurobiol* 22(3):389-396.
- Chen WR, Shepherd GM. 2005. The olfactory glomerulus: a cortical module with specific functions. *Journal of neurocytology* 34(3-5):353-360.
- Chen WR, Xiong W, Shepherd GM. 2000. Analysis of relations between NMDA receptors and GABA release at olfactory bulb reciprocal synapses. *Neuron* 25(3):625-633.
- Chow SF, Wick SD, Riecke H. 2012. Neurogenesis drives stimulus decorrelation in a model of the olfactory bulb. *PLoS Comput Biol* 8(3):e1002398.
- Cleland TA. 2014. Chapter 7 - Construction of Odor Representations by Olfactory Bulb Microcircuits. In: Edi B, Donald AW, eds. *Progress in Brain Research*. Vol Volume 208: Elsevier. p 177-203.
- Cleland TA, Linster C. 2012. On-center/inhibitory-surround decorrelation via intraglomerular inhibition in the olfactory bulb glomerular layer. *Frontiers in integrative neuroscience* 6.
- Cleland TA, Sethupathy P. 2006. Non-topographical contrast enhancement in the olfactory bulb. *BMC Neurosci* 7:7.
- Clemett DA, Punhani T, S. Duxon M, Blackburn TP, Fone KCF. 2000. Immunohistochemical localisation of the 5-HT_{2C} receptor protein in the rat CNS. *Neuropharmacology* 39(1):123-132.
- Colucci-D'Amato L, Bonavita V, di Porzio U. 2006. The end of the central dogma of neurobiology: stem cells and neurogenesis in adult CNS. *Neurol Sci* 27(4):266-270.
- Cornelisse LN, van Elburg RAJ, Meredith RM, Yuste R, Mansvelde HD. 2007. High Speed Two-Photon Imaging of Calcium Dynamics in Dendritic Spines: Consequences for Spine Calcium Kinetics and Buffer Capacity. *Plos One* 2(10).
- Corthell JT, Olcese J, Trombley PQ. 2014. Melatonin in the mammalian olfactory bulb. *Neuroscience* 261:74-84.
- Coss RG, Globus A. 1978. Spine stems on tectal interneurons in jewel fish are shortened by social stimulation. *Science* 200(4343):787-790.
- Cox CL. 2014. Complex regulation of dendritic transmitter release from thalamic interneurons. *Current opinion in neurobiology* 29:126-132.
- Cummings DM, Snyder JS, Brewer M, Cameron HA, Belluscio L. 2014. Adult neurogenesis is necessary to refine and maintain circuit specificity. *J Neurosci* 34(41):13801-13810.

- Cummings JA, Mulkey RM, Nicoll RA, Malenka RC. 1996. Ca²⁺ signaling requirements for long-term depression in the hippocampus. *Neuron* 16(4):825-833.
- D'Souza RD, Vijayaraghavan S. 2012. Nicotinic receptor-mediated filtering of mitral cell responses to olfactory nerve inputs involves the alpha3beta4 subtype. *J Neurosci* 32(9):3261-3266.
- Dale H. 1935. Pharmacology and Nerve-endings (Walter Ernest Dixon Memorial Lecture): (Section of Therapeutics and Pharmacology). *Proc R Soc Med* 28(3):319-332.
- David F, Courtiol E, Buonviso N, Fourcaud-Trocmé N. 2015. Competing mechanisms of gamma and beta oscillations in the olfactory bulb based on multimodal inhibition of mitral cells over a respiratory cycle. *eneuro:ENEURO*. 0018-0015.2015.
- Davila NG, Blakemore LJ, Trombley PQ. 2003. Dopamine modulates synaptic transmission between rat olfactory bulb neurons in culture. *Journal of neurophysiology* 90(1):395-404.
- Davis BJ, Macrides F. 1981. The organization of centrifugal projections from the anterior olfactory nucleus, ventral hippocampal rudiment, and piriform cortex to the main olfactory bulb in the hamster: An autoradiographic study. *The Journal of Comparative Neurology* 203(3):475-493.
- Davis BJ, Macrides F, Youngs WM, Schneider SP, Rosene DL. 1978. Efferents and centrifugal afferents of the main and accessory olfactory bulbs in the hamster. *Brain Res Bull* 3(1):59-72.
- de Almeida L, Reiner SJ, Ennis M, Linster C. 2015. Computational modeling suggests distinct, location-specific function of norepinephrine in olfactory bulb and piriform cortex. *Front Comput Neurosci* 9:73.
- De Rosa E, Hasselmo ME, Baxter MG. 2001. Contribution of the cholinergic basal forebrain to proactive interference from stored odor memories during associative learning in rats. *Behav Neurosci* 115(2):314-327.
- De Saint Jan D, Hirnet D, Westbrook GL, Charpak S. 2009. External tufted cells drive the output of olfactory bulb glomeruli. *J Neurosci* 29(7):2043-2052.
- Debarbieux F, Audinat E, Charpak S. 2003. Action potential propagation in dendrites of rat mitral cells in vivo. *J Neurosci* 23(13):5553-5560.
- Dhawale AK, Hagiwara A, Bhalla US, Murthy VN, Albeanu DF. 2010. Non-redundant odor coding by sister mitral cells revealed by light addressable glomeruli in the mouse. *Nat Neurosci* 13(11):1404-1412.
- Dietz SB, Murthy VN. 2005. Contrasting short-term plasticity at two sides of the mitral-granule reciprocal synapse in the mammalian olfactory bulb. *J Physiol* 569(Pt 2):475-488.
- Dong H-W, Heinbockel T, Hamilton KA, Hayar A, Ennis M. 2009. Metabotropic Glutamate Receptors and Dendrodendritic Synapses in the Main Olfactory Bulb. *Annals of the New York Academy of Sciences* 1170:224-238.
- Duchamp-Viret P, Duchamp A, Chaput MA. 2003. Single olfactory sensory neurons simultaneously integrate the components of an odour mixture. *Eur J Neurosci* 18(10):2690-2696.
- Eccles JC, Fatt P, Koketsu K. 1954. Cholinergic and inhibitory synapses in a pathway from motor-axon collaterals to motoneurons. *J Physiol* 126(3):524-562.
- Eckmeier D, Shea SD. 2014. Noradrenergic plasticity of olfactory sensory neuron inputs to the main olfactory bulb. *J Neurosci* 34(46):15234-15243.
- Egger R, Schmitt AC, Wallace DJ, Sakmann B, Oberlaender M, Kerr JN. 2015. Robustness of sensory-evoked excitation is increased by inhibitory inputs to distal apical tuft dendrites. *Proc Natl Acad Sci U S A* 112(45):14072-14077.
- Egger V. 2008. Synaptic sodium spikes trigger long-lasting depolarizations and slow calcium entry in rat olfactory bulb granule cells. *Eur J Neurosci* 27(8):2066-2075.
- Egger V, Nevian T, Bruno RM. 2008. Subcolumnar dendritic and axonal organization of spiny stellate and star pyramid neurons within a barrel in rat somatosensory cortex. *Cereb Cortex* 18(4):876-889.
- Egger V, Stroh O. 2009. Calcium buffering in rodent olfactory bulb granule cells and mitral cells. *J Physiol* 587(Pt 18):4467-4479.

- Egger V, Svoboda K, Mainen ZF. 2003. Mechanisms of lateral inhibition in the olfactory bulb: Efficiency and modulation of spike-evoked calcium influx into granule cells. *J Neurosci* 23:7551-7558.
- Egger V, Svoboda K, Mainen ZF. 2005. Dendrodendritic synaptic signals in olfactory bulb granule cells: Local spine boost and global low-threshold spike. *J Neurosci* 25:3521-3530.
- Egger V, Urban NN. 2006. Dynamic connectivity in the mitral cell-granule cell microcircuit. *Semin Cell Dev Biol* 17(4):424-432.
- Endevelt-Shapira Y, Shushan S, Roth Y, Sobel N. 2014. Disinhibition of olfaction: human olfactory performance improves following low levels of alcohol. *Behav Brain Res* 272:66-74.
- Engert F, Bonhoeffer T. 1999. Dendritic spine changes associated with hippocampal long-term synaptic plasticity. *Nature* 399(6731):66-70.
- Ennis M, Hamilton K, Hayar A. 2007. Neurochemistry of the main olfactory system. *Handbook of neurochemistry and molecular neurobiology*: Springer. p 137-204.
- Ennis M, Zhou FM, Ciombor KJ, Aroniadou-Anderjaska V, Hayar A, Borrelli E, Zimmer LA, Margolis F, Shipley MT. 2001. Dopamine D2 receptor-mediated presynaptic inhibition of olfactory nerve terminals. *J Neurophysiol* 86(6):2986-2997.
- Escanilla O, Yuhas C, Marzan D, Linster C. 2009. Dopaminergic modulation of olfactory bulb processing affects odor discrimination learning in rats. *Behav Neurosci* 123(4):828-833.
- Eyre MD, Antal M, Nusser Z. 2008. Distinct deep short-axon cell subtypes of the main olfactory bulb provide novel intrabulbar and extrabulbar GABAergic connections. *J Neurosci* 28(33):8217-8229.
- Fagundo AB, Jimenez-Murcia S, Giner-Bartolome C, Islam MA, de la Torre R, Pastor A, Casanueva FF, Crujeiras AB, Granero R, Banos R, Botella C, Fernandez-Real JM, Fruhbeck G, Gomez-Ambrosi J, Menchon JM, Tinahones FJ, Fernandez-Aranda F. 2015. Modulation of Higher-Order Olfaction Components on Executive Functions in Humans. *PLoS One* 10(6):e0130319.
- Famiglietti EV. 1970. Dendro-dendritic synapses in the lateral geniculate nucleus of the cat. *Brain research* 20(2):181-191.
- Fantana AL, Soucy ER, Meister M. 2008. Rat olfactory bulb mitral cells receive sparse glomerular inputs. *Neuron* 59(5):802-814.
- Feierstein CE. 2012. Linking adult olfactory neurogenesis to social behavior. *Frontiers in neuroscience* 6.
- Finger TE, Böttger B, Hansen A, Anderson KT, Alimohammadi H, Silver WL. 2003. Solitary chemoreceptor cells in the nasal cavity serve as sentinels of respiration. *Proceedings of the National Academy of Sciences* 100(15):8981-8986.
- Fleming A, Vaccarino F, Tambosso L, Chee P. 1979. Vomeronasal and olfactory system modulation of maternal behavior in the rat. *Science* 203(4378):372-374.
- Fletcher ML, Chen WR. 2010. Neural correlates of olfactory learning: Critical role of centrifugal neuromodulation. *Learn Mem* 17(11):561-570.
- Fourcaud-Trocme N, Courtiol E, Buonviso N. 2014. Two distinct olfactory bulb sublamina networks involved in gamma and beta oscillation generation: a CSD study in the anesthetized rat. *Front Neural Circuits* 8:88.
- Friedman D, Strowbridge BW. 2003. Both electrical and chemical synapses mediate fast network oscillations in the olfactory bulb. *J Neurophysiol* 89(5):2601-2610.
- Fuentealba Luis C, Obernier K, Alvarez-Buylla A. 2012. Adult Neural Stem Cells Bridge Their Niche. *Cell Stem Cell* 10(6):698-708.
- Fukunaga I, Berning M, Kollo M, Schmaltz A, Schaefer AT. 2012. Two distinct channels of olfactory bulb output. *Neuron* 75(2):320-329.
- Fukunaga I, Herb JT, Kollo M, Boyden ES, Schaefer AT. 2014. Independent control of gamma and theta activity by distinct interneuron networks in the olfactory bulb. *Nat Neurosci* 17(9):1208-1216.
- Gadziola MA, Tylicki KA, Christian DL, Wesson DW. 2015. The olfactory tubercle encodes odor valence in behaving mice. *J Neurosci* 35(11):4515-4527.

- Gaillard I, Rouquier S, Giorgi D. 2004. Olfactory receptors. *Cell Mol Life Sci* 61(4):456-469.
- Galizia CG, Lledo P-M. 2013. Olfaction. *Neurosciences-From molecule to behavior: a university textbook*: Springer. p 253-284.
- Gao Y, Strowbridge BW. 2009. Long-term plasticity of excitatory inputs to granule cells in the rat olfactory bulb. *Nat Neurosci* 12(6):731-733.
- Garcia I, Quast KB, Huang L, Herman AM, Selever J, Deussing JM, Justice NJ, Arenkiel BR. 2014. Local CRH signaling promotes synaptogenesis and circuit integration of adult-born neurons. *Dev Cell* 30(6):645-659.
- Gelperin A, Tank DW. 1990. Odour-modulated collective network oscillations of olfactory interneurons in a terrestrial mollusc. *Nature* 345(6274):437-440.
- Gerkin RC, Castro JB. 2015. The number of olfactory stimuli that humans can discriminate is still unknown. *Elife* 4:e08127.
- Getchell TV, Margolis FL, Getchell ML. 1984. Perireceptor and receptor events in vertebrate olfaction. *Prog Neurobiol* 23(4):317-345.
- Ghatpande AS, Gelperin A. 2009. Presynaptic muscarinic receptors enhance glutamate release at the mitral/tufted to granule cell dendrodendritic synapse in the rat main olfactory bulb. *J Neurophysiol* 101(4):2052-2061.
- Ghatpande AS, Sivaraaman K, Vijayaraghavan S. 2006. Store calcium mediates cholinergic effects on mIPSCs in the rat main olfactory bulb. *J Neurophysiol* 95(3):1345-1355.
- Ghosh S, Larson SD, Hefzi H, Marnoy Z, Cutforth T, Dokka K, Baldwin KK. 2011. Sensory maps in the olfactory cortex defined by long-range viral tracing of single neurons. *Nature* 472(7342):217-220.
- Giessel AJ, Datta SR. 2014. Olfactory maps, circuits and computations. *Curr Opin Neurobiol* 24(1):120-132.
- Gire DH, Franks KM, Zak JD, Tanaka KF, Whitesell JD, Mulligan AA, Hen R, Schoppa NE. 2012. Mitral cells in the olfactory bulb are mainly excited through a multistep signaling path. *J Neurosci* 32(9):2964-2975.
- Giustetto M, Kirsch J, Fritschy JM, Cantino D, Sassoè-Pognetto M. 1998. Localization of the clustering protein gephyrin at GABAergic synapses in the main olfactory bulb of the rat. *Journal of Comparative Neurology* 395(2):231-244.
- Goldman PS, Nauta WJ. 1977. An intricately patterned prefronto-caudate projection in the rhesus monkey. *Journal of Comparative Neurology* 171(3):369-385.
- Gracia-Llanes FJ, Blasco-Ibanez JM, Nacher J, Varea E, Liberia T, Martinez P, Martinez-Guijarro FJ, Crespo C. 2010a. Synaptic connectivity of serotonergic axons in the olfactory glomeruli of the rat olfactory bulb. *Neuroscience* 169(2):770-780.
- Gracia-Llanes FJ, Crespo C, Blasco-Ibanez JM, Nacher J, Varea E, Rovira-Esteban L, Martinez-Guijarro FJ. 2010b. GABAergic basal forebrain afferents innervate selectively GABAergic targets in the main olfactory bulb. *Neuroscience* 170(3):913-922.
- Gray EG. 1959. Electron microscopy of synaptic contacts on dendrite spines of the cerebral cortex. *Nature* 183(4675):1592-1593.
- Grienberger C, Konnerth A. 2012. Imaging calcium in neurons. *Neuron* 73(5):862-885.
- Gross-Isseroff R, Lancet D. 1988. Concentration-dependent changes of perceived odor quality. *Chemical senses* 13(2):191-204.
- Grosmaître X, Santarelli LC, Tan J, Luo M, Ma M. 2007. Dual functions of mammalian olfactory sensory neurons as odor detectors and mechanical sensors. *Dual functions of mammalian olfactory sensory neurons as odor detectors and mechanical sensors* 10(3):348-354.
- Grunditz Å, Holbro N, Tian L, Zuo Y, Oertner TG. 2008. Spine Neck Plasticity Controls Postsynaptic Calcium Signals through Electrical Compartmentalization. *The Journal of Neuroscience* 28(50):13457-13466.
- Guthrie KM, Pullara JM, Marshall JF, Leon M. 1991. Olfactory deprivation increases dopamine D2 receptor density in the rat olfactory bulb. *Synapse* 8(1):61-70.

- Gutierrez-Mecinas M, Crespo C, Blasco-Ibanez JM, Gracia-Llanes FJ, Marques-Mari AI, Nacher J, Varea E, Martinez-Guijarro FJ. 2005. Distribution of D2 dopamine receptor in the olfactory glomeruli of the rat olfactory bulb. *Eur J Neurosci* 22(6):1357-1367.
- Haberly LB, Bower JM. 1989. Olfactory cortex: model circuit for study of associative memory? *Trends in neurosciences* 12(7):258-264.
- Haddad R, Lanjuin A, Madisen L, Zeng H, Murthy VN, Uchida N. 2013. Olfactory cortical neurons read out a relative time code in the olfactory bulb. *Nat Neurosci* 16(7):949-957.
- Halabisky B, Friedman D, Radojicic M, Strowbridge BW. 2000. Calcium influx through NMDA receptors directly evokes GABA release in olfactory bulb granule cells. *J Neurosci* 20(13):5124-5134.
- Halabisky B, Strowbridge BW. 2003. Gamma-frequency excitatory input to granule cells facilitates dendrodendritic inhibition in the rat olfactory Bulb. *J Neurophysiol* 90(2):644-654.
- Hall B, Delaney K. 2001. Cholinergic modulation of odor-evoked oscillations in the frog olfactory bulb. *The Biological Bulletin* 201(2):276-277.
- Halpern M. 2003. Structure and function of the vomeronasal system: an update. *Progress in Neurobiology* 70(3):245-318.
- Hamada S, Senzaki K, Hamaguchi-Hamada K, Tabuchi K, Yamamoto H, Yamamoto T, Yoshikawa S, Okano H, Okado N. 1998. Localization of 5-HT_{2A} receptor in rat cerebral cortex and olfactory system revealed by immunohistochemistry using two antibodies raised in rabbit and chicken. *Molecular brain research* 54(2):199-211.
- Harding B. 1971. Dendro-dendritic synapses, including reciprocal synapses, in the ventrolateral nucleus of the monkey thalamus. *Brain Research* 34(1):181-185.
- Hardy A, Palouzier-Paulignan B, Duchamp A, Royet JP, Duchamp-Viret P. 2005. 5-Hydroxytryptamine action in the rat olfactory bulb: in vitro electrophysiological patch-clamp recordings of juxtglomerular and mitral cells. *Neuroscience* 131(3):717-731.
- Harris KM, Stevens JK. 1989. Dendritic spines of CA 1 pyramidal cells in the rat hippocampus: serial electron microscopy with reference to their biophysical characteristics. *J Neurosci* 9(8):2982-2997.
- Harvey CD, Svoboda K. 2007. Locally dynamic synaptic learning rules in pyramidal neuron dendrites. *Nature* 450(7173):1195-1200.
- Hasselmo ME, Sarter M. 2011. Modes and models of forebrain cholinergic neuromodulation of cognition. *Neuropsychopharmacology* 36(1):52-73.
- Hayar A, Heyward PM, Heinbockel T, Shipley MT, Ennis M. 2001. Direct excitation of mitral cells via activation of α 1-noradrenergic receptors in rat olfactory bulb slices. *Journal of Neurophysiology* 86(5):2173-2182.
- Hayar A, Karnup S, Ennis M, Shipley MT. 2004a. External tufted cells: a major excitatory element that coordinates glomerular activity. *J Neurosci* 24(30):6676-6685.
- Hayar A, Karnup S, Shipley MT, Ennis M. 2004b. Olfactory bulb glomeruli: external tufted cells intrinsically burst at theta frequency and are entrained by patterned olfactory input. *J Neurosci* 24(5):1190-1199.
- Heinbockel T, Laaris N, Ennis M. 2007. Metabotropic glutamate receptors in the main olfactory bulb drive granule cell-mediated inhibition. *J Neurophysiol* 97(1):858-870.
- Herrada G, Dulac C. 1997. A novel family of putative pheromone receptors in mammals with a topographically organized and sexually dimorphic distribution. *Cell* 90(4):763-773.
- Hildebrand JG, Shepherd GM. 1997. Mechanisms of olfactory discrimination: converging evidence for common principles across phyla. *Annu Rev Neurosci* 20:595-631.
- Hoglinger GU, Alvarez-Fischer D, Arias-Carrion O, Djufri M, Windolph A, Keber U, Borta A, Ries V, Schwarting RK, Scheller D, Oertel WH. 2015. A new dopaminergic nigro-olfactory projection. *Acta Neuropathol* 130(3):333-348.
- Holmgren C, Harkany T, Svennenfors B, Zilberter Y. 2003. Pyramidal cell communication within local networks in layer 2/3 of rat neocortex. *The Journal of physiology* 551(1):139-153.

- Homma R, Kovalchuk Y, Konnerth A, Cohen LB, Garaschuk O. 2013. In vivo functional properties of juxtglomerular neurons in the mouse olfactory bulb. *Front Neural Circuits* 7:23.
- Howard JD, Plailly J, Grueschow M, Haynes J-D, Gottfried JA. 2009. Odor quality coding and categorization in human posterior piriform cortex. *Nature neuroscience* 12(7):932-938.
- Hsieh YC, Puche AC. 2014. GABA modulation of SVZ-derived progenitor ventral cell migration. *Dev Neurobiol*.
- Huang L, Garcia I, Jen H-I, Arenkiel BR. 2013. Reciprocal connectivity between mitral cells and external plexiform layer interneurons in the mouse olfactory bulb. *Frontiers in Neural Circuits* 7.
- Huang S, Moody SA. 1998. Dual expression of GABA or serotonin and dopamine in *Xenopus* amacrine cells is transient and may be regulated by laminar cues. *Vis Neurosci* 15(5):969-977.
- Huang YB, Hu CR, Zhang L, Yin W, Hu B. 2015. In Vivo Study of Dynamics and Stability of Dendritic Spines on Olfactory Bulb Interneurons in *Xenopus laevis* Tadpoles. *PLoS One* 10(10):e0140752.
- Hubel DH, Wiesel TN. 1962. Receptive fields, binocular interaction and functional architecture in the cat's visual cortex. *The Journal of physiology* 160(1):106.
- Huisman E, Uylings HB, Hoogland PV. 2004. A 100% increase of dopaminergic cells in the olfactory bulb may explain hyposmia in Parkinson's disease. *Mov Disord* 19(6):687-692.
- Hummel T, Nordin S. 2005. Olfactory disorders and their consequences for quality of life. *Acta otolaryngologica* 125(2):116-121.
- Hummel T, Olgun S, Gerber J, Huchel U, Frasnelli J. 2013. Brain responses to odor mixtures with sub-threshold components. *Frontiers in psychology* 4.
- Igarashi KM, Ieki N, An M, Yamaguchi Y, Nagayama S, Kobayakawa K, Kobayakawa R, Tanifuji M, Sakano H, Chen WR, Mori K. 2012. Parallel Mitral and Tufted Cell Pathways Route Distinct Odor Information to Different Targets in the Olfactory Cortex. *The Journal of Neuroscience* 32(23):7970-7985.
- Imai T, Sakano H. 2008. Odorant receptor-mediated signaling in the mouse. *Curr Opin Neurobiol* 18(3):251-260.
- Imai T, Sakano H, Vosshall LB. 2010. Topographic mapping--the olfactory system. *Cold Spring Harbor perspectives in biology* 2(8):a001776.
- Isaacson JS. 1999. Glutamate spillover mediates excitatory transmission in the rat olfactory bulb. *Neuron* 23(2):377-384.
- Isaacson JS. 2001. Mechanisms governing dendritic gamma-aminobutyric acid (GABA) release in the rat olfactory bulb. *Proc Natl Acad Sci U S A* 98(1):337-342.
- Isaacson JS, Murphy GJ. 2001. Glutamate-mediated extrasynaptic inhibition: direct coupling of NMDA receptors to Ca(2+)-activated K⁺ channels. *Neuron* 31(6):1027-1034.
- Isaacson JS, Strowbridge BW. 1998. Olfactory reciprocal synapses: dendritic signaling in the CNS. *Neuron* 20(4):749-761.
- Isaacson JS, Vitten H. 2003. GABA(B) receptors inhibit dendrodendritic transmission in the rat olfactory bulb. *J Neurosci* 23(6):2032-2039.
- Jahr CE, Nicoll RA. 1982. Noradrenergic modulation of dendrodendritic inhibition in the olfactory bulb. *Nature* 297(5863):227-229.
- Jan YN, Jan LY, Kuffler SW. 1979. A peptide as a possible transmitter in sympathetic ganglia of the frog. *Proceedings of the National Academy of Sciences* 76(3):1501-1505.
- Johnson DM, Illig KR, Behan M, Haberly LB. 2000. New features of connectivity in piriform cortex visualized by intracellular injection of pyramidal cells suggest that "primary" olfactory cortex functions like "association" cortex in other sensory systems. *J Neurosci* 20(18):6974-6982.
- Jonas P, Bischofberger J, Sandkuhler J. 1998. Corelease of two fast neurotransmitters at a central synapse. *Science* 281(5375):419-424.
- Jones E, Powell T. 1969. Morphological variations in the dendritic spines of the neocortex. *Journal of cell science* 5(2):509-529.
- Jones N, Rog D. 1998. Olfaction: a review. *The Journal of Laryngology & Otology* 112(01):11-24.

- Jones W. 2013. Olfactory carbon dioxide detection by insects and other animals. *Mol Cells* 35(2):87-92.
- Jourdain P, Fukunaga K, Muller D. 2003. Calcium/Calmodulin-Dependent Protein Kinase II Contributes to Activity-Dependent Filopodia Growth and Spine Formation. *Journal of Neuroscience* 23(33):10645-10649.
- Kaba H, Keverne E. 1988. The effect of microinfusions of drugs into the accessory olfactory bulb on the olfactory block to pregnancy. *Neuroscience* 25(3):1007-1011.
- Kaba H, Rosser A, Keverne B. 1989. Neural basis of olfactory memory in the context of pregnancy block. *Neuroscience* 32(3):657-662.
- Kang N, Baum MJ, Cherry JA. 2009. A direct main olfactory bulb projection to the 'vomeronasal' amygdala in female mice selectively responds to volatile pheromones from males. *Eur J Neurosci* 29(3):624-634.
- Kaplan MS, Hinds JW. 1977. Neurogenesis in the adult rat: electron microscopic analysis of light radioautographs. *Science* 197(4308):1092-1094.
- Kapoor V, Urban NN. 2006. Glomerulus-specific, long-latency activity in the olfactory bulb granule cell network. *J Neurosci* 26:11706-11719.
- Kasowski HJ, Kim H, Greer CA. 1999. Compartmental organization of the olfactory bulb glomerulus. *J Comp Neurol* 407(2):261-274.
- Kato HK, Chu MW, Isaacson JS, Komiyama T. 2012. Dynamic sensory representations in the olfactory bulb: modulation by wakefulness and experience. *Neuron* 76(5):962-975.
- Kato HK, Gillet SN, Peters AJ, Isaacson JS, Komiyama T. 2013. Parvalbumin-expressing interneurons linearly control olfactory bulb output. *Neuron* 80(5):1218-1231.
- Kay LM. 2003. Two Species of Gamma Oscillations in the Olfactory Bulb: Dependence on Behavioral State and Synaptic Interactions. *Journal of Integrative Neuroscience* 02(01):31-44.
- Kay LM. 2005. Theta oscillations and sensorimotor performance. *Proc Natl Acad Sci U S A* 102(10):3863-3868.
- Kay LM. 2015. Olfactory system oscillations across phyla. *Curr Opin Neurobiol* 31:141-147.
- Kay LM, Beshel J. 2010. A beta oscillation network in the rat olfactory system during a 2-alternative choice odor discrimination task. *J Neurophysiol* 104(2):829-839.
- Kay LM, Sherman SM. 2007. An argument for an olfactory thalamus. *Trends Neurosci* 30(2):47-53.
- Kay RB, Brunjes PC. 2014. Diversity among principal and GABAergic neurons of the anterior olfactory nucleus. *Front Cell Neurosci* 8:111.
- Ke MT, Fujimoto S, Imai T. 2013. SeeDB: a simple and morphology-preserving optical clearing agent for neuronal circuit reconstruction. *Nat Neurosci* 16(8):1154-1161.
- Kendrick KM, Levy F, Keverne EB. 1992. Changes in the sensory processing of olfactory signals induced by birth in sleep. *Science* 256(5058):833-836.
- Kikuta S, Fletcher ML, Homma R, Yamasoba T, Nagayama S. 2013. Odorant response properties of individual neurons in an olfactory glomerular module. *Neuron* 77(6):1122-1135.
- Kim DH, Phillips ME, Chang AY, Patel HK, Nguyen KT, Willhite DC. 2011. Lateral connectivity in the olfactory bulb is sparse and segregated. *Frontiers in Neural Circuits* 5.
- Kim S, Ziff EB. 2014. Calcineurin Mediates Synaptic Scaling Via Synaptic Trafficking of Ca²⁺-Permeable AMPA Receptors.
- Kiselycznyk CL, Zhang S, Linster C. 2006. Role of centrifugal projections to the olfactory bulb in olfactory processing. *Learn Mem* 13(5):575-579.
- Kiyokage E, Pan YZ, Shao Z, Kobayashi K, Szabo G, Yanagawa Y, Obata K, Okano H, Toida K, Puche AC, Shipley MT. 2010. Molecular identity of periglomerular and short axon cells. *J Neurosci* 30(3):1185-1196.
- Koch U, Magnusson AK. 2009. Unconventional GABA release: mechanisms and function. *Curr Opin Neurobiol* 19(3):305-310.
- Kollo M, Schmaltz A, Abdelhamid M, Fukunaga I, Schaefer AT. 2014. 'Silent' mitral cells dominate odor responses in the olfactory bulb of awake mice. *Nature neuroscience* 17(10):1313-1315.

- Komano-Inoue S, Manabe H, Ota M, Kusumoto-Yoshida I, Yokoyama TK, Mori K, Yamaguchi M. 2014. Top-down inputs from the olfactory cortex in the postprandial period promote elimination of granule cells in the olfactory bulb. *European Journal of Neuroscience* 40(5):2724-2733.
- Kopel H, Schechtman E, Groysman M, Mizrahi A. 2012. Enhanced synaptic integration of adult-born neurons in the olfactory bulb of lactating mothers. *J Neurosci* 32(22):7519-7527.
- Kosaka K, Kosaka T. 2005. synaptic organization of the glomerulus in the main olfactory bulb: compartments of the glomerulus and heterogeneity of the periglomerular cells. *Anat Sci Int* 80(2):80-90.
- Kosaka K, Kosaka T. 2007a. Chemical properties of type 1 and type 2 periglomerular cells in the mouse olfactory bulb are different from those in the rat olfactory bulb. *Brain Res* 1167:42-55.
- Kosaka K, Toida K, Aika Y, Kosaka T. 1998. How simple is the organization of the olfactory glomerulus?: the heterogeneity of so-called periglomerular cells. *Neurosci Res* 30(2):101-110.
- Kosaka T, Deans MR, Paul DL, Kosaka K. 2005. Neuronal gap junctions in the mouse main olfactory bulb: morphological analyses on transgenic mice. *Neuroscience* 134(3):757-769.
- Kosaka T, Kosaka K. 2007b. Heterogeneity of nitric oxide synthase-containing neurons in the mouse main olfactory bulb. *Neurosci Res* 57(2):165-178.
- Kosaka T, Kosaka K. 2008. Tyrosine hydroxylase-positive GABAergic juxtglomerular neurons are the main source of the interglomerular connections in the mouse main olfactory bulb. *Neurosci Res* 60(3):349-354.
- Kosaka T, Kosaka K. 2009. Two types of tyrosine hydroxylase positive GABAergic juxtglomerular neurons in the mouse main olfactory bulb are different in their time of origin. *Neurosci Res* 64(4):436-441.
- Kosaka T, Kosaka K. 2011. "Interneurons" in the olfactory bulb revisited. *Neurosci Res* 69(2):93-99.
- Kovalchuk Y, Homma R, Liang Y, Maslyukov A, Hermes M, Thestrup T, Griesbeck O, Ninkovic J, Cohen LB, Garaschuk O. 2015. In vivo odourant response properties of migrating adult-born neurons in the mouse olfactory bulb. *Nat Commun* 6:6349.
- Kozlov AS, Angulo MC, Audinat E, Charpak S. 2006. Target cell-specific modulation of neuronal activity by astrocytes. *Proc Natl Acad Sci U S A* 103(26):10058-10063.
- Kriegstein A, Alvarez-Buylla A. 2009. The glial nature of embryonic and adult neural stem cells. *Annual review of neuroscience* 32:149.
- Kumar R, Kaur R, Auffarth B, Bhondekar AP. 2015. Understanding the Odour Spaces: A Step towards Solving Olfactory Stimulus-Percept Problem. *PLoS One* 10(10):e0141263.
- Laaris N, Puche A, Ennis M. 2007. Complementary postsynaptic activity patterns elicited in olfactory bulb by stimulation of mitral/tufted and centrifugal fiber inputs to granule cells. *J Neurophysiol* 97(1):296-306.
- Labarrera C, London M, Angelo K. 2013. Tonic inhibition sets the state of excitability in olfactory bulb granule cells. *J Physiol* 591(Pt 7):1841-1850.
- Lagier S, Panzanelli P, Russo RE, Nissant A, Bathellier B, Sassoe-Pognetto M, Fritschy JM, Lledo PM. 2007. GABAergic inhibition at dendrodendritic synapses tunes gamma oscillations in the olfactory bulb. *Proc Natl Acad Sci U S A* 104(17):7259-7264.
- Larsen C, Grattan D. 2012. Prolactin, neurogenesis, and maternal behaviors. *Brain, behavior, and immunity* 26(2):201-209.
- Lazarini F, Gabellec MM, Moigneu C, de Chaumont F, Olivo-Marin JC, Lledo PM. 2014. Adult neurogenesis restores dopaminergic neuronal loss in the olfactory bulb. *J Neurosci* 34(43):14430-14442.
- Lazarini F, Lledo P-M. 2011. Is adult neurogenesis essential for olfaction? *Trends in Neurosciences* 34(1):20-30.
- Le Y, Oppenheim JJ, Wang JM. 2001. Pleiotropic roles of formyl peptide receptors. *Cytokine & Growth Factor Reviews* 12(1):91-105.
- Lee S, Yoon BE, Berglund K, Oh SJ, Park H, Shin HS, Augustine GJ, Lee CJ. 2010. Channel-mediated tonic GABA release from glia. *Science* 330(6005):790-796.

- Lei H, Mooney R, Katz LC. 2006. Synaptic integration of olfactory information in mouse anterior olfactory nucleus. *J Neurosci* 26(46):12023-12032.
- Lepousez G, Lledo P-M. 2013. Odor Discrimination Requires Proper Olfactory Fast Oscillations in Awake Mice. *Neuron* 80(4):1010-1024.
- Lepousez G, Mouret A, Loudes C, Epelbaum J, Viollet C. 2010. Somatostatin contributes to in vivo gamma oscillation modulation and odor discrimination in the olfactory bulb. *The Journal of Neuroscience* 30(3):870-875.
- Lepousez G, Nissant A, Bryant AK, Gheusi G, Greer CA, Lledo PM. 2014. Olfactory learning promotes input-specific synaptic plasticity in adult-born neurons. *Proc Natl Acad Sci U S A* 111(38):13984-13989.
- Lepousez G, Valley MT, Lledo P-M. 2013. The Impact of Adult Neurogenesis on Olfactory Bulb Circuits and Computations. *Annual Review of Physiology* 75(1):339-363.
- Leypold BG, Yu CR, Leinders-Zufall T, Kim MM, Zufall F, Axel R. 2002. Altered sexual and social behaviors in *trp2* mutant mice. *Proceedings of the National Academy of Sciences* 99(9):6376-6381.
- Li G, Linster C, Cleland TA. 2015. Functional differentiation of cholinergic and noradrenergic modulation in a biophysical model of olfactory bulb granule cells. *J Neurophysiol*:jn 00324 02015.
- Liberia T, Blasco-Ibanez JM, Nacher J, Varea E, Zwafink V, Crespo C. 2012. Characterization of a population of tyrosine hydroxylase-containing interneurons in the external plexiform layer of the rat olfactory bulb. *Neuroscience* 217:140-153.
- Lin W, Ogura T, Margolskee RF, Finger TE, Restrepo D. 2008. TRPM5-expressing solitary chemosensory cells respond to odorous irritants. *Journal of neurophysiology* 99(3):1451-1460.
- Liu S, Aungst JL, Puche AC, Shipley MT. 2012. Serotonin modulates the population activity profile of olfactory bulb external tufted cells. *J Neurophysiol* 107(1):473-483.
- Liu S, Plachez C, Shao Z, Puche A, Shipley MT. 2013. Olfactory bulb short axon cell release of GABA and dopamine produces a temporally biphasic inhibition-excitation response in external tufted cells. *J Neurosci* 33(7):2916-2926.
- Liu S, Shao Z, Puche A, Wachowiak M, Rothermel M, Shipley MT. 2015. Muscarinic receptors modulate dendrodendritic inhibitory synapses to sculpt glomerular output. *J Neurosci* 35(14):5680-5692.
- Liu X, Popescu IR, Denisova JV, Neve RL, Corriveau RA, Belousov AB. 2008. Regulation of cholinergic phenotype in developing neurons. *J Neurophysiol* 99(5):2443-2455.
- Livneh Y, Adam Y, Mizrahi A. 2014. Odor processing by adult-born neurons. *Neuron* 81(5):1097-1110.
- Livneh Y, Mizrahi A. 2012. Experience-dependent plasticity of mature adult-born neurons. *Nat Neurosci* 15(1):26-28.
- Lledo PM, Alonso M, Grubb MS. 2006. Adult neurogenesis and functional plasticity in neuronal circuits. *Nat Rev Neurosci* 7(3):179-193.
- Lledo PM, Gheusi G, Vincent JD. 2005. Information processing in the mammalian olfactory system. *Physiol Rev* 85(1):281-317.
- Lledo PM, Merkle FT, Alvarez-Buylla A. 2008. Origin and function of olfactory bulb interneuron diversity. *Trends Neurosci* 31(8):392-400.
- Lledo PM, Saghatelian A. 2005. Integrating new neurons into the adult olfactory bulb: joining the network, life-death decisions, and the effects of sensory experience. *Trends Neurosci* 28(5):248-254.
- Lodovichi C, Belluscio L, Katz LC. 2003. Functional topography of connections linking mirror-symmetric maps in the mouse olfactory bulb. *Neuron* 38(2):265-276.
- Lowe G. 2002. Inhibition of backpropagating action potentials in mitral cell secondary dendrites. *J Neurophysiol* 88(1):64-85.
- Lowry CA, Kay LM. 2007. Chemical factors determine olfactory system beta oscillations in waking rats. *J Neurophysiol* 98(1):394-404.

- Ludwig M. 2005. Dendritic neurotransmitter release: Springer Science & Business Media.
- Luskin MB, Price JL. 1983. The topographic organization of associational fibers of the olfactory system in the rat, including centrifugal fibers to the olfactory bulb. *J Comp Neurol* 216(3):264-291.
- Ma J, Dankulich-Nagrudny L, Lowe G. 2013. Cholecystokinin: an excitatory modulator of mitral/tufted cells in the mouse olfactory bulb. *PLoS One* 8(5):e64170.
- Ma M, Luo M. 2012. Optogenetic activation of basal forebrain cholinergic neurons modulates neuronal excitability and sensory responses in the main olfactory bulb. *J Neurosci* 32(30):10105-10116.
- Magavi SS, Mitchell BD, Szentirmai O, Carter BS, Macklis JD. 2005. Adult-born and preexisting olfactory granule neurons undergo distinct experience-dependent modifications of their olfactory responses in vivo. *J Neurosci* 25(46):10729-10739.
- Maher BJ, Westbrook GL. 2008. Co-transmission of dopamine and GABA in periglomerular cells. *J Neurophysiol* 99(3):1559-1564.
- Maier JX, Blankenship ML, Li JX, Katz DB. 2015. A Multisensory Network for Olfactory Processing. *Curr Biol* 25(20):2642-2650.
- Majewska A, Brown E, Ross J, Yuste R. 2000. Mechanisms of calcium decay kinetics in hippocampal spines: role of spine calcium pumps and calcium diffusion through the spine neck in biochemical compartmentalization. *J Neurosci* 20(5):1722-1734.
- Malenka RC, Nicoll RA. 1999. Long-term potentiation--a decade of progress? *Science* 285(5435):1870-1874.
- Malun D, Brunjes PC. 1996. Development of olfactory glomeruli: temporal and spatial interactions between olfactory receptor axons and mitral cells in opossums and rats. *Journal of Comparative Neurology* 368(1):1-16.
- Manabe H, Mori K. 2013. Sniff rhythm-paced fast and slow gamma-oscillations in the olfactory bulb: relation to tufted and mitral cells and behavioral states. *J Neurophysiol* 110(7):1593-1599.
- Mandairon N, Ferretti CJ, Stack CM, Rubin DB, Cleland TA, Linster C. 2006. Cholinergic modulation in the olfactory bulb influences spontaneous olfactory discrimination in adult rats. *Eur J Neurosci* 24(11):3234-3244.
- Mandairon N, Kermen F, Charpentier C, Sacquet J, Linster C, Didier A. 2014. Context-driven activation of odor representations in the absence of olfactory stimuli in the olfactory bulb and piriform cortex. *Frontiers in behavioral neuroscience* 8.
- Mandairon N, Linster C. 2009. Odor perception and olfactory bulb plasticity in adult mammals. *J Neurophysiol* 101(5):2204-2209.
- Mandairon N, Peace S, Karnow A, Kim J, Ennis M, Linster C. 2008. Noradrenergic modulation in the olfactory bulb influences spontaneous and reward-motivated discrimination, but not the formation of habituation memory. *Eur J Neurosci* 27(5):1210-1219.
- Marei HE, Lashen S, Farag A, Althani A, Afifi N, A AE, Rezk S, Pallini R, Casalbore P, Cenciarelli C. 2015. Human olfactory bulb neural stem cells mitigate movement disorders in a rat model of Parkinson's disease. *J Cell Physiol* 230(7):1614-1629.
- Margrie TW, Schaefer AT. 2003. Theta oscillation coupled spike latencies yield computational vigour in a mammalian sensory system. *J Physiol* 546(Pt 2):363-374.
- Marin-Burgin A, Mongiat LA, Pardi MB, Schinder AF. 2012. Unique processing during a period of high excitation/inhibition balance in adult-born neurons. *Science* 335(6073):1238-1242.
- Markopoulos F, Rokni D, Gire DH, Murthy VN. 2012. Functional properties of cortical feedback projections to the olfactory bulb. *Neuron* 76(6):1175-1188.
- Martin C, Beshel J, Kay LM. 2007. An olfacto-hippocampal network is dynamically involved in odor-discrimination learning. *J Neurophysiol* 98(4):2196-2205.
- Martin C, Gervais R, Messaoudi B, Ravel N. 2006. Learning-induced oscillatory activities correlated to odour recognition: a network activity. *Eur J Neurosci* 23(7):1801-1810.
- Martin C, Ravel N. 2014. Beta and gamma oscillatory activities associated with olfactory memory tasks: different rhythms for different functional networks? *Front Behav Neurosci* 8:218.

- Maruniak J, Wysocki C, Taylor J. 1986. Mediation of male mouse urine marking and aggression by the vomeronasal organ. *Physiology & behavior* 37(4):655-657.
- Masurkar AV, Chen WR. 2012. The influence of single bursts versus single spikes at excitatory dendrodendritic synapses. *Eur J Neurosci* 35(3):389-401.
- Matsumoto H, Kobayakawa K, Kobayakawa R, Tashiro T, Mori K, Sakano H, Mori K. 2010. Spatial arrangement of glomerular molecular-feature clusters in the odorant-receptor class domains of the mouse olfactory bulb. *J Neurophysiol* 103(6):3490-3500.
- Matsunami H, Buck LB. 1997. A multigene family encoding a diverse array of putative pheromone receptors in mammals. *Cell* 90(4):775-784.
- Matsushita N, Okada H, Yasoshima Y, Takahashi K, Kiuchi K, Kobayashi K. 2002. Dynamics of tyrosine hydroxylase promoter activity during midbrain dopaminergic neuron development. *Journal of neurochemistry* 82(2):295-304.
- Matsutani S. 2010. Trajectory and terminal distribution of single centrifugal axons from olfactory cortical areas in the rat olfactory bulb. *Neuroscience* 169(1):436-448.
- Matsutani S, Yamamoto N. 2008. Centrifugal innervation of the mammalian olfactory bulb. *Anat Sci Int* 83(4):218-227.
- Matsuzaki M, Honkura N, Ellis-Davies GC, Kasai H. 2004. Structural basis of long-term potentiation in single dendritic spines. *Nature* 429(6993):761-766.
- Matthews HR, Reisert J. 2003. Calcium, the two-faced messenger of olfactory transduction and adaptation. *Current Opinion in Neurobiology* 13(4):469-475.
- Max SR, Bossio A, Iacovitti L. 1996. Co-expression of tyrosine hydroxylase and glutamic acid decarboxylase in dopamine differentiation factor-treated striatal neurons in culture. *Developmental Brain Research* 91(1):140-142.
- McDole B, Isgor C, Pare C, Guthrie K. 2015. BDNF over-expression increases olfactory bulb granule cell dendritic spine density in vivo. *Neuroscience* 304:146-160.
- McLean JH, Darby-King A, Sullivan RM, King SR. 1993. Serotonergic influence on olfactory learning in the neonate rat. *Behav Neural Biol* 60(2):152-162.
- McLean JH, Shipley MT, Nickell WT, Aston-Jones G, Reyher CK. 1989. Chemoanatomical organization of the noradrenergic input from locus coeruleus to the olfactory bulb of the adult rat. *J Comp Neurol* 285(3):339-349.
- Mechawar N, Saghatelian A, Grailhe R, Scoriels L, Gheusi G, Gabellec MM, Lledo PM, Changeux JP. 2004. Nicotinic receptors regulate the survival of newborn neurons in the adult olfactory bulb. *Proc Natl Acad Sci U S A* 101(26):9822-9826.
- Meister M. 2015. On the dimensionality of odor space. *Elife* 4:e07865.
- Merkle FT, Fuentealba LC, Sanders TA, Magno L, Kessaris N, Alvarez-Buylla A. 2014. Adult neural stem cells in distinct microdomains generate previously unknown interneuron types. *Nat Neurosci* 17(2):207-214.
- Merkle FT, Mirzadeh Z, Alvarez-Buylla A. 2007. Mosaic organization of neural stem cells in the adult brain. *Science* 317(5836):381-384.
- Meyer D, Bonhoeffer T, Scheuss V. 2014. Balance and stability of synaptic structures during synaptic plasticity. *Neuron* 82(2):430-443.
- Migeotte I, Communi D, Parmentier M. 2006. Formyl peptide receptors: A promiscuous subfamily of G protein-coupled receptors controlling immune responses. *Cytokine & Growth Factor Reviews* 17(6):501-519.
- Migliore M, Hines ML, Shepherd GM. 2005. The role of distal dendritic gap junctions in synchronization of mitral cell axonal output. *J Comput Neurosci* 18(2):151-161.
- Miller JP, Rall W, Rinzel J. 1985. Synaptic amplification by active membrane in dendritic spines. *Brain Res* 325(1-2):325-330.
- Milosevic A, Noctor SC, Martinez-Cerdeno V, Kriegstein AR, Goldman JE. 2008. Progenitors from the postnatal forebrain subventricular zone differentiate into cerebellar-like interneurons and cerebellar-specific astrocytes upon transplantation. *Mol Cell Neurosci* 39(3):324-334.

- Mion G, Villevieille T. 2013. Ketamine pharmacology: an update (pharmacodynamics and molecular aspects, recent findings). *CNS Neurosci Ther* 19(6):370-380.
- Miyamichi K, Amat F, Moussavi F, Wang C, Wickersham I, Wall NR, Taniguchi H, Tasic B, Huang ZJ, He Z. 2011. Cortical representations of olfactory input by trans-synaptic tracing. *Nature* 472(7342):191-196.
- Miyamichi K, Serizawa S, Kimura HM, Sakano H. 2005. Continuous and overlapping expression domains of odorant receptor genes in the olfactory epithelium determine the dorsal/ventral positioning of glomeruli in the olfactory bulb. *J Neurosci* 25(14):3586-3592.
- Miyamichi K, Shlomai-Fuchs Y, Shu M, Weissbourd BC, Luo L, Mizrahi A. 2013. Dissecting local circuits: parvalbumin interneurons underlie broad feedback control of olfactory bulb output. *Neuron* 80(5):1232-1245.
- Mizrahi A. 2007. Dendritic development and plasticity of adult-born neurons in the mouse olfactory bulb. *Nat Neurosci* 10(4):444-452.
- Mombaerts P. 1996. Targeting olfaction. *Current Opinion in Neurobiology* 6(4):481-486.
- Mombaerts P. 2004. Genes and ligands for odorant, vomeronasal and taste receptors. *Nat Rev Neurosci* 5(4):263-278.
- Moreno MM, Bath K, Kuczewski N, Sacquet J, Didier A, Mandairon N. 2012. Action of the noradrenergic system on adult-born cells is required for olfactory learning in mice. *J Neurosci* 32(11):3748-3758.
- Moreno MM, Linster C, Escanilla O, Sacquet J, Didier A, Mandairon N. 2009. Olfactory perceptual learning requires adult neurogenesis. *Proc Natl Acad Sci U S A* 106(42):17980-17985.
- Mori K. 2014. Piriform Cortex and Olfactory Tubercle. *The Olfactory System*: Springer. p 161-175.
- Mori K, Kishi K, Ojima H. 1983. Distribution of dendrites of mitral, displaced mitral, tufted, and granule cells in the rabbit olfactory bulb. *J Comp Neurol* 219(3):339-355.
- Mori K, Manabe H, Narikiyo K, Onisawa N. 2013. Olfactory consciousness and gamma oscillation couplings across the olfactory bulb, olfactory cortex, and orbitofrontal cortex. *Front Psychol* 4:743.
- Mori K, Satou M, Takagi SF. 1979. Axonal projection of anterior olfactory nuclear neurons to the olfactory bulb bilaterally. *Experimental neurology* 64(2):295-305.
- Mountcastle VB. 1957. Modality and topographic properties of single neurons of cat's somatic sensory cortex. *Journal of neurophysiology* 20(4):408-434.
- Mouret A, Gheusi G, Gabellec MM, de Chaumont F, Olivo-Marin JC, Lledo PM. 2008. Learning and Survival of Newly Generated Neurons: When Time Matters. *Journal of Neuroscience* 28(45):11511-11516.
- Mouret A, Lepousez G, Gras J, Gabellec MM, Lledo PM. 2009. Turnover of newborn olfactory bulb neurons optimizes olfaction. *J Neurosci* 29(39):12302-12314.
- Mundinano IC, Caballero MC, Ordonez C, Hernandez M, DiCauldo C, Marcilla I, Erro ME, Tunon MT, Luquin MR. 2011. Increased dopaminergic cells and protein aggregates in the olfactory bulb of patients with neurodegenerative disorders. *Acta Neuropathol* 122(1):61-74.
- Munger SD, Leinders-Zufall T, Zufall F. 2009. Subsystem organization of the mammalian sense of smell. *Annu Rev Physiol* 71:115-140.
- Murphy GJ, Darcy DP, Isaacson JS. 2005. Intraglomerular inhibition: signaling mechanisms of an olfactory microcircuit. *Nat Neurosci* 8(3):354-364.
- Murthy VN. 2011. Olfactory maps in the brain. *Annu Rev Neurosci* 34:233-258.
- Mutic S, Parma V, Brunner YF, Freiherr J. 2015. You Smell Dangerous: Communicating Fight Responses Through Human Chemosignals of Aggression. *Chem Senses*.
- Nagayama S, Homma R, Imamura F. 2014. Neuronal organization of olfactory bulb circuits. *Front Neural Circuits* 8:98.
- Nai Q, Dong HW, Hayar A, Linster C, Ennis M. 2009. Noradrenergic regulation of GABAergic inhibition of main olfactory bulb mitral cells varies as a function of concentration and receptor subtype. *J Neurophysiol* 101(5):2472-2484.

- Nai Q, Dong HW, Linster C, Ennis M. 2010. Activation of $\alpha 1$ and $\alpha 2$ noradrenergic receptors exert opposing effects on excitability of main olfactory bulb granule cells. *Neuroscience* 169(2):882-892.
- Najac M, Sanz Diez A, Kumar A, Benito N, Charpak S, De Saint Jan D. 2015. Intraglomerular lateral inhibition promotes spike timing variability in principal neurons of the olfactory bulb. *J Neurosci* 35(10):4319-4331.
- Nakagawa T, Vosshall LB. 2009. Controversy and consensus: noncanonical signaling mechanisms in the insect olfactory system. *Current Opinion in Neurobiology* 19(3):284-292.
- Naritsuka H, Sakai K, Hashikawa T, Mori K, Yamaguchi M. 2009. Perisomatic-targeting granule cells in the mouse olfactory bulb. *The Journal of Comparative Neurology* 515(4):409-426.
- Neuner J, Ovsepian SV, Dorostkar M, Filser S, Gupta A, Michalakis S, Biel M, Herms J. 2014. Pathological α -synuclein impairs adult-born granule cell development and functional integration in the olfactory bulb. *Nature Communications* 5:3915.
- Neville KR, Haberly LB. 2004. Olfactory cortex. *The synaptic organization of the brain* 5:415-454.
- Nickell WT, Behbehani MM, Shipley MT. 1994. Evidence for GABAB-mediated inhibition of transmission from the olfactory nerve to mitral cells in the rat olfactory bulb. *Brain Res Bull* 35(2):119-123.
- Ninkovic J, Gotz M. 2013. Fate specification in the adult brain--lessons for eliciting neurogenesis from glial cells. *Bioessays* 35(3):242-252.
- Ninkovic J, Mori T, Gotz M. 2007. Distinct modes of neuron addition in adult mouse neurogenesis. *J Neurosci* 27(40):10906-10911.
- Ninkovic J, Pinto L, Petricca S, Lepier A, Sun J, Rieger MA, Schroeder T, Cvekl A, Favor J, Gotz M. 2010. The transcription factor Pax6 regulates survival of dopaminergic olfactory bulb neurons via crystallin alphaA. *Neuron* 68(4):682-694.
- Nissant A, Bardy C, Katagiri H, Murray K, Lledo PM. 2009. Adult neurogenesis promotes synaptic plasticity in the olfactory bulb. *Nat Neurosci* 12(6):728-730.
- Nunes D, Kuner T. 2015. Disinhibition of olfactory bulb granule cells accelerates odour discrimination in mice. *Nat Commun* 6.
- Nunez-Parra A, Li A, Restrepo D. 2014. Coding odor identity and odor value in awake rodents. *Prog Brain Res* 208:205-222.
- Nunez-Parra A, Maurer RK, Krahe K, Smith RS, Araneda RC. 2013. Disruption of centrifugal inhibition to olfactory bulb granule cells impairs olfactory discrimination. *Proceedings of the National Academy of Sciences of the United States of America* 110(36):14777-14782.
- Nusser Z, Sieghart W, Mody I. 1999. Differential regulation of synaptic GABAA receptors by cAMP-dependent protein kinase in mouse cerebellar and olfactory bulb neurones. *J Physiol* 521 Pt 2:421-435.
- O'Keefe GC, Barker RA, Caldwell MA. 2009. Dopaminergic modulation of neurogenesis in the subventricular zone of the adult brain. *Cell Cycle* 8(18):2888-2894.
- Oertner TG, Matus A. 2005. Calcium regulation of actin dynamics in dendritic spines. *Cell Calcium* 37(5):477-482.
- Orona E, Scott JW, Rainer EC. 1983. Different granule cell populations innervate superficial and deep regions of the external plexiform layer in rat olfactory bulb. *J Comp Neurol* 217(2):227-237.
- Otazu GH, Chae H, Davis MB, Albeanu DF. 2015. Cortical Feedback Decorrelates Olfactory Bulb Output in Awake Mice. *Neuron* 86(6):1461-1477.
- Padmanabhan K, Urban NN. 2010. Intrinsic biophysical diversity decorrelates neuronal firing while increasing information content. *Nature neuroscience* 13(10):1276-1282.
- Pantages E, Dulac C. 2000. A novel family of candidate pheromone receptors in mammals. *Neuron* 28(3):835-845.
- Panzanelli P, Fritschy JM, Yanagawa Y, Obata K, Sassoè-Pognetto M. 2007. GABAergic phenotype of periglomerular cells in the rodent olfactory bulb. *The Journal of Comparative Neurology* 502(6):990-1002.

- Panzanelli P, Homanics GE, Ottersen OP, Fritschy JM, Sassoe-Pognetto M. 2004. Pre- and postsynaptic GABA receptors at reciprocal dendrodendritic synapses in the olfactory bulb. *Eur J Neurosci* 20(11):2945-2952.
- Panzanelli P, Perazzini AZ, Fritschy JM, Sassoe-Pognetto M. 2005. Heterogeneity of gamma-aminobutyric acid type A receptors in mitral and tufted cells of the rat main olfactory bulb. *J Comp Neurol* 484(1):121-131.
- Parrish-Aungst S, Shipley MT, Erdelyi F, Szabo G, Puche AC. 2007. Quantitative analysis of neuronal diversity in the mouse olfactory bulb. *The Journal of Comparative Neurology* 501(6):825-836.
- Patin A, Pause BM. 2015. Human amygdala activations during nasal chemoreception. *Neuropsychologia* 78:171-194.
- Payton CA, Wilson DA, Wesson DW. 2012. Parallel Odor Processing by Two Anatomically Distinct Olfactory Bulb Target Structures. *PLoS ONE* 7(4):e34926.
- Peretto P, Paredes RG. 2014. 13 Social Cues, Adult Neurogenesis, and Reproductive Behavior. *Neurobiology of Chemical Communication*:367.
- Peters A, Kaiserman-Abramof IR. 1970. The small pyramidal neuron of the rat cerebral cortex. The perikaryon, dendrites and spines. *American Journal of Anatomy* 127(4):321-355.
- Petreanu L, Alvarez-Buylla A. 2002. Maturation and death of adult-born olfactory bulb granule neurons: role of olfaction. *J Neurosci* 22(14):6106-6113.
- Petzold GC, Hagiwara A, Murthy VN. 2009. Serotonergic modulation of odor input to the mammalian olfactory bulb. *Nat Neurosci* 12(6):784-791.
- Pignatelli A, Belluzzi O. 2008. Cholinergic modulation of dopaminergic neurons in the mouse olfactory bulb. *Chem Senses* 33(4):331-338.
- Pignatelli A, Borin M, Fogli Isepe A, Gambardella C, Belluzzi O. 2013. The h-current in periglomerular dopaminergic neurons of the mouse olfactory bulb. *PloS one* 8(2).
- Pignatelli A, Kobayashi K, Okano H, Belluzzi O. 2005. Functional properties of dopaminergic neurones in the mouse olfactory bulb. *J Physiol* 564(Pt 2):501-514.
- Pinato G, Midtgaard J. 2005. Dendritic sodium spikelets and low-threshold calcium spikes in turtle olfactory bulb granule cells. *J Neurophysiol* 93(3):1285-1294.
- Pinching AJ, Powell TP. 1971a. The neuron types of the glomerular layer of the olfactory bulb. *J Cell Sci* 9(2):305-345.
- Pinching AJ, Powell TP. 1971b. The neuropil of the glomeruli of the olfactory bulb. *J Cell Sci* 9(2):347-377.
- Pinching AJ, Powell TP. 1971c. The neuropil of the periglomerular region of the olfactory bulb. *J Cell Sci* 9(2):379-409.
- Platel J-C, Dave KA, Gordon V, Lacar B, Rubio ME, Bordey A. 2010. NMDA receptors activated by subventricular zone astrocytic glutamate are critical for neuroblast survival prior to entering a synaptic network. *Neuron* 65(6):859-872.
- Pompeiano M, Palacios JM, Mengod G. 1992. Distribution and cellular localization of mRNA coding for 5-HT_{1A} receptor in the rat brain: correlation with receptor binding. *The Journal of neuroscience* 12(2):440-453.
- Pompeiano M, Palacios JM, Mengod G. 1994. Distribution of the serotonin 5-HT₂ receptor family mRNAs: comparison between 5-HT_{2A} and 5-HT_{2C} receptors. *Molecular Brain Research* 23(1):163-178.
- Poo C, Isaacson JS. 2009. Odor representations in olfactory cortex: "sparse" coding, global inhibition, and oscillations. *Neuron* 62(6):850-861.
- Popovic MA, Carnevale N, Rozsa B, Zecevic D. 2015. Electrical behaviour of dendritic spines as revealed by voltage imaging. *Nat Commun* 6:8436.
- Pressler RT, Inoue T, Strowbridge BW. 2007. Muscarinic receptor activation modulates granule cell excitability and potentiates inhibition onto mitral cells in the rat olfactory bulb. *J Neurosci* 27(41):10969-10981.
- Price JL, Powell TP. 1970a. An electron-microscopic study of the termination of the afferent fibres to the olfactory bulb from the cerebral hemisphere. *J Cell Sci* 7(1):157-187.

- Price JL, Powell TP. 1970b. An experimental study of the origin and the course of the centrifugal fibres to the olfactory bulb in the rat. *J Anat* 107(Pt 2):215-237.
- Price JL, Powell TP. 1970c. The morphology of the granule cells of the olfactory bulb. *J Cell Sci* 7(1):91-123.
- Price JL, Powell TP. 1970d. The synaptology of the granule cells of the olfactory bulb. *J Cell Sci* 7(1):125-155.
- Puopolo M, Bean BP, Raviola E. 2005. Spontaneous activity of isolated dopaminergic periglomerular cells of the main olfactory bulb. *J Neurophysiol* 94(5):3618-3627.
- Rahayel S, Frasnelli J, Joubert S. 2012. The effect of Alzheimer's disease and Parkinson's disease on olfaction: a meta-analysis. *Behav Brain Res* 231(1):60-74.
- Raineki C, Pickenhagen A, Roth TL, Babstock DM, McLean JH, Harley CW, Lucion AB, Sullivan RM. 2010. The neurobiology of infant maternal odor learning. *Braz J Med Biol Res* 43(10):914-919.
- Rajan R, Clement JP, Bhalla US. 2006. Rats smell in stereo. *Science* 311(5761):666-670.
- Rall W, Shepherd GM. 1968. Theoretical reconstruction of field potentials and dendrodendritic synaptic interactions in olfactory bulb. *J Neurophysiol* 31(6):884-915.
- Rall W, Shepherd GM, Reese TS, Brightman MW. 1966. Dendrodendritic synaptic pathway for inhibition in the olfactory bulb. *Exp Neurol* 14(1):44-56.
- Rammes G, Gravius A, Ruitenber M, Wegener N, Chambon C, Sroka-Saidi K, Jeggo R, Staniaszek L, Spanswick D, O'Hare E, Palmer P, Kim EM, Bywalez W, Egger V, Parsons CG. 2015. MRZ-99030 - A novel modulator of Abeta aggregation: II - Reversal of Abeta oligomer-induced deficits in long-term potentiation (LTP) and cognitive performance in rats and mice. *Neuropharmacology* 92:170-182.
- Ressler KJ, Sullivan SL, Buck LB. 1993. A zonal organization of odorant receptor gene expression in the olfactory epithelium. *Cell* 73(3):597-609.
- Ressler KJ, Sullivan SL, Buck LB. 1994. Information coding in the olfactory system: evidence for a stereotyped and highly organized epitope map in the olfactory bulb. *Cell* 79(7):1245-1255.
- Reyher CK, Lubke J, Larsen WJ, Hendrix GM, Shipley MT, Baumgarten HG. 1991. Olfactory bulb granule cell aggregates: morphological evidence for interperikaryal electrotonic coupling via gap junctions. *J Neurosci* 11(6):1485-1495.
- Rinberg D, Koulakov A, Gelperin A. 2006. Sparse odor coding in awake behaving mice. *J Neurosci* 26(34):8857-8865.
- Rivière S, Challet L, Fluegge D, Spehr M, Rodriguez I. 2009. Formyl peptide receptor-like proteins are a novel family of vomeronasal chemosensors. *Nature* 459(7246):574-577.
- Rojas-Libano D, Frederick DE, Egana JI, Kay LM. 2014. The olfactory bulb theta rhythm follows all frequencies of diaphragmatic respiration in the freely behaving rat. *Front Behav Neurosci* 8:214.
- Roman FS, Simonetto I, Soumireu-Mourat B. 1993. Learning and memory of odor-reward association: selective impairment following horizontal diagonal band lesions. *Behav Neurosci* 107(1):72-81.
- Romano C, Sesma MA, McDonald CT, O'malley K, van den Pol AN, Olney JW. 1995. Distribution of metabotropic glutamate receptor mGluR5 immunoreactivity in rat brain. *Journal of Comparative Neurology* 355(3):455-469.
- Rothermel M, Carey RM, Puche A, Shipley MT, Wachowiak M. 2014. Cholinergic inputs from Basal forebrain add an excitatory bias to odor coding in the olfactory bulb. *The Journal of Neuroscience* 34(13):4654-4664.
- Rothermel M, Wachowiak M. 2014. Functional imaging of cortical feedback projections to the olfactory bulb. *Frontiers in neural circuits* 8.
- Roux L, Madar A, Lacroix MM, Yi C, Benchenane K, Giaume C. 2015. Astroglial Connexin 43 Hemichannels Modulate Olfactory Bulb Slow Oscillations. *J Neurosci* 35(46):15339-15352.
- Rowe TB, Shepherd GM. 2015. Role of ortho-retronasal olfaction in mammalian cortical evolution. *J Comp Neurol*.

- Saino-Saito S, Sasaki H, Volpe BT, Kobayashi K, Berlin R, Baker H. 2004. Differentiation of the dopaminergic phenotype in the olfactory system of neonatal and adult mice. *J Comp Neurol* 479(4):389-398.
- Saito TR, Kamata K, Nakamura M, Inaba M. 1988. Maternal behavior in virgin female rats following removal of the vomeronasal organ. *Zoological science* 5(5):1141-1143.
- Salin PA, Lledo PM, Vincent JD, Charpak S. 2001. Dendritic glutamate autoreceptors modulate signal processing in rat mitral cells. *J Neurophysiol* 85(3):1275-1282.
- Sanai N, Berger MS, Garcia-Verdugo JM, Alvarez-Buylla A. 2007. Comment on "Human Neuroblasts Migrate to the Olfactory Bulb via a Lateral Ventricular Extension". *Science* 318(5849):393.
- Sanai N, Tramontin AD, Quiñones-Hinojosa A, Barbaro NM, Gupta N, Kunwar S, Lawton MT, McDermott MW, Parsa AT, Verdugo JM-G. 2004. Unique astrocyte ribbon in adult human brain contains neural stem cells but lacks chain migration. *Nature* 427(6976):740-744.
- Sarrafcchi A, Odhammer AM, Salazar LTH, Laska M. 2013. Olfactory sensitivity for six predator odorants in CD-1 mice, human subjects, and spider monkeys.
- Sassoe-Pognetto M, Fritschy JM. 2000. Mini-review: gephyrin, a major postsynaptic protein of GABAergic synapses. *Eur J Neurosci* 12(7):2205-2210.
- Sawada M, Kaneko N, Inada H, Wake H, Kato Y, Yanagawa Y, Kobayashi K, Nemoto T, Nabekura J, Sawamoto K. 2011. Sensory input regulates spatial and subtype-specific patterns of neuronal turnover in the adult olfactory bulb. *J Neurosci* 31(32):11587-11596.
- Schaefer AT, Margrie TW. 2012. Psychophysical properties of odor processing can be quantitatively described by relative action potential latency patterns in mitral and tufted cells. *Front Syst Neurosci* 6:30.
- Scherfler C, Esterhammer R, Nocker M, Mahlknecht P, Stockner H, Warwitz B, Spielberger S, Pinter B, Donnemiller E, Decristoforo C, Virgolini I, Schocke M, Poewe W, Seppi K. 2013. Correlation of dopaminergic terminal dysfunction and microstructural abnormalities of the basal ganglia and the olfactory tract in Parkinson's disease. *Brain* 136(Pt 10):3028-3037.
- Scheuss V, Bonhoeffer T. 2014. Function of dendritic spines on hippocampal inhibitory neurons. *Cereb Cortex* 24(12):3142-3153.
- Scheuss V, Yasuda R, Sobczyk A, Svoboda K. 2006. Nonlinear [Ca²⁺] signaling in dendrites and spines caused by activity-dependent depression of Ca²⁺ extrusion. *J Neurosci* 26(31):8183-8194.
- Schmidt LJ, Strowbridge BW. 2014. Modulation of olfactory bulb network activity by serotonin: synchronous inhibition of mitral cells mediated by spatially localized GABAergic microcircuits. *Learn Mem* 21(8):406-416.
- Schneider SP, Macrides F. 1978. Laminar distributions of interneurons in the main olfactory bulb of the adult hamster. *Brain Res Bull* 3(1):73-82.
- Schoenfeld TA, Marchand JE, Macrides F. 1985. Topographic organization of tufted cell axonal projections in the hamster main olfactory bulb: an intrabulbar associational system. *Journal of Comparative Neurology* 235(4):503-518.
- Schoppa NE. 2005. Neurotransmitter mechanisms at dendrodendritic synapses in the olfactory bulb. *Dendritic Neurotransmitter Release*: Springer. p 101-115.
- Schoppa NE. 2006. AMPA/Kainate receptors drive rapid output and precise synchrony in olfactory bulb granule cells. *J Neurosci* 26(50):12996-13006.
- Schoppa NE, Kinzie JM, Sahara Y, Segerson TP, Westbrook GL. 1998. Dendrodendritic inhibition in the olfactory bulb is driven by NMDA receptors. *J Neurosci* 18(17):6790-6802.
- Schoppa NE, Westbrook GL. 1999. Regulation of synaptic timing in the olfactory bulb by an A-type potassium current. *Nat Neurosci* 2(12):1106-1113.
- Schoppa NE, Westbrook GL. 2001. Glomerulus-specific synchronization of mitral cells in the olfactory bulb. *Neuron* 31(4):639-651.
- Scott JW, McDonald JK, Pemberton JL. 1987. Short axon cells of the rat olfactory bulb display NADPH-diaphorase activity, neuropeptide Y-like immunoreactivity, and somatostatin-like immunoreactivity. *Journal of Comparative Neurology* 260(3):378-391.

- Segev I, Rall W. 1998. Excitable dendrites and spines: earlier theoretical insights elucidate recent direct observations. *Trends in Neurosciences* 21(11):453-460.
- Seidenfaden R, Desoeuvre A, Bosio A, Virard I, Cremer H. 2006. Glial conversion of SVZ-derived committed neuronal precursors after ectopic grafting into the adult brain. *Molecular and Cellular Neuroscience* 32(1):187-198.
- Seo H-S, Jeon KJ, Hummel T, Min B-C. 2009. Influences of olfactory impairment on depression, cognitive performance, and quality of life in Korean elderly. *European Archives of Oto-Rhino-Laryngology* 266(11):1739-1745.
- Seubert J, Kellermann T, Loughhead J, Boers F, Brensinger C, Schneider F, Habel U. 2010. Processing of disgusted faces is facilitated by odor primes: a functional MRI study. *Neuroimage* 53(2):746-756.
- Shepherd GM. 1991. Computational structure of the olfactory system. *Olfaction: A model system for computational neuroscience*:3-42.
- Shepherd GM. 2011. The microcircuit concept applied to cortical evolution: from three-layer to six-layer cortex. *Front Neuroanat* 5:30.
- Shepherd GM, Chen WR, Willhite D, Migliore M, Greer CA. 2007. The olfactory granule cell: from classical enigma to central role in olfactory processing. *Brain research reviews* 55(2):373-382.
- Shepherd GM, Greer CA. 2004. Olfactory bulb. In: Shepherd GM, ed. *The Synaptic Organization of the Brain*. 3rd ed. New York: Oxford University Press. p 133-169.
- Shipley MT, Adamek GD. 1984. The connections of the mouse olfactory bulb: a study using orthograde and retrograde transport of wheat germ agglutinin conjugated to horseradish peroxidase. *Brain Res Bull* 12(6):669-688.
- Shipley MT, Ennis M. 1996. Functional organization of olfactory system. *Journal of neurobiology* 30(1):123-176.
- Shipley MT, Halloran FJ, de la Torre J. 1985. Surprisingly rich projection from locus coeruleus to the olfactory bulb in the rat. *Brain Res* 329(1-2):294-299.
- Sin WC, Haas K, Ruthazer ES, Cline HT. 2002. Dendrite growth increased by visual activity requires NMDA receptor and Rho GTPases. *Nature* 419(6906):475-480.
- Sinding C, Coureaud G, Chabanet C, Chambault A, Béno N, Dosne T, Schaal B, Thomas-Danguin T. *Perceptual Interactions in Complex Odor Mixtures: The Blending Effect*; 2013. Academic Press. p 27.
- Singer A, Clancy A, Macrides F, Agosta W, Bronson F. 1988. Chemical properties of a female mouse pheromone that stimulates gonadotropin secretion in males. *Biology of reproduction* 38(1):193-199.
- Smith RS, Hu R, DeSouza A, Eberly CL, Krahe K, Chan W, Araneda RC. 2015. Differential Muscarinic Modulation in the Olfactory Bulb. *J Neurosci* 35(30):10773-10785.
- Sorra KE, Harris KM. 2000. Overview on the structure, composition, function, development, and plasticity of hippocampal dendritic spines. *Hippocampus* 10(5):501-511.
- Soucy ER, Albeanu DF, Fantana AL, Murthy VN, Meister M. 2009. Precision and diversity in an odor map on the olfactory bulb. *Nature Neuroscience* 12(2):210-220.
- Spehr M, Spehr J, Ukhanov K, Kelliher KR, Leinders-Zufall T, Zufall F. 2006. Parallel processing of social signals by the mammalian main and accessory olfactory systems. *Cell Mol Life Sci* 63(13):1476-1484.
- Spors H, Albeanu DF, Murthy VN, Rinberg D, Uchida N, Wachowiak M, Friedrich RW. 2012. Illuminating vertebrate olfactory processing. *J Neurosci* 32(41):14102-14108.
- Spruston N. 2008. Pyramidal neurons: dendritic structure and synaptic integration. *Nat Rev Neurosci* 9(3):206-221.
- Steinfeld R, Herb JT, Sprengel R, Schaefer AT, Fukunaga I. 2015. Divergent innervation of the olfactory bulb by distinct raphe nuclei. *J Comp Neurol* 523(5):805-813.
- Stettler DD, Axel R. 2009. Representations of Odor in the Piriform Cortex. *Neuron* 63(6):854-864.
- Stevenson RJ. 2010. An initial evaluation of the functions of human olfaction. *Chemical senses* 35(1):3-20.

- Stowers L, Holy TE, Meister M, Dulac C, Koentges G. 2002. Loss of sex discrimination and male-male aggression in mice deficient for TRP2. *Science* 295(5559):1493-1500.
- Strata P, Harvey R. 1999. Dale's principle. *Brain Res Bull* 50(5-6):349-350.
- Stroh O, Freichel M, Kretz O, Birnbaumer L, Hartmann J, Egger V. 2012. NMDA receptor-dependent synaptic activation of TRPC channels in olfactory bulb granule cells. *J Neurosci* 32(17):5737-5746.
- Sullivan JM, Sandeman DC, Benton JL, Beltz BS. 2007. Adult neurogenesis and cell cycle regulation in the crustacean olfactory pathway: from glial precursors to differentiated neurons. *J Mol Histo* 38(6):527-542.
- Svoboda K, Tank DW, Denk W. 1996. Direct measurement of coupling between dendritic spines and shafts. *Science* 272(5262):716-719.
- Tan J, Savigner A, Ma M, Luo M. 2010. Odor information processing by the olfactory bulb analyzed in gene-targeted mice. *Neuron* 65(6):912-926.
- Thomann PA, Dos Santos V, Seidl U, Toro P, Essig M, Schroder J. 2009. MRI-derived atrophy of the olfactory bulb and tract in mild cognitive impairment and Alzheimer's disease. *J Alzheimers Dis* 17(1):213-221.
- Tobin VA, Hashimoto H, Wacker DW, Takayanagi Y, Langnaese K, Caquineau C, Noack J, Landgraf R, Onaka T, Leng G, Meddle SL, Engelmann M, Ludwig M. 2010. An intrinsic vasopressin system in the olfactory bulb is involved in social recognition. *Nature* 464(7287):413-417.
- Toida K, Kosaka K, Heizmann CW, Kosaka T. 1994. Synaptic contacts between mitral/tufted cells and GABAergic neurons containing calcium-binding protein parvalbumin in the rat olfactory bulb, with special reference to reciprocal synapses between them. *Brain Res* 650(2):347-352.
- Tonnesen J, Katona G, Rozsa B, Nagerl UV. 2014. Spine neck plasticity regulates compartmentalization of synapses. *Nat Neurosci* 17(5):678-685.
- Triller A, Boulden EA, Churchill A, Hatt H, Englund J, Spehr M, Sell CS. 2008. Odorant-receptor interactions and odor percept: a chemical perspective. *Chem Biodivers* 5(6):862-886.
- Trombley P, Westbrook GL. 1992. L-AP4 inhibits calcium currents and synaptic transmission via a G-protein-coupled glutamate receptor. *The Journal of neuroscience* 12(6):2043-2050.
- Trombley PQ. 1992. Norepinephrine inhibits calcium currents and EPSPs via a G-protein-coupled mechanism in olfactory bulb neurons. *J Neurosci* 12(10):3992-3998.
- Trombley PQ, Hill BJ, Horning MS. 1999. Interactions between GABA and glycine at inhibitory amino acid receptors on rat olfactory bulb neurons. *Journal of neurophysiology* 82(6):3417-3422.
- Trombley PQ, Shepherd GM. 1992. Noradrenergic inhibition of synaptic transmission between mitral and granule cells in mammalian olfactory bulb cultures. *J Neurosci* 12(10):3985-3991.
- Trombley PQ, Shepherd GM. 1994. Glycine exerts potent inhibitory actions on mammalian olfactory bulb neurons. *J Neurophysiol* 71(2):761-767.
- Trudeau LE, Gutierrez R. 2007. On cotransmission & neurotransmitter phenotype plasticity. *Mol Interv* 7(3):138-146.
- Vaaga CE, Borisovska M, Westbrook GL. 2014. Dual-transmitter neurons: functional implications of co-release and co-transmission. *Curr Opin Neurobiol* 29:25-32.
- van den Pol AN, Gorcs T. 1988. Glycine and glycine receptor immunoreactivity in brain and spinal cord. *The Journal of neuroscience* 8(2):472-492.
- Vanderwolf CH, Zibrowski EM. 2001. Piriform cortex beta-waves: odor-specific sensitization following repeated olfactory stimulation. *Brain Res* 892(2):301-308.
- Vassar R, Chao SK, Sitcheran R, Nun~ez JM, Vosshall LB, Axel R. 1994. Topographic organization of sensory projections to the olfactory bulb. *Cell* 79(6):981-991.
- Verhagen JV, Wesson DW, Netoff TI, White JA, Wachowiak M. 2007. Sniffing controls an adaptive filter of sensory input to the olfactory bulb. *Nat Neurosci* 10(5):631-639.
- Veyrac A, Didier A, Colpaert F, Jourdan F, Marien M. 2005. Activation of noradrenergic transmission by alpha2-adrenoceptor antagonists counteracts deafferentation-induced neuronal death and cell proliferation in the adult mouse olfactory bulb. *Exp Neurol* 194(2):444-456.
- Wachowiak M. 2011. All in a sniff: olfaction as a model for active sensing. *Neuron* 71(6):962-973.

- Wang C, Liu F, Liu YY, Zhao CH, You Y, Wang L, Zhang J, Wei B, Ma T, Zhang Q, Zhang Y, Chen R, Song H, Yang Z. 2011. Identification and characterization of neuroblasts in the subventricular zone and rostral migratory stream of the adult human brain. *Cell Res* 21(11):1534-1550.
- Wang YJ, Okutani F, Murata Y, Taniguchi M, Namba T, Kaba H. 2013. Histone acetylation in the olfactory bulb of young rats facilitates aversive olfactory learning and synaptic plasticity. *Neuroscience* 232:21-31.
- Wang ZJ, Sun L, Heinbockel T. 2012. Cannabinoid receptor-mediated regulation of neuronal activity and signaling in glomeruli of the main olfactory bulb. *J Neurosci* 32(25):8475-8479.
- Wesson DW, Wilson DA. 2010. Smelling sounds: olfactory-auditory sensory convergence in the olfactory tubercle. *J Neurosci* 30(8):3013-3021.
- Whitaker-Azmitia PM, Clarke C, Azmitia EC. 1993. Localization of 5-HT_{1A} receptors to astroglial cells in adult rats: implications for neuronal-glia interactions and psychoactive drug mechanism of action. *Synapse* 14(3):201-205.
- Whitesell JD, Sorensen KA, Jarvie BC, Hentges ST, Schoppa NE. 2013. Interglomerular lateral inhibition targeted on external tufted cells in the olfactory bulb. *J Neurosci* 33(4):1552-1563.
- Whitman MC, Greer CA. 2007a. Adult-generated neurons exhibit diverse developmental fates. *Developmental Neurobiology* 67(8):1079-1093.
- Whitman MC, Greer CA. 2007b. Synaptic integration of adult-generated olfactory bulb granule cells: basal axodendritic centrifugal input precedes apical dendrodendritic local circuits. *J Neurosci* 27(37):9951-9961.
- Whitman MC, Greer CA. 2009. Adult neurogenesis and the olfactory system. *Prog Neurobiol* 89(2):162-175.
- Whitten W. 1959. Occurrence of anoestrus in mice caged in groups. *Journal of Endocrinology* 18(1):102-107.
- Willhite DC, Nguyen KT, Masurkar AV, Greer CA, Shepherd GM, Chen WR. 2006. Viral tracing identifies distributed columnar organization in the olfactory bulb. *Proc Natl Acad Sci USA* 103:12592-12597.
- Woolf TB, Shepherd GM, Greer CA. 1991. Serial reconstructions of granule cell spines in the mammalian olfactory bulb. *Synapse* 7(3):181-192.
- Woolsey TA, Van der Loos H. 1970. The structural organization of layer IV in the somatosensory region (SI) of mouse cerebral cortex. The description of a cortical field composed of discrete cytoarchitectonic units. *Brain Res* 17(2):205-242.
- Xu F, Greer CA, Shepherd GM. 2000. Odor maps in the olfactory bulb. *J Comp Neurol* 422(4):489-495.
- y Cajal SR. 1888. Estructura de los centros nerviosos de las aves.
- Yamaguchi M, Mori K. 2005. Critical period for sensory experience-dependent survival of newly generated granule cells in the adult mouse olfactory bulb. *Proc Natl Acad Sci U S A* 102(27):9697-9702.
- Yokoyama Takeshi K, Mochimaru D, Murata K, Manabe H, Kobayakawa K, Kobayakawa R, Sakano H, Mori K, Yamaguchi M. 2011. Elimination of Adult-Born Neurons in the Olfactory Bulb Is Promoted during the Postprandial Period. *Neuron* 71(5):883-897.
- Young WS, 3rd, Kuhar MJ. 1980. Noradrenergic alpha 1 and alpha 2 receptors: light microscopic autoradiographic localization. *Proc Natl Acad Sci U S A* 77(3):1696-1700.
- Youngstrom IA, Strowbridge BW. 2015. Respiratory Modulation of Spontaneous Subthreshold Synaptic Activity in Olfactory Bulb Granule Cells Recorded in Awake, Head-Fixed Mice. *The Journal of Neuroscience* 35(23):8758-8767.
- Yu Y, Migliore M, Hines ML, Shepherd GM. 2014. Sparse coding and lateral inhibition arising from balanced and unbalanced dendrodendritic excitation and inhibition. *J Neurosci* 34(41):13701-13713.
- Yuan Q, Harley CW, McLean JH. 2003. Mitral cell beta1 and 5-HT_{2A} receptor colocalization and cAMP coregulation: a new model of norepinephrine-induced learning in the olfactory bulb. *Learn Mem* 10(1):5-15.

- Yue EL, Cleland TA, Pavlis M, Linster C. 2004. Opposing effects of D1 and D2 receptor activation on odor discrimination learning. *Behav Neurosci* 118(1):184-190.
- Zaborszky L, van den Pol A, Gyengesi E. 2012. The Basal Forebrain Cholinergic Projection System in Mice. 684-718.
- Zeilhofer HU, Studler B, Arabadzisz D, Schweizer C, Ahmadi S, Layh B, Bösl MR, Fritschy JM. 2005. Glycinergic neurons expressing enhanced green fluorescent protein in bacterial artificial chromosome transgenic mice. *Journal of Comparative Neurology* 482(2):123-141.
- Zelles T, Boyd JD, Hardy AB, Delaney KR. 2006. Branch-specific Ca²⁺ influx from Na⁺-dependent dendritic spikes in olfactory granule cells. *J Neurosci* 26:30-40.
- Zheng LM, Caldani M, Jourdan F. 1988. Immunocytochemical identification of luteinizing hormone-releasing hormone-positive fibres and terminals in the olfactory system of the rat. *Neuroscience* 24(2):567-578.
- Zhou Z, Belluscio L. 2008. Intrabulbar projecting external tufted cells mediate a timing-based mechanism that dynamically gates olfactory bulb output. *The Journal of Neuroscience* 28(40):9920-9928.
- Zhou Z, Belluscio L. 2012. Coding odorant concentration through activation timing between the medial and lateral olfactory bulb. *Cell reports* 2(5):1143-1150.
- Zimnik NC, Treadway T, Smith RS, Araneda RC. 2013. alpha(1A)-Adrenergic regulation of inhibition in the olfactory bulb. *J Physiol* 591(Pt 7):1631-1643.

6. Appendix

6.1. Nomenclature / Abbreviations

5-HT	serotonin
AB	adult-born neural progenitor cell
ACh	acetylcholine
AD	Alzheimer's disease
AMPA	α -amino-3-hydroxy-5-methyl-4-isoxazolepropionic
AN	amygdaloid nuclei
AON	anterior olfactory nucleus
AP	action potential
APC	anterior PC
BC	Blanes cell
BF	basal forebrain
BK	big conductance potassium channel
CA1	Cornu Ammonis region 1
Ca ²⁺	calcium (ion form)
cAMP	cyclic adenosine monophosphate
CC	calcium channel
CCK	cholecystokinin
CF	centrifugal fibers
CO	carbon monoxide
CO ₂	carbon dioxide
CRH	corticotropin-releasing hormone
D/DA/DAergic	dopamine/dopaminergic
DAT	dopamine transporter
dGC	deep GC
DJ	dopaminergic juxtglomerular neuron
DNI	4-methoxy-5,7-dinitroindoliny
DR KC	delayed rectifier potassium channel
dSAC	deep SAC
EPL	external plexiform layer
ETC	external TC
FFN102	false fluorescent neurotransmitter 102 (DAT-specific probe)
GABA/GABAergic	γ -aminobutyric acid/GABAergic
GAD65/GAD67	glutamate decarboxylase 65/67 isoforms
GC	granule cell
GCL	granule cell layer
GFP	green fluorescent protein
GL	glomerular layer
Glu	glutamate
GTP	guanosine triphosphate
HDB	horizontal limb of the diagonal band of Broca
HVACC	high voltage activated calcium channel
IBP	intraulbar projection
I _{CAN}	calcium-activated non-selective cation current
IN	interneuron
IPL	internal plexiform layer
JG/JGC/JGN	juxtglomerular cell
KC	potassium channel

K _{DR}	delayed rectifier potassium channel
LC	locus ceruleus
LEC	lateral entorhinal cortex
LOT	lateral olfactory tract
LTP	long-term potentiation
MC	mitral cell
mGluR	metabotropic glutamate receptor
MNI	4-Methoxy-7-nitroindoliny
MOB	main olfactory bulb
MOE	main olfactory epithelium
mTC	medial TC
MTC	mitral/tufted cell
NA	noradrenaline
Na _v	voltage gated sodium channel
NLOT	nucleus of the lateral olfactory tract
NMDA	N-Methyl-D-aspartic acid
OB	olfactory bulb
OC	olfactory cortex
ONL	olfactory nerve layer
OR	olfactory receptor
OSN	olfactory sensory neuron
OT	olfactory tubercle
PC	piriform cortex
PD	Parkinson's disease
pdSAC	projecting deep SAC
PG/PGC/PGN	periglomerular cell
PN	projection neuron
PPC	posterior PC
PV	parvalbumin
RMS	rostral migratory stream
RN	raphe nuclei
SAC	short-axon cell
SEZ	subependymal zone
sGC	superficial GC
SN	substantia nigra
sSAC	superficial SAC
sTC	superficial TC
SVZ	subventricular zone
TC	tufted cell
TH	tyrosine hydroxylase
TPLSM	two-photon laser scanning microscopy
TRPC	transient receptor potential cation channel
TT	tenia tecta
vdSAC	vertical column deep SAC
VNO	vomer nasal organ
vsSAC	vertical column superficial SAC

6.2. Acknowledgements

Thank you...

Veronica Egger for your continuous support and supervision throughout the thesis and at the same time giving me plenty of rope for own scientific decisions and development, while keeping me funded throughout the thesis. Of course I also cherished the occasional nonscientific and informal chats about everything and anything after work hours or during conferences.

Volker Scheuss and Marc Spehr for taking on the time consuming job of being secondary reviewers of my thesis and your cordial and informal company outside of professional ties.

Andreas Schäfer, Hans Straka Volker Scheuss and Mario Wullimann for very valuable input and lively discussions during my advisory committee meetings and beyond.

The whole SPP 1392 for all the funding and providing a secure, friendly and extremely stimulating scientific framework for my PhD project and by that becoming the equivalent of a scientific family (students and likewise very approachable PIs and Mihaela of course). Let me just exemplarily point out Jan and Tobi with whom I hope to drink a beer even 50 years from now.

The GSN staff (Julia, Lena, Alex, Renate, Raluca, Catherine, Stefanie, Benedikt ...) for being very helpful chaperones of the graduate program and accompanying me throughout the thesis professionally and amicably.

Simone Fischer, Kathrin Koros, Sera Camyesil, Cornelia Besand and Eva-Maria Hofmann, the women secretly wielding the real power and responsibility at universities – for being dear and helpful colleagues in a thousand different tasks in university routine and for shoveling away tons of bureaucracy associated with my scientific work.

Benedikt Grothe and Inga Neumann for providing lab and office space for me and my work group, especially during the long limbo states of our relocations.

My current and former work group (Veronica, Fernando, both Michaels, Mahua, Max, Vanessa, Tiffany, Anne, Hortenzia) for creating a lively scientific and personal environment that constantly made me feel excited about going to work every day.

Anne, Hortenzia, Olga, Hilde, Gabi, for great technical assistance throughout difficult projects and for finding a convenient solution for any problem.

My collaboration partners in all the projects – let me just point out a few representative for the many which shared my work – Vanessa, Michael, Tiffany from

my group, Dinu, Andreas Herz, Martin Stemmler from the LMU, Gerhard Rammes from the TUM and all the others - thank you for the fruitful and successful teamwork.

Everyone sharing an office space with me, and therefore also some laughs and moans. (Fernando, Mahua, Michael, Max, Vanessa, Daniel, Nicole, Chrisi, Jana).

All the PIs, postdocs, PhDs, TAs and students at the LMU and UR for sharing amazing talks, good beer and fluctuating levels of quality of mensa food with me day by day. Thanks for all the professional acquaintances and friendships far beyond that, which I could experience in different work spaces, homes or conferences – with many more people than I could name in a few lines.

My dear parents, my brother and the rest of my family for their unconditional love, care and support.

Maren, for being my love and the best partner anyone could ever imagine throughout these busy years.

6.3. Short scientific curriculum vitae

Name: Wolfgang Georg Bywalez
Date/place of birth: June 24th, 1986, in Schweinfurt
Nationality: German

Academic Studies

2012 to date: Graduate School of Systemic Neurosciences (GSN) member
2011 to date: PhD thesis - LMU München/Universität Regensburg, AG Egger
(Physiology of interneurons in the olfactory bulb)
2010: Diploma thesis – JMU Würzburg, AG Förster
(The circadian cycle of *Drosophila melanogaster* under varying
conditions)
2010: Diploma exams
(neurobiology - 1.0, pharmaceutical biology 1.0, genetics 1.0)
2005 - 2010: Biology studies (Diploma) at the JMU Würzburg

Selected conferences and workshops

November 2015: Universitätsklinikum Regensburg Neuroscience Seminar (Oral
presentation)
September 2015: SPP Main Meeting Aachen (Chair and oral presentation)
July 2015: Summer School on Human Olfaction 2015 (by Prof Dr. Thomas
Hummel)
March 2015: NWG Göttingen (Poster Presentation)
November 2014: SFN Conference Washington D.C. (Poster Presentation)
December 2013: SPP PhD Meeting München (Organized by W. Bywalez and D.
Biechl, oral presentation)
February 2013: GSN Workshop Quality Papers (by Dr. Peter Moore)
October 2012: GSN Workshop Optogenetics (Organized by Prof. Dr. Venkatesh
Murthy and W. Bywalez)
March 2012: Visual Impact: The use and abuse of visual information in
science and beyond (by Dr. Barrett Klein)

Publication list

Bywalez W, Menegazzi P, Rieger D, Schmid B, Helfrich-Forster C, Yoshii T. 2012. The dual-oscillator system of *Drosophila melanogaster* under natural-like temperature cycles. *Chronobiol Int* 29(4):395-407.

Bywalez WG, Patirniche D, Rupprecht V, Stemmler M, Herz AV, Palfi D, Rozsa B, Egger V. 2015. Local postsynaptic voltage-gated sodium channel activation in dendritic spines of olfactory bulb granule cells. *Neuron* 85(3):590-601.

Rammes G, Gravius A, Ruitenbergh M, Wegener N, Chambon C, Sroka-Saidi K, Jeggo R, Staniaszek L, Spanswick D, O'Hare E, Palmer P, Kim EM, **Bywalez W**, Egger V, Parsons CG. 2015. MRZ-99030 - A novel modulator of Abeta aggregation: II - Reversal of Abeta oligomer-induced deficits in long-term potentiation (LTP) and cognitive performance in rats and mice. *Neuropharmacology* 92:170-182.

Submissions

Bywalez W, Ona Jodar, T, Lukas M, Ninkovic J, Egger V. 2015. Subtype diversity of dopaminergic neurons within the rat and mouse olfactory bulb glomerular layer. Submitted, December 2015 in *Journal of Comparative Neurology*

6.4. Contributions

Project 1: Local postsynaptic voltage-gated sodium channel activation in dendritic spines of olfactory bulb granule cells

Veronica Egger (V.E.) and Wolfgang Bywalez (W.B.) designed experiments and established a functional setup. W.B., Vanessa Rupprecht (V.R.), and V.E. performed experiments and analyzed data. V.E., W.B., Dinu Patirniche (D.P.) and Martin Stemmler (M.S.) wrote the manuscript. W.B., V.E. and D.P. prepared the figures. D.P. performed the simulations, in close collaboration with M.S., Andreas Herz (A.H.), V.E. and W.B.. Dénes Pálfi (De.Pa.) and Balázs Rózsa (B.R.) provided DNI-caged glutamate and data on DNI properties. W.B., V.E., D.P., A.H., M.S., and V.R. edited and revised the manuscript and all authors approved the final version.

Publication in *Neuron* 85, 590–601, February 4, 2015

doi: 10.1016/j.neuron.2014.12.051

Project 2: Subtype diversity of dopaminergic neurons within the rat and mouse olfactory bulb glomerular layer

Wolfgang Bywalez (W.B.) and Veronica Egger (V.E.) designed experiments. W.B., V.E. and Michael Lukas (M.L.) interpreted data. W.B. and Tiffany Ona Jodar (T.O.J.) performed experiments. W.B., T.O.J. and V.R. analyzed data. W.B. and V.E. wrote the manuscript. W.B. prepared the figures. W.B., V.E. and M.L. critically revised the manuscript. Jovica Ninkovic (J.N.) provided transgenic animals.

Submitted to *Journal of Comparative Neurology*, December 2015

Unterschrift / signature Wolfgang Bywalez

Unterschrift /signature Veronica Egger (thesis supervisor and first reviewer)

6.5. Eidesstattliche Versicherung/Affidavit

Hiermit versichere ich an Eides statt, dass ich die vorliegende Dissertation „Physiology of rodent olfactory bulb interneurons“ selbstständig angefertigt habe, mich außer der angegebenen keiner weiteren Hilfsmittel bedient und alle Erkenntnisse, die aus dem Schrifttum ganz oder annähernd übernommen sind, als solche kenntlich gemacht und nach ihrer Herkunft unter Bezeichnung der Fundstelle einzeln nachgewiesen habe.

I hereby confirm that the dissertation „Physiology of olfactory bulb interneurons“ is the result of my own work and that I have only used sources or materials listed and specified in the dissertation.

München, den
Munich, date

Unterschrift
signature

6.6. Erratum

Erratum: Physiology of olfactory bulb interneurons - Project 1: Subtype diversity of dopaminergic neurons within the rat and mouse olfactory bulb glomerular layer

The novel fluorescent probe FFN102 was published as a specific substrate for dopamine transporter (DAT) and vesicular monoamine transporter 2 (VMAT2) in the striatum and ventral midbrain of mice (Rodriguez et al., 2013). Since dopaminergic cells are the only population of resident monoaminergic cells in the olfactory bulb, the marker FFN102 should be specific for this cell population. However, in a set of revision experiments we had to realize that the probe did not specifically stain dopaminergic cells, but rather the majority of juxtglomerular neurons, mostly GABAergic interneurons, as observed via a strong overlap with a marker specific for the vesicular GABA transporter (VGAT). Therefore, only the clasping cell type described in the first project about juxtglomerular neurons is certainly a dopaminergic cell type, as identified by the marker DAT. The other discussed interneurons are likely to encompass mostly previously described populations of GABAergic cell types, namely classical periglomerular cells (the majority of the 'uniglomerular' cell population as well as the putative majority of 'intermediate' and 'reduced' cells). The findings and resulting deductions have been carefully revised and a corrected manuscript for this project has been resubmitted to the Journal of Comparative Neurology in June 2016 under the following title: Dendrosomatic specializations and arborization patterns of small juxtglomerular interneuron subtypes within the mouse and rat olfactory bulb. The authors would like to apologize for any inconvenience this has caused to the reviewers and readers of this dissertation.